POST-LATE CRETACEOUS ROTATIONAL EVOLUTION OF NEOTETHYAN SUTURES AROUND ANKARA REGION

A THESIS SUBMITTED TO
THE GRADUATE SCHOOL OF NATURAL AND APPLIED SCIENCES
OF
MIDDLE EAST TECHNICAL UNIVERSITY

BY

MURAT ÖZKAPTAN

IN PARTIAL FULFILLMENT OF THE REQUIREMENTS
FOR
THE DEGREE OF DOCTOR OF PHILOSOPHY
IN
GEOLOGICAL ENGINEERING

JANUARY 2016

Approval of the thesis:

POST-LATE CRETACEOUS ROTATIONAL EVOLUTION OF NEOTETHYAN SUTURES AROUND ANKARA REGION

submitted by **MURAT ÖZKAPTAN** in partial fulfillment of the requirements for the degree of **Doctor of Philosophy in Geological Engineering Department, Middle East Technical University** by,

Prof. Dr. Gülbin Dural Ünver _____

Dean, Graduate School of **Natural and Applied Sciences**

Prof. Dr. Erdin Bozkurt _____

Head of Department, **Geological Engineering**

Prof. Dr. Nuretdin Kaymakcı _____

Supervisor**, Geological Engineering Dept., METU**

Assist. Prof. Dr. A. Arda Özacar. _____

Co-Supervisor**, Geological Engineering Dept., METU**

Examining Committee Members:

Prof. Dr. Erdin Bozkurt _____

Geological Engineering Dept., METU

Prof. Dr. Nuretdin Kaymakcı _____

Supervisor, Geological Engineering Dept., METU

Prof. Dr. Kadir Dirik _____

Geological Engineering Dept., HÜ

Prof. Dr. Hasan Sözbilir _____

Geological Engineering Dept., DEÜ

Assist. Prof. Dr. Erman Özsayın _____

Geological Engineering Dept., HÜ

Date: 27.01.2016

I hereby declare that all information in this document has been obtained and presented in accordance with academic rules and ethical conduct. I also declare that, as required by these rules and conduct, I have fully cited and referenced all material and results that are not original to this work.

Name, Surname: Murat ÖZKAPTAN

Signature:

ABSTRACT

POST-LATE CRETACEOUS ROTATIONAL EVOLUTION OF NEOTETHYAN SUTURES AROUND ANKARA REGION

Özkaptan, Murat

Ph.D., Department of Geological Engineering

Supervisor: Prof. Dr. Nuretdin Kaymakcı

Co-Supervisor: Assist. Prof. Dr. A. Arda Özacar

January 2016, 200 pages

The central Anatolia comprises various continental fragments belonging to Laurasia at the north and Gondwana at the south. These amalgamated continental fragments (micro continents) delineated by ophiolitic remnants of Tethyan oceanic lithosphere which were consumed due to ~N to S convergence. Around Haymana Basin the closure of the Neotethys Oceans lead to amalgamation of the Pontides (Laurasian affinity) in the north, Tauride and Kırşehir blocks (Gondwana affinity) in the south. The main purpose of this study is to unravel vertical axis rotations in around Haymana Basin using paleomagnetic tools and its deformation history and kinematics using Anisotropy of Magnetic Susceptibility vectors. In this respect, late Cretaceous to Pliocene infill of the Haymana and adjacent basins namely, Alcı-Orhaniye, Tuz Gölü and Kırıkkale-Bala basins in the central Anatolia are systematically sampled and around ~5000 sedimentary paleomagnetic samples for paleomagnetic purposes from 119 different locations within a 250 km diameter area were collected. Before the demagnetization process, nearly 3000 core specimens were measured for anisotropy of magnetic susceptibility (AMS) to reveal their magnetofabric characteristics.

The paleomagnetic results show, that the region underwent strong clockwise and counterclockwise rotations -even more than 90° in places- resulting the present geometry of the suture zones. Overall Haymana Basin has rotated more than 90° counterclockwise while its northern and south parts and northern part of the Tuz

Gölü Basin rotated approximately 30° clockwise senses, which disagrees with almost all the published paleomagnetic data from the region. The restored orientations, based on the new data indicate that Haymana, Tuz Gölü Basin and the Kırıkkle-Bala Basin which constitutes the SW continuation of the Çankırı Basin were initially oriented in N-S direction prior to Eocene. These results are greatly differing from previously published results from the region which assumes that the İzmir-Ankara-Erzincan Suture Zone was oriented E-W. These imply that almost all of the paleogeographical maps and evolutionary scenarios and models of the region requires major re-thinking and serious revisions.

Keywords: Paleomagnetism, Rotation, anisotropic Magnetic Susceptibility (AMS), Central Anatolia, Haymana Basin, İzmir-Ankara Suture, Intra-Tauride Suture.

ÖZ

ANKARA BÖLGESİ CİVARINDA NEO-TETIS KENET KUŞAĞININ GEÇ KRETASEDEN GÜNÜMÜZE ROTASYONAL EVRİMİ

Özkaptan, Murat
Doktora, Jeoloji Mühendisliği Bölümü
Tez Yöneticisi: Prof. Dr. Nuretdin Kaymakcı
Yardımcı Tez Yöneticisi: Yrd. Doç. Dr. A. Arda Özacar
Ocak 2016, 200 sayfa

İç Anadolu geçmişte iki büyük kıta olan kuzeydeki Lavrasya ve güneydeki Gondvana'nın farklı kıtasal parçalarının birleşmesiyle oluşmuştur. Bu bütünleşik kıtasal bloklar (mikro kıtalar) yaklaşık kuzey-güney yönünde daralma sonucunda Tetis okyanusal litosferininin yitiminden kalan parçalarla çevrelenmiştir. Haymana Havzası ve civarında Noe-Tetis okyanusunun kapanmasıyla kuzeydeki Pontide (Lavrasya'nın parçası) ile güneydeki Toros ve Kırşehir Blokları (Gondvana'nın parçaları) bütünleşmiştir. Bu çalışmanın ana amacı Haymana Havzası ve civarinda paleomanyetik yöntemler kullanarak düşey eksen blok rotasyonlarını belirlemek ve anizotropik manyetik duyarlılık (süseptibilite) vektörlerini de kullanarak bölgenin kinematik evrimini ortaya koymaktır. Bu kapsamda Haymana Havzası ve civarındaki havzalardan; Alcı-Orhaniye, Tuzgölü ve Kırıkkale-Bala havza dolgularından geç Kretase – Piliyosen zaman aralığına ait sistematik örnekleme yapılarak yaklaşık 250 km^2 'lik bir alanda toplamda 119 farklı lokasyondan 5000 civarında paleomanyetik amaçlı tortul kaya örneği derlenmiştir. Manyetik temizleme (demanyetizasyon) işlemlerinden önce yaklaşık 3000 örnek üzerinde anizotropik manyetik duyarlılık ölçümleri yapılarak manyetofabrik karakteristikleri ortaya konulmustur.

Paleomanyetik sonuçlar bölgenin saat yönünde ve tersi istikamette yer yer 90°'leri geçen aşırı miktarlarda rotasyona maruz kalarak bölgedeki kenet kuşaklarının günümüzdeki geometrilerini kazanmasına neden olmuştur. Genel olarak Haymana Havzası'nın tamamı 90°'lere yakın miktarlarda saatin tersi yönde rotasyona

uğrarken, Çankırı Havza'sının güneybatı devamını oluşturan Kırıkkale-Bala ve Tuz Gölü Havza'sının kuzey bölümünden oluşan bölge yaklaşık 30° saat yönünde dönmeye maruz kalmıştır. Bu sonuçlar bölgede yapılan daha önceki paleomanyetizma çalışmalarından oldukça fazla farklılık göstermektedir. Bu çalışma sonucunda ortaya çıkan yeni verilere göre bölge restore edildiğinde Haymana, Tuz Gölü, ve Kırıkale-Bala havzalarının Eosen öncesinde K-G doğrultulu oldukları ortaya çıkmaktadır. Önceki bir çok çalışmanın İzmir-Ankara-Erzincan Kenet Kuşağının yönünün D-B olduğunu farz ettiği dikkate alındığında, bu yeni sonuçlar; literatürde bölge için önerilmiş olan paleocoğrafik haritaların, tektonik evrim senaryoların ve modellerin tekrar gözden geçirilmesini zorunlu kılmaktadır.

Anahtar Kelimeler: Paleomanyetizma, rotasyon, Anizotropik Manyetik Duyarlılık (AMD), Orta Anadolu, Haymana Havzası, İzmir-Ankara Kenedi, Intra-Torid Kenedi.

To all those who take part in this research

ACKNOWLEDGEMENTS

There are many people to thank who have helped me complete this thesis.

First and foremost, I would like to thank to my supervisor Prof. Dr. Nuretdin Kaymakcı, for his guidance and support in every steps of this study. He always standing beside me throughout my career and also improved the scientific content of this thesis.

I would also like to express my deepest gratitude to Prof. Dr. Cor Langereis who thought me paleomagnetic measurement and interpretation techniques. I also would like to him his hospitability, openness, being always ready to help and providing an excellent working environment while I was in Utrecht.

I would like to express my appreciation to my co-supervisor Dr. A. Arda Özacar for his time, support, and his valuable advices.

My Ph.D. committee members, Dr. Erdin Bozkurt, Dr. F. Hasan Sözbilir, Dr. Kadir Dirik and Dr. Erman Özsayın are deeply appreciated for their critical reading and suggestions for improving and increasing the quality of this thesis.

I am indebted to Forth Hoofddijk Paleomagnetic Laboratory team members; especially Mark Dekkers whom patiently thought me how to use paleomagnetic equipment and always provided a pleasant environment and time shifts for the measurements.

I would like to thank to my dear friends Dr. Erhan Gülyüz, Mrs. Nilay Gülyüz, and Abdul Qayyum for company and help during fieldworks. My hard and long field studies could not have been completed without their assistance.

A special thanks to my new sisters Mrs. Pınar Ertepınar Kaymakcı and Öykü Ertepınar for their endless support and Öykü's delicious cooking. Thank you dear.

In Utrecht, thanks to Ahmet Peynircioğlu and Derya Güerer from Utrecht University, the Netherlands, for collaboration and their warm hospitality.

At last but definitely not the least, I am grateful to Mrs. Tuğçe Özvural for her endless help, patience and motivation during my study. Without her company and the bright and practical solutions she provides, this study could not have been completed.

Finally, I would like to express my gratitude to my parents. Without the support of my family, this study would not have been accomplished.

TABLE OF CONTENTS

LIST OF TABLES

TABLES

LIST OF FIGURES

FIGURES

CHAPTER 1

INTRODUCTION

1.1 General

Discovery of the lodestone or loadstone (magnetite) which name was derived from middle English word load, meaning “way” or “course” loadstone was literally a “course stone” that help to travelers and navigators to find their way in ancient times (Lowrie, 2007).

Earth magnetic field, since it’s first realized by Chinese navigators, still one of the most magnificent features of the Earth and has been used not only navigation purpose but it is also helps to illuminate solving some significant geological problems which are the first and foremost clear geophysical evidence into the plate tectonics.

Regarding the paleomagnetism, intensity and orientation of earth’s past magnetic field is recorded by the help of certain magnetic minerals contained within the sedimentary, igneous and metamorphic rocks that provide information about the characteristics and orientation of the magnetic vector of the earth and how it changed in time. Using this phenomenon the position and rotation amounts of tectonic blocks in different time intervals throughout geological past can be reconstructed (Butler 1998; Tauxe 2010). In general, the paleomagnetism has both geochronological and tectonic applications. The age of a rock can be determined with high precision by correlating it with the established geomagnetic pattern of the earth through time and by obtaining the magnetic declination of a rock and comparing it with respect to present magnetic vector (declination, inclination) provides information about how tectonically the rocks might have been deformed (Susman and Weil 2004) and by the use of paleoinclination values the paleo-latitudunal positions of tectonic blocks can be determined (Tauxe 2010).

Paleomagnetic applications in Turkey dates back to 1960's and after the pioneering work of Vander Voo (1968) which aimed at determination of paleolattitudinal position of Pontide belt during the Mesozoic, a number of paleomagnetic studies have been conducted especially in 1990's most of which are related to fault block rotations related to North Anatolian fault Zone (e.g. Platzman *et al.* 1994; Tatar *et al.*, 1995, 1996; Gürsoy *et al.*, 1997). During this time interval a number of magnetostratigraphical studies have also been conducted (e.g. Gallet *et al.*, 1992, 1993, 1994, 2000; Krijgsman *et al.* 1996). In 2000's the number of paleomagnetic studies have increased significantly and are varied. In this time interval, a number of studies related to tectonic block rotations related to paleotectonic period have also been conducted (e.g. Kaymakcı *et al.* 2003; İşseven *et al.* 2006; Meijers *et al.* 2010; van Hinsbergen 2010a, b; Çinku *et al.* 2011, 2013; Uzel *et al.* 2015; Koç 2016).

The main concern of this thesis is determination of vertical axis block rotations in north central Anatolia along the Izmir-Ankara and Intra-Tauride suture zones which demarcates the former position of the Neotethys Ocean that subducted and obliterated completely by the end of Cretaceous to early Paleogene (Okay *et al.* 1984; Okay and Tüysüz 1999; Kaymakcı *et al.* 2000 & 2009; Pourteau *et al.* 2015).Therefore, the study is concentrated mainly around the Haymana and adjacent basins that include northern continuation of Haymana Basin into the Alcı-Orhaniye sub-basin (Koçyiğit *et al.*, 1988; Koçyiğit 1989; Rojay and Süzen 1997), southwestern continuation of Çankırı Basin around Kırıkkale-Bala region (Kaymakcı *et al.* 2009), and exposed Paleogene sector of the Tuz Gölü Basin (Çemen *et al.* 1999).

1.2. Purpose and scope

The main objective of this study is to determine the amount and timing of vertical axes rotations in Haymana and adjacent basins in order to unravel the evolution of the Izmir-Ankara and Intra-Tauride suture zones in relation to the terminal subduction of the Neotethyan Oceanic lithosphere and subsequent collision of the intervening continental blocks that include Taurides and the Kırşehir Block (sensu Görür *et al.* 1984) into the Pontides. The Izmir-Ankara Suture Zone demarcates the former position of the Neotehys Ocean between Pontides in the north and Taurides

and Kırşehir Block in the south while Intra-Tauride Suture Zone separates Taurides from the Kırşehir Block (Görür *et al.*, 1984; Kaymakcı *et al.*, 2009; Pourteau *et al.* 2015, van Hinsbergen *et al.* 2016).

In order to accomplish this purpose, a very detailed and extensive field study and comprehensive sampling strategy have been performed in the study for the time interval extending from the Late Cretaceous to Pliocene. Sampling is performed mainly on the fine grained clastic sedimentary rocks and clayey limestone units as well. During sampling a pseudo magnetostratigraphical sampling strategy was followed so that sampling was performed at different levels of each lithostratigraphical units, in each site, for certain time intervals. The purpose of such sampling strategy was to determine the exact timing of the inception and cessation of rotational deformation (Figure 1.1) in the region. In addition to this, a detailed rock magnetic property analysis has also been performed on each sample, in order to determine variations in the intrinsic versus tectonically induced changes in the magnetic properties of the samples. The obtained results are analyzed and the ones related to tectonic processes are scrutinized accordingly.

Determination of tectonic block rotations and related finite strain tensors by the help of magneto-fabric analysis are very important in terms of understanding the styles and modes of deformation, which in turn provide crucial information about geodynamical evolution in an area.

In summary, the main purpose of this research is to determine vertical-axis block rotations in Haymana and adjacent central Anatolian basins for late Cretaceous to Pliocene period in order to understand the tectonic relationship between Izmir-Ankara-Erzincan and the Intra-Tauride suture zones and their temporal and spatial evolution since the Late Cretaceous. The obtained results are evaluated in relation to the terminal subduction of the Neotehys and collision of intervening continental blocks during the Late Cretaceous to Late Paleogene and to the transcurrent tectonics that has been dominated in much areas of Turkey during the late Neogene and Quaternary.

1.3. Tectonic Setting of the Study area

The study area is located in a zone where İzmir-Ankara and Intra-Tauride suture zones meet in north central Anatolia (Turkey). İzmir-Ankara Suture represents the western sector of the Izmir-Ankara-Erzincan Suture Zone and is the suture between Taurides in the south and Pontides in the north, while the eastern sector demarcates the suture between Pontides in the north and the Kırşehir Block in the east. On the other hand, the Intra-Tauride suture developed between Taurides in the south and southwest and the Kırşehir Block in the east and northeast (Figure 1.1). All of these suture zones demarcate the former position of Neotethys Ocean in Turkey which completely subducted and obliterated at the end of Cretaceous to earliest Paleogene (Kaymakcı *et al.*, 2009; Pourteau *et al.*, 2010, 2013; van Hinsbergen *et al.*, 2016).

The geometry, position and tectonic relationships of different parts of the İzmir-Ankara-Erzincan suture is relatively well known (e.g. Görür *et al.*, 1984; Okay and Tüysüz 1999; Kaymakcı *et al.*, 2009). However, its relationship with the Intra-Tauride suture is relatively unknown and the number of studies that addresses this problem is relatively limited, except for Görür *et al.* (1984) which proposed the existence of Intra-Tauride Suture, Okay and Tüysüz (1999), Pourteau *et al.* (2010 and 2013), van Hinsbergen *et al.* (2016). Understanding of the geometry and tectonic relationship between these suture zones constitutes one of the main objectives of this study.

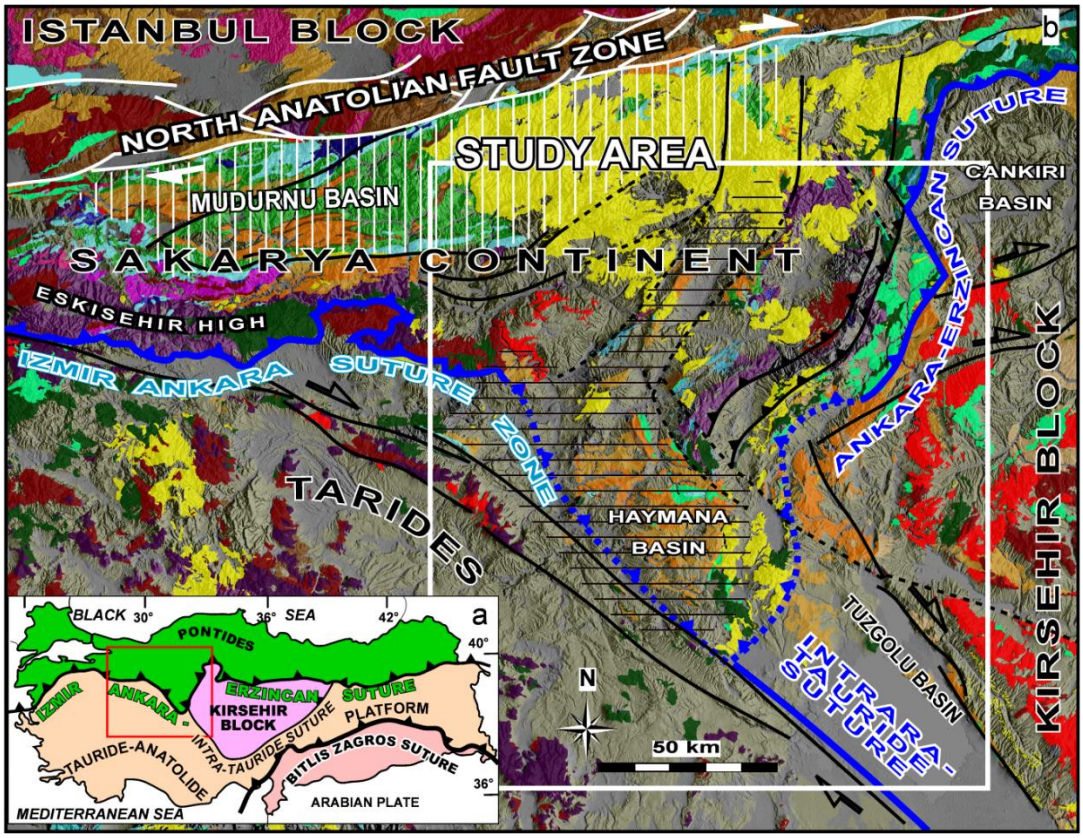

Figure 1.1. Tectonic setting of the study area. **a)** simplified pre-Neogene tectonic configuration of Turkey, **b)** simplified geological map of north central Anatolia overlaid on shaded topographic relief (adopted from revised 1/500.000 Geological Map of Turkey released in 2003 by Turkish General Directorate of Mineral Research and Exploration).

1.4. Method of study and Data

In order to unravel the tectonic evolution of the study area, it is important that to document deformation history of the basins which record the tectonic events during the deposition of basin infills. This research relies mostly on paleomagnetic analysis of the infill of the central Anatolian Basins (Figure 1.2) and targeted the restoration of the central Anatolian Basins and as well their continental basements during the Upper Cretaceous to Recent development.

For this purpose more than 7000 oriented samples from 119 sites have been collected. The samples were dominantly collected from sedimentary sequences spanning from Upper Cretaceous to Pliocene. Among these collected samples 4500

of them are measured and analyzed in Fort Hoofddijk Paleomagnetic laboratory in Utrecht University, the Netherlands. The remaining samples are stored for further analyses. The analyses of the samples are performed on the basis of the tectonic domain they are collected.

For this purpose, the study area is divided into four basins based on their characteristics and position with respect to the involved tectonic blocks. These basins (Figure 1.1 and 1.2) include **1)** Kırıkkale-Bala Basin: It is located at the interaction zone of Çankırı and Tuz Gölü basins. Kaymakcı *et al.* (2009) argued that it is the SW continuation of Çankırı Basin. Since its basement is constituted by Kırşehir Block and thrusted over from the north by the Pontide related units. It also comprises mainly similar lithologies with the Çankırı Basin and related to the development of the Ankara-Erzincan Suture Zone. **2)** Tuz Gölü Basin: It straddles the Kırşehir Block in the east and Taurides in the west therefore it is related to the development of the Intra-Tauride Suture zone. **3)** Haymana Basin: it straddles the İzmir-Ankara Suture Zone where Pontides thrusted over the Taurides from north to south. The basement of Haymana Basin is constituted mainly by Late Cretaceous ophiolitic mélange and its southern boundary with the Taurides is obscured by Neogene cover. **4)** Alcı-Orhaniye Basin is developed mainly on the Pontides and connects the Haymana Basin to the Mudurnu-Alcı Basin (Figure 1.2).

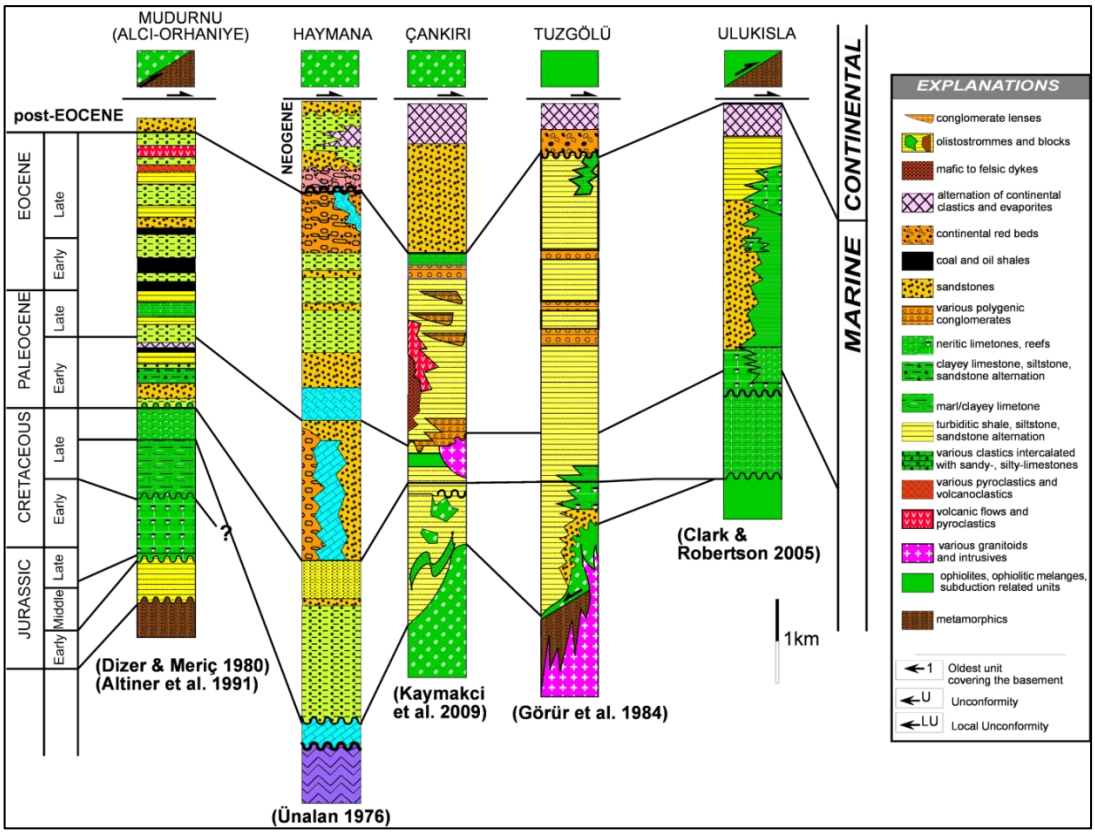

Figure 1.2. Correlation of stratigraphy of central Anatolian basins.

1.5 Stratigraphy of Study Area

The stratigraphy of the study are is represented by the Haymana basin which has the most complete and the thickest exposed stratigraphy among the sampled basins. The basin stratigraphy is established mainly by Ünalan (1976) and almost all other younger studies followed the stratigraphical scheme of him. The Haymana Basin developed mainly on the Late Cretaceous ophiolitic mélange related to subduction of the Neotethys Ocean if not on the Sakarya Continent. The basement of the basin is constituted by lithologies belonging to basement of the Sakarya Continent represented by pre-Triassic metamorphic rocks, Triassic slightly metamorphosed blocky mélange of Karakaya Complex and Mesozoic mainly carbonate dominated cover rocks that unconformably overlie the basement of the Sakarya Complex (Figure 1.3) (Koçyiğit *et al.*, 1988; Koçyiğit 1989).

According to Ünalan (1976) the infill of the Haymana basin comprises five stratigraphical cycles. The oldest cycle in the basins comprises Haymana and

Beyobası formations. Haymana Formation comprises mainly alternation of turbiditic sandstone, siltstone, shale and marl. The base of the formation can be observed around Haymana and in the southern part of the basin.

At the base it is characterized by boulder to block sized conglomerates which very rapidly fines and thins upwards. The thickness of these very coarse clastics reaches up to 10 m around Hayman and may reach to 30 m in the southern part of the basin. The boundary between Haymana and Beyobası formation is gradational and Beyobası Formation is characterized relatively thinner and distal turbiditic facies dominated by sandstone, sandy marl and organic rich layers with occasional thin coal seams (Figure 1.3).

The second cycle in the basin infill comprises laterally and vertically grading Kartal, Çaldağ and Yeşilyurt formations. Kartal Formation composed mainly of continental red beds while Çaldağ Formation comprises mainly of neritic carbonates dominated by reefal limestones and Yeşilyurt Formation comprises mainly distal fine clastics dominated by marls. These units conformably overlies the Late Cretaceous units and are of Paleocene in age (Ünalan 1976).

The third cycle in the basin fill comprises relatively carbonate dominated proximal Kırkkavak Formation which laterally and vertically grades into Ilgınlıkdere Formation of medial to distal turbidites dominated by sandstone, siltstone and shale. It grades vertically into Eskipolatlı Formation which is composed of medial to distal turbidites intercalated with nummulites bearing marls and limestones. The age of the third cycle rocks span from Late Palaeocene to Middle Eocene according to fossil fauna they contain (Ünalan *et al.* 1976, Prof.Dr. Ercan Özcan of Istanbul Technical University, personal communication 2014).

The fourth cycle comprises Beldede, Çayraz and Yamak formations. Although the boundary between third and fourth cycles is gradational in most parts of the Haymana Basin, However, around 5 km north of Haymana a local angular unconformities separates Çayraz Formation from the underlying second cycle units. Beldede Formation comprises mainly continental red clastics while Çayraz Formation is characterized by nummulitic limestones and Yamak Formation

comprises alternation of conglomerates, sandstones, shale and marl of turbiditic origin.

The fifth cycle comprises Neogene cover rocks. These units are generally characterized by fluvio-lacustrine associations. They are not bound to Haymana or any other basins in the study area and belong to tectonic regimes that postdate Late Cretaceous to Early Miocene subduction and subsequent collisional convergence (Kaymakci *et al.* 2009, Gülyüz 2015).

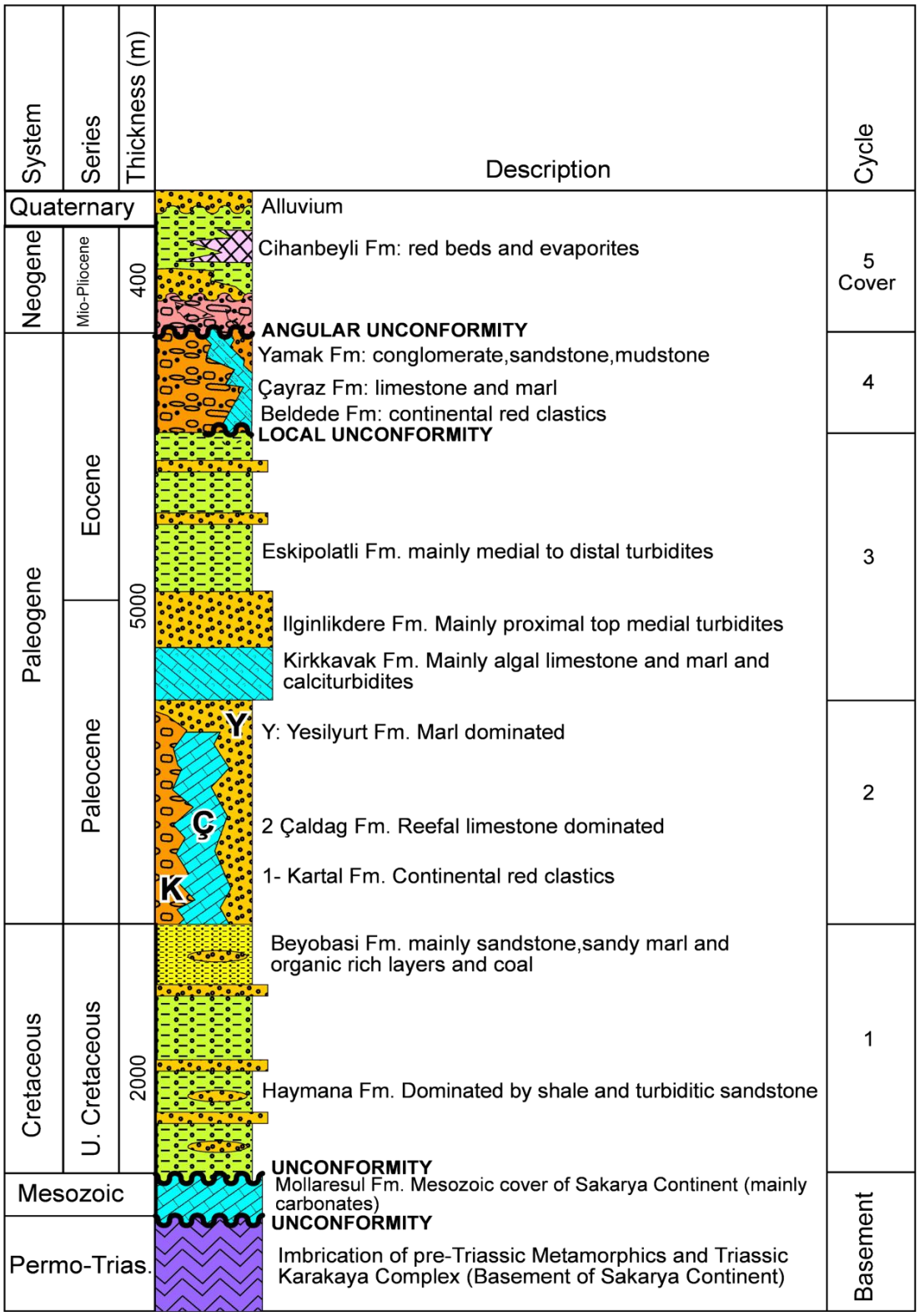

Figure 1.3. Generalized stratigraphic section of Haymana Basin which is used as representative section for whole study area (modified from Ünalan 1976).

CHAPTER 2

ANISOTROPIC MAGNETIC SUSCEPTIBILITY: DETERMINATION OF PRINCIPAL STRAIN DIRECTIONS IN THE CENTRAL ANATOLIA

2.1. Introduction

The Anisotropy of Magnetic Susceptibility (AMS) is often determined by directional variances of induced magnetization strength properties of a rock sample when measuring in different directions within the certain amount of applied magnetic field (Owens and Bamford, 1976; Hrouda, 1982; Borradaile, 1988). It delineates preferred orientation of the magnetic properties (susceptibility) of minerals within a rock unit. In spite of the fact that the initial systematic background was introduced by Voight and Kinoshita (1907), the first applications of AMS as a petro-fabric marker was investigated by Ising (1942), who realized that magnetic susceptibility increase as the measurement orientation become perpendicular to the bedding plane which has the minimum Eigen values (Schmidt 2007). Graham (1966) proposed that the AMS is related to the finite strain and could be used as a strain marker in the deformed rocks. In the following years, increasing number of AMS studies, carried out on various rock types to unconsolidated lose sediments, progressively populated the literature. Some of the most notable of these studies include Fuller (1964), Hrouda & Janâk (1976), Kneen (1976), Kligfield *et al.* (1977), Hrouda (1982), Tarling and Hrouda (1993), and Duermeijer *et al.* (1998). Following these studies AMS became a standard tool for determination of strain ellipsoid in the rocks.

The AMS technique can be used in nearly all types of rocks, even in the case of absence of lineation and foliation and provides non-destructive, fast, accurate and inexpensive way to determine the petro-fabric characteristics of minerals and their preferred orientations within a rock. The principal directions of anisotropy in the rocks are generally related to orientation of folds, faults, foliations and lineations of the rock units (Hrouda and Janak 1976, Borradaile 1988; Averbuch *et al.* 1992, Robion *et al.*

2007; Borradaile and Jackson 2010). Although the technique has great advantages, however, it has inherited complications since the AMS results are the combination of factor(s) that include mineral physical properties, crystal structure, mixture of mineral compositions, tectonic and metamorphic processes such as current directions from sediments, flow-directions from magma, finite-strain directions from tectonized rocks and stress-orientations from low-strain, low-temperature, environments, etc. (Borradaile and Henry 1997; Borradaile and Jackson 2004). In order to obtain an accurate correct understanding of the AMS results, all of these variables needed to be taken into consideration.

The anisotropy of magnetic susceptibility (AMS) technique as a paleomagnetic tool has been increasingly applied on wide range of application in geology since last decades. The weakly deformed sedimentary rocks under a contractional regime orient its minimum susceptibility axis (k_{min}) perpendicular to the bedding plane or maximum susceptibility axis (k_{max}) perpendicular to the direction of main shortening axis, parallel to fold axis, thrust faults, and local bedding strike (Lee *et al.*, 1990; Tarling and Hrouda 1993). However under the extensional regime, the maximum susceptibility axis aligns perpendicular to normal faults and parallel to bedding dip direction. Increasing the intensity of extensional deformation converts the susceptibility ellipsoid to have more prolate geometry (Lee *et al.*, 1990; Tarling and Hrouda, 1993) than oblate and finally become triaxial in shape.

In this regard, the AMS technique is successfully applied to the infill of the Haymana and adjacent basins within the study area. The analyses have shown that the technique has merits and produced compatible results with the large scale structures in the study area.

2.2. Sampling

In three years of field work, we carried out a very comprehensive paleomagnetic sampling in the central Anatolia (Turkey). More than 3000 cylindrical cores with 1” (2.54 cm) diameter and more than 2” (>5 cm) length (oriented cores) have been collected from 110 sites. The samples were collected from rock units ranging in age from late Cretaceous to Pliocene. Most of the samples were collected largely from

sedimentary rocks, although volcanic rock samples were also collected in places (Figure 2.1 and 2.2; Table 2.1).

In general, dominantly clayey, thinly bedded fine grained lithologies were sampled. For each site, at least 15 oriented cores were collected that is distributed within approximately 15-20 meters in stratigraphic thickness, in order to avoid possible paleo-secular variation effect.

The samples were collected using a portative gasoline powered motor drill and an electrical drill with generator, based on the ease of drillability of the rock units. Since the length of a single core was longer than 2", they often provided multiple specimens on which various measurement techniques were applied on the same sample. Consequently, the amount of measured specimens are higher than the number of sampled cores. Core orientations (drilling position) and bedding attitude were measured by using a magnetic compass. The present day declination value for the study area is 4.5° (to the east) (http://www.ngdc.noaa.gov/geomag-web/#declination, National Oceanic and Atmospheric Administration, last visited on January 2016) during the time of sampling and each sample was corrected according to this value.

2.3. Measurement and Analysis

The laboratory analyses were conducted at the Forth Hoofddijk paleomagnetic laboratory at the Utrecht University (Utrecht, the Netherlands). All the samples were cut in to the standard paleomagnetic measurement size (2.54 cm diameter and 1.3 cm height). The specimens were measured an automatic field variations (low field, 200 A/m) using the Multi-Function Kappabridge MFK1-FA (AGICO-Brno, Czech Republic) equipped with an up-down mechanism and a rotator. The sensitivity is 10^{-8} SI which is critical to measurement in weak magnetic carries of the carbonate rocks. The measurement was operated by rotation of the specimen in three perpendicular plane positions while the magnetic moment in the applied field monitored following the spinning specimen method. This gives an opportunity for computing the principal susceptibility axes of an AMS ellipsoid following the procedure introduced by Jelinek (1997).

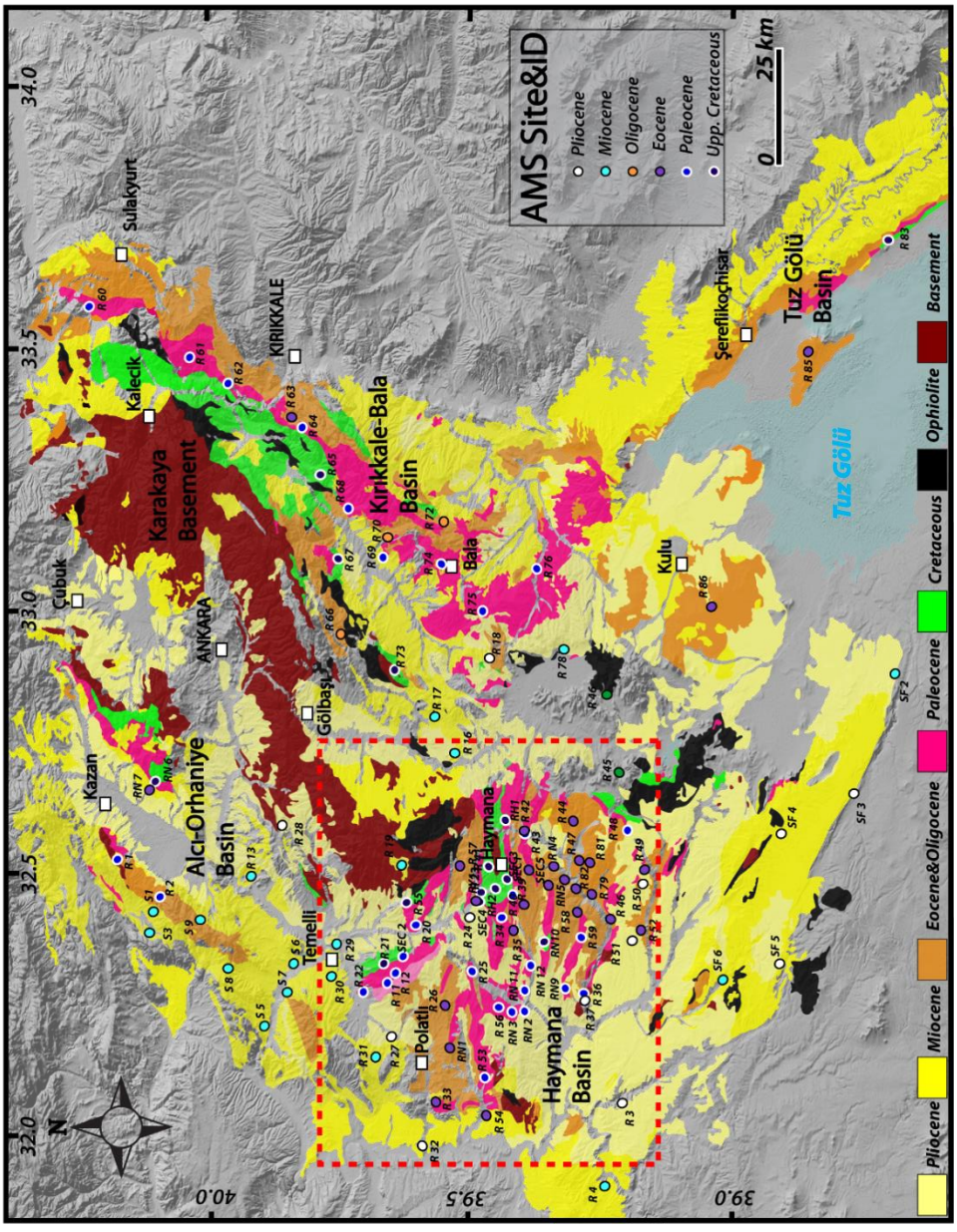

Figure 2.1. Simplified geological and sample locations draped onto shaded relief image.

Table 2.1. Summary of the anisotropy of magnetic susceptibility parameters from 106 Upper Cretaceous to Pliocene sites in the study area.

Site	*Geog. Coord. (deg)*		N_{AMS}	*Bedding*	k_m*(SI)*	*L*	*F*	*Pj*	*T*	*D/I* (k_{max})	*D/I* (k_{min})	e_1	e_2	e_3
	Lat. (N)	*Long. (E)*		*Azi / dip*										
Pliocene														
R 3	39.21949	32.06600	05	+	4.98E-05	1.001	1.003	1.004	0.316	196.6/05.2	055.7/83.3	17.2	18.6	13.2
R 24	39.49088	32.42698	17	278 / 15	8.77E-04	1.000	1.000	1.001	-0.184	205.3/14.5	100.1/45.5	43.6	65.2	65.0
R 27	39.63345	32.19992	12	195 / 18	5.67E-03	1.003	1.024	1.030	0.756	184.2/09.1	324.8/78.2	25.9	25.9	06.4
R 28	39.85070	32.60247	16	277 / 22	5.12E-05	1.002	1.005	1.007	0.504	124.7/36.6	249.8/37.7	68.2	69.6	63.4
R 37	39.26698	32.26085	07	046 / 14	1.86E-05	1.028	1.011	1.040	-0.447	344.3/07.6	076.4/15.8	25.4	60.8	60.3
R 50	39.15034	32.50766	10	+	1.27E-03	1.003	1.014	1.018	0.634	018.8/00.3	282.1/87.3	25.8	25.7	08.4
R 51	39.17460	32.39708	10	+	1.10E-03	1.017	1.055	1.076	0.521	018.9/08.9	180.6/80.7	14.9	14.7	04.8
SF3	38.79057	32.57749	20	+	2.85E-06	1.120	1.085	1.216	-0.163	288.8/09.4	023.8/27.6	59.8	61.6	67.2
SF4	38.89749	32.60258	16	+	2.26E-03	1.011	1.015	1.027	0.173	187.9/69.8	290.3/04.5	16.6	16.7	14.5
Miocene														
R 4	39.22803	31.90884	38	143 / 14	7.84E-05	1.003	1.003	1.006	-0.046	016.9/09.8	235.7/77.6	33.8	38.0	33.6
R 13	39.90372	32.50336	06	+	4.26E-02	1.003	1.022	1.028	0.737	334.2/16.9	137.4/72.4	39.5	38.9	18.0
R 16	39.50370	32.74693	17	282 / 13	4.32E-05	1.002	1.001	1.003	-0.053	227.7/47.8	084.0/36.2	57.0	64.1	64.3
R 17	39.55369	32.82139	17	068 / 24	2.55E-04	1.003	1.011	1.014	0.599	002.7/09.6	156.4/79.4	47.9	47.9	12.3
R 18	39.44065	32.93658	18	250 / 14	3.32E-04	1.002	1.002	1.005	0.048	238.3/65.6	110.0/15.7	58.8	65.4	59.0
R 19	39.61479	32.52476	10	+	9.40E-05	1.000	1.001	1.001	0.391	153.6/06.5	323.6/83.4	79.1	79.4	63.2
R 29	39.73686	32.37431	05	+	2.15E-05	1.003	1.004	1.007	0.035	124.7/27.1	019.3/27.5	18.3	29.2	28.6
R 30	39.75496	32.32426	06	165 / 34	2.45E-05	1.016	1.011	1.027	-0.174	168.4/07.3	258.5/01.0	40.0	46.4	42.4
R 31	39.66499	32.16552	16	+	9.62E-04	1.002	1.000	1.002	-0.605	082.9/86.6	237.5/03.1	54.2	75.2	74.4
R 32	39.57138	31.99519	10	+	8.67E-05	1.001	1.000	1.001	-0.635	261.2/11.1	170.3/04.6	47.9	76.5	76.5

R 45	39.20876	32.70327	19	+	1.97E-03	1.004	1.009	1.014	0.366	076.0/20.1	252.9/69.8	47.6	48.0	34.2
R 46	39.21776	32.85851	09	+	1.15E-02	1.002	1.011	1.014	0.641	201.5/15.2	071.4/67.1	29.7	30.0	09.8
R 78	39.31113	32.93993	18	281 / 07	3.87E-05	1.015	1.083	1.107	0.683	244.7/09.5	083.9/79.9	37.0	37.1	11.9
RN7	40.10062	32.67606	21	218 / 32	4.16E-06	1.006	1.053	1.065	0.786	342.9/07.4	197.3/81.1	88.1	88.1	69.0
S 1	40.09339	32.43849	08	211 / 18	1.21E-04	1.001	1.001	1.002	-0.301	303.5/57.8	044.9/07.1	52.6	53.1	45.8
S 3	40.10604	32.40219	12	087 / 23	1.61E-04	1.004	1.005	1.009	0.060	038.0/03.9	307.5/06.9	19.2	18.4	19.5
S 5	39.87782	32.22427	21	091 / 24	1.67E-04	1.005	1.005	1.010	0.008	338.7/13.4	211.7/68.5	16.5	17.1	16.7
S 6	39.81832	32.33579	14	160 / 45	9.17E-05	1.001	1.002	1.003	0.280	020.7/70.1	245.3/14.5	59.9	59.6	55.6
SF2	38.63961	32.85627	20	+	2.06E-04	1.001	1.002	1.003	0.330	017.4/57.2	140.9/19.6	64.1	63.8	51.7
SF5	38.89064	32.33443	09	+	7.41E-04	1.004	1.003	1.007	-0.131	168.2/42.1	056.2/22.8	40.4	41.0	34.1
SF6	38.98257	32.33974	16	+	2.86E-03	1.002	1.007	1.009	0.565	319.1/12.2	089.7/71.6	34.4	34.4	17.7
Eocene&Oligocene														
R 23	39.47332	32.46083	13	228 / 35	1.95E-03	1.008	1.016	1.025	0.303	241.1/20.7	123.0/51.2	24.5	28.9	24.6
R 26	39.53736	32.24681	22	071 / 49	1.67E-03	1.016	1.020	1.037	0.131	282.6/29.5	118.4/59.5	19.8	33.5	31.2
R 33	39.55413	32.07114	09	305 / 44	5.27E-04	1.018	1.022	1.040	0.100	276.3/20.4	075.0/68.2	38.6	41.6	25.2
R 35	39.39997	32.40371	18	232 / 18	3.62E-03	1.010	1.025	1.036	0.442	304.0/29.1	116.2/60.7	12.5	13.5	10.4
R 40	39.38760	32.44978	20	153 / 37	7.40E-04	1.033	1.052	1.088	0.217	237.9/02.4	141.0/71.0	07.9	14.3	15.3
R 42	39.39413	32.59785	15	110 / 78	4.53E-04	1.005	1.015	1.021	0.535	025.5/10.5	172.7/77.6	16.9	18.1	14.8
R 44	39.29012	32.61395	20	276 / 74	5.72E-04	1.019	1.078	1.104	0.607	111.9/16.4	264.0/71.6	14.5	14.4	09.2
R 47	39.28483	32.54474	08	044 / 22	2.43E-04	1.010	1.008	1.019	-0.125	270.3/17.8	102.7/71.8	06.5	06.9	04.8
R 49	39.14827	32.51619	07	314 / 68	2.48E-04	1.001	1.011	1.014	0.892	357.9/16.3	131.4/67.0	61.4	61.3	10.5
R 52	39.15480	32.40322	13	114 / 71	1.15E-03	1.014	1.005	1.019	-0.446	096.6/10.3	005.4/06.8	12.4	27.9	27.2
R 54	39.46095	32.05102	08	175 / 09	2.22E-04	1.006	1.004	1.011	-0.245	307.8/12.0	194.9/61.4	68.0	77.9	77.7
R 57	39.51085	32.52564	06	115 / 54	3.80E-03	1.017	1.019	1.037	0.063	115.0/04.7	342.5/83.1	09.3	13.0	12.8

R 58	39.28255	32.45181	11	335 / 13	2.99E-04	1.006	1.023	1.030	0.602	091.7/05.4	191.3/60.8	15.6	15.7	07.0
R 63	39.82211	33.39003	09	053 / 74	-1.14E-07	-0.608	0.360	0.000	0.000	264.3/70.7	035.7/13.0	53.5	53.9	31.0
R 66	39.73907	32.98141	10	179 / 27	2.99E-03	1.021	1.020	1.041	-0.009	122.6/11.1	353.5/72.6	07.8	08.2	05.2
R 70	39.64818	33.15610	18	196 / 41	2.65E-03	1.023	1.061	1.088	0.453	233.5/01.4	328.1/72.8	06.6	06.6	04.6
R 72	39.54100	33.19489	07	047 / 46	6.31E-05	1.005	1.013	1.018	0.449	113.4/01.6	207.8/69.6	26.3	26.3	10.3
R 79	39.24738	32.47380	12	086 / 39	2.03E-04	1.005	1.016	1.022	0.502	079.1/04.9	193.2/78.2	13.5	12.7	08.7
R 80	39.21889	32.42476	05	141 / 40	4.71E-04	1.021	1.058	1.083	0.467	237.1/05.1	352.1/78.1	06.9	11.5	12.7
R 81	39.26321	32.49518	14	334 / 19	2.61E-04	1.005	1.031	1.039	0.699	264.7/12.2	079.7/77.8	03.5	11.6	04.6
R 82	39.27460	32.47375	14	312 / 18	8.72E-04	1.006	1.036	1.046	0.692	068.7/06.7	175.7/68.1	15.6	15.7	08.3
R 85	38.84238	33.51440	17	110 / 13	1.22E-04	1.001	1.008	1.010	0.694	344.2/00.6	251.8/76.3	62.1	62.1	18.0
R 86	39.02141	33.02820	05	115 / 30	2.01E-04	1.002	1.011	1.014	0.688	359.6/14.7	198.0/74.5	43.9	43.7	09.0
RN1	39.52899	32.17783	14	282 / 23	5.86E-04	1.006	1.047	1.059	0.762	275.0/16.9	063.5/70.4	19.0	19.1	04.8
RN4	39.32555	32.51482	19	333 / 49	8.92E-04	1.003	1.005	1.008	0.284	207.7/26.3	342.4/55.0	33.5	42.8	42.0
RN5	39.28051	32.48407	17	332 / 23	1.59E-03	1.004	1.020	1.025	0.663	240.1/01.7	145.8/68.0	24.6	24.6	06.6
SEC1	39.37553	32.52444	225	240 / 71	1.78E-03	1.011	1.038	1.052	0.554	272.7/06.4	164.2/70.4	30.2	30.5	14.5
SEC5	39.33560	32.49780	396	060 / 37	1.26E-03	1.013	1.024	1.038	0.279	286.7/08.0	059.2/78.3	27.8	32.2	28.5
S 7	39.84019	32.28449	22	328 / 32	6.98E-05	1.002	1.008	1.011	0.646	187.3/01.6	047.7/87.9	74.8	74.8	27.8
S 8	39.94585	32.33197	18	185 / 31	2.42E-04	1.018	1.019	1.037	0.043	231.2/58.4	102.4/21.1	22.3	23.1	20.7
S 9	39.99441	32.41776	09	032 / 43	9.33E-05	1.001	1.001	1.002	0.134	039.2/14.2	157.0/61.6	36.9	56.1	54.2
Paleocene														
R 01	40.16496	32.53870	57	358 / 13	1.54E-04	1.001	1.005	1.007	0.739	147.4/04.0	005.1/85.0	58.9	58.8	16.4
R 02	40.09047	32.46817	16	064 / 19	2.49E-05	1.006	1.012	1.019	0.291	164.5/13.1	071.6/12.5	60.9	60.7	41.9
R 11	39.63310	32.29312	13	155 / 34	1.18E-03	1.003	1.003	1.006	0.103	312.5/10.2	054.4/48.9	38.8	42.5	42.6
R 12	39.62637	32.30051	15	145 / 20	1.84E-03	1.008	1.019	1.028	0.424	163.4/03.2	062.9/72.9	36.4	36.2	13.4
R 20	39.58484	32.41188	16	318 / 36	-9.25E-06	1.004	1.001	1.005	-0.657	231.4/32.5	128.9/18.7	84.5	84.5	66.0

R 22	39.66605	32.28952	15	161 / 29	1.32E-03	1.002	1.047	1.055	0.907	116.0/30.4	267.6/56.3	22.9	22.1	10.9
R 25	39.48710	32.31312	13	268 / 56	3.96E-04	1.008	1.019	1.028	0.378	084.6/12.7	331.7/59.9	14.6	14.3	09.0
R 34	39.42330	32.42497	06	072 / 22	-6.25E-06	1.009	1.012	1.021	0.161	187.8/63.2	307.0/13.8	70.1	64.7	73.4
R 36	39.26847	32.27213	17	052 / 43	1.26E-04	1.004	1.004	1.008	-0.055	225.8/74.4	006.6/12.2	24.2	21.2	22.4
R 39	39.40370	32.47808	10	096 / 72	2.59E-05	1.003	1.007	1.010	0.388	132.7/50.6	028.3/11.5	61.3	61.6	42.9
R 43	39.38718	32.59634	09	104 / 34	3.41E-04	1.011	1.005	1.016	-0.355	206.1/22.3	113.9/05.3	17.0	23.9	23.9
R 48	39.18192	32.59336	14	168 / 26	1.26E-04	1.001	1.007	1.009	0.712	304.7/01.5	036.4/47.2	30.9	30.3	13.9
R 53	39.45942	32.11865	20	305 / 33	5.47E-04	1.021	1.054	1.079	0.432	293.0/04.4	057.5/82.3	08.7	08.9	07.1
R 56	39.43051	32.24960	12	085 / 59	1.47E-04	1.004	1.013	1.018	0.523	231.9/11.1	030.3/78.1	22.3	22.3	08.8
R 59	39.27679	32.39393	21	272 / 59	1.54E-04	1.009	1.006	1.015	-0.250	067.3/10.5	169.3/48.3	06.6	11.8	11.5
R 60	40.19579	33.60275	13	199 / 26	2.32E-04	1.009	1.003	1.012	-0.550	354.4/08.2	159.0/81.5	12.7	27.0	27.1
R 61	40.03112	33.51727	06	347 / 69	4.15E-03	1.016	1.026	1.043	0.238	317.3/05.0	185.7/82.5	11.6	10.2	07.5
R 62	39.95102	33.45625	15	007 / 75	7.82E-03	1.029	1.045	1.076	0.214	137.6/02.6	262.8/85.5	10.8	10.5	05.6
R 64	39.81216	33.37347	11	172 / 59	1.91E-04	1.002	1.006	1.008	0.522	340.7/18.3	176.1/71.1	19.0	20.6	13.4
R 68	39.71815	33.21623	07	071 / 88	2.01E-04	1.001	1.009	1.011	0.777	282.2/01.0	188.9/72.1	44.0	44.0	06.7
R 69	39.65083	33.13674	15	026 / 32	1.95E-04	1.001	1.007	1.009	0.750	134.6/15.6	294.0/73.4	39.2	39.2	12.1
R 74	39.54773	33.11896	06	186 / 24	3.78E-04	1.007	1.005	1.012	-0.113	084.9/20.5	190.0/34.8	07.8	19.7	20.0
R 75	39.46966	33.01845	14	166 / 45	7.30E-04	1.017	1.043	1.063	0.429	131.6/13.9	349.7/72.5	08.5	08.9	08.1
R 76	39.36283	33.09148	14	284 / 13	2.98E-04	1.000	1.021	1.025	0.973	286.5/10.2	144.5/77.2	72.6	72.6	08.3
RN2	39.38881	32.25795	05	122 / 87	1.28E-04	1.003	1.003	1.007	0.007	113.3/13.4	204.4/04.6	18.8	17.7	11.6
RN3	39.39294	32.26118	17	105 / 62	1.40E-04	1.001	1.013	1.015	0.886	123.0/05.2	309.7/84.7	47.6	47.6	07.0
RN9	39.30177	32.29844	21	105 / 51	1.94E-04	1.006	1.004	1.010	-0.183	292.0/09.5	034.7/54.0	13.1	17.7	19.3
RN10	39.34098	32.37492	16	092 / 20	-9.24E-06	1.004	1.003	1.008	-0.118	006.6/017	144.0/67.0	66.2	72.0	72.0
RN11	39.38253	32.26836	18	092 / 20	7.72E-05	1.006	1.012	1.018	0.360	311.0/044	048.9/07.8	24.7	24.8	18.2
RN12	39.36638	32.32919	18	315 /25	1.98E-04	1.011	1.001	1.013	-0.775	157.9/09.9	050.1/60.4	09.5	67.3	67.3
SEC2	39.59471	32.34523	200	158 / 38	1.51E-03	1.009	1.015	1.025	0.255	349.7/00.9	224.4/88.5	29.1	30.2	26.1

Upper Cretaceous

R 21	39.64864	32.33886	18	145 / 30	1.30E-03	1.009	1.044	1.057	0.652	344.2/02.8	090.6/80.1	24.2	24.4	10.5
R 41	39.45675	32.51812	21	249 / 33	1.30E-03	1.004	1.027	1.033	0.767	279.6/20.2	091.3/69.6	44.7	44.8	16.5
R 55	39.61401	32.45400	11	147 / 18	2.95E-04	1.001	1.026	1.031	0.915	192.6/07.4	046.4/81.1	47.4	47.4	10.3
R 65	39.76183	33.27043	08	032 / 71	3.34E-03	1.005	1.013	1.018	0.455	226.9/02.2	118.2/83.0	57.3	57.3	23.9
R 67	39.75144	33.13353	19	110 / 11	1.68E-04	1.001	1.009	1.011	0.777	262.5/00.5	168.2/83.4	43.6	43.6	10.9
R 73	39.63160	32.91753	13	039 / 87	1.35E-03	1.009	1.010	1.019	0.078	288.9/17.1	091.5/72.1	23.8	33.9	34.9
R 83	38.68441	33.73607	12	320 / 23	1.55E-03	1.004	1.025	1.031	0.712	227.3/15.3	022.0/73.2	27.8	27.3	08.5
RH 1	39.41609	32.61153	31	125 / 48	4.87E-04	1.024	1.028	1.053	0.077	284.7/02.1	017.6/54.6	07.6	07.1	07.7
RH 2	39.43985	32.48446	19	229 / 56	6.14E-04	1.013	1.068	1.088	0.666	266.1/04.3	140.0/82.8	13.6	13.2	07.2
RY 1	39.46935	32.46973	40	244 / 63	1.40E-04	1.012	1.015	1.027	0.107	251.9/10.1	116.5/76.0	12.5	12.6	08.1
RN6	40.09111	32.68306	19	230 / 57	1.98E-03	1.026	1.066	1.097	0.428	168.1/00.6	046.0/88.9	08.9	09.1	05.2
SEC3	39.42022	32.51139	80	131 / 37	9.19E-04	1.021	1.073	1.100	0.541	087.5/09.5	316.1/75.7	12.9	12.6	10.8
SEC4	39.46639	32.45941	27	228 / 49	7.86E-05	1.006	1.017	1.024	0.485	226.8/05.3	119.5/72.6	26.6	26.8	11.5

Lat: Lattitude, **Long**: Longitude, $\mathbf{N_{AMS}}$: number of measured specimens; **km(SI)**=(k_{max}+k_{int}+k_{min})/3 mean susceptibility; **L**=k_{max}/k_{int} (magnetic lineation); **F**=k_{int}/k_{min} (magnetic foliation); **Pj**= $\exp\sqrt{\{2[(n1-n)^2+(n2-n)^2+(n3-n)^2]\}}$, degree of anisotropy (corrected) (Jelinek, 1981); **T**= 2ln (k_{int} / k_{min}) / ln (k_{max} / k_{min}) −1, shape parameter (Jelinek, 1981); **D/I**= declination/inclination of the principal susceptibilities after tilt correction; **kmax/kmin**: maximum/minimum normed principal susceptibility values; **e**: semi-angle of the 95% confidence ellipse around the k_{max} axis in three planes (k_{max}-k_{int}, k_{int}-k_{min}, k_{max}-k_{min}). $n1 = \ln kmax,\ n2 = \ln kint,\ n3 = \ln kmin,\ n = (n1+n2+n3)/3$.

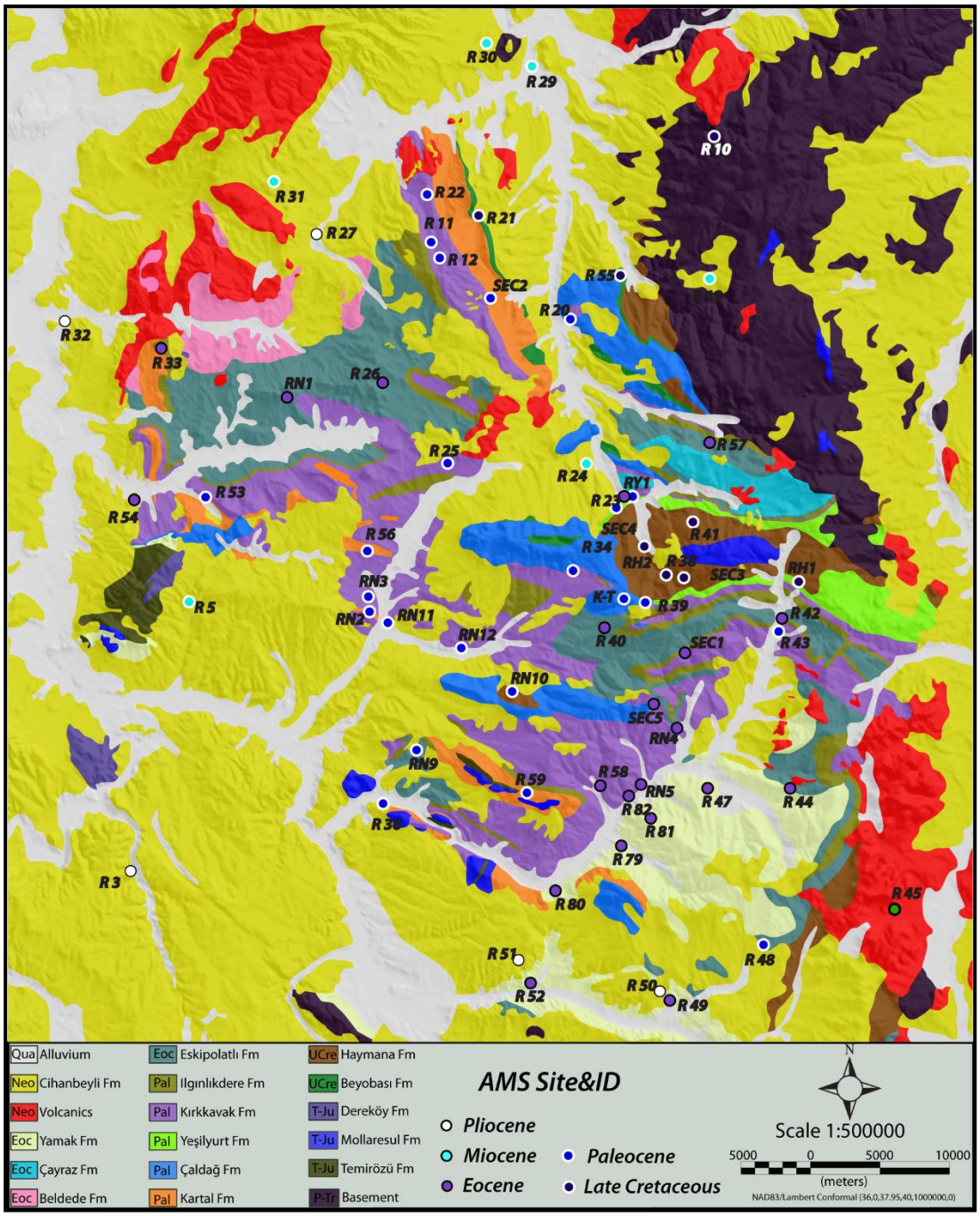

Figure 2.2 Blow-up map of the Haymana Basin area showing the location of sampling sites.

During the measurements, the specimen was rotated subsequently about three perpendicular plane positions for anisotropy and one for the bulk susceptibility as dictated by the spinning specimen measurement method. Between these steps, the bridge was zeroed before inserting the specimen in to the measuring coil. So, differences between the steps were determined more precisely and susceptibility

tensor enhanced from the measurement on the lowest possible, therefore most sensitive range. Herewith, with combining of four values a complete susceptibility tensor was calculated.

Most of the rocks have mix of minerals with ferromagnetic, paramagnetic or diamagnetic properties which ranges from negative values (10^{-5} SI) for diamagnetic, to positive values but low in paramagnetic (10^{-4}-10^{-5} SI) and high in ferromagnetic ($\geq 10^{-4}$ SI) (Nagata, 1961).

Generally, sedimentary sequences show low susceptibility ($<10^{-4}$ SI) and anisotropy (<5%) values. The results for each specimen can be enhanced due to a variety of mineral composition in the rocks.

The AMS susceptibility or deformation ellipsoid is defined by three principal axes; kmax≥ kint≥ kmin namely maximum, intermediate, and minimum susceptibility values per specimen, respectively. The shape of the magnetic susceptibility ellipsoid corresponds to these strain axes. When the kmin smaller than kmax, kint, the shape of the AMS ellipsoid become oblate and kmin clustering perpendicular to the bedding plane, kint&kmax scattering parallel to the bedding plane that is the in common in sedimentary rocks. Increasing the deformation range and other dynamic effects (i.e. paleocurrent), oblate shape transforms into prolate and kmin axis is not perpendicular to the bedding plane, while parallel to the strike indicate maximum extension direction or perpendicular to the maximum principal stress direction in weakly deformed sedimentary units. There are great variety of parameters that have been used to qualify susceptibility magnitude and the other shape features. Some are given at below as an example;

Pj= corrected degree of AMS, exp {2[(n1 - n) 2 + (n2 – n2) + (n3 - n) 2]} 1/2

L: magnetic lineation, = k_{min}/k_{int}

F: magnetic foliation, = k_{int}/k_{min}

T: shape parameter, "= (2n2 - n1 - n3)/ (n1 - n3)"

Where, n1 = ln k1, n2 = ln k2, n3 = ln k3, n = (n1+ n2 +n3)/3, proposed by Jelinek (1981).

km: the mean magnetic susceptibility (km) is calculated as km = (k1 + k2 + k3)/3 (Nagata, 1961), and is related to the qualitative and quantitative content of magnetic mineral composition in a rock. The mean magnetic susceptibility to express the fabric intensity as a measure of eccentricity,

Pj indicates the intensity of preferred orientation of the magnetic lineations in a rock,

T gives information about to the shape of the susceptibility ellipsoid that the value varies in between -1 to 1 responsible for an oblate to prolate ellipsoid shape, respectively.

All the data are converted first to specimen coordinate system to geographic orientations, similarly the same concept is followed for tilt (bedding) correction (also known as tectonic correction-TC). The results, from both, each specimen and the site means, were obtained by applying Jelinek statistics (1977, 1978) and are illustrated by Anisoft 4.2 program (Chadima and Jelinek, 2009).

2.4. Magnetofabric characteristic

Before the interpretation of the AMS lineament results, magnetic mineralogical properties (e.g. anisotropy degree, bulk susceptibility) and their shape parameters (magnetic foliations and lineations) are analyzed for the sites. All the results from 106 sites analyzed based on their age and separated into five age groups; **1)** the first group comprises 13 late Cretaceous sites, **2)** the second group includes 31 Paleocene sites, **3)** Eocene to Oligocene sites number is 31, **4)** for Miocene total number of 21 sites, and **5)** the last group includes 9 Pliocene sites. These sites collected from four sub areas which include; Haymana, Tuz Gölü, Kırıkkale-Bala, and the Alci-Orhaniye basins.

2.4.1. Late Cretaceous sites

The study area is represented by 16 Upper Cretaceous sedimentary AMS sites. The sites mainly composed of alternation of yellowish to reddish and brown to greenish sandstone-mudstone alternations. The mean magnetic susceptibility (km) of all sites ranging from 78.6×10^{-6} SI to 1980×10^{-6} SI indicating a major contribution of the paramagnetic to small percentage of ferromagnetic constituent minerals of the rocks

to the bulk susceptibility results (Rochette, 1987; Sagnotti *et al.*, 1998) (Figure 2.3; Table 2.1).

The results from various lithologies indicated that the magnetic susceptibility magnitudes controlled by the nature of the rocks. The site degrees of corrected anisotropy (Pj) values relatively low (<1.1) and the specimen results varies in wide range from 1.008 to 1.175 indicate only poorly developed magnetic fabric (Figure 2.3; Table 2.1). The shape of the anisotropy ellipsoids ranges from prolate (T<0 and L>F; SEC3) to neutral (T~=0 and L/F~=1; RY1, RH1, R73, R 65) and rest of them strong oblate (T>0 and F>L) (Table 2.1).

In the Figure 2.3; the last diagram illustrates distribution of sum of results of mean magnetic susceptibility and Jelinek (T versus Pj) results in 16 sites. The results show both prolate and oblate in shape.

2.4.2. Paleocene Sites

31 Paleocene sites were analyzed for rock magnetic properties in the study area. The susceptibility and Jelinek diagrams for Paleocene sites are depicted in Figure 2.4. The 31 Paleocene sites contain samples collected only from sedimentary rocks that include limestone and clastic rocks (red to green mudstone-sandstone and claystone). Rock magnetic properties of these samples are closely connected with their position and matrix ingredients and there is no relationship with their ages. The site mean susceptibility values range between a minimum of -9.25×10^{-6} SI and maximum of 7820×10^{-6} SI indicating three types of magnetic contributions; diamagnetic from limestone (R20, R34, RN10), paramagnetic and ferromagnetic dominant minerals in the rest (Table 2.1).

The shape parameters indicate that the anisotropy ellipsoids change from prolate (T<0 and L>F; R20, R 43, R 59, R60, RN10, RN11, and RN12) to neutral (T~=0 and L/F~=1; R11, R34, R36, R74, RN2) and rest of them show strong oblate geometry (T>0 and F>L) (Table 2.1).

As seen in the combined results of the sites (the last plot in the Figure 2.4), Pmean susceptibility (km) and corrected anisotropy degree varies in wide range. In addition, the resultant shape parameters indicate the variation both from prolate to oblate.

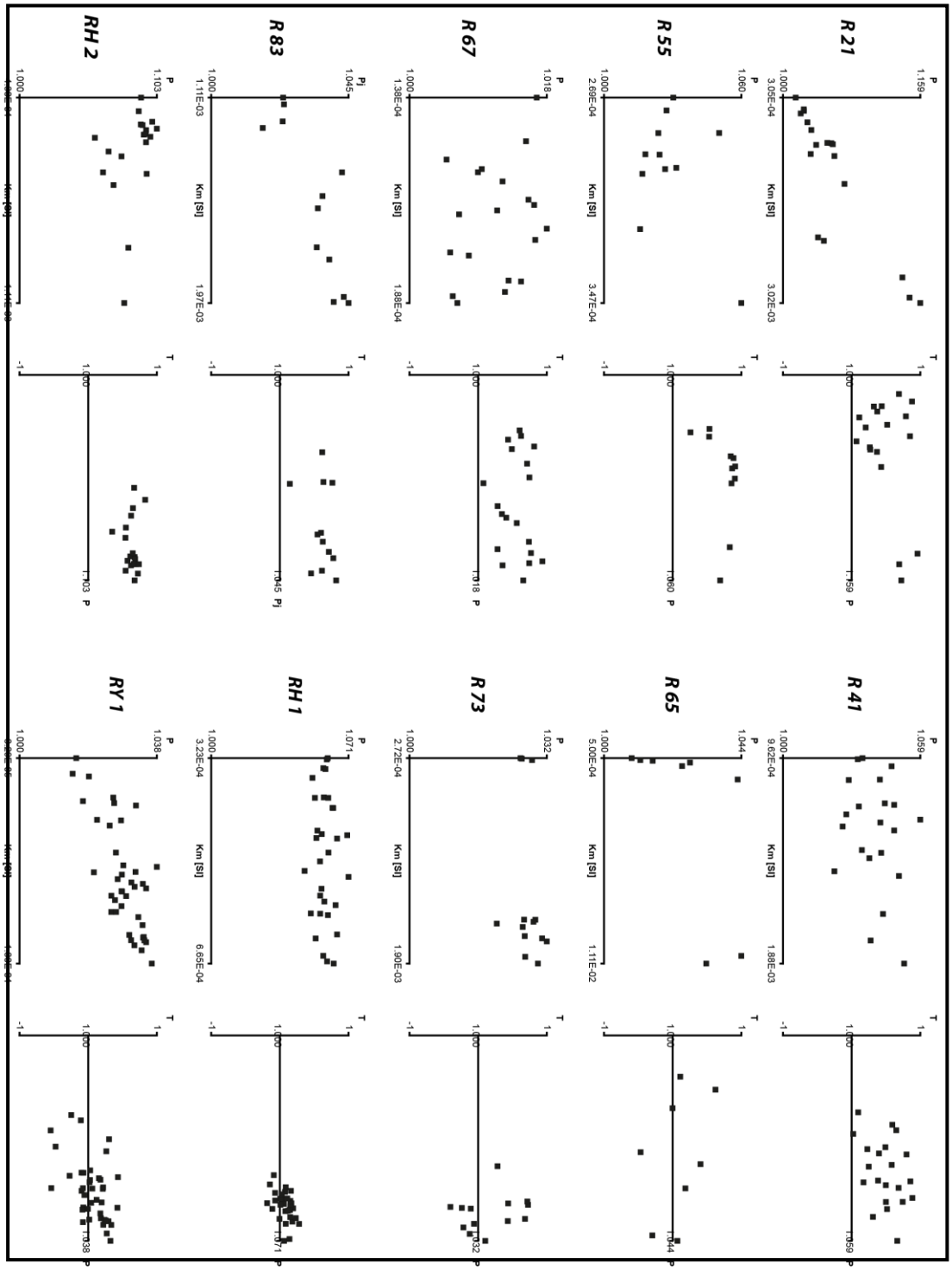

Figure 2.3. Magneto-fabric parameters of 13 Upper Cretaceous sites and one combined result. The site mean shape parameter (T) vs. corrected anisotropy degree (Pj) plot (Jelinek Diagram) is on the right, the corrected anisotropy degree (Pj) vs. magnetic bulk susceptibility (km) plot is on the left. Oblate susceptibility ellipsoids fall in the T>0 and F>L domain, while prolate susceptibility ellipsoids are in the T<0 and L>F domain.

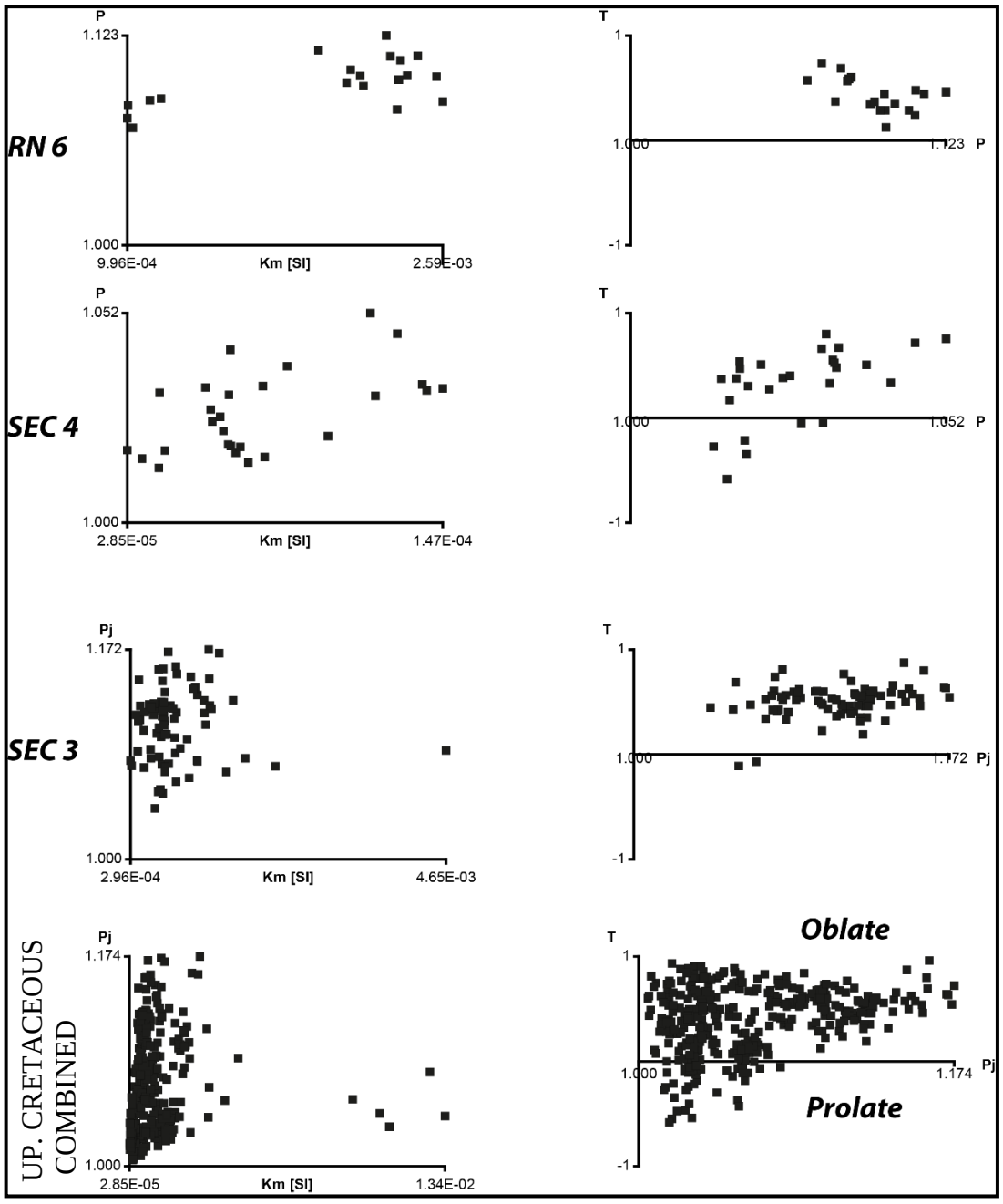

(**Figure 2.3 continued**)

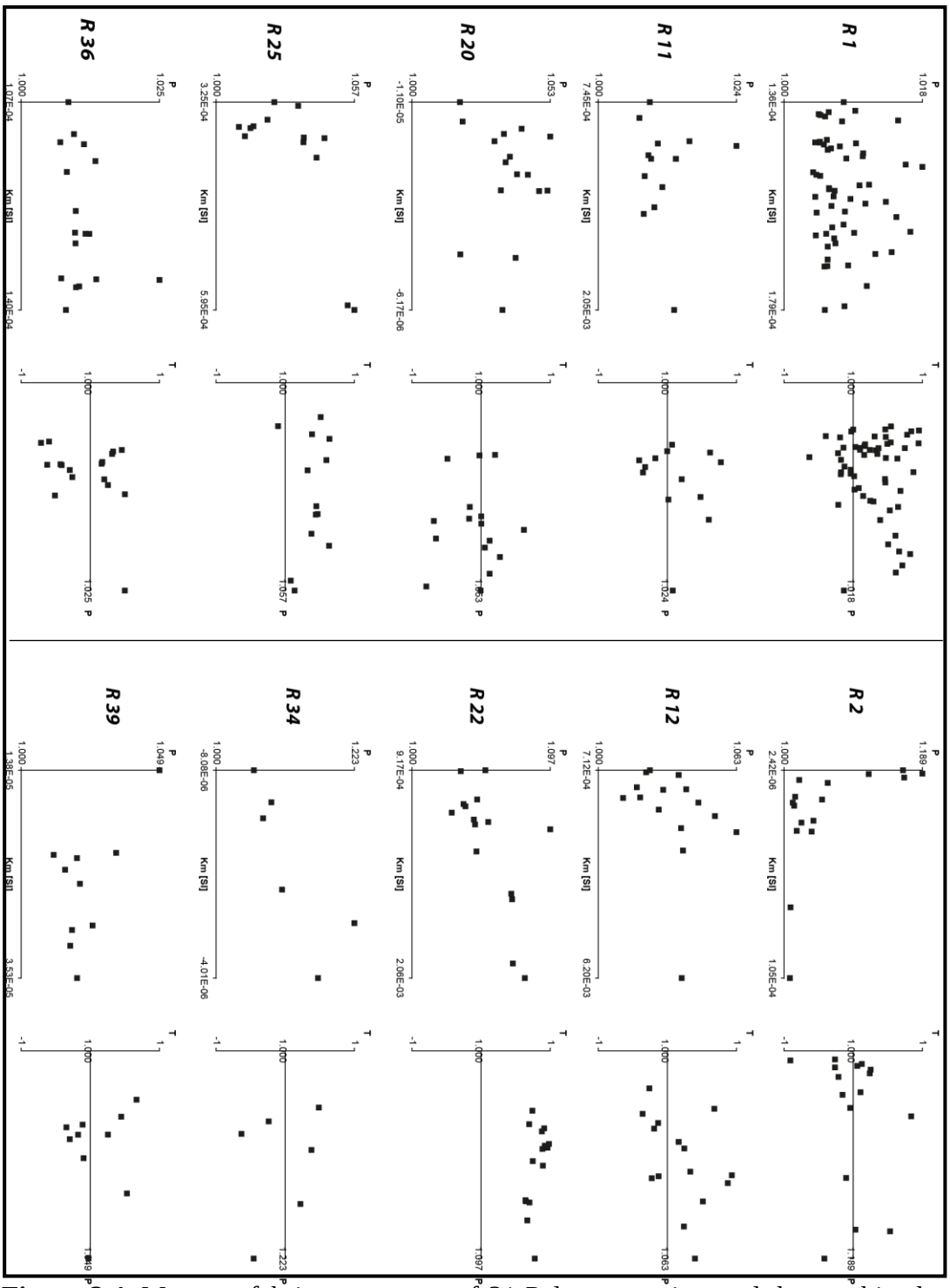

Figure 2.4. Magneto-fabric parameters of 31 Palaeocene sites and the combined result. The site mean shape parameter (T) vs. corrected anisotropy degree (Pj) plot (Jelinek Diagram) is on the right, the corrected anisotropy degree (Pj) vs. magnetic bulk susceptibility (km) plot is on the left. Oblate susceptibility ellipsoids fall in the T>0 and F>L domain, while prolate susceptibility ellipsoids are in the T<0 and L>F domain.

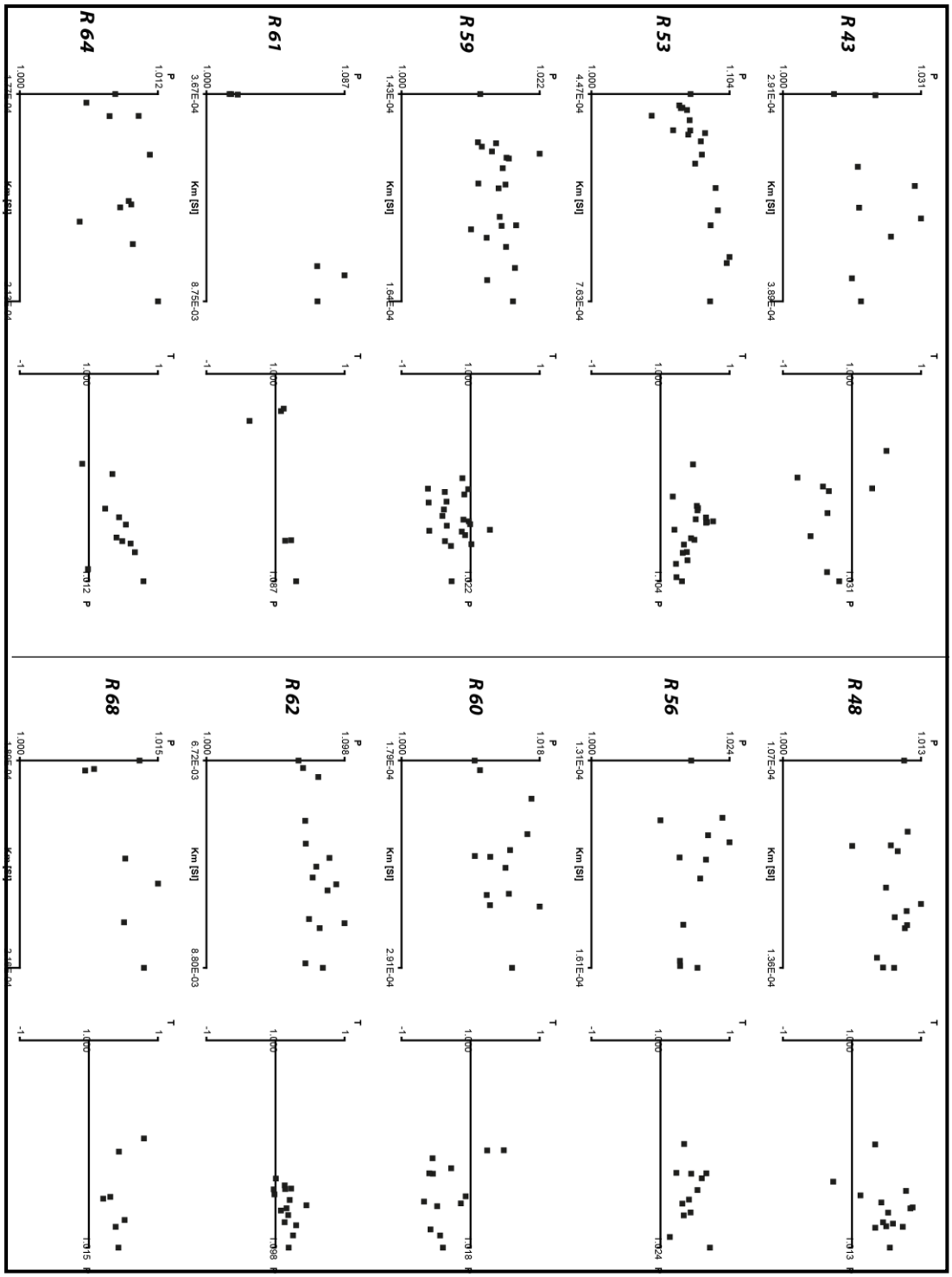

(Figure 2.4 continued)

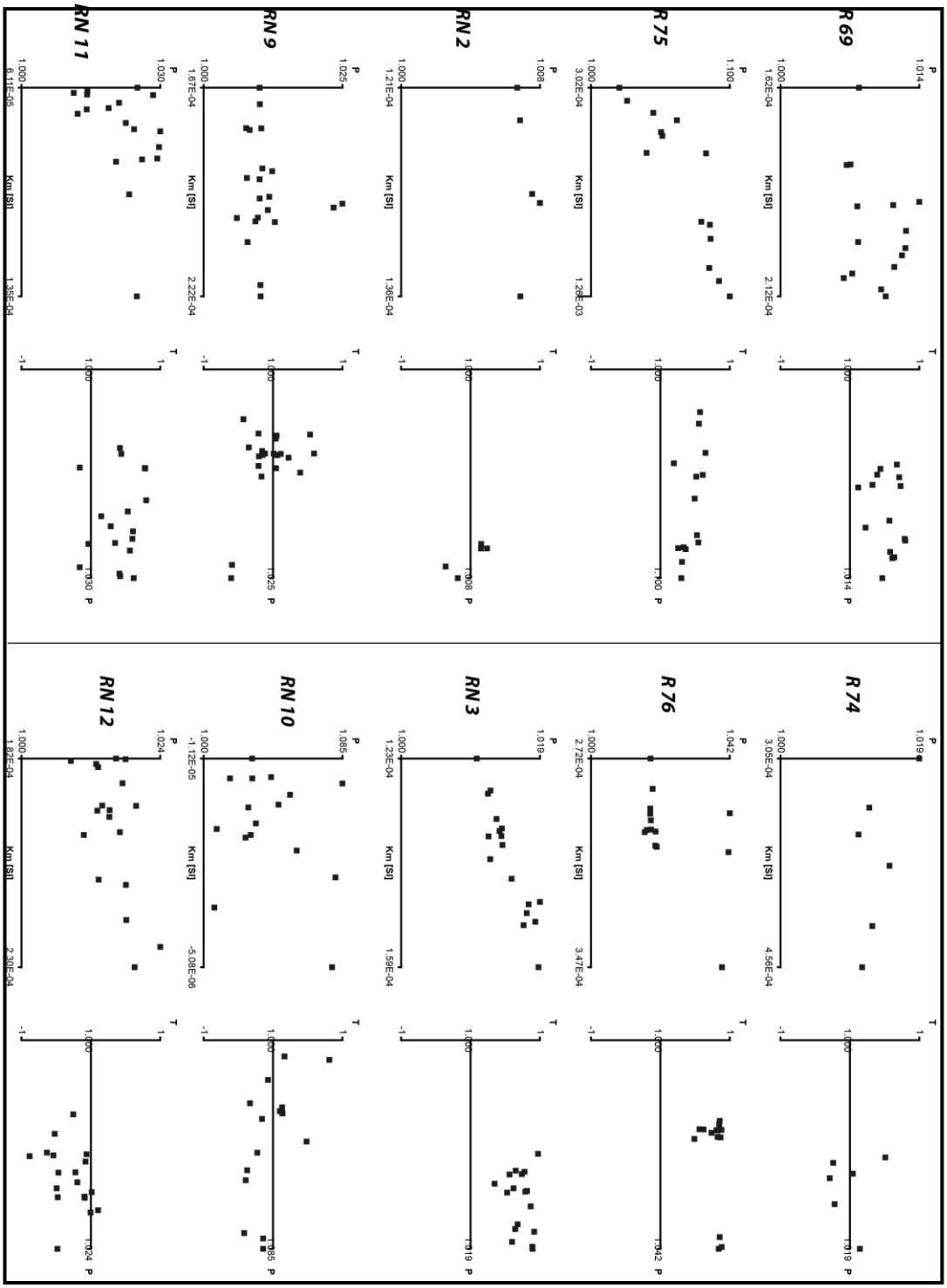

(Figure 2.4 continued)

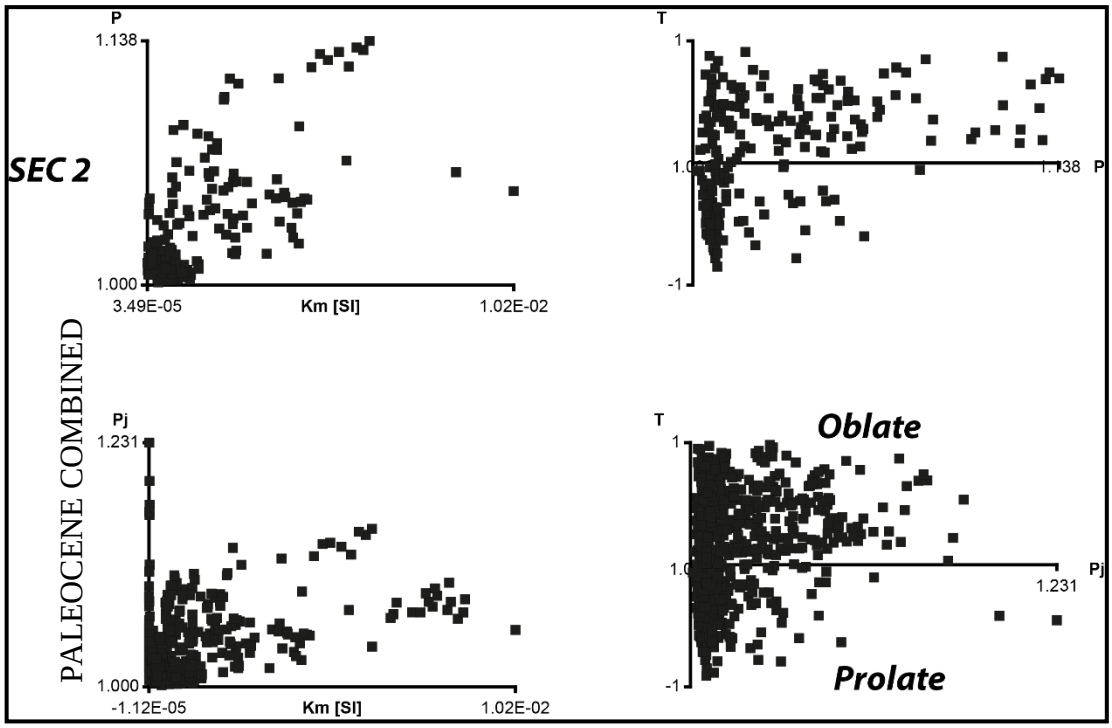

(Figure 2.4 continued)

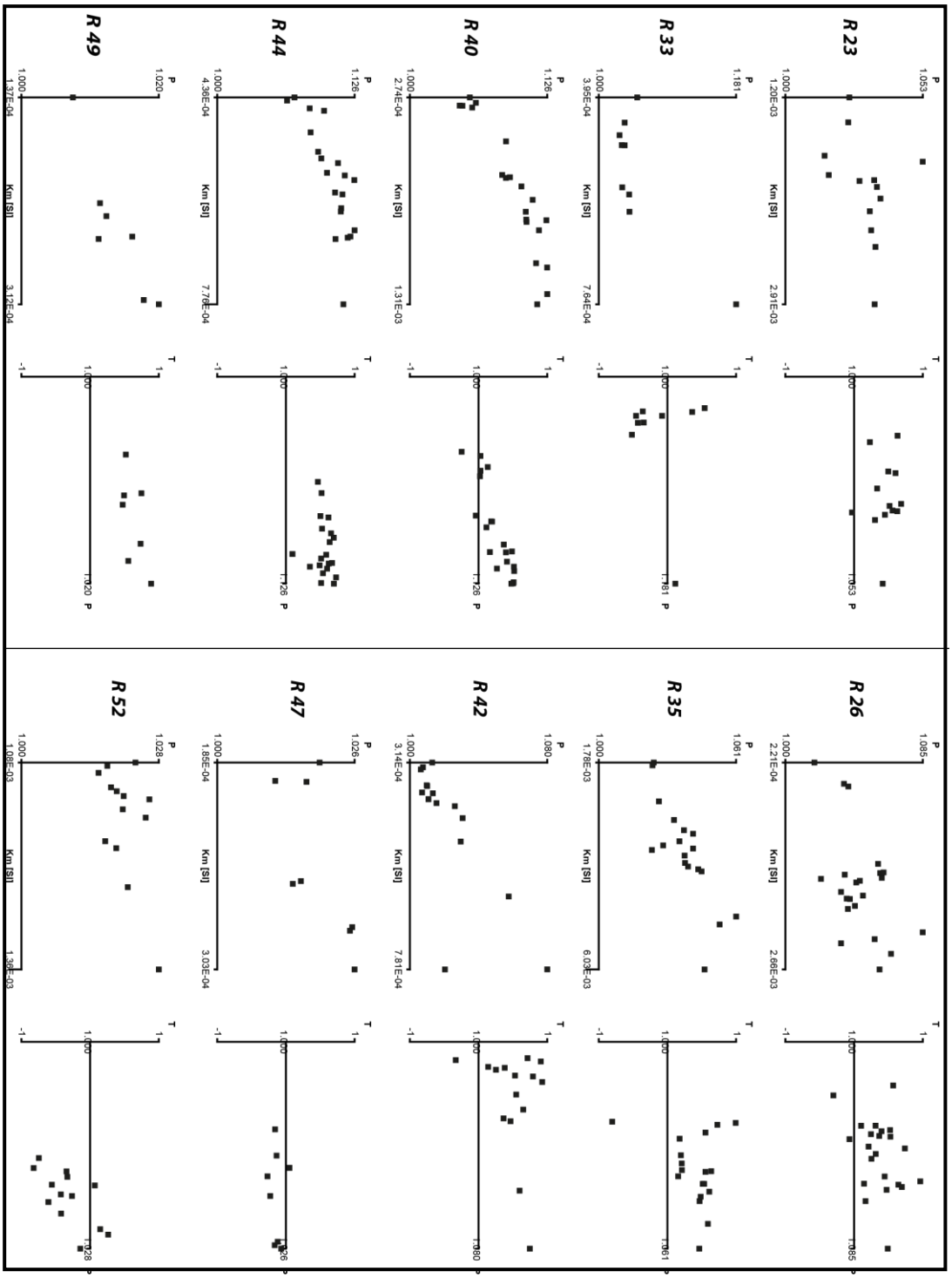

Figure 2.5. Magneto-fabric parameters of 31 Eocene-Oligocene sites and their combined results. The site mean shape parameter (T) vs. corrected anisotropy degree (Pj) plot (Jelinek Diagram) on the right, the corrected anisotropy degree (Pj) vs. magnetic bulk susceptibility (km) plot in on the left. Oblate susceptibility ellipsoids fall in the T>0 and F>L domain, while prolate susceptibility ellipsoids are in the T<0 and L>F domain.

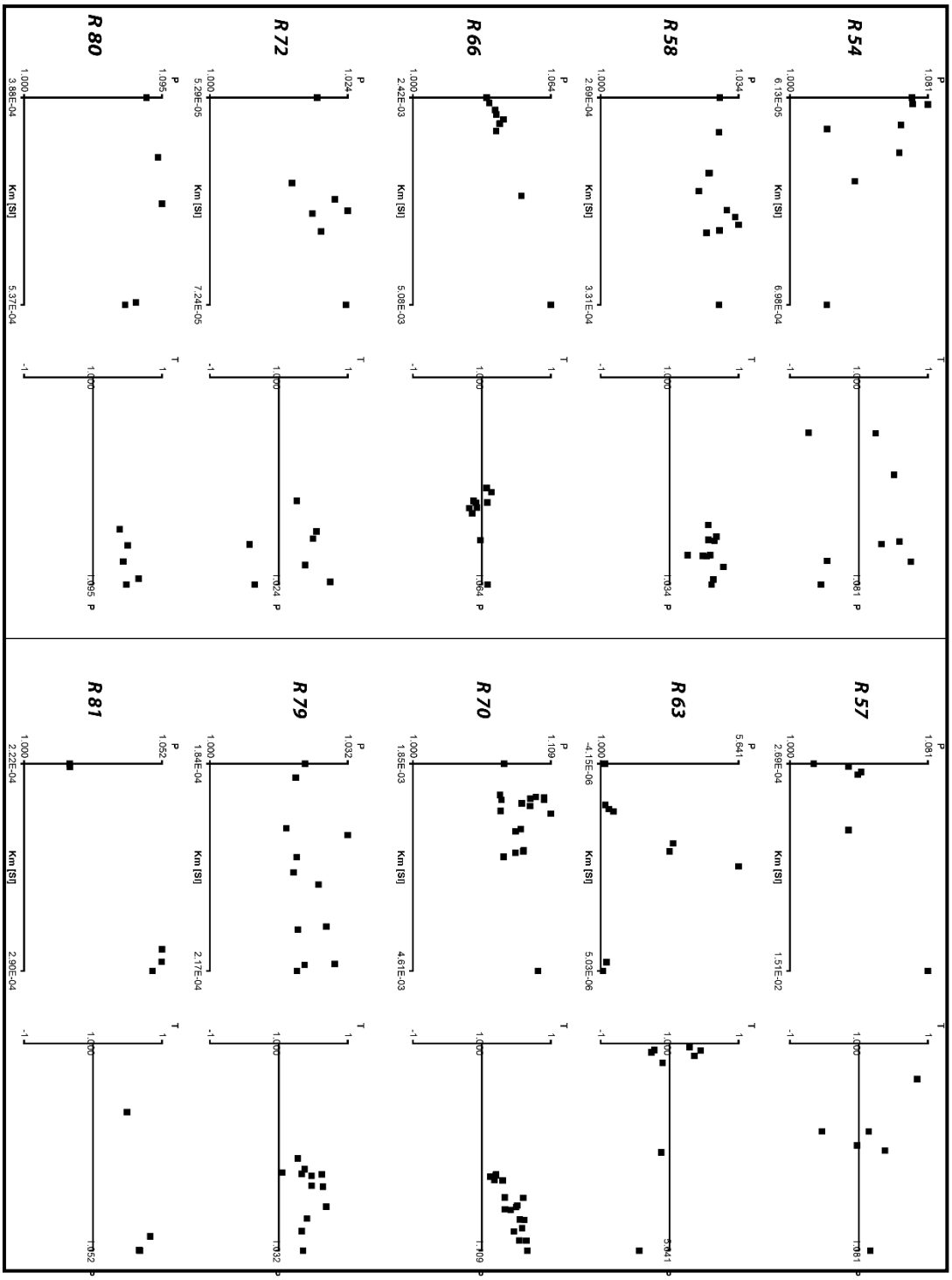

(Figure 2.5 continued)

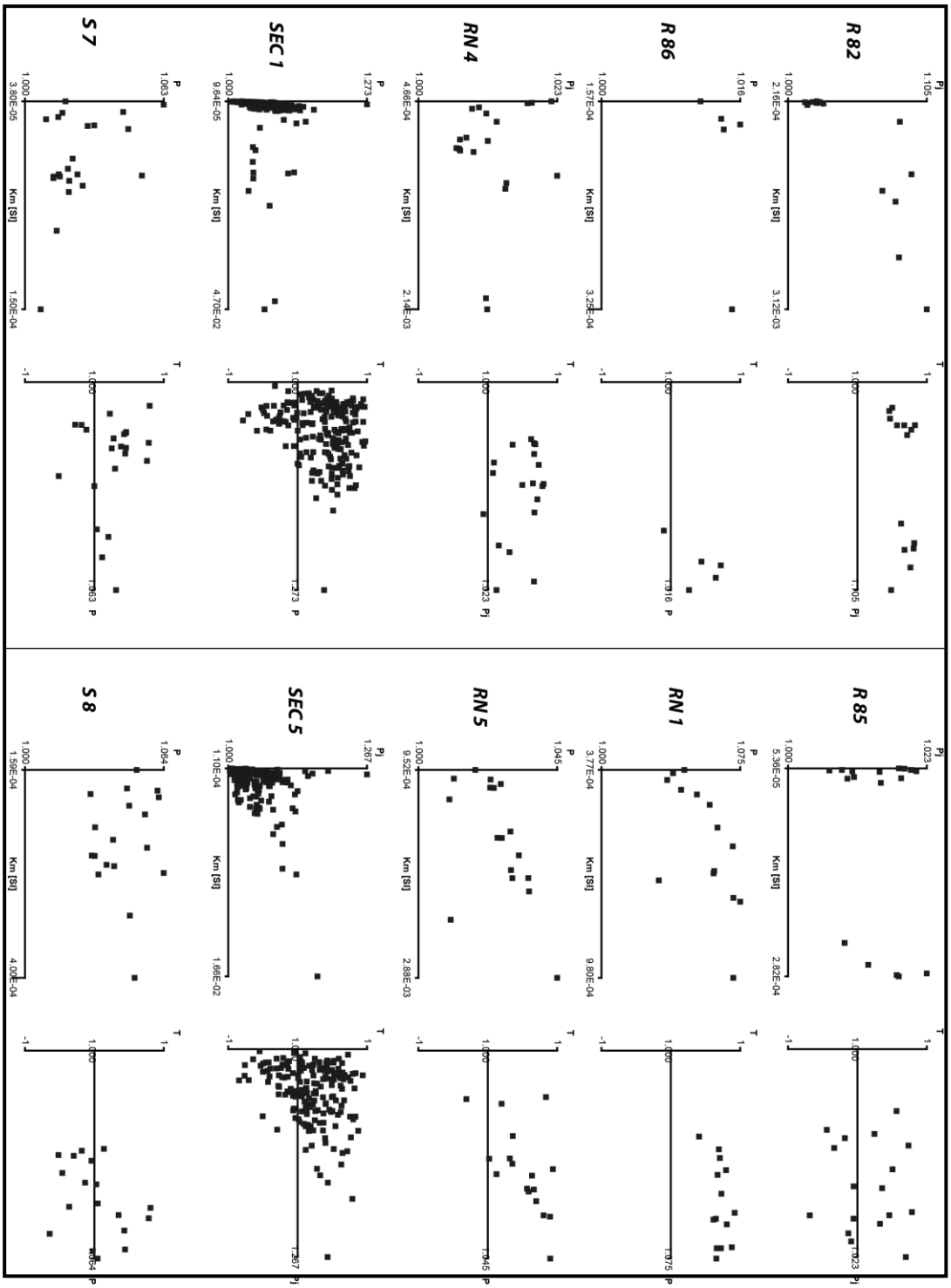

(Figure 2.5 continued)

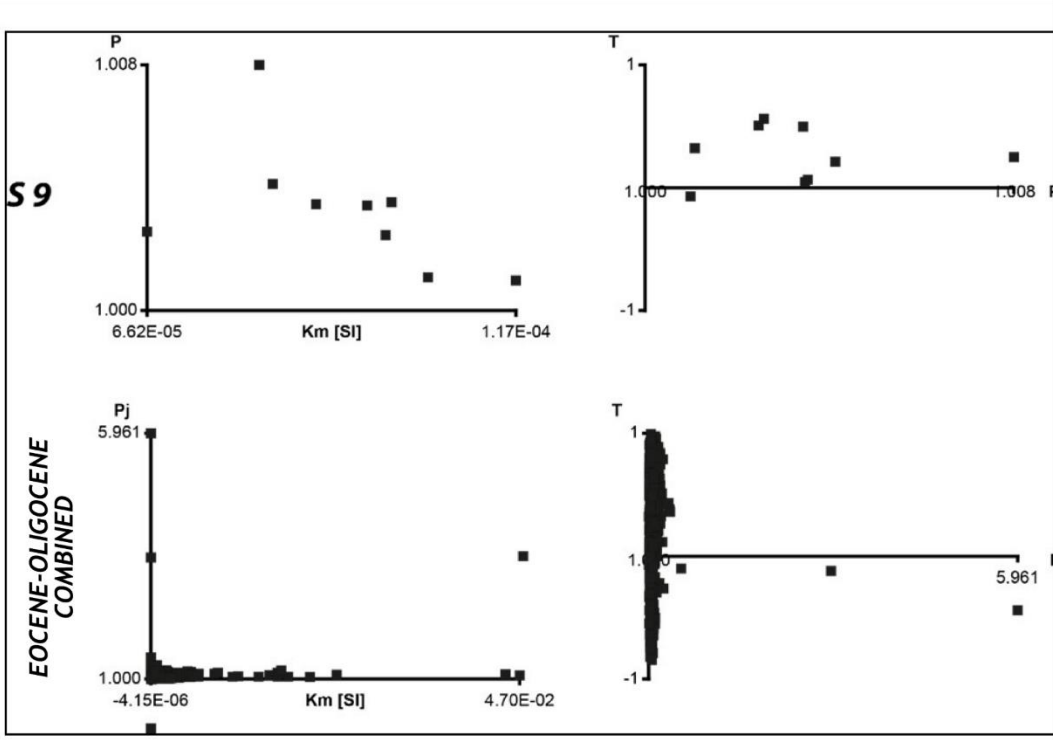

(Figure 2.5 continued)

2.4.3. Eocene-Oligocene sites

The Eocene-Oligocene rocks composed of sandstone-claystone-mudstone alternations intercalated with various carbonate rocks. The 31 sampling sites distributed relatively homogeneously in the study area unlike sites belong to other sampled time intervals (Figure 2.1 and 2.2). The magnetic property analysis results show that they are controlled by the position of the sampling site. The km (SI) values are swinging between negative values which indicate diamagnetic properties (e.g. R63) to moderate values ranging between ~$90x10^{-6}$ – $1500x10^{-6}$ (SI) and very high values that exceed >1500 SI. They indicate ferromagnetic minerals that dominate most of Eocene-Oligocene samples (Figure 2.5; Table 2.1).

The shape parameters show AMS ellipsoids from prolate (T<0 and L>F) to neutral (T~=0 and L/F~=1) and strong oblate geometry (T>0 and F>L) (Table 2.1). The last diagrams in the Figure 2.5 illustrate combined results of all Eocene-Oligocene sites.

2.4.4. Miocene sites

Miocene is represented by 21 sites (Figure 2.6; Table 2.1.) The km values are generally lower in the carbonate rocks (Figure 2.6; Table 2.1). Interestingly there are no negative (diamagnetic) mean susceptibility results in the measurements. On the other hand, the volcanic rocks (e.g. R13, R 45, and R46) produced very high mean susceptibility values (11500-42600 SI) clearly indicating their volcanic origin.

The AMS ellipsoids of Miocene sites are oblate to neutral and only few sites produced neutral to prolate shapes (R3, R37, and R50).

2.4.5. Pliocene sites

For Pliocene time interval only 9 AMS results are available. The sites generally distributed in the southern part of the study area (Figure 2.1 and 2.2). Almost all of the samples belongs to lacustrine deposits. They are composed of fine grained clastics such as siltstone and mudstone, and marl alternations. Likewise other sedimentary rock samples their mean magnetic susceptibility values are relatively low compare to older rocks (Eocene and older) (Table 2.1). The km values change between 2.85 to 5670 SI. Similar to the Miocene sites, there is no negative (diamagnetic) susceptibility values, possibly due to the contribution of Miocene and younger volcanism in the region.

The magnetic susceptibility magnitude values changes according to the lithology in each sites. The results of corrected anisotropy (Pj) values relatively low (<1.05, except for the site SF3 which has 1.02). This implies low degree of deformation and indicate poorly developed magnetic fabric possibly related to tectonic deformation (Figure 2.7; Table 2.1). The AMS ellipsoids dominantly have oblate shape (T>0 and F>L; R27, R50, R51) to neutral (T~=0 and L/F~=1; R37, SF3, SF4) and rest of them have mixed geometries (Figure 2.7 and Table 2.1).

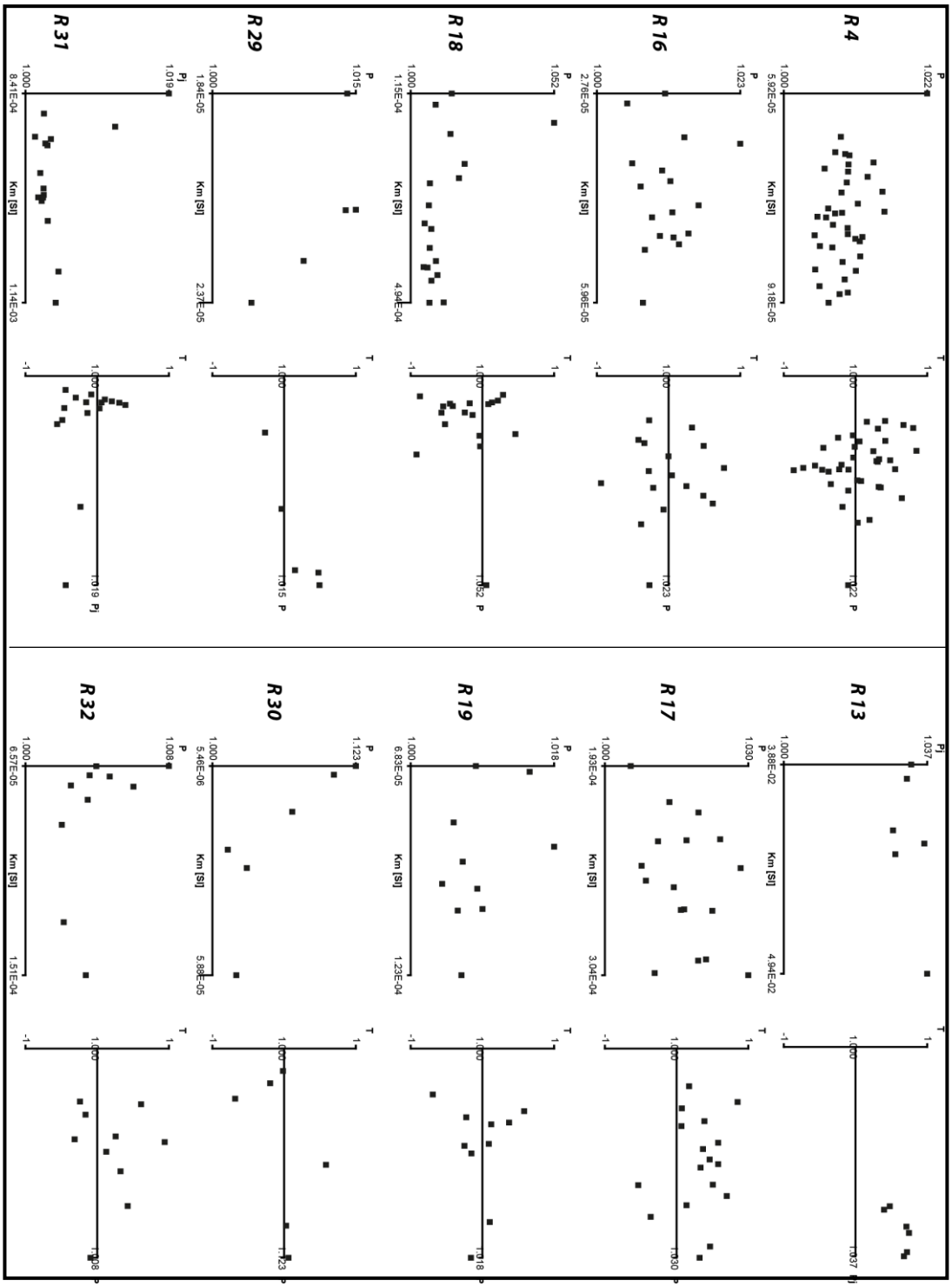

Figure 2.6. Magneto-fabric parameters of Miocene 21 sites and one combined result. The site means shape parameter (T) vs. corrected anisotropy degree (Pj) plot (Jelinek Diagram) (right). The corrected anisotropy degree (Pj) vs. magnetic bulk susceptibility (km) plot (left). Oblate susceptibility ellipsoids fall in the T>0 and F>L domain, while prolate susceptibility ellipsoids are in the T<0 and L>F domain.

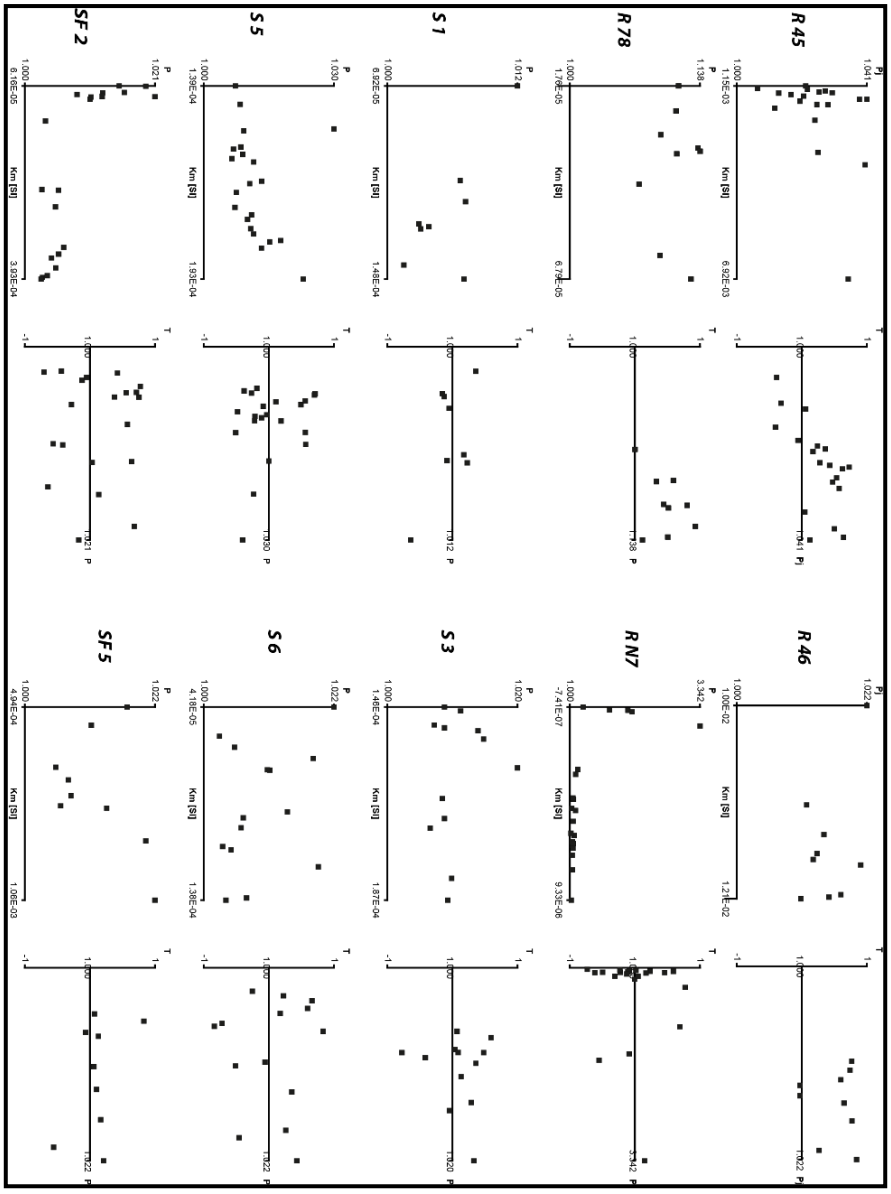

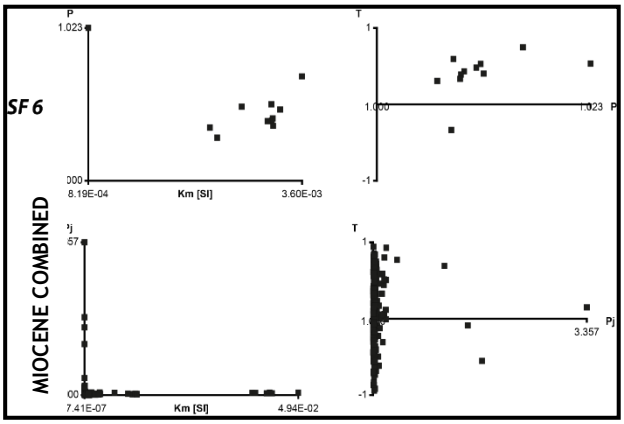

(Figure 2.6 continued)

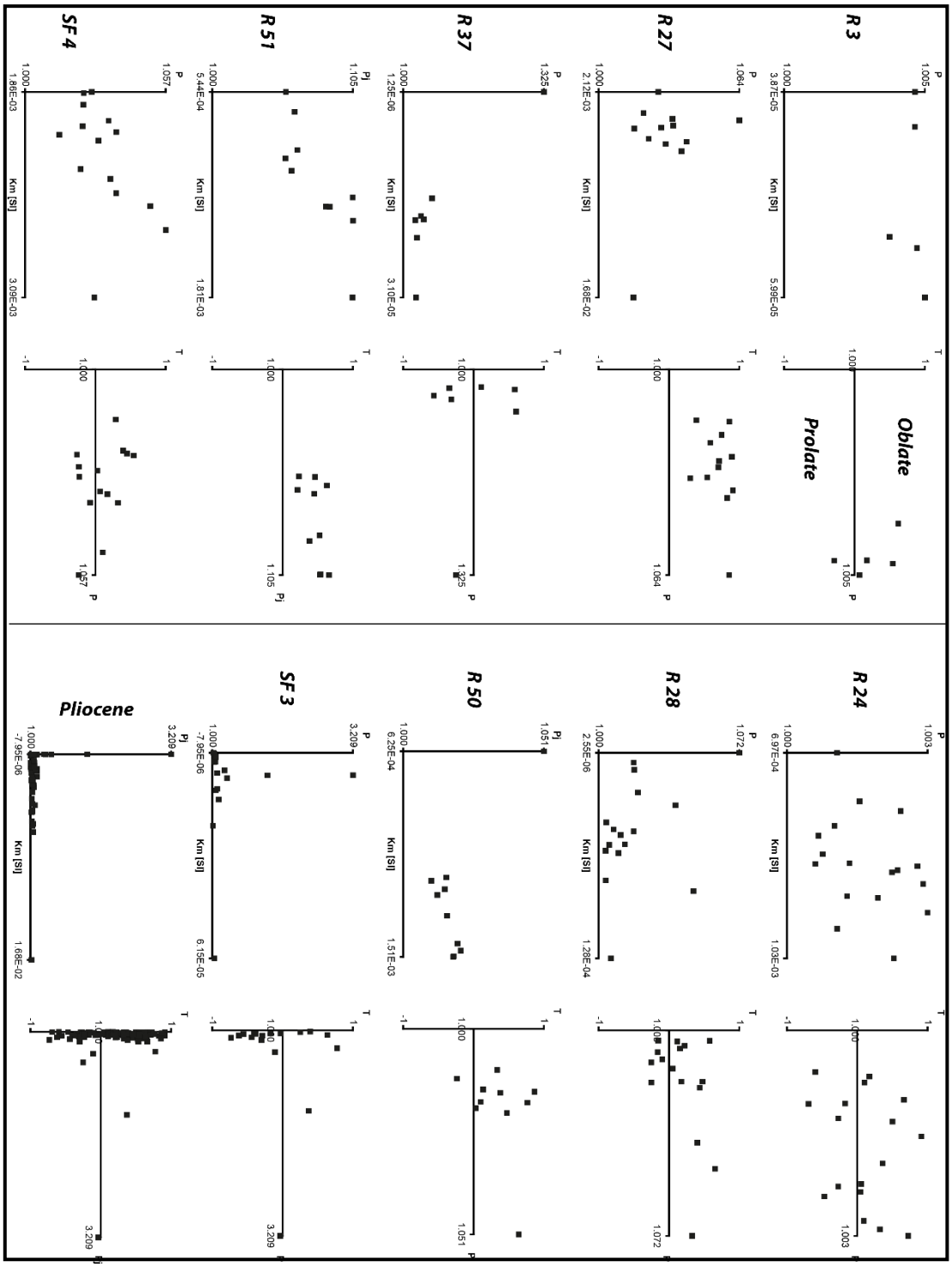

Figure 2.7. Magneto-fabric parameters of Pliocene 9 sites and their combined result (indicated as Pliocene). The site means shape parameter (T) vs. corrected anisotropy degree (Pj) plots (Jelinek Diagram) on the right, the corrected anisotropy degree (Pj) vs. magnetic bulk susceptibility (km) plot on the left. Oblate susceptibility ellipsoids fall in the T>0 and F>L domain, while prolate susceptibility ellipsoids are in the T<0 and L>F domain.

2.5. Evaluation of the AMS results

The anisotropy of magnetic susceptibility results show that the magnetic lineations are sensitive indicators of progressive deformation in the study area. They can be used to differentiate the stages of deformation in the sedimentary rocks. In the study are the obtained results can be categorized in three deformation stages with increasing in the intensity of the tectonic deformation from primary sedimentary fabric (depositional anisotropy) to cleavage development (intense deformation). Theoretically, the stages of deformation related magnetic lineations are as follows;

- ✓ The first case includes the no deformation phase. In this case the minimum susceptibility axis (k_{min}) is perpendicular to the bedding plane and is related to the compaction of the unconsolidated sediments. In this case, the maximum and intermediate susceptibility axes (k_{max} and k_{int}) are not constrained and therefore they form a girdle distribution, characteristics of an oblate susceptibility ellipsoid.

- ✓ The second case is the intermediate tectonic deformation phase. In this case, k_{max} is well constrained and parallel to the extension direction while k_{int} and k_{min} makes a pencil structure perpendicular to k_{max}. The shape of the anisotropy ellipsoid transform from oblate to prolate geometry.

- ✓ The final stage determines full tectonic deformation phase and cleavage structures occur. The minimum susceptibility axis changes into a well-defined cluster that is almost parallel to the bedding plane or normal to the cleavage plane (minimum strain axis), while k_{int} and k_{max} are fairly clustered. Cleavages can be developed in the specimens at final stage.

The constructed AMS ellipsoids in the study indicate typical of weakly to intermediate deformation phases. The AMS ellipsoid patterns changes from region to region and are independent from the age and lithological characteristics imply tectonic origin for the ellipsoids.

In this section, 106 Upper Cretaceous to Pliocene AMS sites are analyzed from the four basins in the study area namely Alcı-Orhaniye, Kırıkkale-Bala, Tuz Gölü and

Haymana basins (Figure 2.1, 2.2). The kmax (also named as AMS lineament) results are presented before and after tilt correction, for five time intervals that include 1) late Cretaceous, 2) Paleocene, 3) Eocene-Oligocene, 4) Miocene, 5) Pliocene.

2.5.1 Late Cretaceous AMS Results

The late Cretaceous results are well clustered in all directions parallel to k_{max}, k_{int}, k_{min}. However, the orientations of the AMS lineaments vary basin to basin. The k_{max} results from site R65 and R67 are almost parallel and indicate NE-SW direction of maximum susceptibility in the Kırıkkale-Bala Basin. They are almost parallel with the bedding strike at the sites. In the site R73, the k_{max} is oriented NW-SE almost perpendicular to the bedding strike and also to the results of the sites R65 and R67 (Figure 2.8).

In the Tuz Gölü Basin the only Upper Cretaceous site (R83) indicate NE-SW oriented k_{max} and it is perpendicular to the bedding strike and the long axis of the basin (NW-SE) which is controlled in it eastern margin by the NW-SE tending Tuzgölü Fault (Figure 2.8).

Similarly, Alcı-Orhaniye Basin is also represented by only one site (R6). The orientation of the k_{max} is NNW-SSE before and after tilt correction and the result not pairing with the site bedding attitude which is NE-SW striking (Table 2.1).

The rest of 9 sites from the Haymana Basin can be divided in two part according to kmax lineaments. The first group comprise the sites R21 and R55 which are located NW of the Haymana Basin near the Temelli (Figure 2.8 and 2.9). The results show NNW to NW and SSW to SW kmax directions considerably matching with the local bedding strikes of the sites (Figure 2.9)

In the central of the Haymana Basin, from 7 sites indicate more or less E-W direction of kmax results which are also perfectly fit to the bedding strikes of the sites (Figure 2.9).

2.5.2 Paleocene AMS Results

The Paleocene sites are not present in all basins. For example, the Paleocene sites in the Tuzgölü basin did not produce and appreciable results and only two sites in the Alcı-Orhaniye Basin produced interpretable results (Figure 2.10).

In the Kırıkkale-Bala Basin, the AMS k_{max} directions gradually changes from almost N-S to NW then to E-W from north to south. At the transition zone from Kırıkkale-Bala to Tuzgölü basins, the K_{max} orientations become E-W (Figure 2.10).

The two sites (R1, R2) in the Alcı-Orhaniye Basin have parallel k_{max} orientation and are oriented NNW-SSE. They are also parallel to the northern part of the Kırıkkale-Bala Basin (Figure 2.10). In these sites the k_{max} directions and the bedding strikes are not parallel to each other neither before nor after tilt correction (Table 2.1).

In the Haymana Basin, mainly two groups of k_{max} orientations can be discriminated. The first group has NW-SE orientation while the second group is oriented NE-SW. The NW-SE striking sites are approximately parallel to the Upper Cretaceous sites and are located mainly at the northwestern part of the basin. The other group located mainly at the central part of the basin and the Paleocene and late Cretaceous orientations are normal to each other (compare Figures 2.10 and 2.11). The second group is positioned at the central part of the Haymana Basin and indicates dominantly E-W k_{max} directions (Figure 2.11).

2.5.3 Eocene-Oligocene AMS Results

Eocene-Oligocene is represented by 31 sites and are relatively well distributed in the study area (Figure 2.12). The AMS susceptibility directions have moderate to low degree of error margins in three directions (Table 2.1).

In the Kırıkkale-Bala Basin two sets of K_{max} directions are determined from four Eocene-Oligocene sites. The first set is compatible with the general orientation of bedding strikes and folds in the basin. They are oriented NE-SW. The second set of AMS data gives NW-SE k_{max} directions which area normal to the first set. Whereas they are parallel to the local (site) bedding strikes (Figure 2.12).

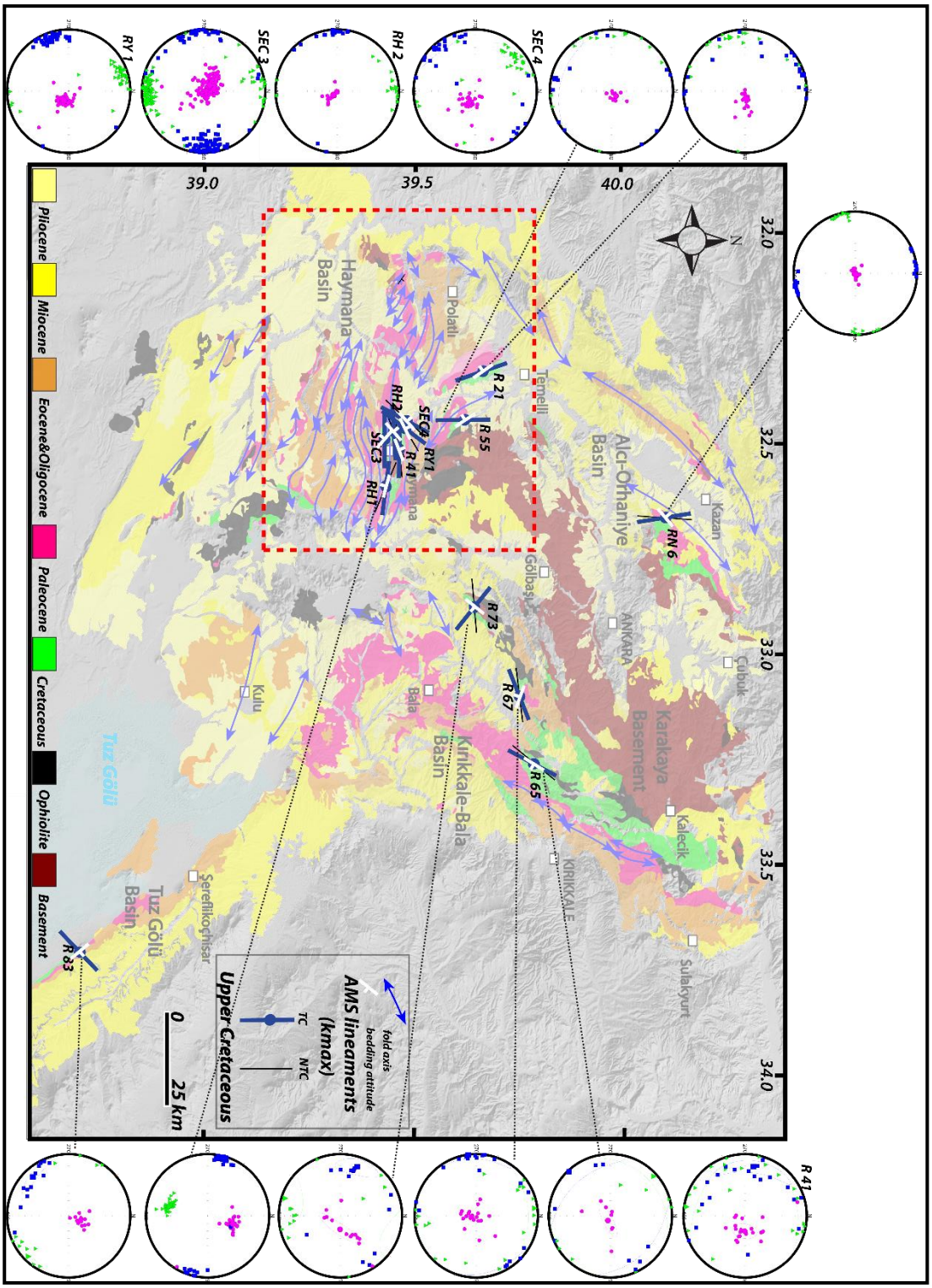

Figure 2.8. Map showing late Cretaceous k_{max} orientations, in-situ and after tectonic correction, and the strike of the bedding planes at the site. The circles outside the map are distributions of magnetic susceptibility directions; k_{max} (blue square), k_{int} (green triangle), and k_{min} (purple circle) (equal area, lower hemisphere projection). Red dashed box is the coverage area of Figure 2.8.

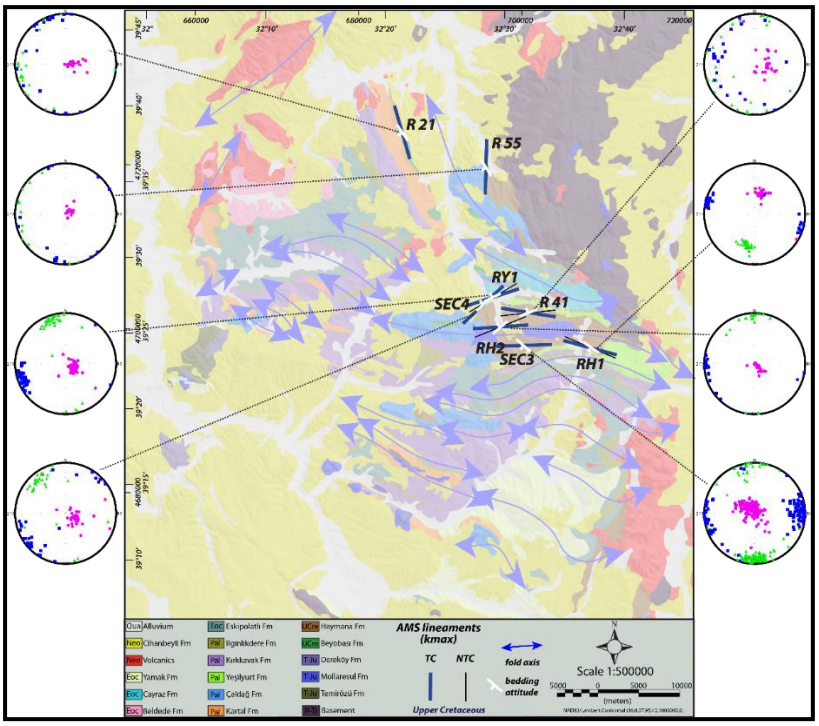

Figure 2.9. Blow up view of the Haymana Basin (see Figure 2.8 for its location) showing late Cretaceous k_{max} orientations, in-situ and after tectonic correction, and the strike of the bedding planes at the site. The circles outside the map are distributions of magnetic susceptibility directions; k_{max} (blue square), k_{int} (green triangle), and k_{min} (purple circle) (equal area, lower hemisphere projection).

Three sites are produced reliable results from the Alcı-Orhaniye Basin. They are very consistent with each other and also with the bedding strikes (Figure 2.12). The tilt corrected k_{max} directions are oriented NE-SW. Except one site (S8), the k_{max} results before and after tilt corrections are the same in other two sites.

A large number of Eocene sites are there for the Haymana Basin (Figure 2.13). The AMS k_{max} are oriented generally E-W direction except few sites which are oriented NE-SW (Table 2.1). The most striking characteristics of the Kmax orientations in the Haymana Basin is that almost all of the sites they follow approximately the local fold trends. As the fold axis deviates from linear and become curvilinear, the k_{max} orientations also deviates from general trend and become parallel to the folds axis (Figure 2.12 and Table 2.1).

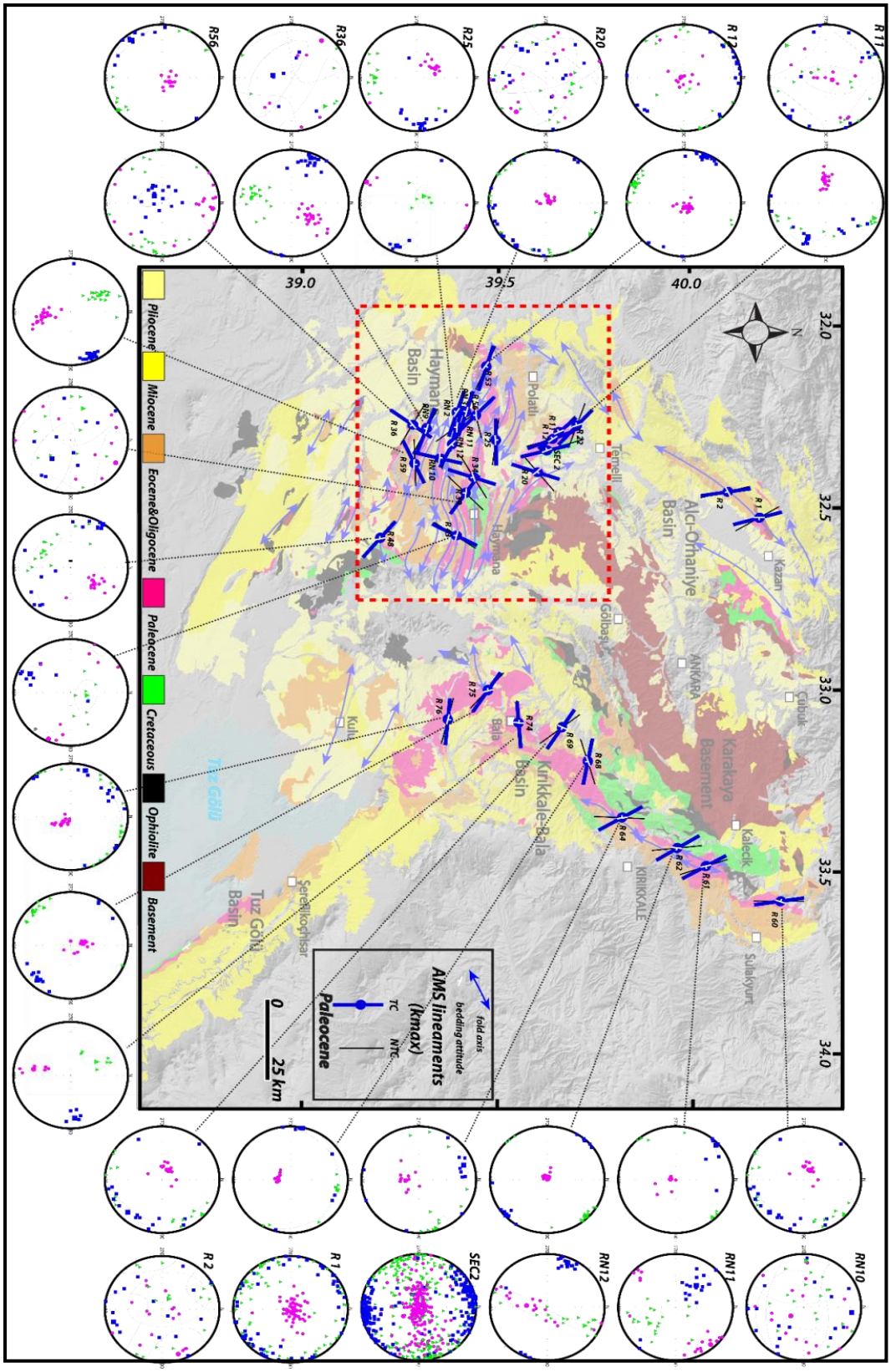

Figure 2.10. Map showing Paleocene k_{max} orientations, in-situ and after tectonic correction, and the strike of the bedding planes at the site. The circles outside the map are distributions of magnetic susceptibility directions; k_{max} (blue square), k_{int} (green triangle), and k_{min} (purple circle) (equal area, lower hemisphere projection). Red dashed box is the coverage area of Figure 2.10.

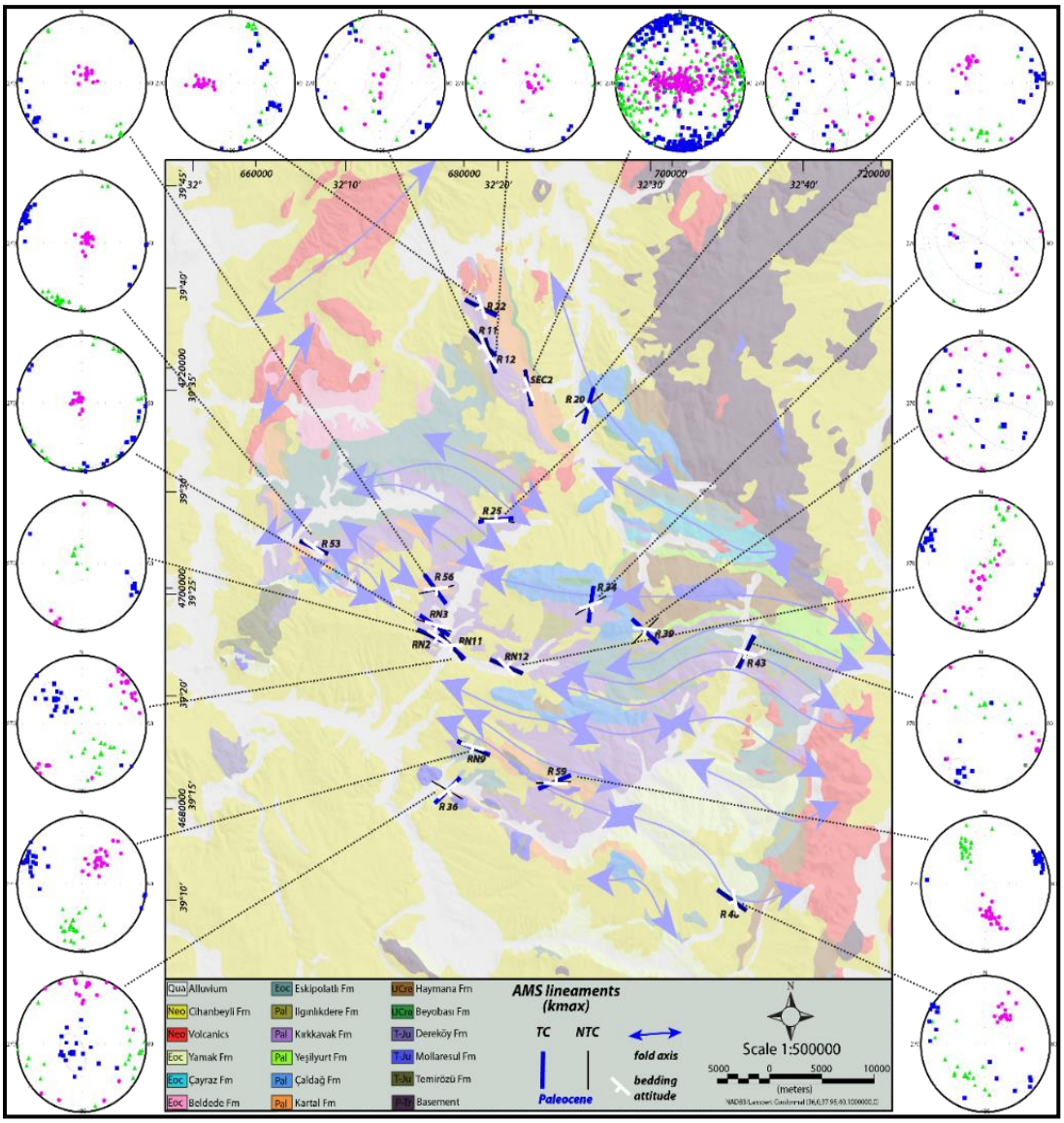

Figure 2.11. Blow up map of the Haymana Basin (see Figure 2.10 for its location) showing Paleocene k_{max} orientations, in-situ and after tectonic correction, and the strike of the bedding planes at the site. The circles outside the map are distributions magnetic susceptibility directions; k_{max} (blue square), k_{int} (green triangle), and k_{min} (purple circle) (equal area, lower hemisphere projection).

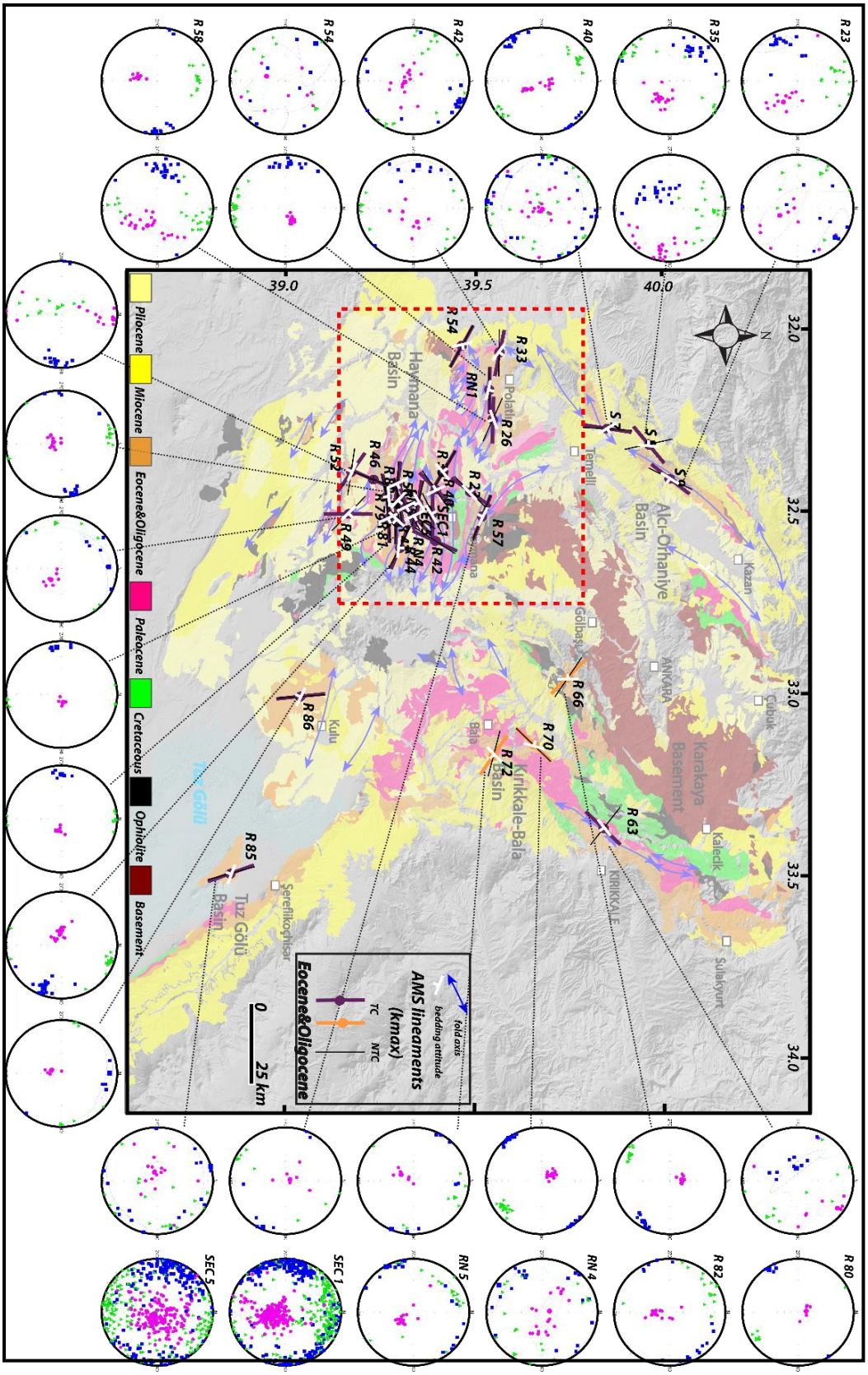

Figure 2.12. Map showing Eocene-Oligocene k_{max} orientations, in-situ and after tectonic correction, and the strike of the bedding planes at the site. The circles outside the map are distributions of magnetic susceptibility directions; k_{max} (blue square), k_{int} (green triangle), and k_{min} (purple circle) (equal area, lower hemisphere projection). Red dashed box is the coverage area of Figure

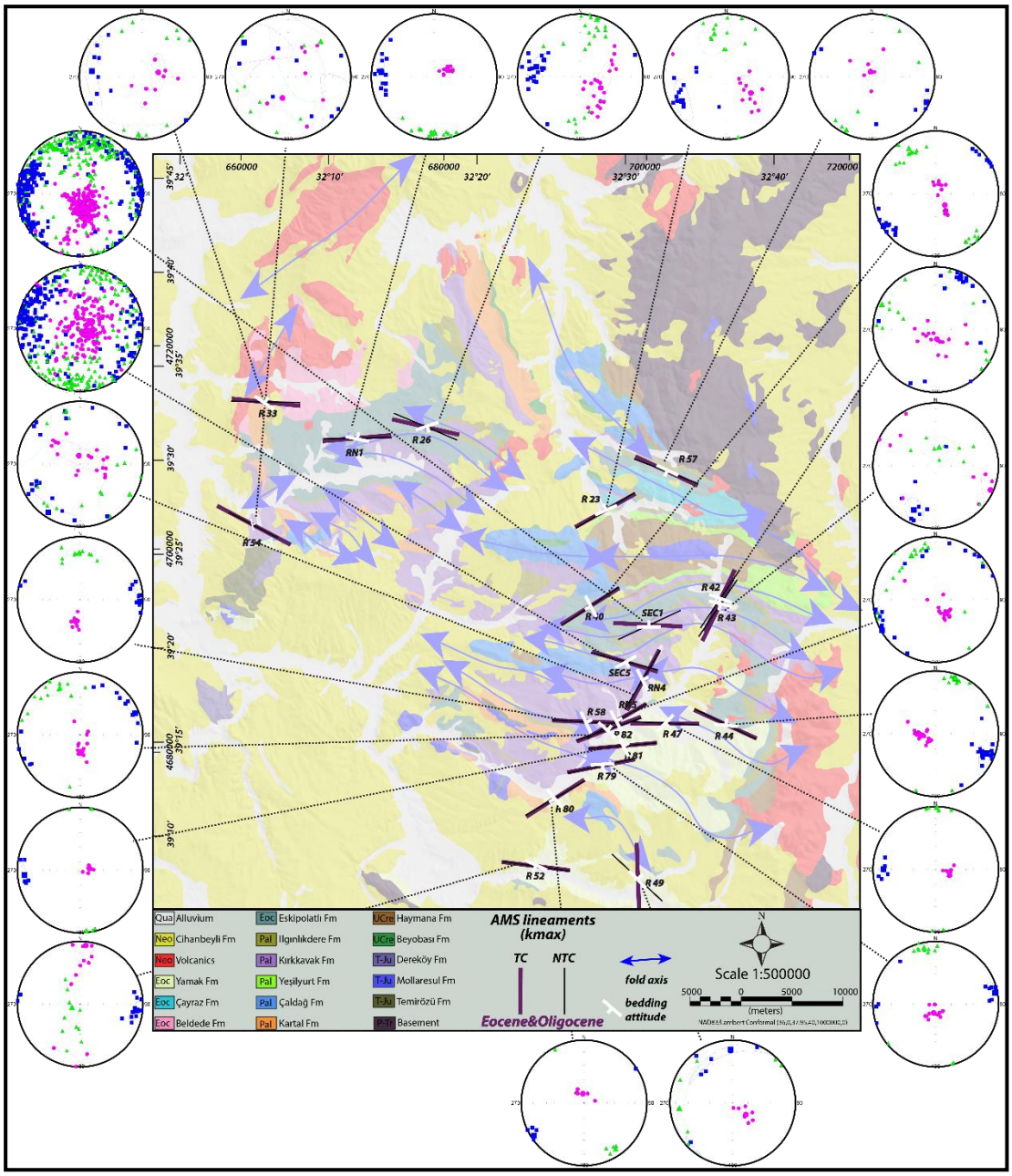

Figure 2.13. Blow up map of the Haymana Basin (see Figure 2.12 for its location) showing Eocene-Oligocene k_{max} orientations, in-situ and after tectonic correction, and the strike of the bedding planes at the site. The circles outside the map are distributions magnetic susceptibility directions; k_{max} (blue square), k_{int} (green triangle), and k_{min} (purple circle) (equal area, lower hemisphere projection).

2.5.4 Miocene AMS Results

The Miocene sites have high error margins in all AMS axes and are sparsely clustered on the equal area diagrams (Table 2.1; Figure 2.14). The k_{max} orientations show almost random direction patterns and they do not indicate a common direction on the regional scale (Figure 2.14). The Kırıkkale-Bala and Tuz Gölü Basins do not have Miocene results. The Alcı-Orhaniye Basin has four sites with reliable results and the indicate NE-SW to NW-SE K_{max} orientations. The k_{max} directions are highly oblique to almost perpendicular to the bedding strikes. The kmax orientations in the northwestern part of the Haymana Basin near Temelli aligned in NW-SE directions similar to the orientations of older units. However, two sites near Polatlı (west of the Haymana Basin) kmax directions are oriented E-W (Figure 2.14 and 2.15) and in the eastern part of the Haymana Basin they become NE-SW. On the other hand, k_{max} orientation at the southernmost part of the Haymana Basin indicates roughly N-S directions.

2.5.5 Pliocene AMS Results

AMS results from only 9 sites represent the Pliocene of the study area. 8 of them belongs to Haymana Basin and only one site belongs to Alcı-Orhaniye Basin. Kırıkkale-Bala and Tuzgölü basins do not have Pliocene AMS results. K_{max} in almost all sites (R3, R24, R27, R37, R51, SF4) are oriented about NNW-SSE to NNE-SSW directions except for R32 which is oriented almost ENE-WSW and two other sites (SF3 and R28) which are oriented NW-SE. In most of the sites, the bedding is almost horizontal if not bedding strike and K_{max} are oblique to each other (Figure 2.16 and 2.17; Table 2.1).

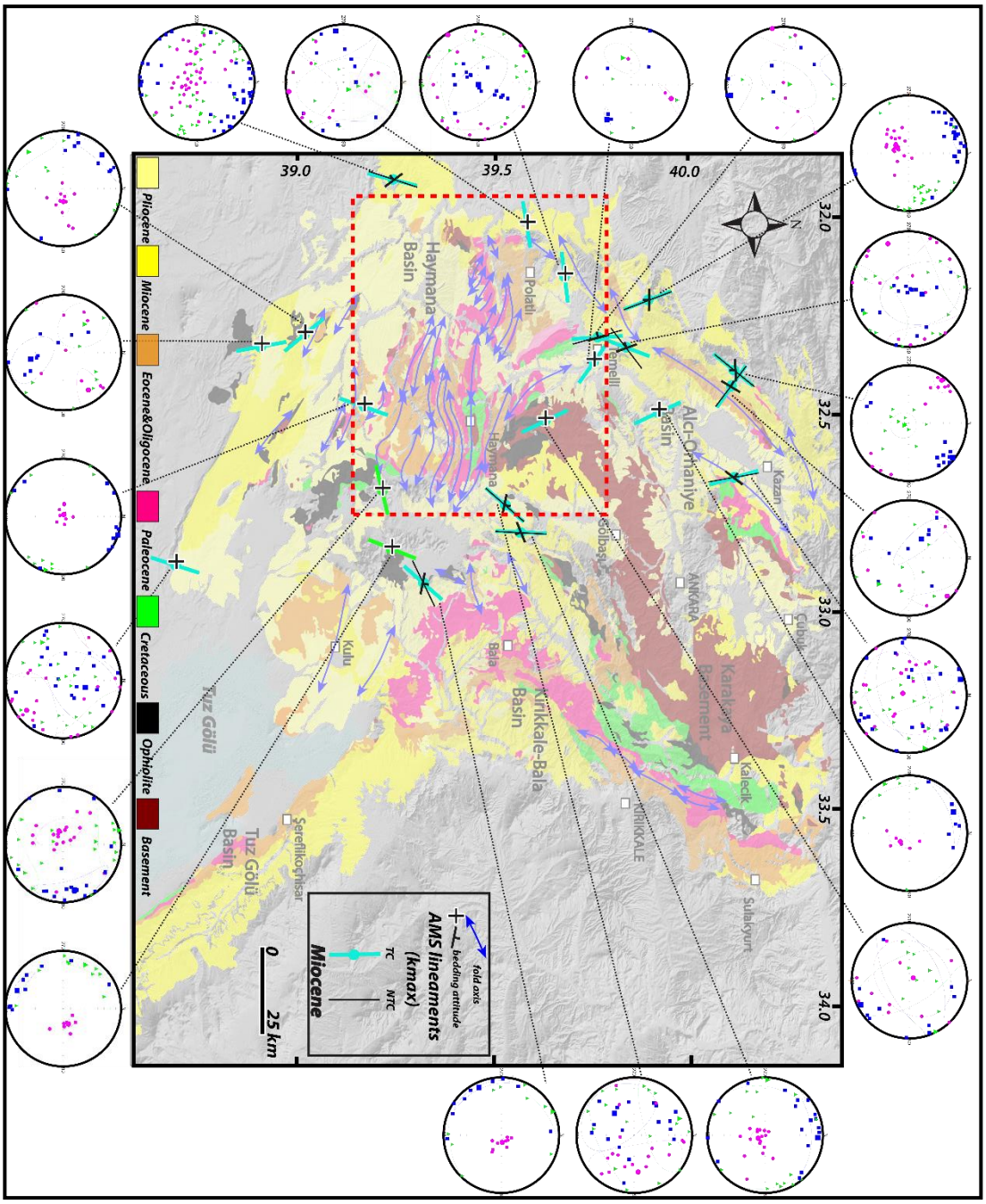

Figure 2.14. Map showing Miocene k_{max} orientations, in-situ and after tectonic correction, and the strike of the bedding planes at the site. The circles outside the map are distributions of magnetic susceptibility directions; k_{max} (blue square), k_{int} (green triangle), and k_{min} (purple circle) (equal area, lower hemisphere projection). Red dashed box is the coverage are of Figure 2.15.

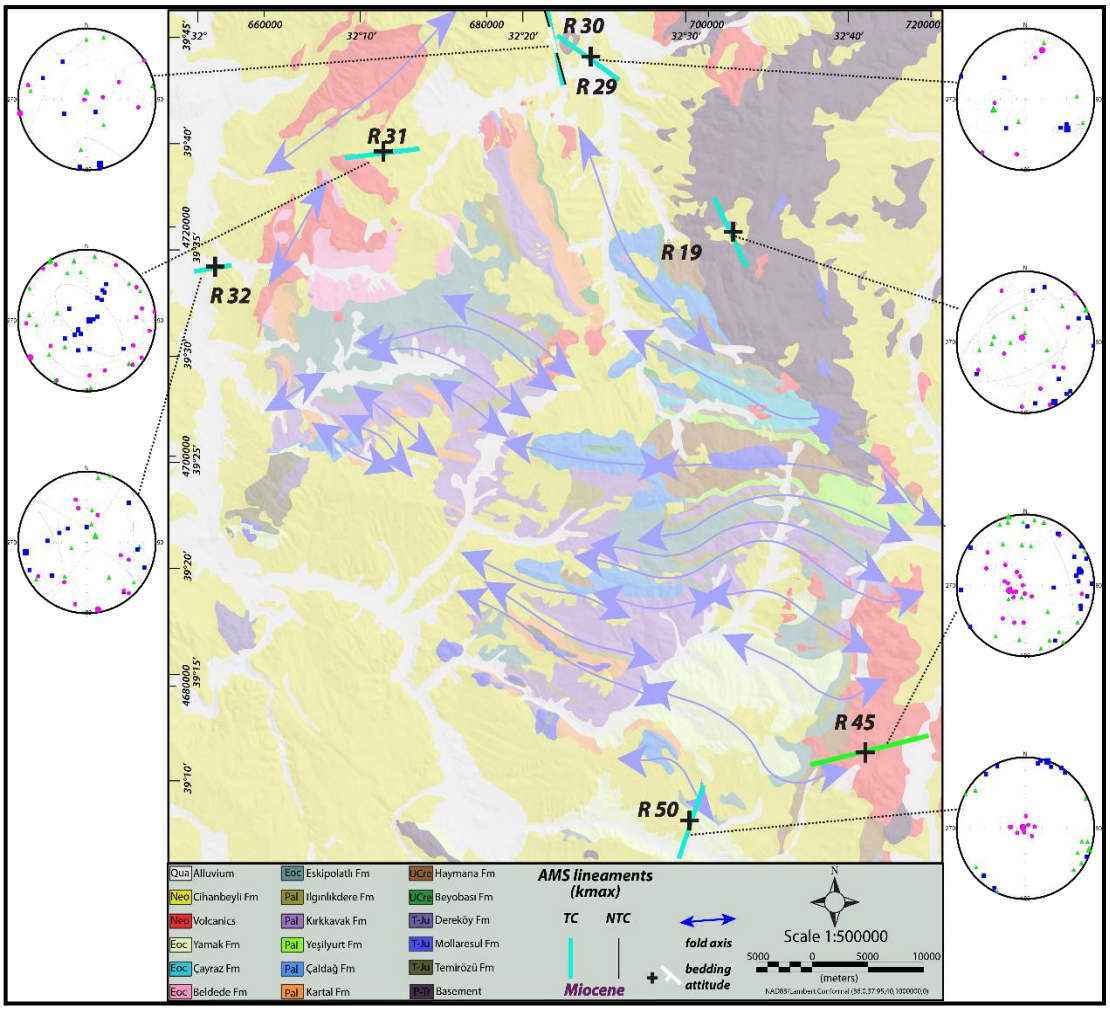

Figure 2.15. Blow up map of the Haymana Basin (see Figure 2.14 for its location) showing Miocene kmax orientations, in-situ and after tectonic correction, and the strike of the bedding planes at the site. The circles outside the map are distributions magnetic susceptibility directions; kmax (blue square), kint (green triangle), and kmin (purple circle) (equal area, lower hemisphere projection).

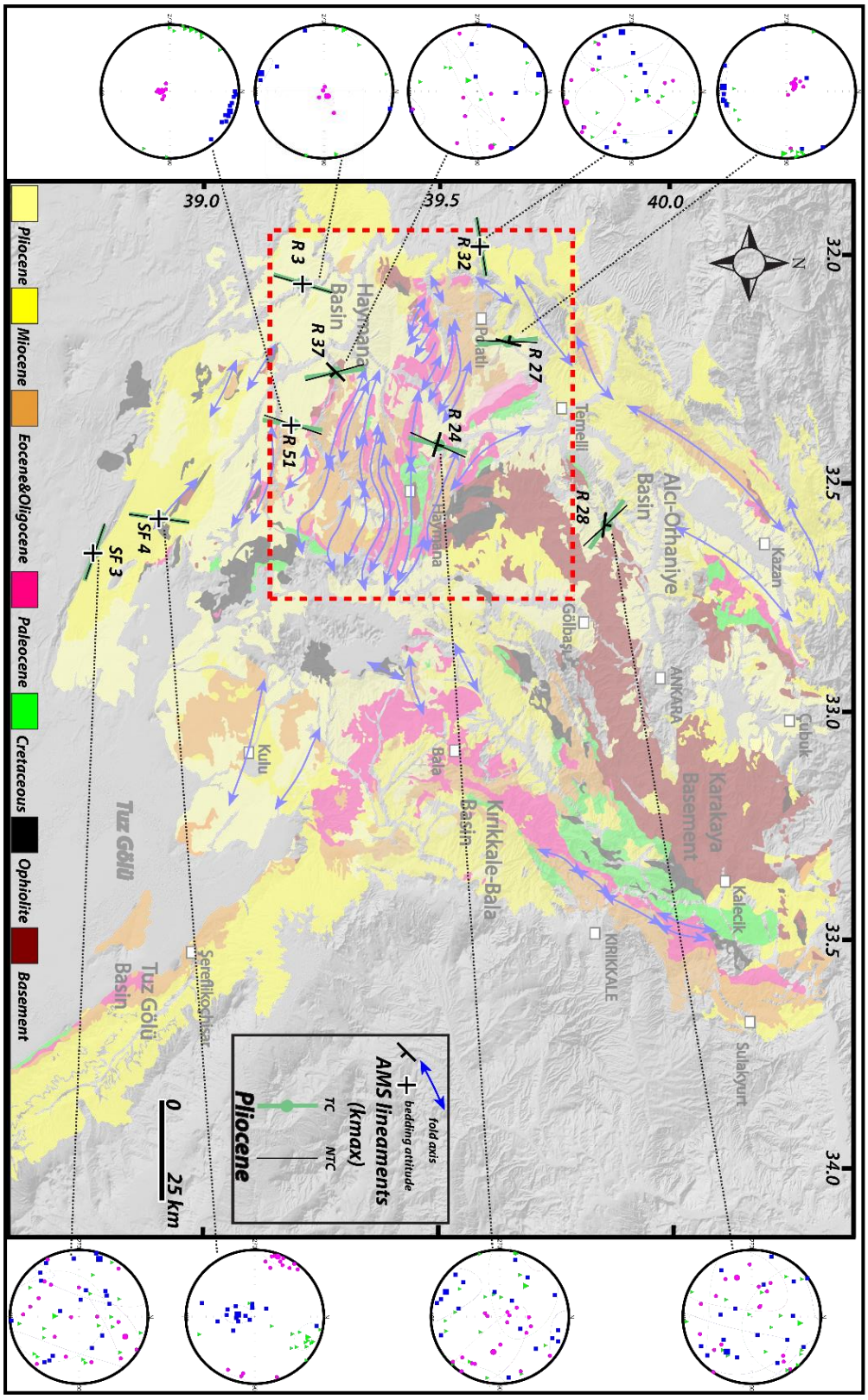

Figure 2.16. Map showing Pliocene k_{max} orientations, in-situ and after tectonic correction, and the strike of the bedding planes at the site. The circles outside the map are distributions of magnetic susceptibility directions; k_{max} (blue square), k_{int} (green triangle), and k_{min} (purple circle) (equal area, lower hemisphere projection). Red dashed box is the coverage area of Figure 2.17.

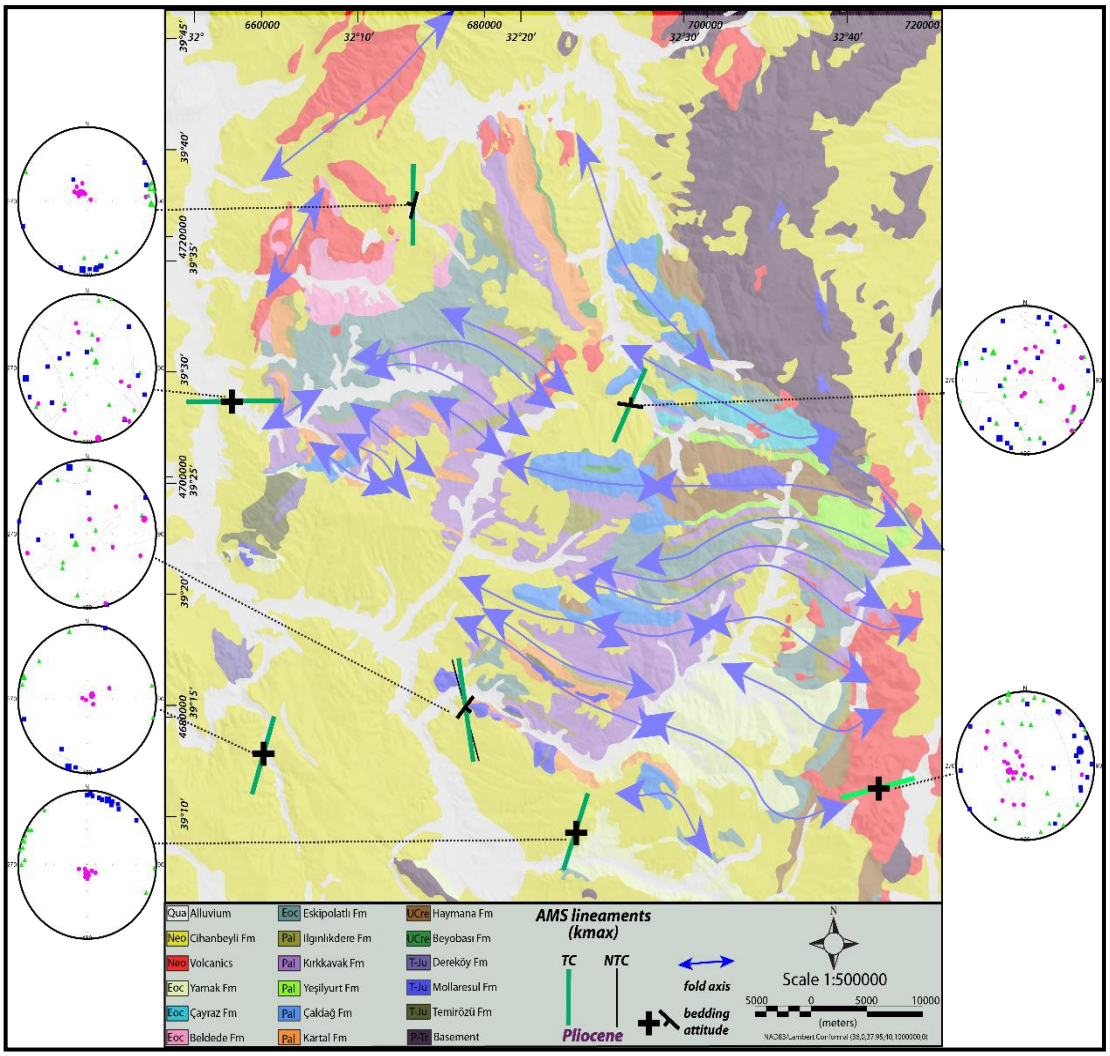

Figure 2.17. Blow up map of the Haymana Basin (see Figure 2.16 for its location) showing Pliocene kmax orientations, in-situ and after tectonic correction, and the strike of the bedding planes at the site. The circles outside the map are distributions magnetic susceptibility directions; kmax (blue square), kint (green triangle), and kmin (purple circle) (equal area, lower hemisphere projection).

2.5. Discussion

2.5.1. Tectonic Implications of AMS Results

The average AMS vectors for each basin for different time intervals is depicted Figure 2.18. As seen in the figure the late Cretaceous maximum susceptibility vectors (k_{max}) are almost parallel to the margin of the Kırıkkale-Bala while the intermediate susceptibility vector (K_{int}) is perpendicular to the basin margin. However, in Alcı-Orhaniye basin K_{max} vectors are parallel to the basin margin while

K_{int} vectors are perpendicular. In Haymana basin the K_{max} vector is almost E-W and parallel to the major structures (folding) while K_{int} vector is N-S and perpendicular to the major structures in the basin. In Tuzgölü basin the K_{max} is perpendicular to the Tuzgölü Fault while K_{int} is parallel to the fault.

In all basins the K_{min} is perpendicular to the bedding plane hence it is related to the compaction of the basin infill. Therefore, the other AMS vectors (K_{int} and K_{max}) are related to tectonic deformation in the study area. In this case, K_{int} is thought to be parallel to maximum contraction while K_{max} is parallel to the maximum extension (stretching). Based on this assumption, during the late Cretaceous, Kırıkkale-Bala and Tuzgölü basins were subjected to NW-SE contraction while Alcı-Orhaniye Basin was subjected to extension in the same direction (NW-SE) and Haymana basin was subjected to N-S contraction and E-W extension.

For Palaeocene time interval there is no information from the Tuzgölü Basin but all other basins were subjected to NE-SW contraction and NW-SE extension.

During the Eo-Oligocene time interval Kırıkkale-Bala and Alcı-Orhaniye basins were subjected to NE-SW extension and NW-SE contraction, while Haymana Basin was subjected to NNE-SSW contraction almost like in Palaeocene and late Cretaceous, however Tuzgölü basin was subjected to NE-SW contraction perpendicular to Tuzgölü Fault.

During the Miocene and Pliocene, the Kmax and Kint (extension and contraction) directions are almost parallel, the only difference took place in the western part of Haymana Basin where N-S compression in the Miocene is replaced by E-W compression. The orientation of extension and contraction directions for Miocene and Pliocene in the Alcı-Orhaniye basin is NW-SE and NE-SW respectively. The central eastern part of Haymana basin is characterized by WNW-ESE compression and ENE-WSW extension for both Miocene and Pliocene time intervals. Kırıkkale-Bala basin only has data for the Miocene time interval and it is parallel to the central and eastern part of the Haymana basin which is characterized by NE-SW extension and NW-SE contraction.

2.6. Conclusions

Analysis of AMS data from 106 sites provided important clues about the deformation styles and major strain directions in the study area since late Cretaceous. Beware that all the interpretations were based on present geographic orientations. No back rotation has been performed for clarity.

The main conclusions of this chapter are as follows;

1. Most of the AMS results are originated from tectonic deformation except for k_{min} which is almost vertical due to compaction of sedimentary rocks.

2. There is a very prominent boundary that separates the domains with similar AMS vector orientations. This boundary corresponds to Dereköy-Hirfanlı Fault Zone.

3. During the late Cretaceous Tuz Gölü and Kırıkkale-Bala basins was subjected to NE-SW extension and NW-SE contraction while Hayman Basin was subjected to NS-contraction and E-W extension. In the same time Alcı-Orhaniye Basin was subjected to NW-SE extension and NE-SW contraction.

4. Most of the AMS results are originated from tectonic deformation except for K_{min} which is almost always due to compaction of sedimentary rocks.

5. There is a very prominent boundary that separate the domains with similar AMS vector orientations. This boundary corresponds to Dereköy-Hirfanlı Fault Zone.

6. During the late Cretaceous Tuz Gölü and Kırıkkale-Bala basins was subjected to NE-SW extension and NW-SE contraction while Hayman Basin was subjected to NS-contraction and E-W extension. In the same time Alcı-Orhaniye Basin was subjected to NW-SE extension and NE-SW contraction.

7. Palaeocene time interval is characterized by NW-SE extension and NE-SW contraction. This is possibly due to regional NE-SW extension in the region.

8. Eocene-Oligocene time interval is characterized by NW-SE contraction in the north of Dereköy-Hirfanlı Fault zone during which N-S contraction in the Haymana Basin and NE-SW contraction in the Tuz Gölü Basin dominated.

9. During the Miocene and Pliocene time intervals Dereköy-Hirfanlı Fault Zone was possibly inactive and there is not much change in the contraction and extension direction in the study area except the western part of Hayman Basin where the contraction and extension directions swapped.

10. AMS results proved that they are useful in understanding the deformation styles in an area.

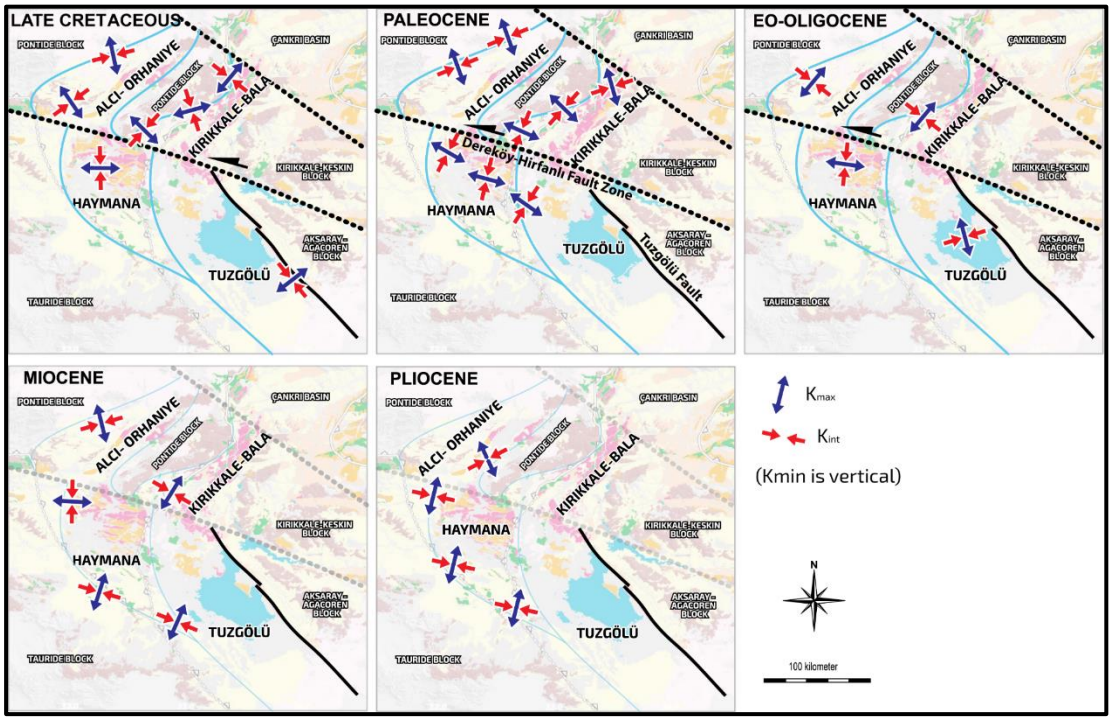

Figure 2.18. Generalized AMS results in the study area. Note that the Dereköy-Hirfanlı Fault Zone controls the deformation in the north and was active possibly during Late Cretaceous to Oligocene and it does not have any control over the Miocene and Pliocene units. Blue lines are approximate boundaries of the basins.

CHAPTER 3

LATE CRETACEOUS TO PLIOCENE VERTICAL AXIS BLOCK ROTATIONS IN NORTH CENTRAL ANATOLIA, TURKEY

3.1. Introduction

This chapter deals with the vertical axes rotations in the study area for the time period from Late Cretaceous to Pliocene. Here, the results of paleomagnetic measurements and their analysis will be presented based on their age. For this purpose, the results are classified into five time periods namely, Late Cretaceous, Paleocene, Eocene-Oligocene, Miocene, and Pliocene epochs. In addition, the results are grouped into clusters based on their spatial distribution and consistency. These spatial domains include Haymana, Alcı-Orhaniye, Kırıkkale-Bala, and Tuz Gölü basins (Figure 3.1). This does not exclude the possibility that these domains were integral parts of now disconnected a large basin complex. However, such a discussion is out of scope of this thesis.

3.2. Paleomagnetic Sampling

Total numbers of 4630 oriented cylindrical samples from 119 sites have been collected in the study area. Out of these samples, only 751 samples from 16 sites belongs to Upper Cretaceous rocks, 1354 samples from 33 sites belongs to Paleocene rocks, 1603 samples from 31 sites belongs to Eocene to Oligocene rocks, the Miocene epoch was represented by 615 samples from 26 sites, and the youngest, Pliocene, rock units are represented by 308 samples from 13 sites. In all of the 119 sites, minimum number of samples per site is 13 while maximum number of samples per site is 64. In addition to these, 648 oriented rock samples were also collected from a single site in a stratigraphic order. Almost all of the samples were collected from sedimentary rocks except for 4 sites where sampling was performed on volcanoclastic rocks (Figure 3.2 and 3.3; Table 3.1).

One site from late Cretaceous granitoids, in the Kırşehir Block, is also collected to check the coherence between cover and basement of the Tuz Gölü Basin. Usually, we obtained multiple specimens from a single core (i.e. long samples cut into 2 or 3 pieces as subsamples) which provided a chance to apply both thermal and alternating field demagnetization procedures as well as rock magnetic measurements on the same sample. It also provided means to compere single core results (AF/TH) for natural remnant magnetization directions (c.f. Gong *et al.*, 2008).

Samples were collected using handheld water cooled diamond coated drill bits, gasoline powered motor drill or with a water cooled-generator powered electric drill, depending of the rock type. Sample orientations and attitude of the bedding were measured with a magnetic compass which were corrected for present declination amounts, which is around 4.5° E for the study sampling period between 2012-14.

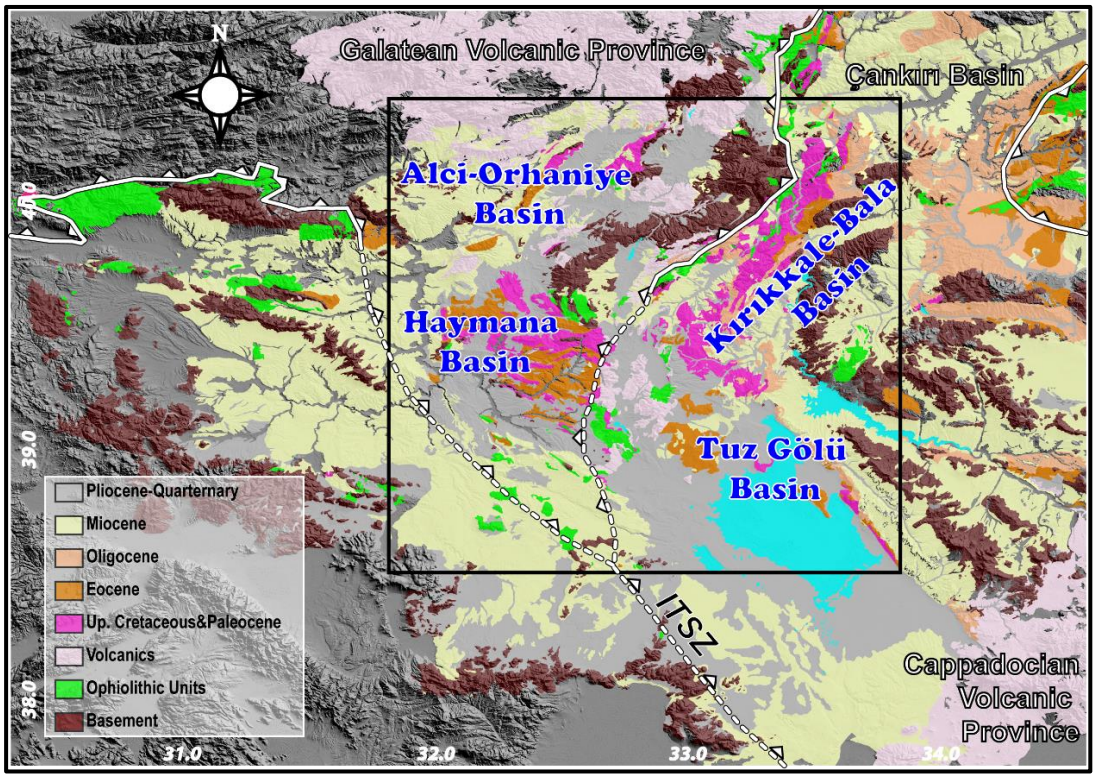

Figure 3.1. Simplified geological map of north central Anatolia. AESZ: Ankara-Erzincan Suture Zone, İASZ: İzmir-Ankara Suture Zone, ITSZ: Intra-Tauride Suture Zone. Box shows the outline of Figure 3.2.

3.3. Paleomagnetic Measurements

3.3.1. Rock Magnetic Properties

The paleomagnetic samples were measured to determine their thermomagnetic behaviors under the different temperatures following the procedure describe in Huang *et al.*, (2013). The measurements were run in air, using a modified horizontal translation type curie balance, with a sensitivity of ~5x10-9 Am2 (Mullender *et al.*, 1993) (Appendix A and B). Approximately 30-90 mg powdered samples were put into a quartz-glass sample holder and were held in place by quartz wool. Temperatures were increased in a number of heating and cooling cycles up to a maximum of 700°C. Heating and cooling rates were 10°C /min.

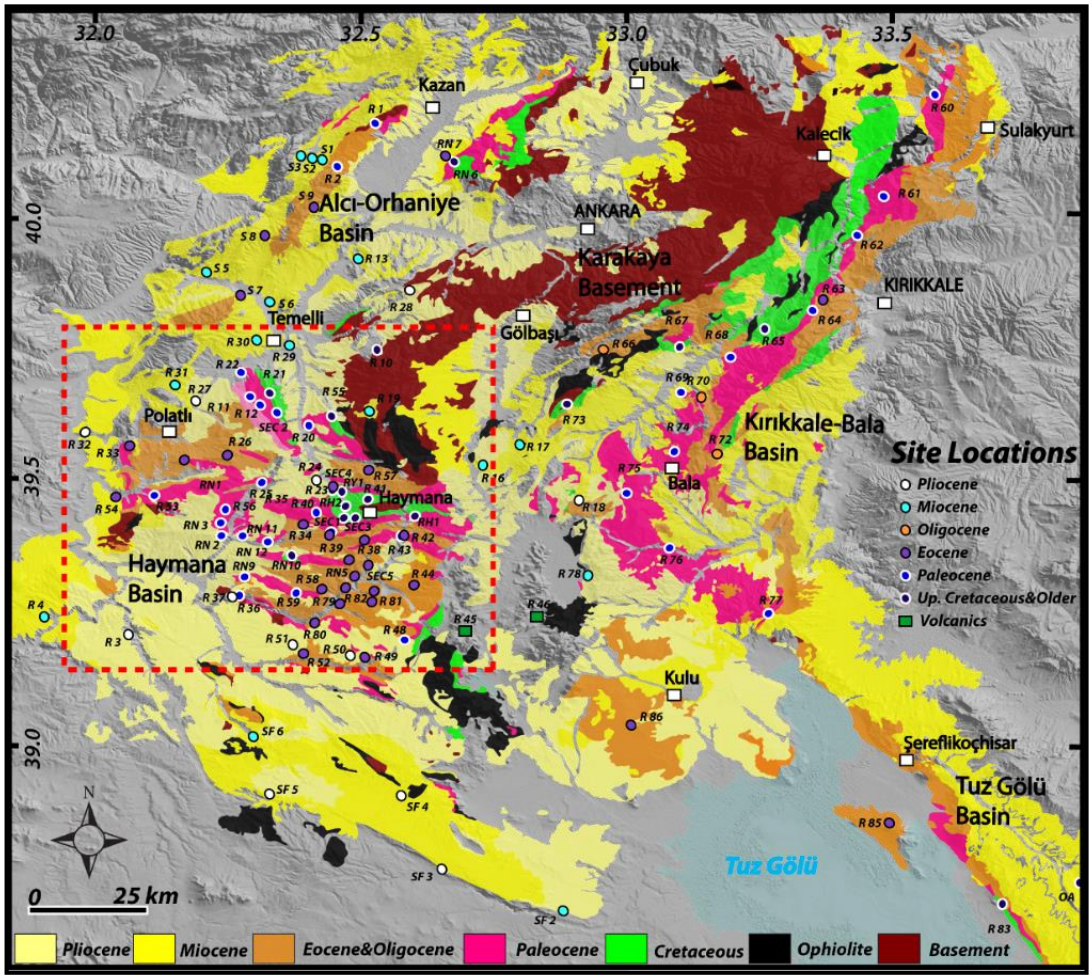

Figure 3.2. a) Simplified geological map of the study area showing the location of the paleomagnetic sites. The red dashed rectangle shows enlarged version of Haymana Basin (simplified from Ünalan *et al.*, 1976, 1/500.000 scale maps of MTA 2002).

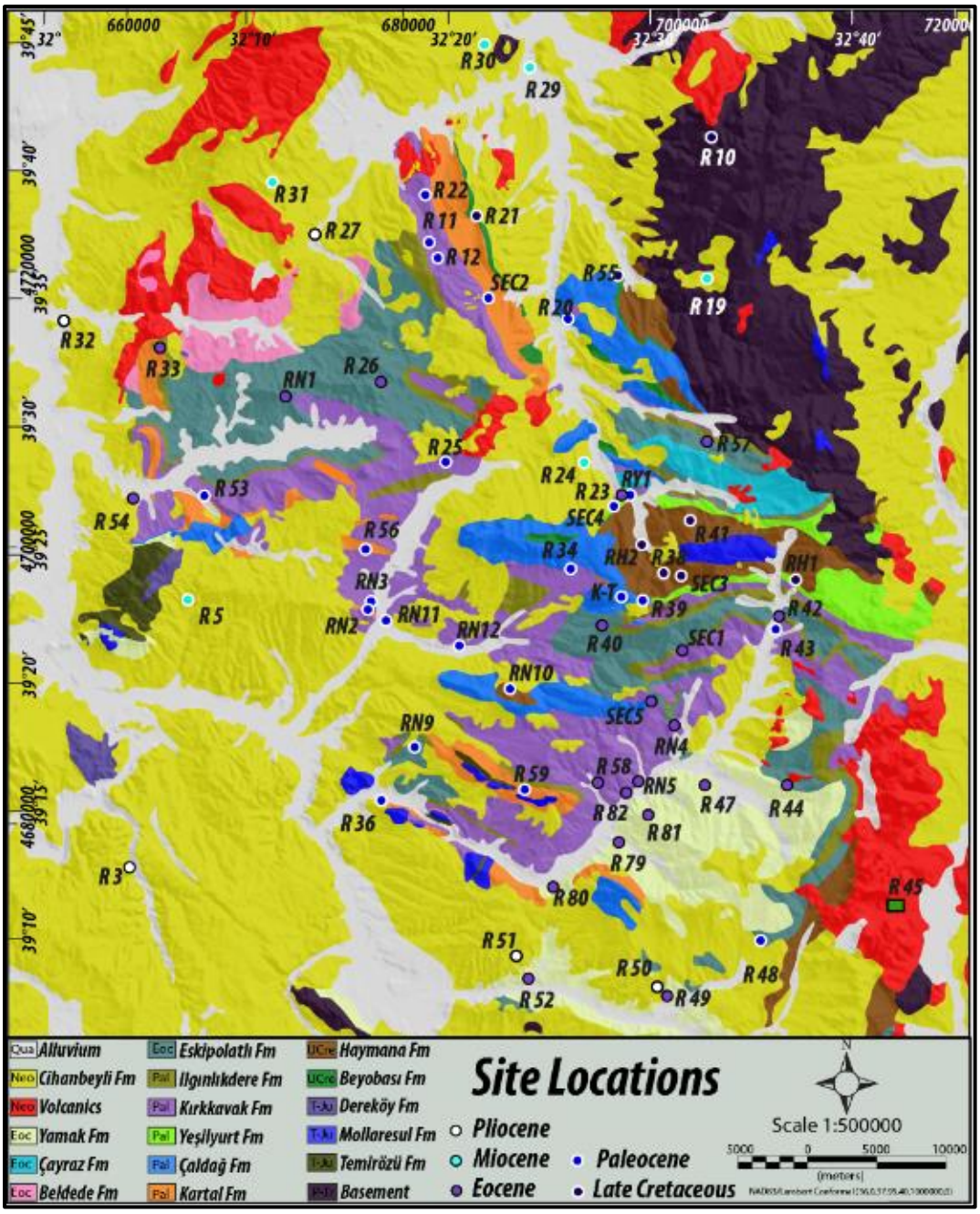

Figure 3.3 Blow up view of the Haymana Basin displaying the sample locations and local geology (simplified from Ünalan *et al.*, 1976, 1/500.000 scale maps of MTA 2002) (see Figure 3.2. for its location).

Table 3.1. Results of all measurements for vertical axis rotations.

Site	Lat.(N)	Lon.(E)	Nc	ChRM Directions (In Situ)							ChRM Directions (Tilt Corrected)										
				Nm/NvD	Dec	ΔDx	Inc	ΔIx	k	a95	Dec	ΔDx	Inc	ΔIx	k	a95	K	λ	$A95_{min}$	A95	$A95_{max}$
PLIOCENE																					
R 3	39.219	32.066	35	26/23	029.5	09.8	65.0	05.1	044.2	04.6	029.5	09.8	65.0	05.1	044.2	04.6	021.7	47.0	04.9	06.6	11.4
R 5	39.398	32.106	23	12/11	205.7	05.9	-25.4	09.9	053.6	06.3	203.4	07.5	-43.1	08.9	053.8	06.3	045.8	25.1	06.5	06.8	18.1
R 24	39.491	32.427	25	24/20	139.7	10.9	-59.8	07.2	028.5	06.2	153.5	08.5	-48.5	08.6	028.5	06.2	020.3	29.4	05.1	07.4	12.4
R 27	39.633	32.200	17	18/17	347.6	07.2	60.7	04.6	085.6	03.9	326.9	05.5	49.4	05.4	085.6	03.9	057.2	30.3	05.5	04.8	13.8
R 28	39.851	32.602	26	20/15	333.2	13.5	62.1	08.1	032.7	07.4	345.2	09.7	46.4	10.4	022.3	08.3	020.9	27.7	05.8	08.6	14.9
R 32	39.571	31.995	32	24/24	004.9	07.0	56.5	05.4	044.7	04.5	004.9	07.0	56.5	05.4	044.7	04.5	028.9	37.1	04.8	05.6	11.1
R 37	39.267	32.261	26	20/15	186.3	08.9	-45.1	09.9	023.3	08.4	202.8	10.9	-52.2	09.7	020.9	08.6	018.5	32.8	05.8	09.1	14.9
R 50	39.150	32.508	20	21/20	214.1	04.8	-56.2	03.7	124.7	02.9	214.1	04.8	-56.2	03.7	124.7	02.9	072.6	36.8	03.6	03.9	12.4
R 51	39.175	32.397	20	19/18	165.1	06.8	-38.7	08.9	036.1	05.8	165.1	06.8	-38.7	08.9	036.1	05.8	031.1	21.8	03.8	06.3	13.3
R 84	38.758	33.791	28	21/21	163.8	03.1	-49.6	03.0	209.9	02.2	163.8	03.1	-49.6	03.0	209.9	02.2	154.4	30.5	05.0	02.6	12.0
SF 1	38.722	32.818	20	14/13	005.9	07.1	42.1	08.6	043.8	06.3	005.9	07.1	42.1	08.6	043.8	06.3	041.5	24.3	04.3	06.5	16.3
SF 3	38.791	32.577	20	10/10	002.7	11.9	59.1	08.1	048.9	07.0	002.7	11.9	59.1	08.1	048.9	07.0	029.4	39.9	04.8	09.1	19.2
SF 4	38.897	32.603	16	16/15	035.5	04.7	35.3	06.7	058.9	05.0	035.5	04.7	35.3	06.7	058.9	05.0	074.9	19.5	04.1	04.4	14.9
MIOCENE																					
R 4	39.228	31.909	46	34/29	337.2	07.4	51.5	06.7	023.8	05.6	319.7	07.0	52.9	06.1	025.3	05.4	022.0	33.5	04.4	05.8	09.8
R 13*	39.904	32.503	22	18/18	001.6	07.9	57.6	05.8	059.9	04.5	-		-				032.2	38.3	05.3	06.2	13.3
R 14	39.691	32.681	14	08/00	-		-				-		-								
R 15	39.597	32.667	28	10/00	-		-				-		-								
R 16	39.504	32.747	29	18/16	211.2	07.2	-49.7	07.0	043.1	05.7	207.5	05.5	-37.2	07.5	043.1	05.7	052.2	20.8	04.0	05.2	14.3
R 17	39.554	32.821	21	18/17	022.2	05.7	50.9	05.3	078.9	04.0	055.5	07.8	63.2	04.5	079.1	04.0	042.4	44.7	03.9	05.5	13.8
R 18	39.441	32.937	33	20/19	341.1	11.3	56.7	08.6	022.7	07.2	344.5	09.0	43.4	10.5	019.9	07.7	018.0	25.3	05.2	08.1	12.8
R 19	39.615	32.525	27	20/18	199.9	07.4	-49.4	07.2	036.0	05.8	199.9	07.4	-49.4	07.2	036.0	05.8	030.4	30.2	03.8	06.4	13.3
R 29	39.737	32.374	18	17/14	330.3	08.6	49.1	08.5	041.2	06.3	330.3	08.6	49.1	08.5	041.2	06.3	029.6	30.0	05.9	07.4	15.6
R 30	39.755	32.324	19	19/15	169.5	13.1	-49.0	13.0	015.7	10.0	134.9	10.4	-40.9	13.0	015.7	09.9	016.9	23.4	05.8	09.6	14.9
R 31	39.665	32.166	34	20/20	349.8	04.6	51.8	04.1	106.2	03.2	349.8	04.6	51.8	04.1	106.2	03.2	072.6	32.4	05.1	03.9	12.4
R 45*	39.209	32.703	34	23/21	198.9	05.1	-44.0	05.9	042.8	04.9	198.9	05.1	-44.0	05.9	042.8	04.9	048.4	25.8	05.0	04.6	12.0
R 46*	39.218	32.859	24	21/21	006.0	04.1	51.0	03.8	099.5	03.2	006.0	04.1	51.0	03.8	099.5	03.2	084.5	31.7	05.0	03.5	12.0
R 71	39.560	33.309	18	17/14	359.1	13.8	55.2	11.0	022.9	08.5	008.0	17.8	63.7	09.9	022.9	08.5	011.2	45.3	05.9	12.4	15.6
R 78	39.311	32.940	20	15/00	-		-				-		-								
RN 7	40.101	32.676	19	21/21	343.7	20.4	74.7	05.8	029.4	06.0	319.9	07.1	44.0	08.2	029.5	06.0	025.4	25.7	03.6	06.4	12.0
RN 8	39.597	32.667	13	11/10	353.4	06.2	44.7	07.0	093.7	05.0	346.7	08.4	56.6	06.4	093.7	05.0	053.1	37.1	04.8	06.7	19.2

S 1	40.093	32.438	24	20/20	347.3	09.2	59.2	06.3	040.7	05.2	332.6	06.5	45.0	07.3	040.7	05.2	032.4	26.6	05.1	05.8	12.4
S 2	40.095	32.426	3	-	-	-	-	-	-	-											
S 3	40.106	32.402	27	20/19	357.6	06.1	52.0	05.5	062.4	04.3	358.3	16.0	75.0	04.5	062.4	04.3	021.0	61.8	05.2	07.5	12.8
S 4	39.994	32.284	24	14/12	339.8	17.2	55.1	13.8	018.7	10.8	322.9	11.0	33.3	16.2	015.2	11.5	018.2	18.2	06.3	10.4	17.1
S 5	39.878	32.224	28	20/14	157.7	08.0	-18.6	14.6	018.1	09.6	151.6	10.5	-40.1	13.3	018.1	09.6	017.9	22.9	05.9	09.7	15.6
S 6	39.818	32.336	39	20/20	354.3	05.0	51.7	04.6	079.0	03.7	303.3	04.2	41.5	05.2	079.0	03.7	071.9	23.9	05.1	03.9	12.4
SF 2	38.640	32.856	20	16/10	027.4	20.9	48.9	20.7	011.7	14.8	-		-				008.1	29.8	04.8	18.0	19.2
SF 5	38.891	32.334	15	12/05	300.4	32.2	48.5	32.0	009.8	25.7	-		-				008.6	29.5	06.3	27.7	29.7
SF 6	38.983	32.340	16	14/14	002.5	08.8	54.6	07.2	048.6	05.8	-		-				031.9	35.1	04.2	07.2	15.6
EOCENE-OLIGOCENE																					
R 23	39.473	32.461	16	16/00	-		-				-		-								
R 26	39.537	32.247	29	21/21	002.1	07.7	61.9	04.7	068.1	03.9	150.5	03.5	-22.2	06.1	068.1	03.9	086.4	11.5	03.6	03.4	12.0
R 33	39.554	32.071	17	17/17	358.0	04.7	57.8	03.4	185.1	02.7	016.3	04.2	18.2	07.6	055.5	04.8	076.0	09.3	05.5	04.1	13.8
R 35	39.400	32.404	25	22/22	252.7	11.4	73.2	03.7	077.5	03.5	287.5	06.3	61.5	03.9	077.5	03.5	045.6	42.7	04.9	04.6	11.7
R 40	39.388	32.450	27	24/24	110.6	07.2	-40.7	09.0	036.5	05.8	296.3	04.6	57.7	03.4	113.4	02.8	067.1	38.3	04.8	03.6	11.1
R 42	39.394	32.598	23	21/13	048.9	08.7	-31.1	13.3	025.7	08.3	052.1	09.5	38.8	12.4	025.7	08.3	023.3	21.9	06.1	08.8	16.3
R 44	39.290	32.614	26	21/21	315.8	06.0	-03.6	12.0	018.8	07.5	283.0	07.8	-38.9	10.1	020.6	07.2	020.5	22.0	05.0	07.2	12.0
R 47	39.285	32.545	27	21/21	356.4	06.0	52.9	05.2	061.1	04.1	028.3	09.2	65.0	04.8	061.1	04.1	026.9	47.0	05.0	06.2	12.0
R 49	39.148	32.516	23	20/20	357.5	11.7	68.3	05.1	049.9	04.7	027.6	04.9	37.8	06.5	048.1	04.8	052.3	21.2	03.6	04.6	12.4
R 52	39.155	32.403	28	21/20	008.0	08.8	56.8	06.6	033.2	05.6	215.1	05.9	-38.3	07.8	033.2	05.6	034.3	21.6	03.6	05.5	12.0
R 54	39.461	32.051	17	17/11	045.6	10.2	46.8	10.9	023.7	09.6	038.2	11.6	53.4	09.9	023.7	09.6	023.6	33.9	04.6	09.6	18.1
R 57	39.511	32.526	19	19/17	355.7	11.5	60.8	07.3	031.5	06.5	232.6	11.2	59.0	07.7	031.5	06.5	018.2	39.8	05.5	08.6	13.8
R 58	39.283	32.452	18	18/17	322.3	10.1	48.1	10.3	021.7	07.8	337.2	10.6	49.3	10.4	021.7	07.8	016.2	30.2	05.5	09.1	13.8
R 63	39.822	33.390	16	16/14	344.3	04.9	30.7	07.6	049.3	05.5	095.4	11.1	65.1	05.8	049.5	05.7	028.6	47.1	05.9	07.6	15.6
R 66	39.739	32.981	15	15/13	231.4	05.2	-44.1	05.9	073.7	04.9	202.5	08.4	-61.5	05.2	073.9	04.9	046.1	42.6	06.1	06.2	16.3
R 70	39.648	33.156	21	15/15	084.3	07.1	12.4	13.6	023.9	08.0	072.4	11.1	49.3	10.9	023.9	08.0	017.0	30.1	05.8	09.5	14.9
R 72	39.541	33.195	21	20/18	166.5	06.5	-58.1	04.6	050.1	04.8	280.1	07.1	-66.5	03.4	115.0	03.2	056.1	49.1	03.8	04.7	13.3
R 79	39.247	32.474	17	17/17	015.5	04.1	28.6	06.6	080.4	04.0	036.6	08.3	63.3	04.7	080.8	04.0	038.1	44.8	03.9	05.9	13.8
R 80	39.219	32.425	11	13/13	315.0	20.6	71.3	07.4	034.4	06.9	254.1	07.6	-39.7	09.7	034.5	07.2	036.2	22.6	04.3	07.0	16.3
R 81	39.263	32.495	14	13/13	023.3	11.5	62.2	06.9	052.4	05.8	038.0	07.4	46.2	08.0	052.4	05.8	040.8	27.5	06.1	06.6	16.3
R 82	39.275	32.474	20	20/20	317.8	06.3	43.8	07.3	030.6	06.0	333.6	05.9	39.5	07.6	030.6	06.0	036.6	22.4	05.1	05.5	12.4
R 85	38.842	33.514	27	21/20	341.7	07.5	53.4	06.4	030.0	06.1	326.7	10.2	62.6	06.0	030.0	06.1	020.8	44.0	05.1	07.3	12.4
R 86	39.021	33.028	13	13/11	348.9	08.4	50.4	08.0	055.4	06.2	304.2	15.0	67.6	06.8	055.4	06.2	024.3	50.5	04.6	09.5	18.1
S 7*	39.840	32.284	23	20/16	190.7	05.7	-48.6	05.7	062.2	04.4	206.3	04.4	-23.2	07.6	056.1	05.0	074.2	12.1	05.6	04.3	14.3
S 8	39.946	32.332	27	20/10	217.2	07.8	-18.4	14.2	074.3	08.9	203.6	07.6	-32.1	11.4	074.3	08.9	112.5	17.4	08.9	07.2	29.7
S 9	39.994	32.418	24	20/17	355.9	09.8	52.1	08.7	026.7	07.0	060.8	10.9	55.5	08.6	026.7	07.0	017.4	36.0	05.5	08.8	13.8

SEC 1	39.376	32.524	610	106/80	125.5	04.2	-38.6	05.5	018.7	03.8	125.5	04.2	-38.6	05.5	018.7	03.8	017.4	21.7	02.1	03.9	05.2
SEC 5	39.336	32.498	396	46/46	052.9	06.6	53.1	05.7	021.4	04.6	052.9	06.6	53.1	05.7	021.4	04.6	015.7	33.6	02.6	05.5	07.3
RN 1	39.529	32.178	19	21/00	-		-				-		-								
RN 4	39.326	32.515	18	21/21	330.6	07.3	69.5	03.0	156.0	02.6	031.4	02.1	34.7	03.0	181.3	02.4	251.4	19.1	05.0	02.0	12.0
RN 5	39.281	32.484	16	21/20	332.4	05.2	54.7	04.3	094.3	03.4	001.1	04.7	48.5	04.8	094.3	03.4	063.8	29.5	05.1	04.1	12.4
PALEOCENE																					
R 1	40.165	32.539	56	34 /30	077.3	08.1	63.6	04.5	039.0	04.3	082.0	05.3	52.0	04.8	041.3	04.1	035.2	32.6	03.1	04.5	09.6
R 2	40.090	32.468	30	26/25	015.5	07.7	46.8	08.1	021.1	06.5	035.4	10.3	58.9	07.2	021.1	06.5	014.3	39.6	04.7	07.9	10.8
R 11	39.633	32.293	24	18/16	009.6	07.9	61.3	04.9	080.0	04.1	301.2	07.9	61.6	04.9	080.0	04.1	041.7	42.7	05.6	05.8	14.3
R 12	39.626	32.301	27	18/18	318.6	10.8	56.8	08.1	024.3	07.2	292.7	07.7	50.0	07.4	024.3	07.2	028.1	30.8	05.3	06.6	13.3
R 20	39.585	32.412	30	20/11	098.8	07.3	-30.1	11.3	034.4	07.5	125.8	09.7	-46.4	10.5	031.5	08.3	029.1	27.7	06.5	08.6	18.1
R 22	39.666	32.290	24	18/16	134.3	05.2	-25.8	08.7	049.8	05.3	127.9	04.6	-16.2	08.5	049.8	05.3	067.4	08.3	05.6	04.5	14.3
R 25	39.487	32.313	18	18/18	110.6	07.2	-40.7	09.0	036.5	05.8	129.4	05.4	-20.9	09.6	036.5	05.8	043.4	10.8	05.3	05.3	13.3
R 34	39.423	32.425	20	19/16	330.9	03.6	38.8	04.7	143.9	03.1	324.4	05.9	60.2	03.9	143.7	03.1	069.3	41.1	04.0	04.5	14.3
R 36	39.268	32.272	26	20/20	192.2	05.7	-47.7	05.8	047.7	04.8	252.1	08.0	-56.6	06.1	047.7	04.8	027.1	37.2	03.6	06.4	12.4
R 39	39.404	32.478	21	20/11	331.6	15.0	39.1	19.5	010.1	15.1	224.1	14.1	48.3	14.3	019.4	11.3	016.5	29.3	04.8	12.3	19.2
R 43	39.387	32.596	16	15/14	009.6	07.6	64.9	04.0	132.6	03.5	205.8	22.0	80.9	03.6	132.6	03.5	037.2	72.1	05.9	06.6	15.6
R 48	39.182	32.593	24	21/15	241.4	10.4	-27.3	16.9	009.6	12.5	229.4	15.9	-52.6	13.9	011.0	12.1	009.3	33.2	05.8	13.2	12.0
R 53	39.459	32.119	25	21/21	031.5	13.6	68.2	06.0	036.4	05.3	033.4	05.8	35.2	08.2	036.4	05.3	035.1	19.4	03.6	05.4	12.0
R 56	39.431	32.250	20	23/23	355.7	11.5	60.8	07.3	031.5	06.5	162.4	05.2	-39.3	06.7	039.8	04.9	041.0	22.2	03.4	04.8	11.4
R 59	39.277	32.394	23	21/17	022.1	10.0	45.6	10.9	018.8	07.7	061.2	18.5	68.2	08.1	024.7	07.3	010.7	51.4	05.5	11.4	13.8
R 60	40.196	33.603	15	15/14	148.9	24.9	-69.2	10.2	021.4	09.2	122.3	11.4	-46.3	12.3	021.9	08.7	016.5	27.6	05.9	10.1	15.6
R 61	40.031	33.517	17	16/16	329.0	06.5	61.2	04.1	100.4	03.7	046.1	03.5	26.9	05.7	100.3	03.7	120.5	14.2	04.0	03.4	14.3
R 62	39.951	33.456	17	16/12	327.2	09.7	49.2	09.5	037.1	07.2	056.0	07.9	36.5	10.8	032.2	07.8	035.6	20.3	04.4	07.4	17.1
R 64	39.812	33.373	18	18/17	040.5	04.5	15.8	08.4	065.4	04.6	004.3	05.2	49.5	05.1	069.4	04.3	063.8	30.3	05.5	04.5	13.8
R 68	39.718	33.216	20	20/20	120.5	06.7	15.5	12.5	015.7	08.5	044.5	07.8	44.9	08.7	029.9	06.1	023.0	26.5	03.6	07.0	12.4
R 69	39.651	33.137	21	19/19	019.2	05.7	64.5	03.1	159.7	02.7	071.5	03.7	52.4	03.3	159.7	02.7	120.0	33.0	05.2	03.1	12.8
R 74	39.548	33.119	16	15/15	344.2	07.1	50.3	06.7	054.1	05.2	324.2	04.9	37.3	06.6	054.1	05.2	071.7	20.9	05.8	04.5	14.9
R 75	39.470	33.018	17	17/16	129.7	19.6	72.8	06.4	036.6	06.2	232.6	09.8	53.1	08.5	036.6	06.2	021.4	33.6	05.6	08.2	14.3
R 76	39.363	33.091	22	22/22	348.7	05.6	49.3	05.5	059.8	04.0	353.5	04.6	37.3	06.2	059.8	04.0	052.7	20.9	04.9	04.3	11.7
R 77	39.244	33.302	25	18/18	339.7	13.5	70.0	05.3	047.3	05.1	077.2	06.1	46.3	06.6	047.3	05.1	042.2	27.6	03.8	05.4	13.3
SEC2	39.595	32.345	648	208/196	314.1	05.5	56.0	04.2	022.7	03.6	314.1	05.5	56.0	04.2	022.7	03.6	015.5	36.6	03.1	04.4	05.5
RN2	39.389	32.258	14	14/08	075.1	22.9	22.6	39.8	004.6	29.2	216.7	19.1	-40.7	23.8	010.9	17.6	011.0	23.3	05.2	17.5	22.1
RN3	39.393	32.261	13	20/18	116.5	15.5	48.6	15.6	008.7	12.4	135.8	15.9	-47.1	16.7	010.4	11.6	007.5	28.3	03.9	14.0	13.8
RN9	39.302	32.298	22	20/20	353.4	15.9	72.2	05.4	045.3	05.0	203.6	06.2	-35.9	08.7	031.0	06.0	031.9	19.9	03.6	05.9	12.4
RN10	39.341	32.375	20	19/10	359.3	15.0	57.8	10.8	033.5	09.0	055.5	24.3	61.6	14.8	013.1	13.9	008.5	42.8	04.8	17.6	19.2

RN11	39.383	32.268	20	20/20	130.6	04.3	-33.1	06.4	044.1	05.0	117.0	05.8	-43.8	06.7	044.1	05.0	039.6	25.6	03.6	05.3	12.4
RN12	39.366	32.329	25	17/17	015.1	10.5	58.6	07.4	035.1	06.1	026.3	07.0	35.6	09.9	035.1	06.1	030.0	19.7	03.9	06.6	13.8
K-T	39.406	32.465	20	20/20	293.8	13.2	41.6	16.1	023.0	11.8	236.6	17.3	51.6	15.7	017.9	12.5	013.5	32.3	07.1	14.5	20.5
OLDER & LATE CRETACEOUS																					
R 21	39.649	32.339	28	020/018	356.4	06.8	51.8	06.2	056.8	04.8	309.4	09.3	55.9	07.2	030.6	06.4	022.5	36.5	05.3	07.5	13.3
R 38	39.423	32.498	24	020/020	344.0	07.3	50.8	06.8	041.4	05.1	299.8	07.1	55.1	05.8	048.3	04.7	032.6	35.6	05.1	05.8	12.4
R 41	39.457	32.518	22	022/021	143.4	11.8	-73.0	03.9	057.1	04.2	148.9	04.6	-48.5	04.6	093.1	03.3	064.6	29.4	05.0	04.0	12.0
R 55	39.614	32.454	26	021/021	023.8	04.5	50.3	04.3	089.0	03.2	321.3	05.4	50.0	05.2	064.4	04.0	048.2	30.8	05.0	04.6	12.0
R 65	39.762	33.270	27	021/021	346.0	06.4	42.3	07.7	028.9	05.9	074.0	07.8	46.2	08.4	028.9	05.9	021.0	27.5	04.9	06.9	11.7
R 67	39.751	33.134	25	021/021	001.0	03.1	58.8	02.1	267.1	01.9	352.0	04.8	68.9	02.0	267.1	01.9	120.1	52.4	05.0	02.9	12.0
R 73	39.632	32.918	17	017/010	175.4	10.7	-19.2	19.3	015.5	12.7	242.3	14.4	-41.9	17.5	015.5	12.7	014.5	24.1	06.8	13.1	19.2
R 83	38.684	33.736	33	021/021	353.8	06.7	58.8	04.6	081.4	03.5	014.3	04.1	42.4	05.0	081.4	03.5	072.2	24.6	05.0	03.8	12.0
RH 1	39.416	32.612	45	024/024	338.9	05.5	44.5	06.2	041.8	04.6	281.7	06.5	49.9	06.3	041.8	04.6	028.6	30.7	04.8	05.6	11.1
RH 2	39.440	32.484	57	026/025	014.7	24.7	77.3	05.7	029.1	05.7	329.4	05.4	28.5	08.6	022.7	06.2	032.2	15.2	04.7	05.2	10.8
RY 1	39.469	32.470	60	022/022	236.0	29.8	79.8	05.3	034.9	05.5	323.7	05.3	27.4	08.7	031.3	05.6	037.0	14.5	04.9	05.2	11.7
SEC3	39.420	32.511	266	283/266	282.2	03.0	60.3	02.0	024.9	01.8	282.2	03.0	60.3	02.0	024.9	01.8	015.5	41.3	01.3	02.3	02.4
SEC4	39.466	32.459	64	035/014	337.1	04.6	17.6	08.5	058.1	05.3	337.1	04.6	17.6	08.5	058.1	05.3	076.2	09.0	05.9	04.6	15.6
RN6	40.091	32.683	20	021/021	244.8	08.4	-53.5	07.2	034.2	05.4	184.2	04.6	-34.4	06.6	034.2	05.4	051.7	18.9	03.5	04.4	11.7
GRANITE																					
OA	38.676	33.983	20	020/007	151.5	18.9	-58.4	13.2	032.0	10.8	151.5	18.9	-58.4	13.2	032.0	10.8	018.2	39.1	07.8	14.5	24.1
TRIASSIC																					
R 10	39.708	32.527	17	017/016	094.0	18.0	67.7	08.1	025.6	08.0	028.5	09.4	49.5	09.2	021.7	08.4	023.2	30.3	05.8	08.1	14.9

*: Volcanic samples, Nc: number of collected sample for each site, Nm: number of demagnetized specimens, NvD: number of specimens included in the calculation for the mean ChRM direction after applying Vandamme cut-off, Dec/I: declination / inclination, ΔDx / (ΔIx): errors in declination / (inclination) determined from the A95 of the poles, k: estimate of the precision parameter determined from the ChRM directions, a95: cone of confidence determined from the mean ChRM directions for in situ and tilt corrected data, K: precision parameter determined from the mean virtual geomagnetic pole directions (VGPs), λ: paleolatitude, A95: cone of confidence determined from the mean VGP direction, $A95_{min}$ / ($A95_{max}$) : minimum / (maximum) value of the A95 for the given dataset based on (Deneen *et al.* 2011, 2014).

Figure 3.4 illustrates 18 representative examples of thermomagnetic experiment results for Upper Cretaceous to Paleocene rock units in the central Anatolia (Appendix A). Thermomagnetic analysis of 18 sites underwent alteration of iron sulphite, transforming above ~400°C to a more magnetic phases from pyrrhotite to magnetite around 580°C and finally above 580-650°C, to hematite (Figure 3.4).

The results show that the samples have various magnetic carriers in each site and a few sites have weak or scarcely distributed magnetic minerals in it (Appendix A). As seen in the thermomagnetic diagrams, we computed total magnetization in a series of runs to increasingly higher temperatures (up to 700°C). Individual data points have been omitted for clarity. Cycling field varied between 150 and 300 mT. In general, pale color marl, silt and limestone samples show very weak magnetization (saturation of remanence) (sites; R10, R20, R34, RN10). The majority of the samples have a reasonable amount of magnetic mineral compositions in them. For example; some samples show a reversible behavior during the heating-cooling cycle (decrease in magnetization with increasing temperature up to ~410°C) that is typical greigite dominant matrix (sites; R38, R53, R55, R60, R65, RH1 and RH2) (Figure 3.4 and Appendix A).

Some samples have reversible smooth decrease in a magnetization between 100–400°C continue with a sharp decline in intensity between 400 - 600°C, which is characteristic for low Ti-Magnetite (sites; R11, R22, R41, R73, SEC2) (Figure 3.4 and Appendix 3.1). Hematite dominant matrix shows smooth decline in the intensity between 20 - 580 °C and meaning fully large enough for paleomagnetic interpretations (sites; R12, R62, R64, R77, R83, SEC3) (Figure 3.4 and Appendix A).

In some sites reversible curves have low intensity values but decreasing up to 650 °C indicate that the hematite mineral is the magnetic carrier (sites; R56, R59, R68, RN2, RN3, RN11) which is characteristic with their red color in the field (Figure 3.4 and Appendix A). The heating curves of some sites show an abrupt decrease in intensity between 20 - 100 °C which can be due to the existence of the goethite, an iron oxyhydroxide mineral.

Most of the sites, apart from some pale color marls and limestone samples, have suitable magnetic bearing mineral composition such as magnetite, ti-magnetite, hematite, pyrrhotite, greigite, etc. (Figure 3.4). Characteristic maximum blocking temperature for the magnetite ~ 580°C or maximum blocking under the magnetic field of 60-100 mT were selected to determine the ChRM direction. For few sites, demagnetization steps go up to 680°C, indicating typical maximum blocking temperature for hematite bearing samples. Some samples show low blocking temperatures around 340 - 475°C and magnetic field between 25-45 mT. This implies that the remanence is mainly carried by greigite (Roberts, 1995; Vasiliev *et al.*, 2008; Rowan *et al.*, 2009).

18 thermomagnetic results belong to the youngest rocks that span between Eocene to Pliocene (Figure 3.5). Here, at least one thermomagnetic measurements were performed for each site and the results are given in Appendix B.

At the NE part of the study area, in the Kırıkkale-Bala Basin; we measured high initial magnetization intensities (total magnetization, 2- $3x10^{-5}$ Am^2 /mg) from the Eocene sedimentary rocks (R17, R66, and R70) (Figure 3.5). Representative specimens show an irreversible decrease in magnetization around 530-580°C, implying the existence of magnetite as magnetic carrier in the sites R66 and R70. At site R17, initial intensity is low ($1.2x10^{-6}$ Am^2 /mg) compared to the other two sites but the show irreversible decreases again around 580°C indicating that magnetite as magnetic carrier for Miocene deposits in the site.

The Tuz Gölü Basin is represented by three thermomagnetic samples from the sites R18 (Miocene), R84 and R86 (both are Eocene) (Figure 3.5). The Eocene sites have high initially intensities (3-$20x10^{-6}Am^2$ /mg) while Miocene site (R18) shows low initially intensity ($5x10^{-7}$ Am^2 /mg) similar to results from the Miocene samples in the Kırıkkkale- Bala Basin.

Two thermomagnetic experiments from Miocene volcanic and sedimentary units and one andesitic rock from the Eocene in the northwestern part of the study area, in the Alcı-Orhaniye Basin, indicate that the Eocene site (sample S7.13C) shows a progressive quasireversible decrease up to ~640°C, followed by a more rapid

decrease up to 700°C so the dominate magnetic carrier is hematite. The last two Miocene sites (R13 and R31); one is volcanic (R13) indicate high initial intensity up to $3x10^{-5}$ Am^2 /mg and irreversible decrease around 580°C indicate magnetite composition. However, the other Miocene sedimentary sample (R31) shows Ti-rich magnetite from its heating curves and decreases around 400°C (Figure 3.5). In the Haymana Basin, between Polatlı and Haymana, three results one from Miocene and two from Eocene show magnetite, pyrrhotite, and Ti-rich magnetite dominance from the sites R24, R57 and SEC1, respectively. Southernmost part of the study area is represented by three sites (two Eocene and one Miocene site). The Thermomagnetic results indicate Ti-rich, pyrrhotite mineral from the Eocene rocks (R 33 and R 58, respectively) and hematite from the Miocene rocks (SF6).

Total number of 36 thermomagnetic results from Upper Cretaceous to Pliocene rocks (Figure 3.4 and 3.5) clearly indicate that the rest of 83 sites have coherent results which have high isolation ranges (both thermal and alternating field) to determine ChRM direction from 119 sites (Appendix B).

3.3.2. Demagnetization Procedure (AF/TH)

Characteristic remnant magnetization (ChRM) directions were isolated by applying both thermal (TH) and alternating field (AF) repeatedly stepwise demagnetization processes. For each sites, minimum number of seven specimens were fully cleaned thermally from secondary magnetic field effects and half of the samples in each sites were measured in AF that first heated and measured up to 150°C thermally before the full AF demagnetization process was applied in order to isolate possible stress in magnetite grains due to oxidation at low temperatures (Van Velzen and Zijderveld, 1995; Gong *et al.*, 2008). TH demagnetization process was performed in a magnetically shielded oven (ASC, model TD48-SC) that has a residual field < 10 nT. Each specimen progressively demagnetized and measured by successive temperature steps at from 20°C, 80°C, 120°C, 150°C, 180°C, 200°C, 225°C, 250°C, 275°C, 300°C, 320°C, 340°C, 380°C, 420°C, 450°C, 450°C, 500°C, 530°C, 560°C, 580°C up to complete demagnetization of the naturel remnant magnetizations (for some samples if the magnetic carrier is hematite, the stepwise heating and measurement performed up to 700°C).

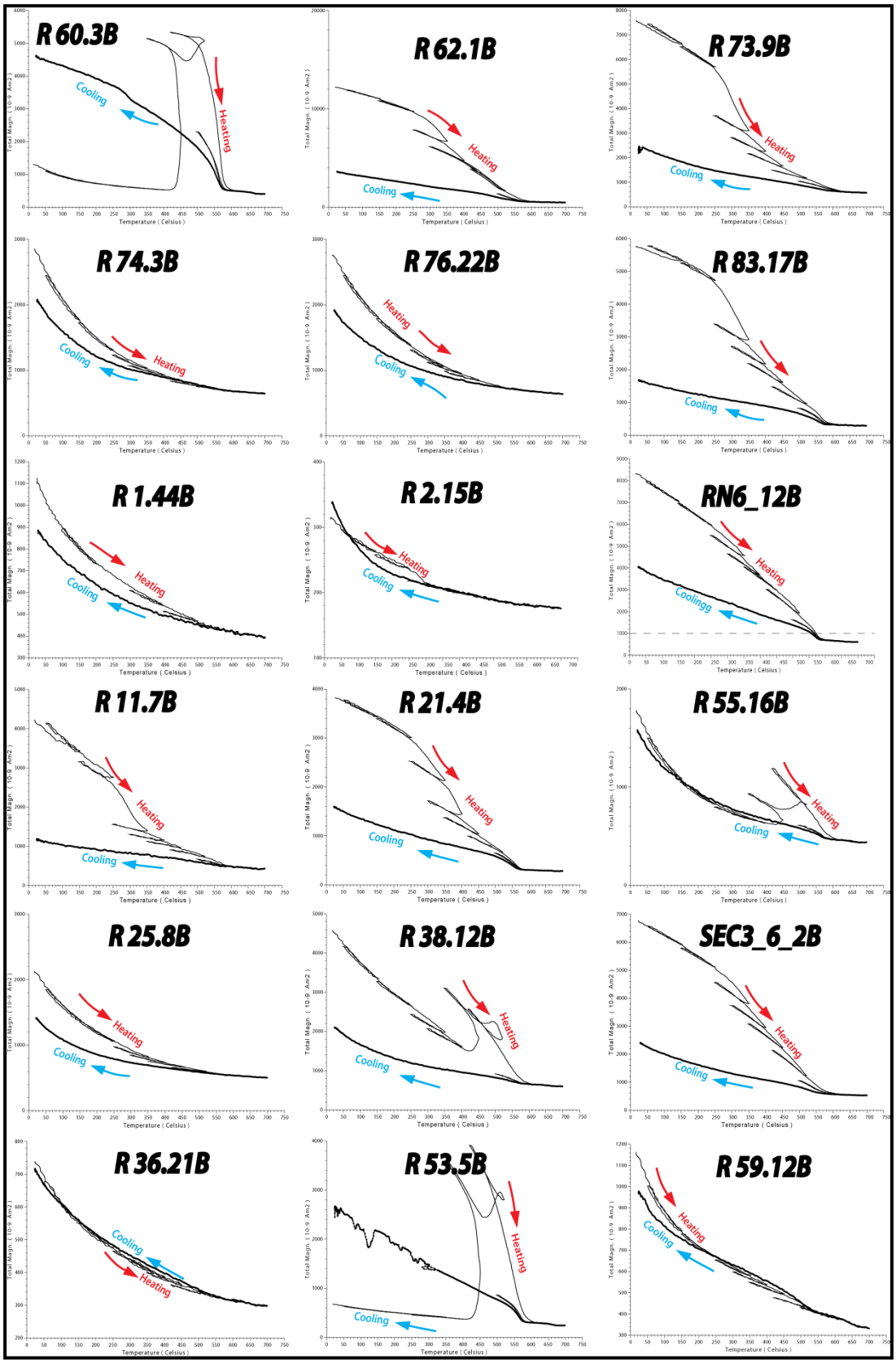

Figure 3.4. Thermomagnetic results measured on a Curie balance (Mullender et al, 1993) for representative of the upper Cretaceous to Paleocene rocks.

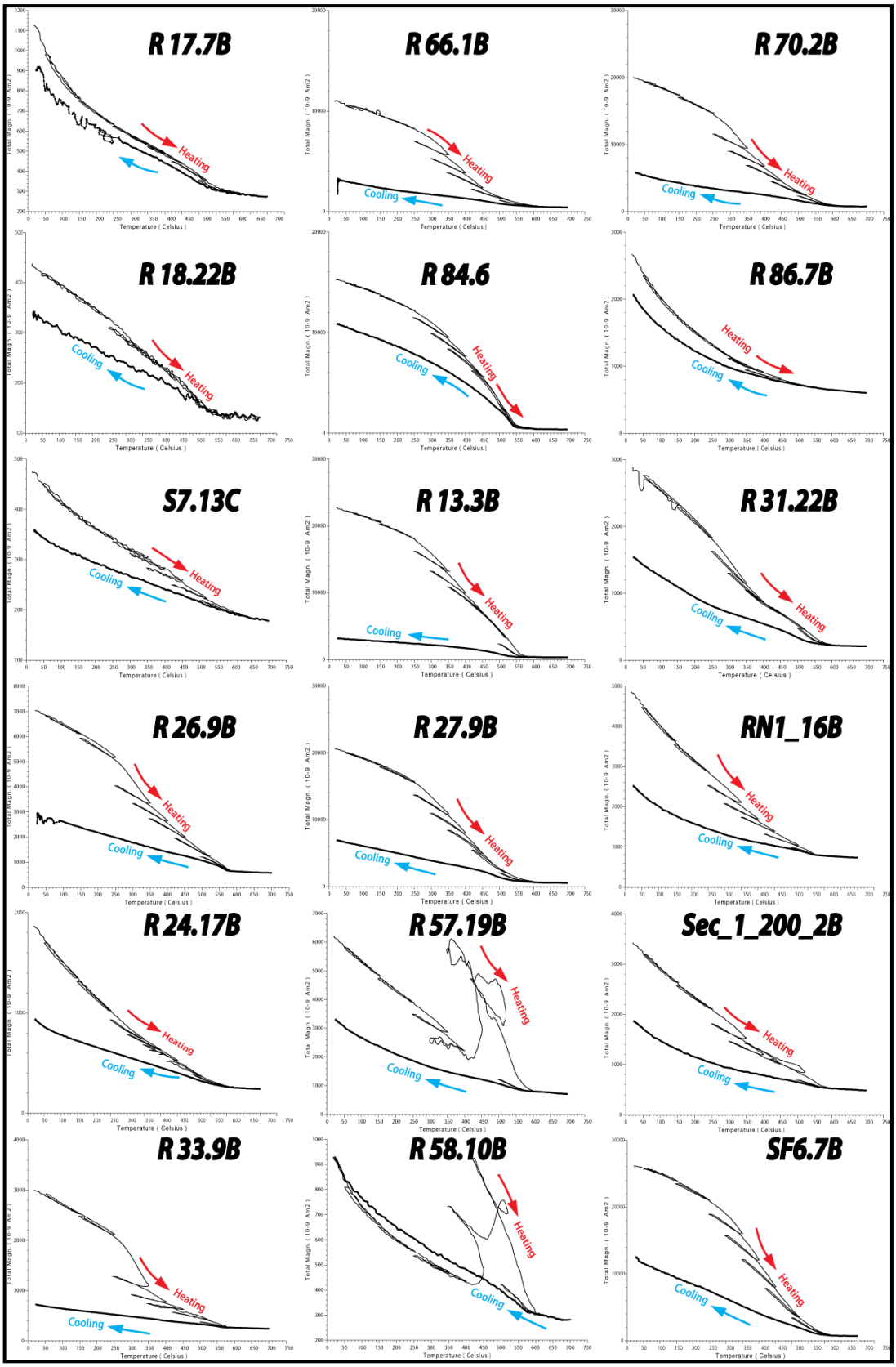

Figure 3.5. Thermomagnetic results measured on a Curie balance (Mullender et al, 1993) for representative of the Eocene to Miocene rocks.

The NRM of the specimens were measured on a 2G Enterprises horizontal 2G DC SQUID cryogenic magnetometer (noise level 3×10^{-12} Am^2) hosted in the Fort Hoofddijk Paleomagnetic Laboratory, Utrecht University (the Netherlands). The AF demagnetization was carried out with increments of 3–10 mT, up to a maximum of 100 mT. The AF demagnetization and measurement process was carried out with an in-house developed robotized sample handler attached to a horizontal pass-through 2G Enterprises DC SQUID cryogenic magnetometer (noise level $1\text{-}2\times10^{-12}$ Am^2) hosted in the magnetically shielded room. Representative results of demagnetization steps of AF and TH are illustrated on the orthogonal vector diagrams. In order to compere AF and TH results in each site, we illustrated both thermal and alternating field demagnetization results in the same figure (Figures 3.6). Detailed information about the results per site is given in Table 3.1 and further details can be found in the Appendices 3.1 and 3.2.

3.3.3. Analysis of ChRM directions

In order to illustrate all the demagnetization results (steps) of the NRM, we used orthogonal vector diagrams (Zijderveld, 1967) (Figure 3.6), as well as the equal area projections of the ChRM (Figure 3.7). In orthogonal diagrams, the ChRM directions were determined using principal component analysis (Kirschvink, 1980) by taking approximately five to seven or more successive points from TH or AF demagnetization steps. Few samples, overprinted at least two overlapping coercivity or temperature components, were analyzed using the great circle approach (McFadden and McElhinny, 1988) (Figure 3.6). With the help of this method, the ChRM directions that lie around a great circle, the average direction from well-defined NRM directions can be determined. Since the results of ChRM distributions effected by the certain amount of secular variation of the Earth's magnetic field after the initial remanence were obtained which is circular at the poles, but gradually becomes more ellipsoid towards the equator (Creer *et al.*, 1959; Tauxe and Kent, 2004, Deenen *et al.*, 2011). Therefore, we calculated from the ChRM directions of each samples, site means (K) as well as virtual geomagnetic poles (VGP) and their means (A95, the 95% cone of confidence of the VGPs) were computed using Fisher statistics (Fisher 1953). A fixed cut-off (45°) was

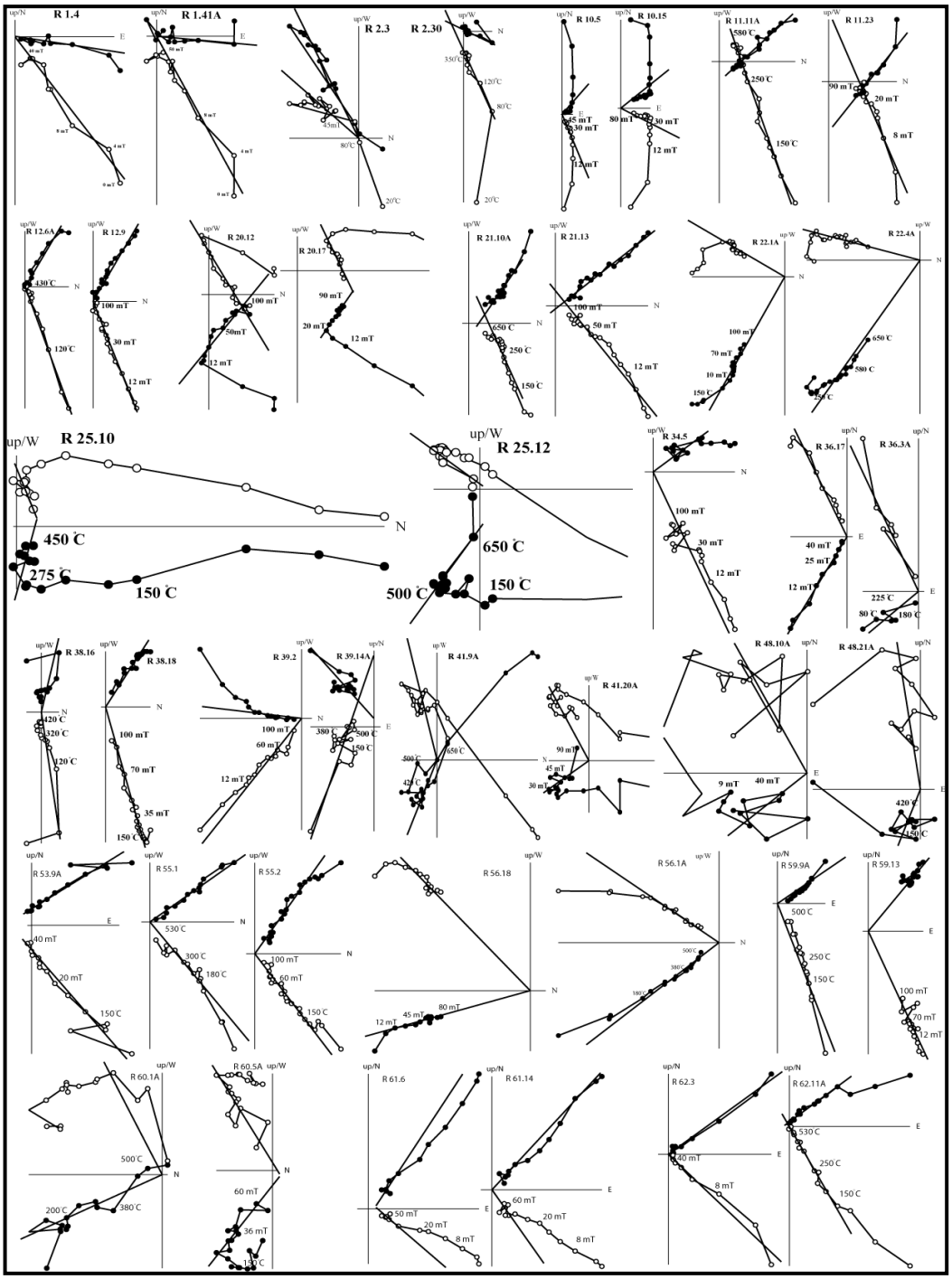

Figure 3.6. Results of orthogonal vector diagrams (Zijderveld, 1967), illustrating representative characteristic demagnetization diagrams for each site comprising the late Cretaceous to Paleocene time interval. Closed (open) circles indicate the projection on the horizontal (vertical) plane. All diagrams converted to their initial bedding (horizontal) positions. Both thermal (steps in °C) and alternating field (milliTesla, mT) demagnetization diagrams are shown for two specimens from the same site for comparison. Note that the site R53 did not produced any TH results.

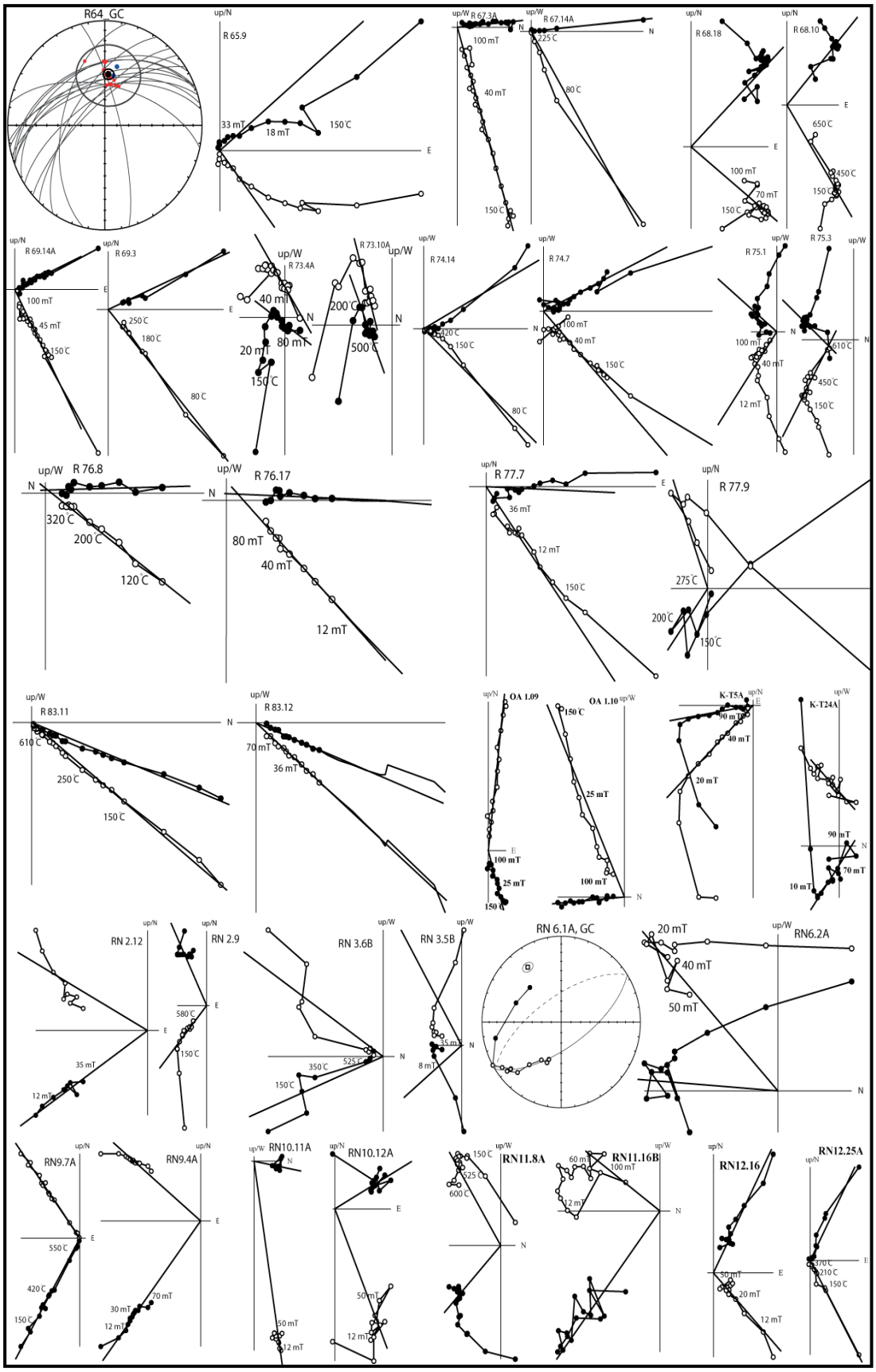

(Figure 3.6 continued)

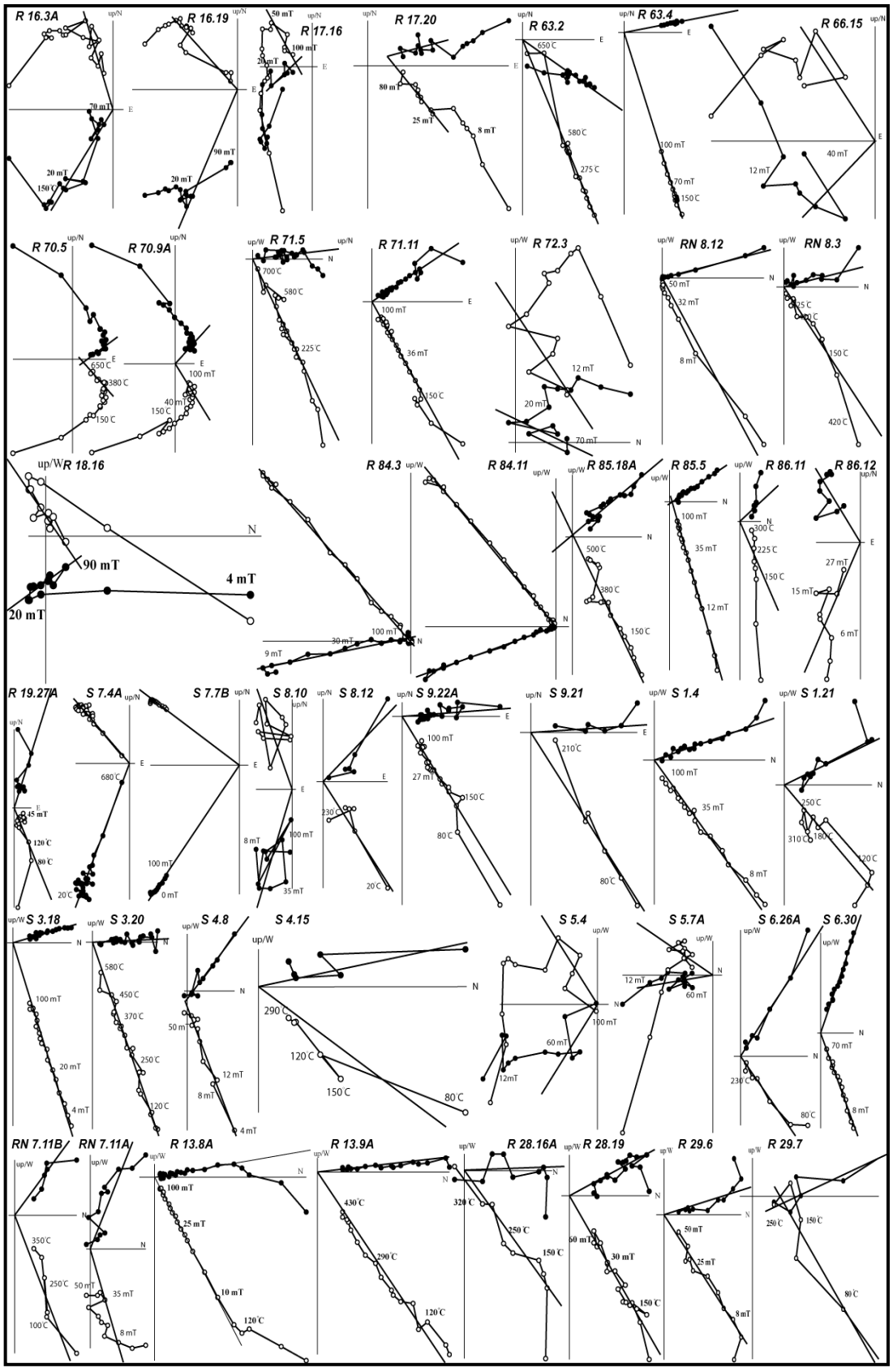

(Figure 3.6 continued)

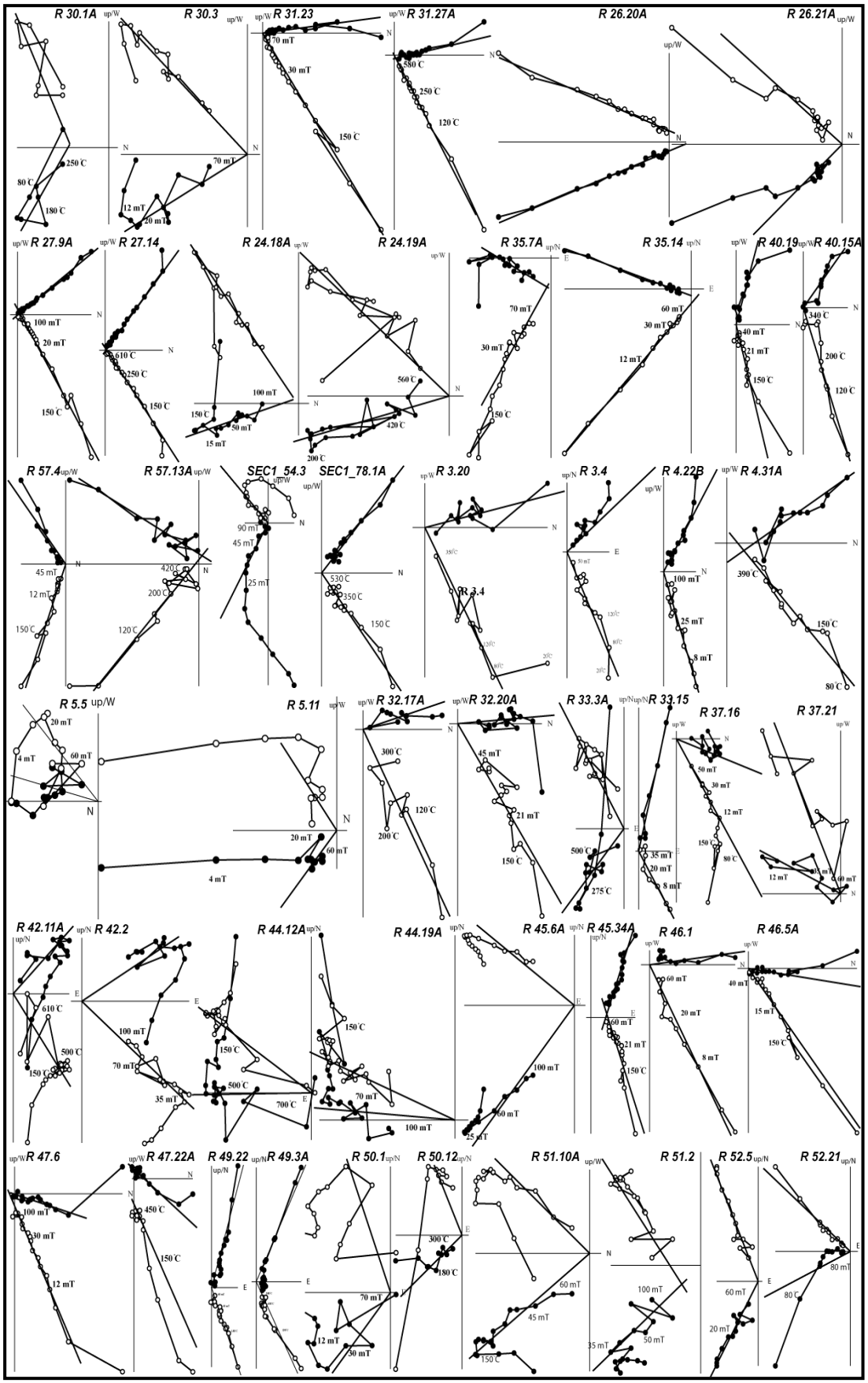

(Figure 3.6 continued)

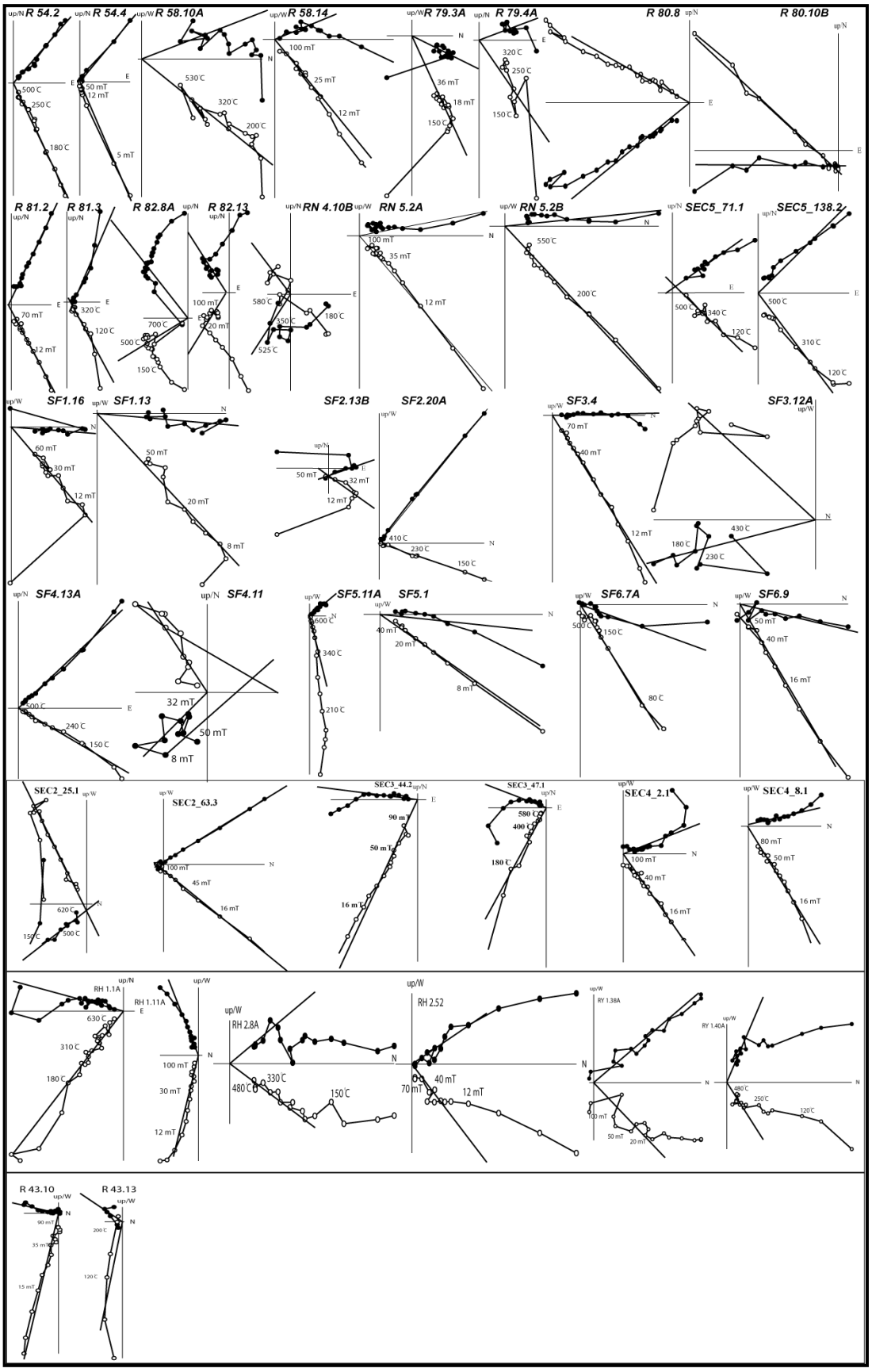

(Figure 3.6 continued)

applied to remove outliers as explained by Deenen *et al.*, (2011, 2014). The VGPs per site and the corresponding errors in declination (ΔDx) and error in inclination (ΔIx) determined individually according to Butler (1992). Deenen *et al.*, (2011, 2014) proposed N-dependent reliability criteria for dataset which assess whether the statistical results may be verified by the secular variations alone or not. On the contrary most of the paleomagnetic studies used the criteria proposed by Van der Voo (1990) but the criteria suggested by Deenen *et al.* (2011) are individually applied for each data set, in this study. In order to identify whether two distributions have a common true mean direction (CTMD), we used the reversal test proposed by McFadden and McElhinny (1990) and their classifications (A, B, C, indeterminate) in terms of the critical angle γc and the angle γ between the means. Since we operate their test with simulation, which is equivalent to Watson (1983)'s Vw statistical parameter.

3.3.4. Data Reliability

In order to verify the reliability of the obtained results following reliability criteria have been applied. Other than six sites which belong to Miocene volcanoclastic rocks in the Haymana Basin and one Permian limestone block from the Karakaya Complex and one site from the late Cretaceous granite (basement of Tuz Gölü Basin), in all other site sedimentary rock units are sampled. It is already known that the secular variation effects are minimal to negligible in the sedimentary rocks due to a fact that 1.3cm thick fine clastic sediment may represent few hundred to thousand year therefore the secular variation is smoothed out. In addition, sedimentary rocks provide good constraints on the position of the paleohorizontal (original horizontality of bedding plane). Therefore, sedimentary rocks are more reliable in terms of secular variations and finding paleohorizontal which is collectively known as tectonic or tilt correction. However, volcanic rocks are prone to secular variation since they are spot readings owing to be cooled off within few hours to days. Paleohorizontal is generally difficult to determine for both volcanic and plutonic rocks are on fine minimized and also the initial bedding positions (accepted horizontal) are more reliable than the intrusive bodies. According to Jackson *et al.* (2000) the paleosecular variations (PSV), might reach up to ± 25° or more depending on the latitude (higher latitudes has higher angular variation).

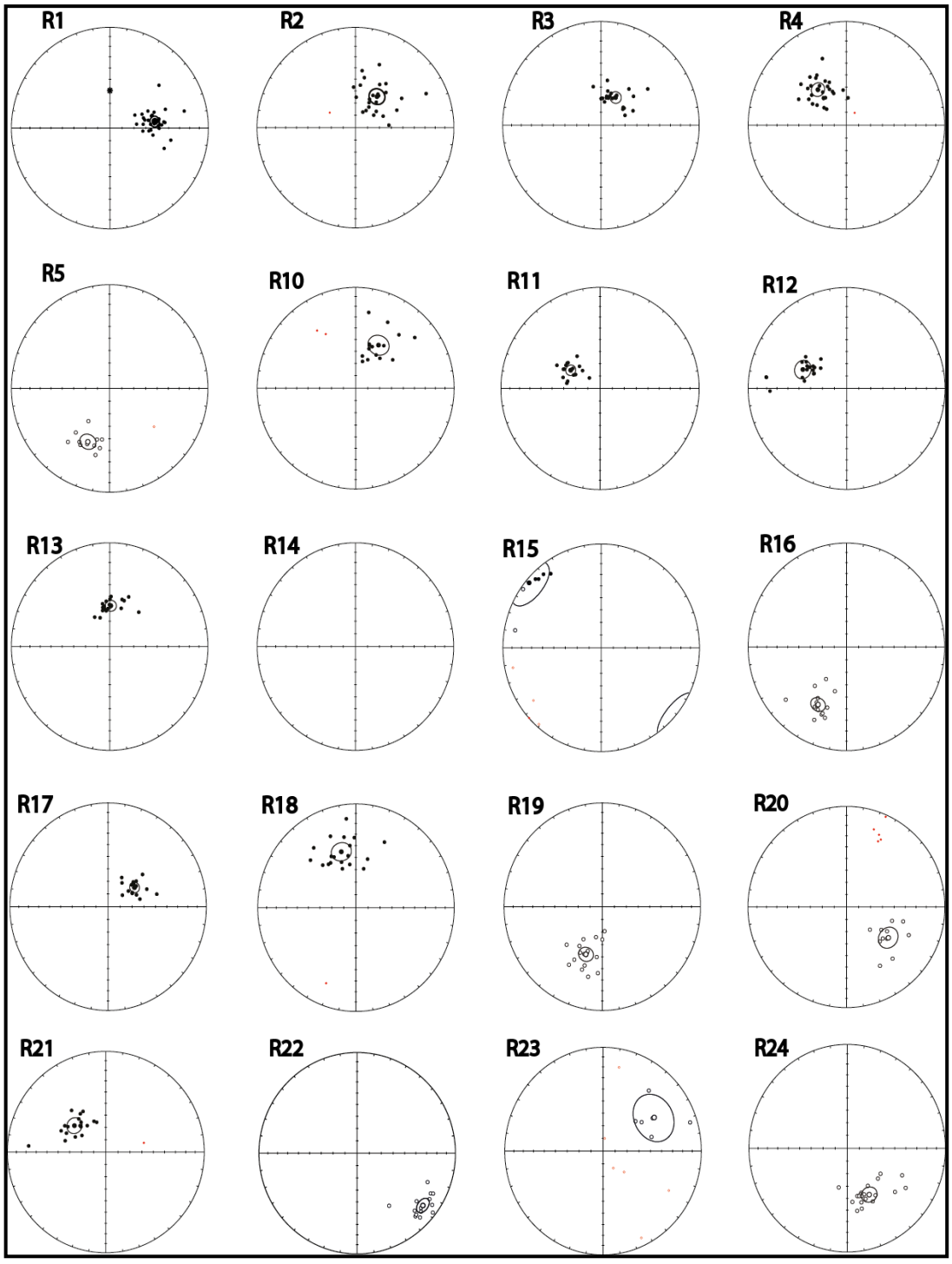

Figure 3.7. Equal area projections of the ChRM directions of all sites from late Cretaceous to Pliocene. Open (solid) symbols denote projection on upper (lower) hemisphere. Large symbols indicate respectively the mean directions and their cone of confidence (a95). Red (small) circles indicate the individual directions rejected by the Vandamme cut-off angle (45°) (Vandamme, 1994). Note that only one site (S2 did not produce any results).

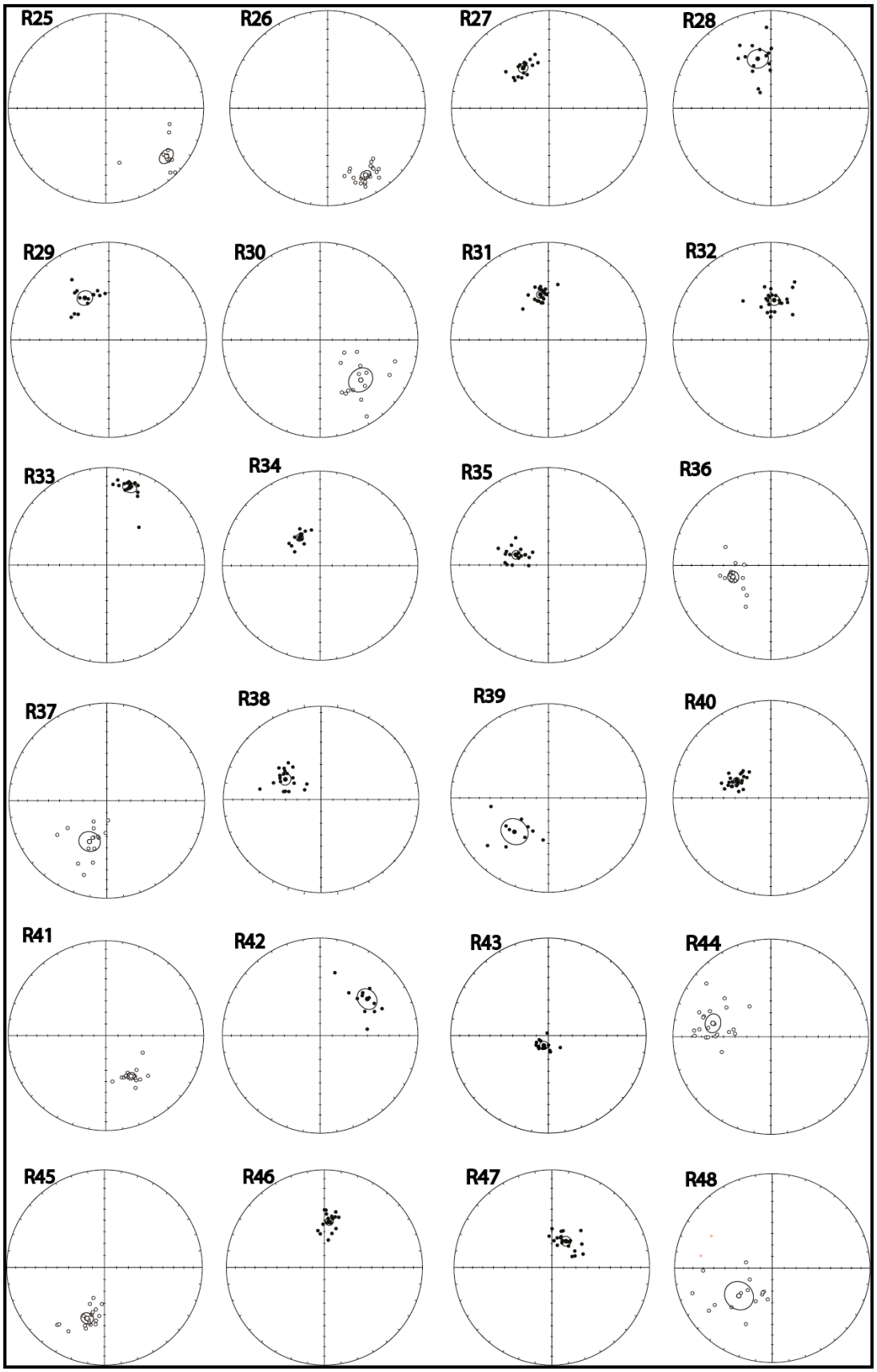

(Figure 3.7 continued)

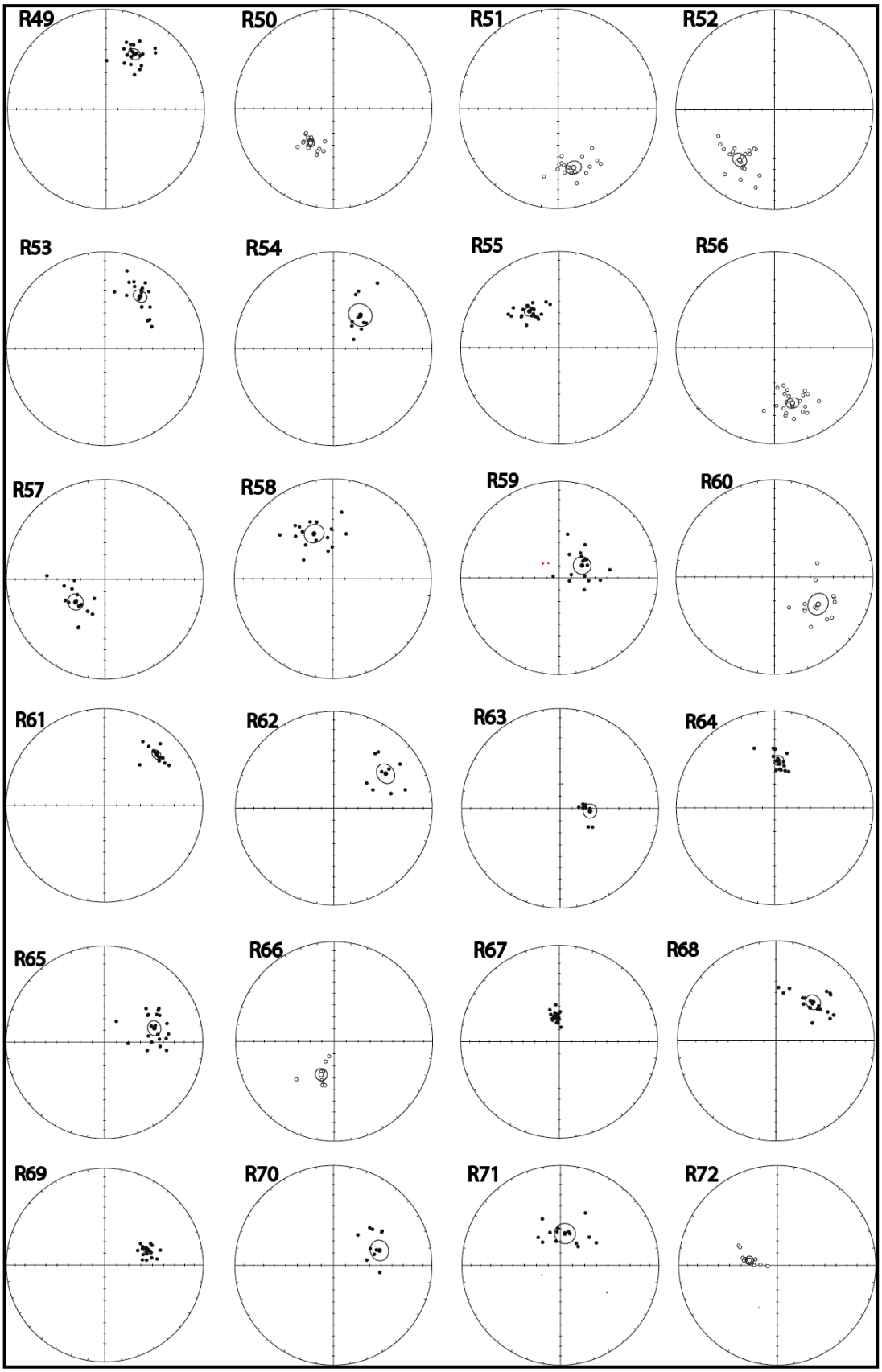

(Figure 3.7 continued)

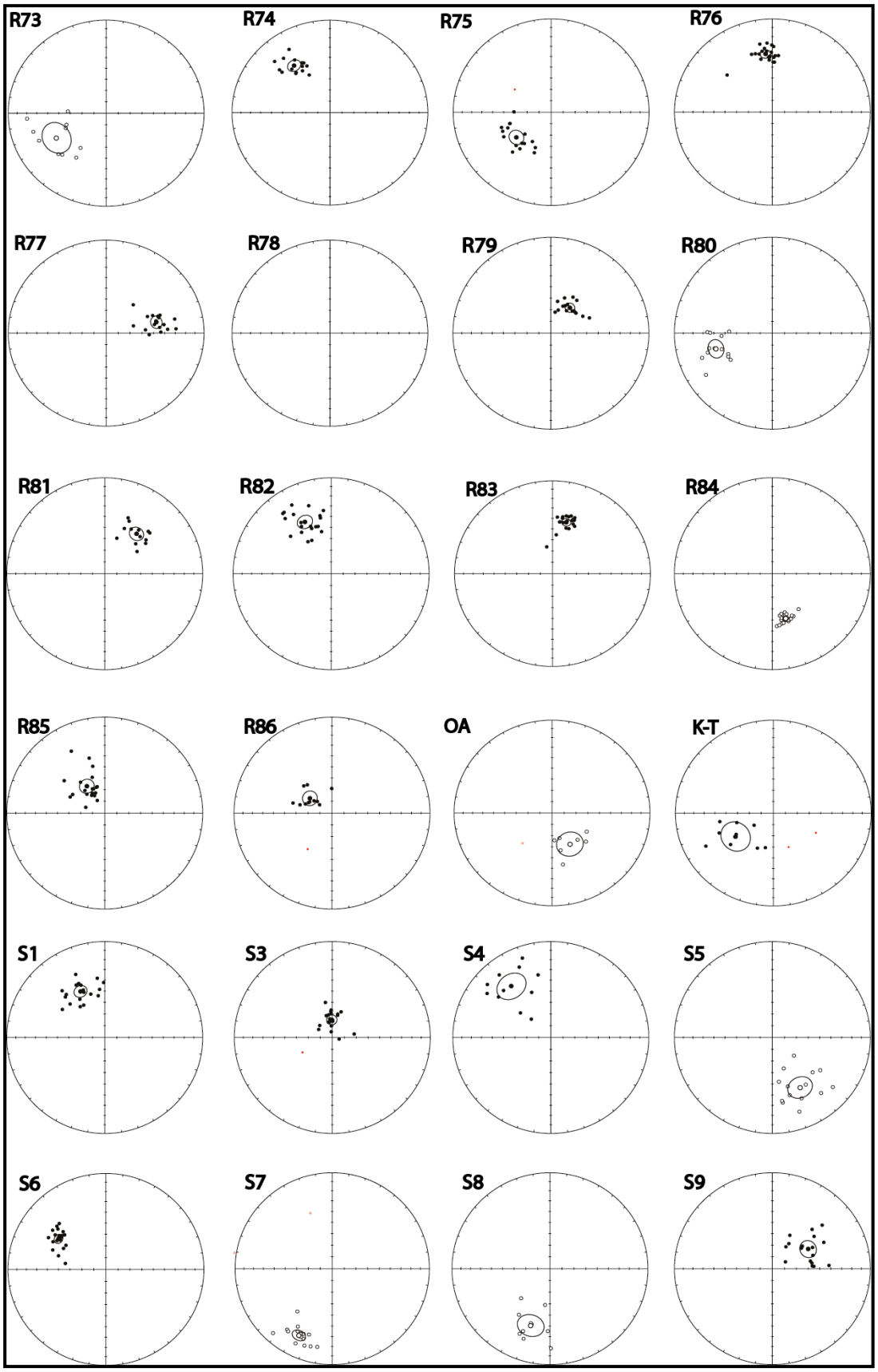

(Figure 3.7 continued)

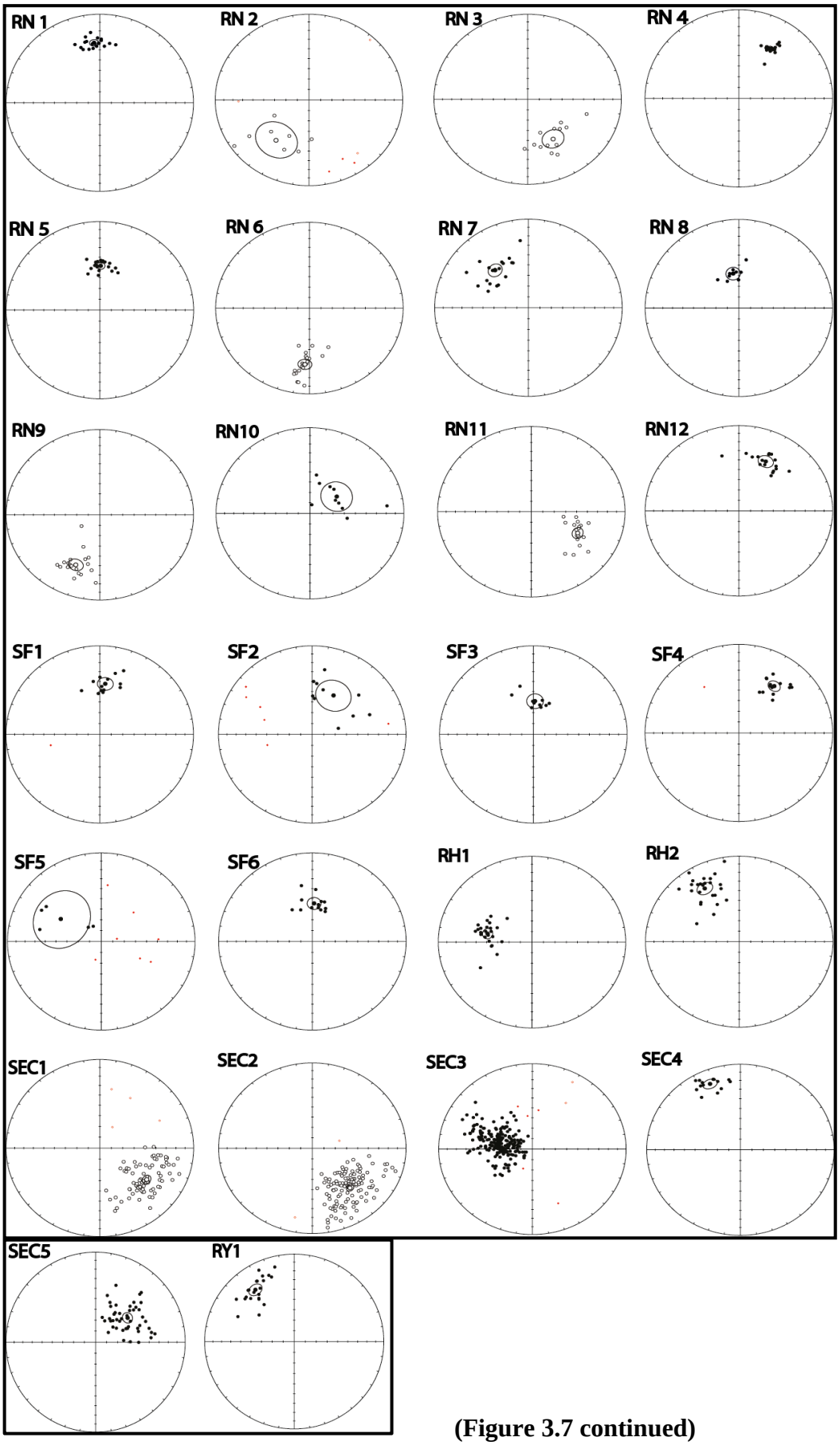

(Figure 3.7 continued)

Although, majority of our samples are collected from sedimentary rocks which have lower chance of paleosecular variations, nevertheless, we followed the criteria proposed by Deneen *et al.* (2011, 2014) in order to overcome this problem. According to these criteria a cone of confidence is determined based on the maximum and minimum values within the $A95_{max}$ and $A95_{min}$ of VGP cone of the site. Any sample with results out of this cone implies that these datasets are influenced by the PSV effect or samples comprise a short time span (spot sampling). If A95 larger than the $A95_{max,}$ the results are not only effected by the secular variations but might as well be affected by the combination of vertical axis rotation and tilt differences within the dataset.

In order to reduce the effect of PSV on results, each sample was collected from different stratigraphical levels and in the sections few meters apart. In order to cover larger thickness and time interval. In some sites, both normal and reverse polarities were measured within the same section, therefore, we applied reversal test to verify the reliability of the data.

However, some of the sites (R43, R60, R75 and R83) (Table 3.1) erratic NRM directions (e.g. N/up, S/down) are detected which do not fit the general mean rotations possibly due to close proximity to a major fault zone or they are struck by lightning. Such sites are refrained from further analysis.

3.4. Paleomagnetic Rotations

Paleomagnetic rotations are evaluated based on their age and location. Spatially the results show very distinct pattern in different part of the study area. For this reason the study area subdivided into sub areas based on the sampled lithologies and tectonic history of the study area. The sub areas include counter-clockwise from SE to NE to NW to SW include Tuz Gölü, Kırıkkale-Bala, Alcı-Orhaniye and Haymana basins (Figure 3.7)

3.4.1. Late Cretaceous & Older Rocks

Upper Cretaceous and older rocks are represented by 16 sites (Figure 3.9a and b, Table 3.1). Among these 16 sites, two of them were rejected because the initial magnetic remanence has been partly overprinted by present day magnetic field in site

R67 and the site R83 produced uninterpretable and unrealistic results (Figure 3.8). The overall rotation results in these rocks indicate a very large swath of rotations as large as ±80° in both clockwise and counter-clockwise senses.

The oldest site belongs to the Permian Limestone blocks of Karakaya Complex (R10). The results from this site shows normal polarity with D=28.5°, I= 49.5° sense. This indicates an approximately 28° clockwise rotation and very high inclination value that is little bit south of present day latitude of the block. Therefore, it must be remagnetized possibly during Eocene or younger periods.

Two Upper Cretaceous sites in the Kırıkkale-Bala Basin show clockwise rotations. The site R 65 has both normal and reverse magnetic polarity and yielded D=74°, I= 46.2° indicating 74° clockwise rotation. The site R 73 has reverse polarity and the yielded D=242.3°, I= -41.9° which indicate as high as 80° clockwise rotations.

There is only one Upper Cretaceous site (RN 6) in the Alcı-Orhaniye Basin and yielded reverse polarity of D=184.2°, I=-34.4° which indicates almost no rotation.

In the Haymana Basin all of the 9 Upper Cretaceous sites yielded counter-clockwise rotations. 7 of the total 9 sites, show strong counter-clockwise rotations with declination values varying between D=281.7°-301.3° and they have both normal and reverse polarities. On the other hand, the declinations seem to decrease in the western part of the Haymana basin around Polatlı. The remaining two sites (R 21 and R 55) in this part of the basin has relatively lower counter-clockwise rotations compared to the eastern sites. R 21 has D=309.4°, I= 55.9° from 28 measurements and R 55 has D=321.3°, I= 50.0° from 26 measurements.

3.4.2. Paleocene vertical axis rotation

Paleocene paleomagnetic data in the study area is represented by 33 sites (Table 3.1, Figures 3.10 and 3.11). They have both clockwise and counter-clockwise senses. The detailed information about the results per sub area is given below.

Apart from one site (R 60) which produced reverse polarity and counter-clockwise rotation (D=122.3°, I= -46.3°) all other 5 Paleocene sites in the Kırıkkale-Bala Basin show consistent clockwise rotations that vary between D=4.3° to 71.5º and have both

normal and reverse polarities. At the southern part of the Kırıkkale-Bala Basin near Bala, the site R 75 produced normal polarity and very large counter-clockwise rotations as high as 128° and the obtained declination and inclination values are as follows D=232.6°, I= 53.1°. Rest of two the sites (R 74 and R 76) shows consistently counter-clockwise rotations with ChRM result; D=324.3°, I= 37.3° for the site R 74 and D=353.5°, I= 37.3° for the site R 76. On the other hand, from the site R 77 which is located at the south-easternmost part of the study area and in the Tuz Gölü Basin and produced clockwise rotations with ChRM results; D=77.2°, I= 46.3°. In this site 7 of the samples were reversely polarized while the remaining 11 of them were normally polarized.

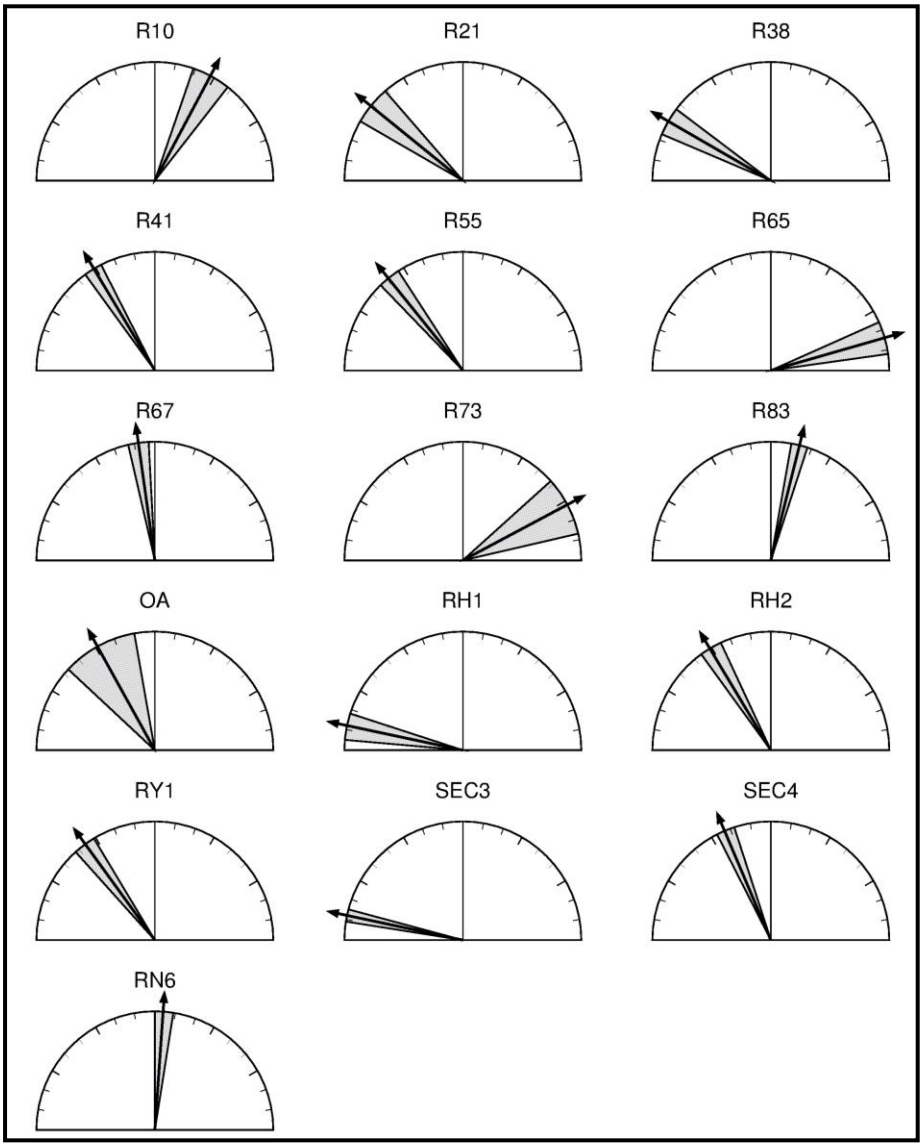

Figure 3.8. Upper Cretaceous and Older age 16 sites vertical axis rotation vectors with their error envelop illustrated in grey.

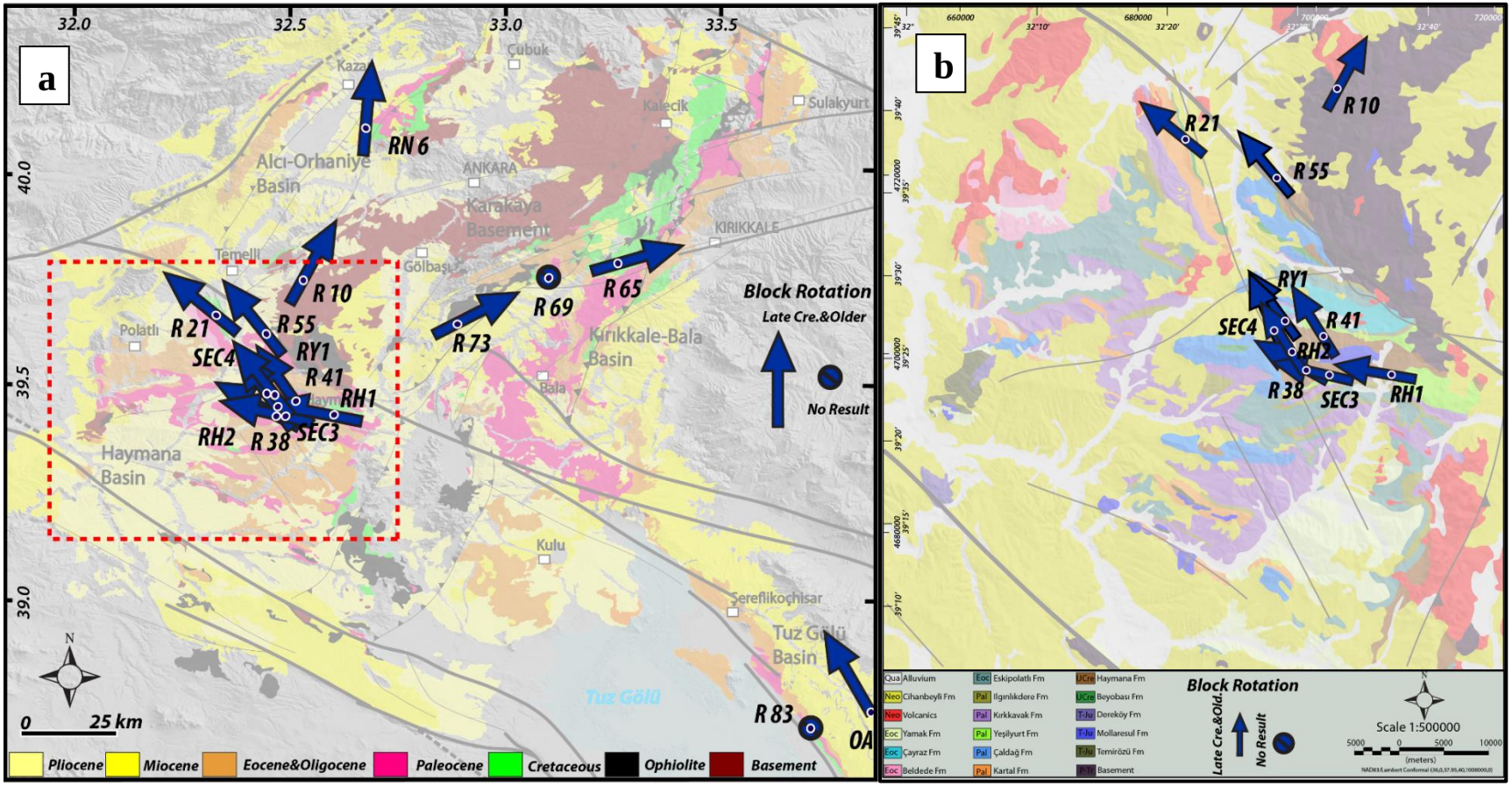

Figure 3.9. a) Late Cretaceous and Older paleomagnetic rotation vectors plotted on the general geological and structural settings in the study area. **b)** Blow up view of the Haymana Basin displaying the results of the Late Cretaceous sites paleomagnetic rotation vectors. Note that R10 belongs to Karakaya complex (pre-Cretaceous) and OA belongs to late Cretaceous granitoids of Kirşehir Block.

From the northwestern part of the study area, in the Alci-Orhaniye Basin, we have only two Paleocene sites (R 1 and R 2) which are consistently produced clockwise rotations with ChRM (N=30) result; D= 82 °, I= 52° in the site R1. In this site 12 specimens were reversely polarized while the remaining 18 of them were normally polarized. The site R2 has ChRM (N=25) results; D=35.4°, I= 58.9°.

At the western part of the area between Temelli and Polatlı, there are 5 Paleocene sites (R 11, R 12, R 20, R 22, and SEC 2). All of these sites show counter-clockwise rotations that vary between D=292.7° - 314.1°. Two sites (R 20 and R 22) have reverse polarity. One site (R 43) has very large declination and inclination values (D: 205°, I: 80°).

In the Haymana Basin two distinct and opposite rotation senses are observed. Near Haymana town center, from 7 sites (R 25, R 56, RN 3, RN 11, R 34, K-T, R 39) counter-clockwise rotations with declination values varying between 236.6°- 334.6° have been obtained (Table 3.1, Figures 3.10 and 3.11b). Towards the southwestern part of the basin the paleomagnetic direction results show opposite senses of (clockwise) rotations in the seven sites (R53, RN2, RN9, R36, R59, R48). The clockwise rotation results change between 23° to 72.1°.

3.4.3. Eocene to Oligocene Rotations

Eocene-Oligocene period is represented by 31 sites. Among these, two sites (R 23 and RN 1) did not pass the Vandamme cut-off (45°) and they are not included in any further analysis (Table 3.1). The rest of 29 sites scattered in the area produces reliably results that show interpretable rotation pattern (Figures 3.12 and 3.13).

From the northeastern part of the study area, in the Kırıkkale-Bala Basin, four Oligocene sites (R63, R66, R70, and R72) produced clockwise rotations. The rotation directions vary between 22.5° up to 100° clockwise sense. In addition, two of these sites have normal polarization while the other two sites were reversely polarized.

The Tuz Gölü Basin is represented only by two Eocene sites they show counter-clockwise rotations (R85: N=21, D=163.8°, I= -49.6° and R 86: N=11, D=304.2°, I= 67.6°). They are all normally polarized and are opposite to the results of the Kırıkkale-Bala Basin which are located at the north and have clockwise rotations.

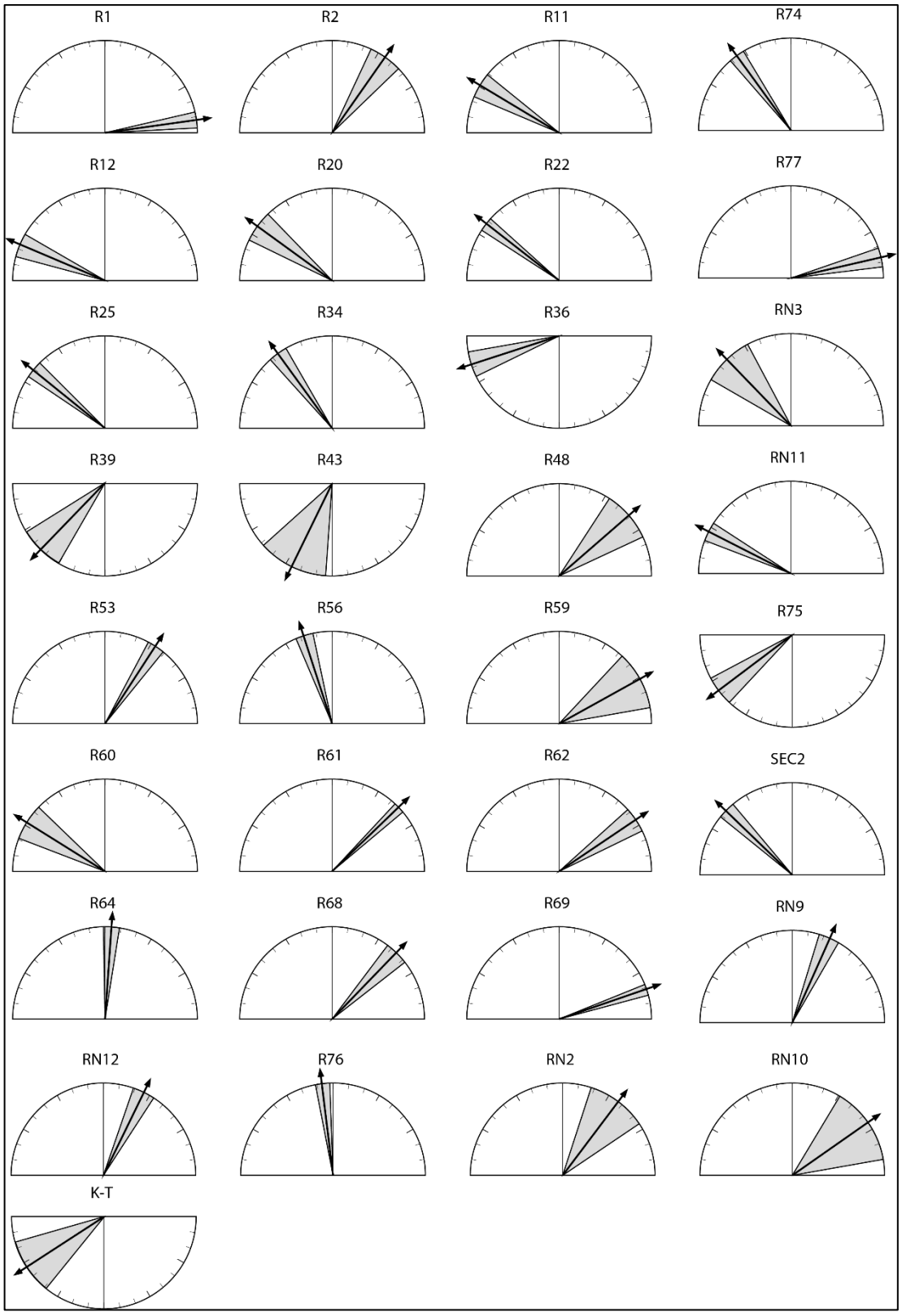

Figure 3.10. Declination values and corresponding error parachutes of 33 Paleocene sites in the study area.

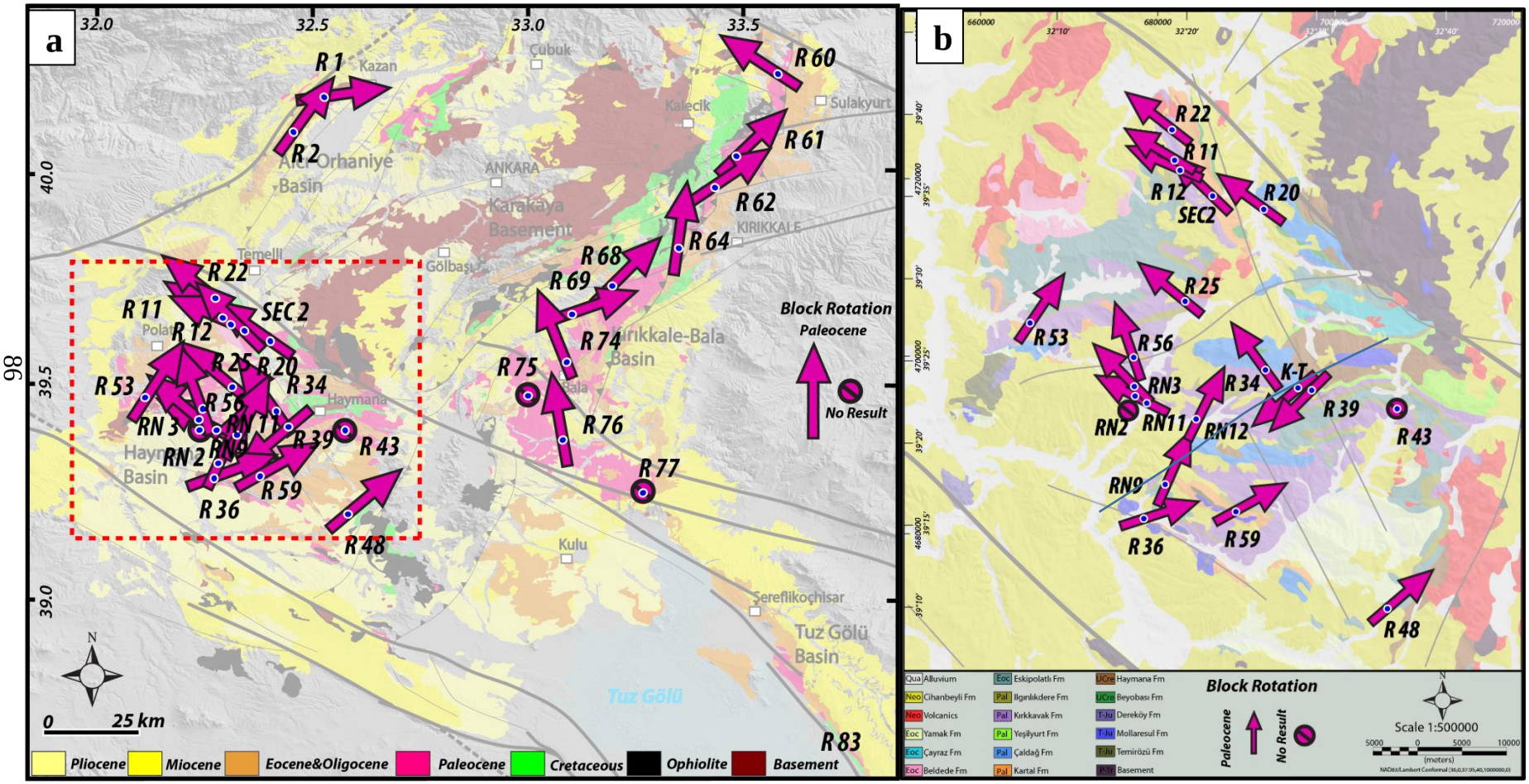

Figure 3.11. a) Paleocene rotation vectors plotted on the general geological and structural settings in the study area. **b)** Blow up view of the Haymana Basin displaying the results of the Paleocene sites paleomagnetic rotation vectors.

In the Alcı-Orhaniye Basin, which is located at the NW part of the study area, three sites yielded clockwise rotations ranging between 18°-60° (S8: N=10, D=198.4°, I= -37.2°; S9: N=17, D=60.8°, I= 55.5°).

Haymana Basin is represented by 24 sites (Table 3.1, Figure 3.13). Two of the sites (RN 1 and R 23) did not yield any appreciable results so they are not used for further analysis. The rest of 22 sites show both clockwise and counter clockwise rotations. Especially near Haymana town center, four sites (R 26, R 40, R 42, R 57) show counter-clockwise rotations, while further south of the town 12 sites (R 33, R 54, R 42, R47, SEC 5, RN 4, R 81, R 79, R 80, R 52, R 49, RN 5) yielded clockwise rotations. However, two sites (R 58 and R 82) within the clockwise domain yielded counter-clockwise rotations contrary to the nearby clockwise sites.

3.4.4. Miocene Rotations

From 26 Miocene sites 615 samples were collected (Table 3.1). Among these 5 sites did not produce any reliable results therefore they are not used is any further analysis. The remaining of 21 sites produced meaningful results. Among them three sites belong to volcanic rocks while the rest of them are collected from sedimentary rocks. The results are depicted in Figures 3.14 and 3.15.

The results are evaluated on the basis of sub areas (basins). In the Kırıkkale-Bala Basin the site R 71 show slightly clockwise rotation (8.0 ±17.8, N=14). Between the Kırıkkale-Bala and the Haymana basins, the rotation vectors show generally clockwise senses except for two sites (R8 and RN18) which yielded counter-clockwise rotations. The other five sites (two of them are volcanic) in the region shows clockwise rotation that vary between 6° to 55° (R46: N=21, D=6°, I= 51°, R 17: N=17, D=55.5°, I= 63.2°). The site R46 has 5 while R17 has 14 reverse polarity samples. The site R 78 did not produce any reliable results from 15 measured specimens.

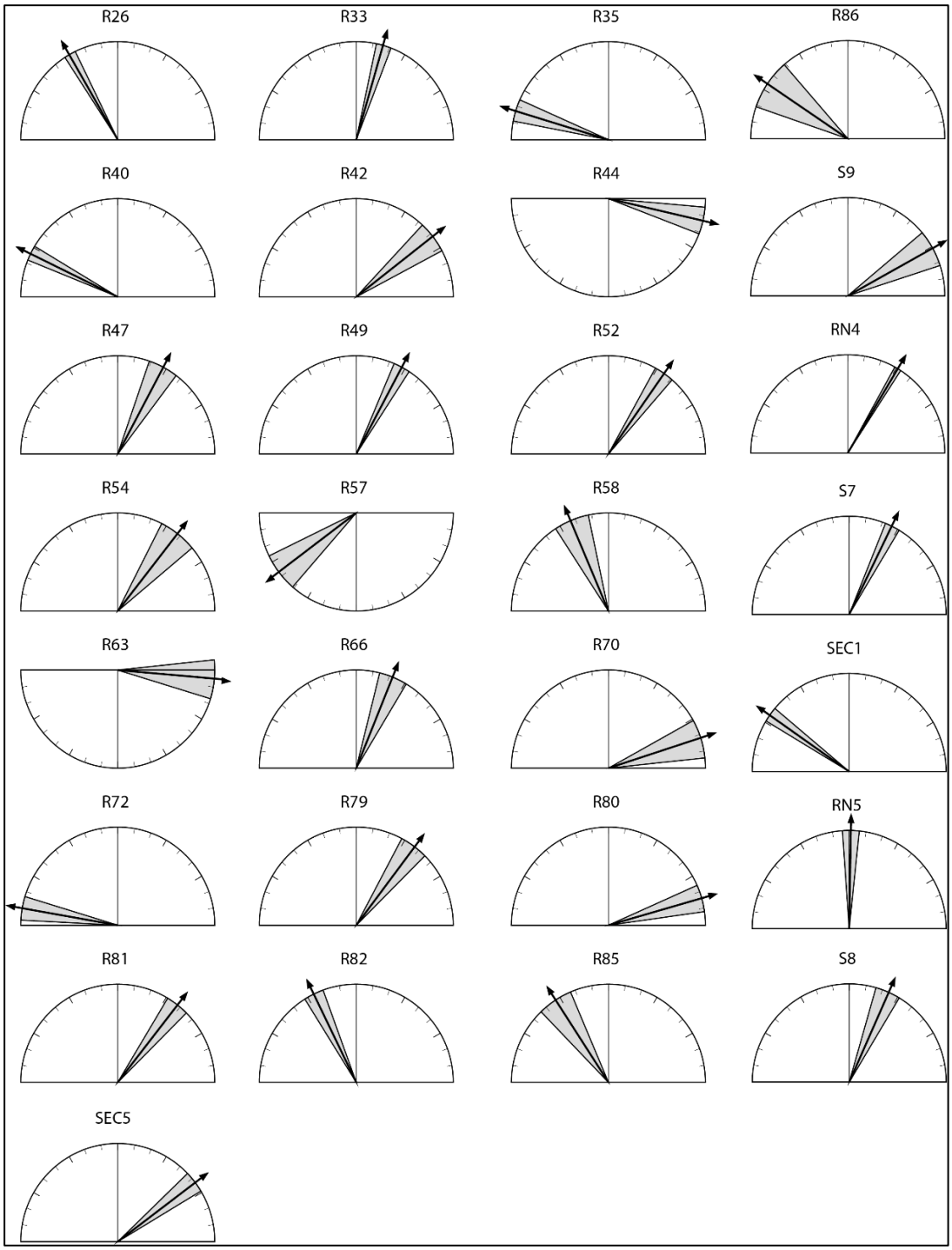

Figure 3.12. Declination values of Eocene sites with their error envelop (grey parachutes).

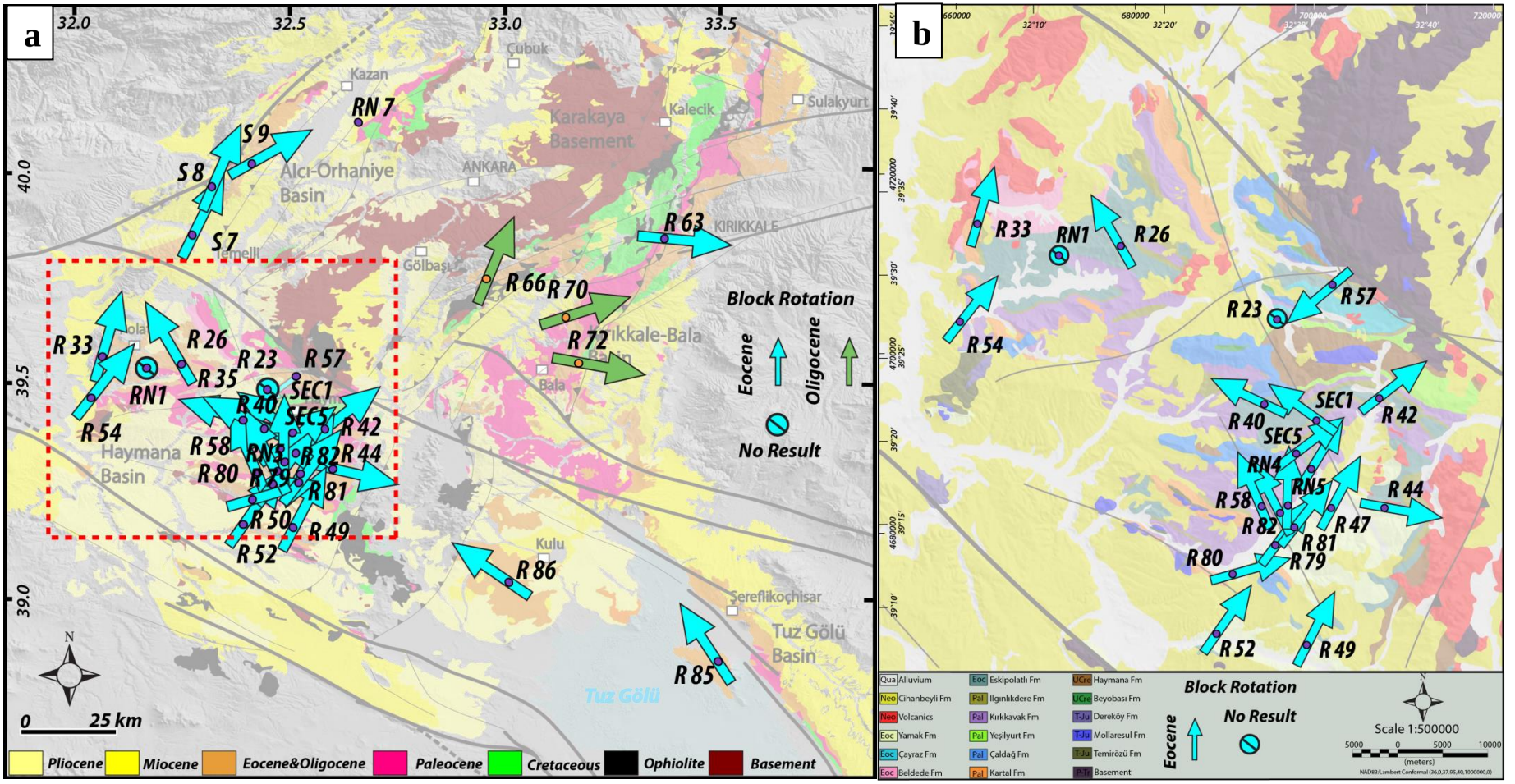

Figure 3.13. a) Eocene to Oligocene rotation vectors plotted on geological map. **b)** Blow up view of the Haymana Basin displaying the results of Eocene rotation vectors.

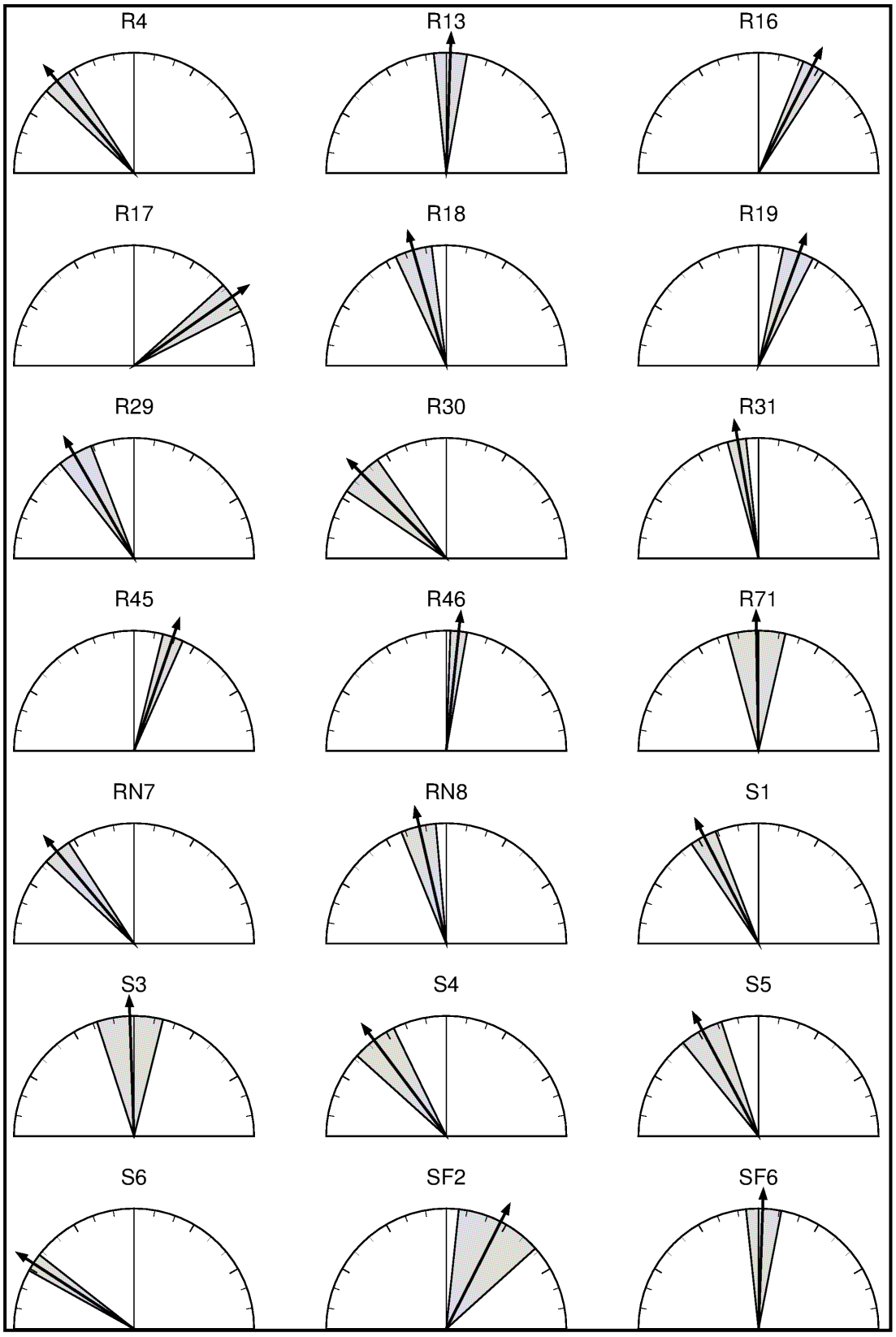

Figure 3.14. Miocene age 21 site rotation vectors with their error envelops illustrated in grey.

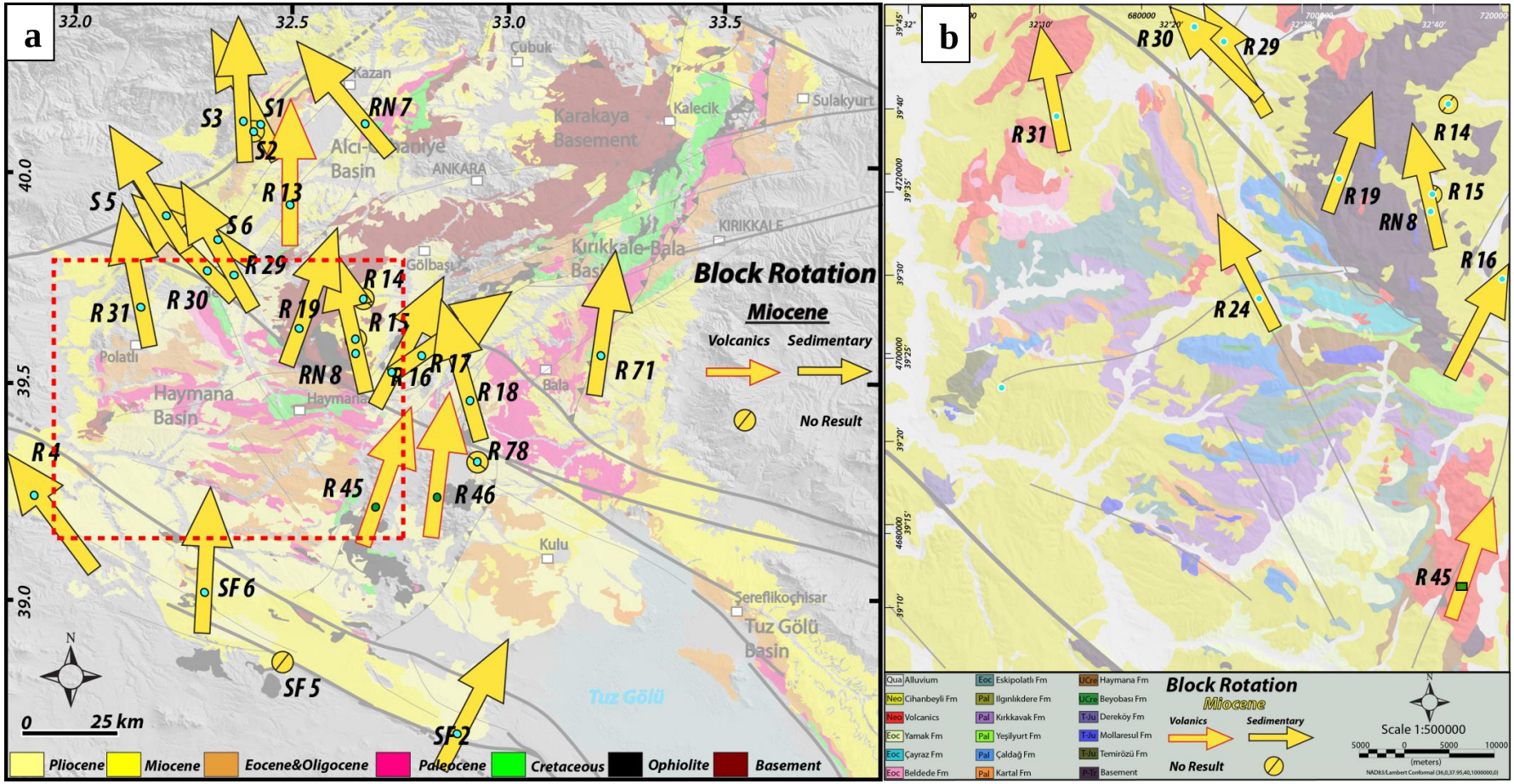

Figure 3.15. a) Miocene rotation vectors plotted on the general geological and structural settings in the study area. **b)** Blow up view of the Haymana Basin displaying the results of the Miocene sites paleomagnetic rotation vectors.

In the Alci-Orhaniye Basin, out of five sites one site (S2) did not produce any reliable result, all of the other four sites (S 1, S 3, R 13, RN 7) show counter-clockwise rotations ranging between 2° to 27° (S3: , N=19, D=358.3°, I= 75° and S1: N=46, D=332.6°, I= 45°). All the specimens show normal polarity. In addition, in the southernmost part of the Alcı-Orhaniye Basin, a cluster of five sites (S5, S6, R29, R30, and R31) show counter-clockwise rotations with mean direction of ~ 340±7°.

The Miocene in Haymana Basin is represented by three sites (Figure 3.15). Among these, one site (R4) shows counter-clockwise rotation (N=29, D=319.7°, I= 52.9°) whereas the other two sites (SF6 and SF2) indicate clockwise directions up to 27° (N=20, D=2.5°, I=54.6°; and N=16, D=27.4°, I= 48.9°, respectively).

3.4.5. Pliocene Rotations

The Pliocene paleomagnetic data comprises, totally 13 sites (Figure 3.16 and 3.17, Table 3.1). There is no paleomagnetic site in the Kirikkale-Bala Basin. Both Tuz Gölü and Alcı-Orhaniye basins are represented by only one site each The site in the Tuz Gölü basin (R84) yielded from 21 specimens D=163.8°, I= -49.6° results. All of the specimens are reversely polarized. On the other hand, only one specimen was reversely polarized while the remaining ones were normally polarized in the single site in the Alci-Orhaniye Basin (R28) and yielded from 15 specimens D=345.2°, I= 46.4°.

The remaining 11 Pliocene sites belong to Haymana Basin. Between Polatlı and Temelli town centers, in other words, in the northern part of the Haymana Basin, two sites yielded counter-clockwise rotations. In site R 25 out of 17 samples D=326.9°, I= 49.4° results are obtained. The other counter-clockwise site is R24 and out of 20 samples it yielded D=153.5°, I= -48.5° results. In this site all specimens were reversely polarized.

In the southern part of the Haymana Basin, all the samples indicate clockwise rotations except for the site R51 that has about 15° counter-clockwise rotation (D=165.1°, I= -38.7°) out of 20 samples. In this site, all the specimens are reversely polarized. The other 8 sites (R3, R5, R 32, R37, R 50, SF 4, SF 3, and SF 1) all have clockwise rotations ranging between 2° to 35°. In this part of the Haymana Basin,

one site (SF5) did not produce any interpretable signal and it is excluded from further analysis. All the result are given in the Table 3.1 and in Appendices.

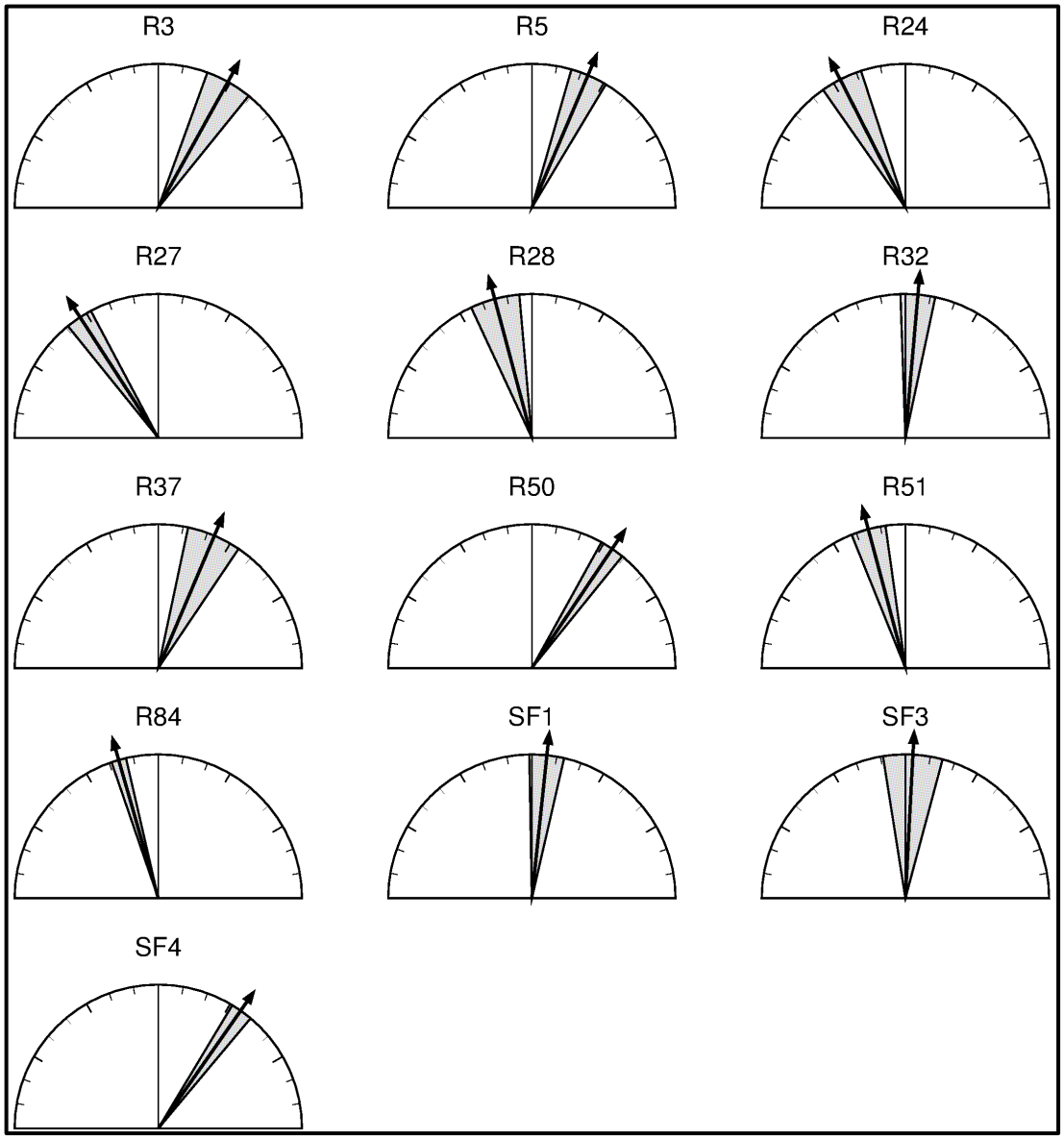

Figure 3.16. Declinations and corresponding error parachutes (grey wedges) of Pliocene sites in the study area.

3.5. Discussions

3.5.1. Evaluation of Paleomagnetic Results

The paleomagnetic results have indicated that the rotation patterns within each basin is relatively consistent (Figure 3.18, Table 3.2). Among these, the results of Tuz Gölü, Kırıkkale-Bala and Alcı-Orhaniye Basin are internally consistent whereas Haymana Basin has controversial results (Figure 3.18).

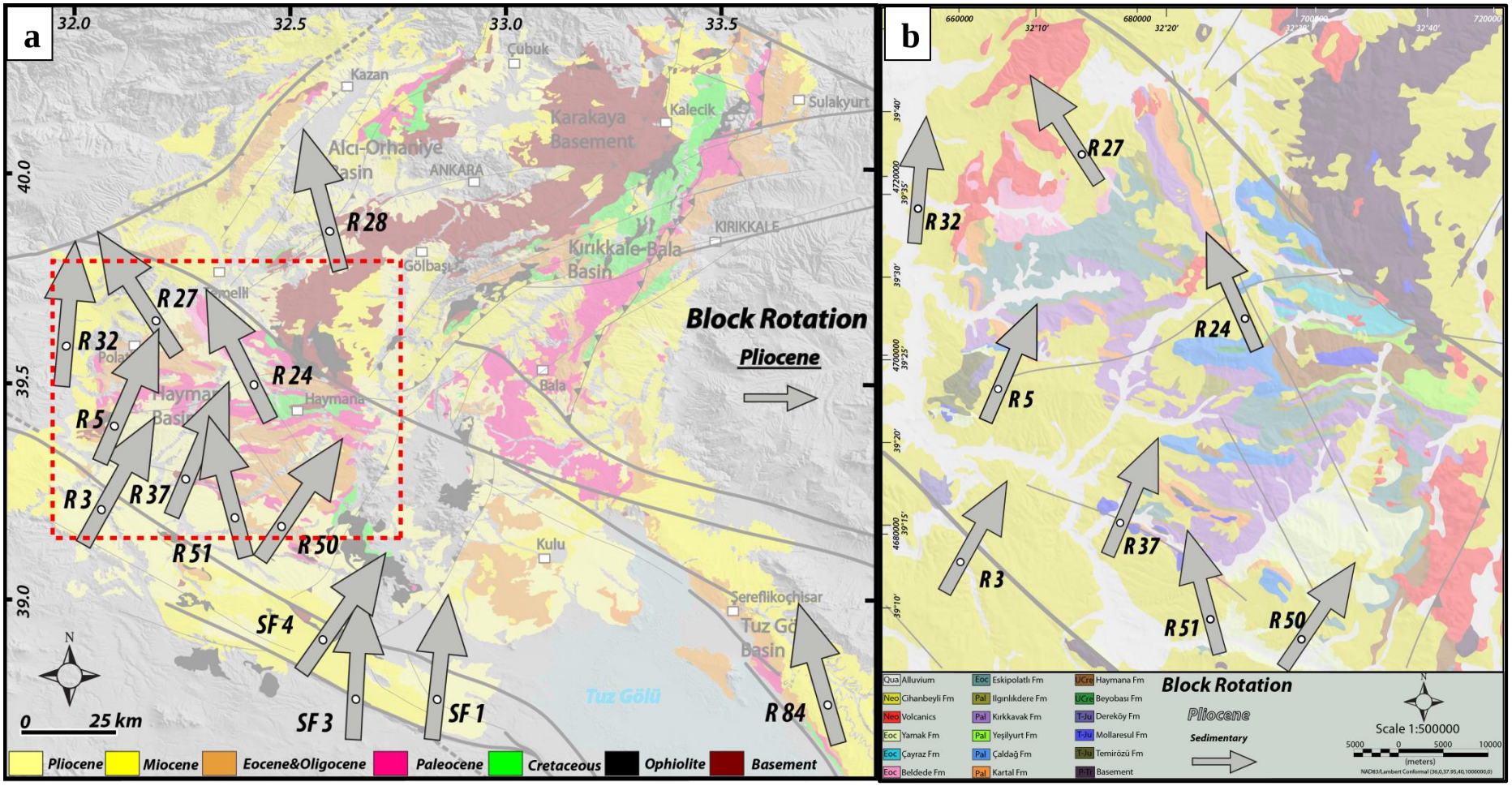

Figure 3.17. a) Mean Pliocene declinations plotted on the geological map. Dash-line box is the location of (b) blow up view of Haymana Basin.

The calculated mean statistics for basins from per locality in each basin are consistent which implies that they can be considered as independent blocks except for Kırıkkale-Bala and Alcı-Orhaniye basins which seems to belong to same block although they are separated by a major metamorphic belt (Figure 3.18.). Nevertheless, for the sake of consistency, each basin will be dealt with separately in the forthcoming section. In order to calculate mean block rotation amounts all the sedimentary data for different time intervals are grouped and analyzed together for each block. In other words, all the sedimentary specimens from each site in each basin are evaluated collectively for each block.

The magmatic rocks due to their intrinsic magnetic properties they are not included in this analysis. During the analysis of the results all the declinations are normalized with respect to north (normal) for statistical reasons (see Appendices and Supplementary).

In the next sections the declination results for each basin and each time interval is discussed.

3.5.1.1. The Kırıkkale-Bala Basin

The mean declinations of 49 Miocene samples from three sites indicate that the Kırıkkale-Bala Basin rotated 34.4±7.3° clockwise. The basin does not have any Pliocene and younger sites.

The Eocene to Oligocene is represented by four sites and they indicate very coherent directions (a95=4.3) (Figure 3.19). The results of the four sites show quite large amounts of clockwise rotations which is 73.7±8.9° (Figure 3.19, Table 3.2).

The Paleogene Kırıkkale-Bala Basin is represented by three Upper Cretaceous, six Paleocene, four Eocene and Oligocene, and three Miocene sites (Figures 3.19 and 3.20, Table 3.2).

Table 3.2. Average rotation values for four sub areas according to their age.

Basins	*Age*	*Mean ChRM Directions (Tilt Corrected)*											
		Nm/NvD	***Dec***	***ΔDx***	***Inc***	***ΔIx***	***k***	***a95***	***K***	***λ***	$A95_{min}$	***A95***	$A95_{max}$
Kırıkkale-Bala	Pliocene	No averages calculated											
	Miocene	49/44	034.4	07.3	54.6	06.0	018.5	05.1	014.1	35.1	02.6	05.9	07.6
	Eo-Oligo.	62/61	073.7	08.9	64.1	04.8	018.5	04.3	009.7	45.8	02.3	06.2	06.2
	Paleo.	84/83	045.7	05.1	44.8	05.7	016.1	04.0	012.7	26.4	02.0	04.5	05.1
	U. Creta.	32/32	070.3	06.9	45.0	07.7	022.2	05.5	017.8	26.6	03.0	06.2	09.2
Tuz Gölü	Pliocene	21/21	163.8	03.1	-49.6	03.0	209.9	02.2	145.4	30.5	05.0	02.6	12.0
	Miocene	20/19	344.5	09.0	43.4	10.5	019.9	07.7	018.0	25.3	05.2	08.1	12.8
	Eo-Oligo.	32/31	319.6	08.9	64.8	04.7	032.1	04.6	019.1	46.7	03.0	06.1	09.4
	Paleo.	37/37	341.7	05.4	38.2	07.2	027.1	04.6	022.9	21.5	02.8	05.0	08.4
	U. Creta.	8/7	151.5	18.9	-58.4	13.2	032.0	10.8	018.2	39.1	07.8	14.5	24.1
Alcı-Orhaniye	Pliocene	15/15	345.2	09.7	46.4	10.4	022.3	08.3	020.9	27.7	05.8	08.6	14.9
	Miocene	136/131	322.9	03.8	46.5	04.1	017.2	03.1	014.3	27.8	01.7	03.4	03.8
	Eo-Oligo.	44/43	033.9	07.2	40.1	09.2	012.2	06.5	011.6	22.8	02.7	06.7	07.7
	Paleo.	56/49	070.1	06.9	56.3	05.3	022.4	04.4	014.7	36.9	02.5	05.5	07.1
	U. Creta.	39/39	010.0	06.5	40.1	08.2	014.8	06.2	015.8	22.9	02.8	05.9	08.2
North Haymana	Pliocene	37/37	330.5	05.2	49.0	05.2	040.9	03.7	028.3	29.9	02.8	04.5	08.4
	Miocene	20/20	349.8	04.6	51.8	04.1	106.2	03.2	072.6	32.4	05.1	03.9	12.4
	Eo-Oligo.	92/76	315.7	04.5	40.9	05.7	015.8	04.2	016.2	23.4	02.1	04.2	05.4
	Paleo.	251/219	312.6	03.0	47.3	03.2	014.2	02.6	013.8	28.5	01.4	02.7	02.8
	U. Creta.	449/397	298.0	02.6	55.5	02.1	017.0	01.8	012.3	36.1	01.1	02.1	01.9
Haymana (south)	Pliocene	152/146	017.2	03.7	52.3	03.3	020.2	02.7	015.4	32.9	01.6	03.1	03.6
	Miocene	30/21	006.3	07.5	51.2	06.9	032.3	05.7	025.8	31.9	03.6	06.4	12.0
	Eo-Oligo.	254/227	034.3	03.0	46.8	03.1	015.6	02.4	013.8	28.0	01.4	02.6	02.7
	Paleo.	115/102	038.3	04.7	46.2	05.0	015.0	03.7	012.4	27.5	01.9	04.1	04.5
	U. Creta.	No averages calculated											

Nm: number of demagnetized specimens/mean ChRM direction per site under AF/TH, NvD: number of specimens/mean direction included in the calculation for the mean ChRM direction after applying the 45° fixed cut-off, Dec/I: declination/inclination, ΔDx / (ΔIx): errors in declination / (inclination) determined from the A95 of the poles, k: estimate of the precision parameter determined from the ChRM directions, a95: cone of confidence determined from the mean ChRM directions for in situ and tilt corrected data, K: precision parameter determined from the mean virtual geomagnetic pole directions (VGPs), λ: paleolatitude, A95: cone of confidence determined from the mean VGP direction, A95min / (A95max) : minimum / (maximum) value of the A95 for the given dataset based on (Deneen *et al.*, 2011, 2014).

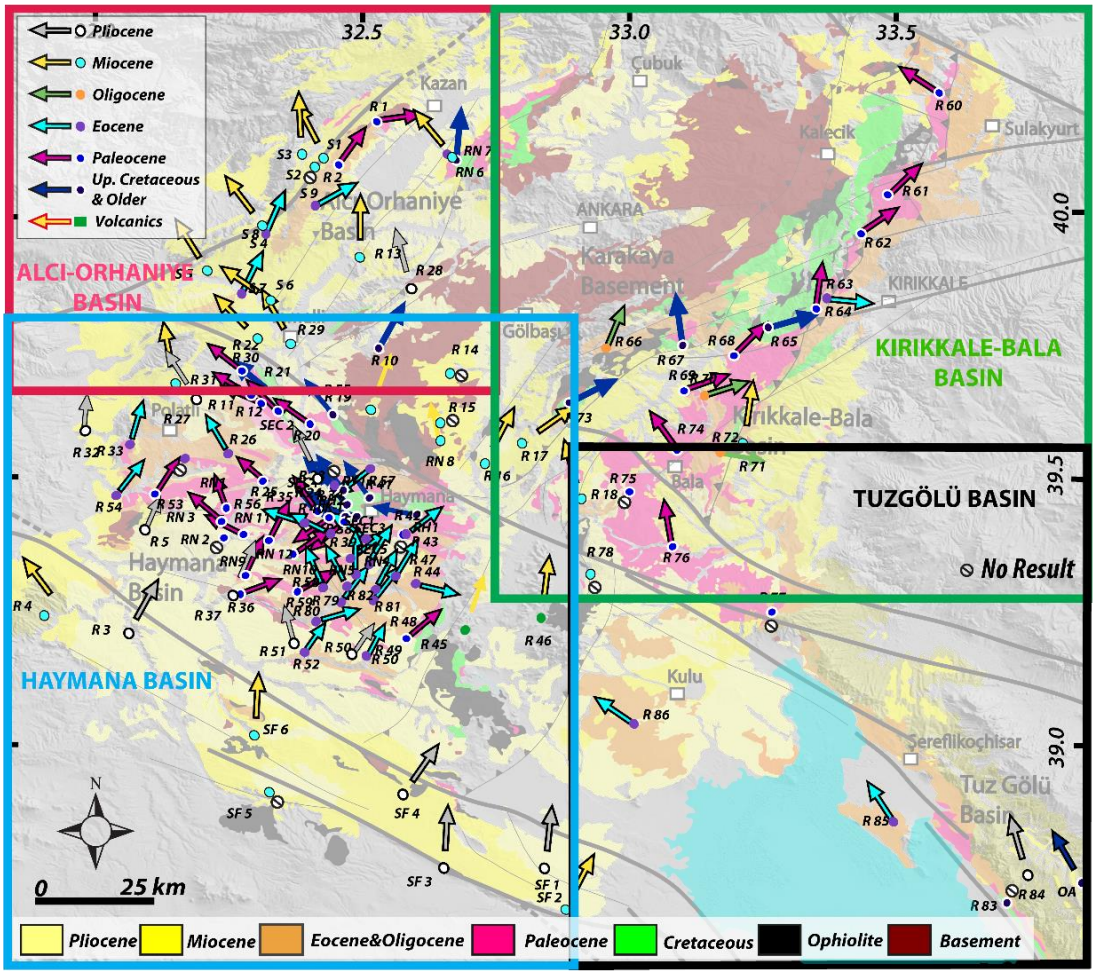

Figure 3.18. Mean declination vectors per site for different time intervals. The boxes indicate the data clustered for each basin to determine mean block rotation vectors.

Paleocene of Kırıkkale-Bala basin is represented by 84 samples from five sites. The average declination vector indicates large clockwise rotation amount of 45.7±5.1° from the Kırıkkale-Bala Basin (Figure 3.19, Table 3.2). All the specimens have normal polarity (Figure 3.20).

The oldest studied time interval in Kırıkkkale-Bala Basin is late Cretaceous and represented by 32 samples from two sites. The mean vector indicates very large clockwise rotations which is 70.3±6.9° (Figure 3.19, Table 3.2).

3.5.1.2. The Tuz Gölü Basin

Only one Pliocene site (R 84) represents the Tuz Gölü Basin. The results of the site indicates 16° counter-clockwise rotation with N=21, D: 163.8±3.1°, I:-49.6 results (Figures 3.21 and 3.22, Table 3.2).

Similarly, the Miocene is also represented by one site (R 18) with 20 samples. The results show that the site mean rotation amount is 15° counter-clockwise (D: 344.5±9.0° and I: 43.4) (Figure 3.21 and 3.22, Table 3.2).

Eocene - Oligocene interval in the Tuz Gölü Basin is represented by two sites (Table 3.2). The results of combination of these two sites out of 32 samples, produced consistent result with 40° counter-clockwise rotations (D: 319.6±8.9°, I:64.8°). All the samples have normal polarity.

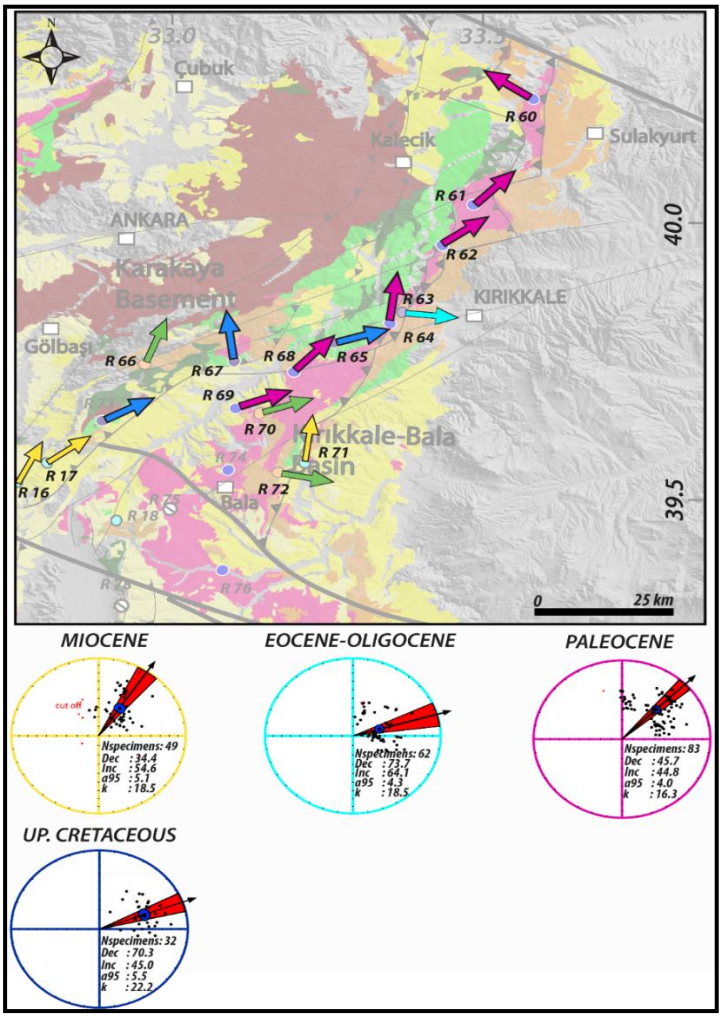

Figure 3.19. Paleomagnetic vector diagrams of Upper Cretaceous to Pliocene rocks in the Kırıkkale-Bala Basin. Equal area projections of the ChRM directions determined from specimens in five time intervals. Open (solid) symbols denote projection on upper (lower) hemisphere. Large symbols indicate respectively the mean directions and their cone of confidence (a95). Red (small) circles indicate the individual directions rejected by the cut-off angle 45° (Vandamme, 1994).

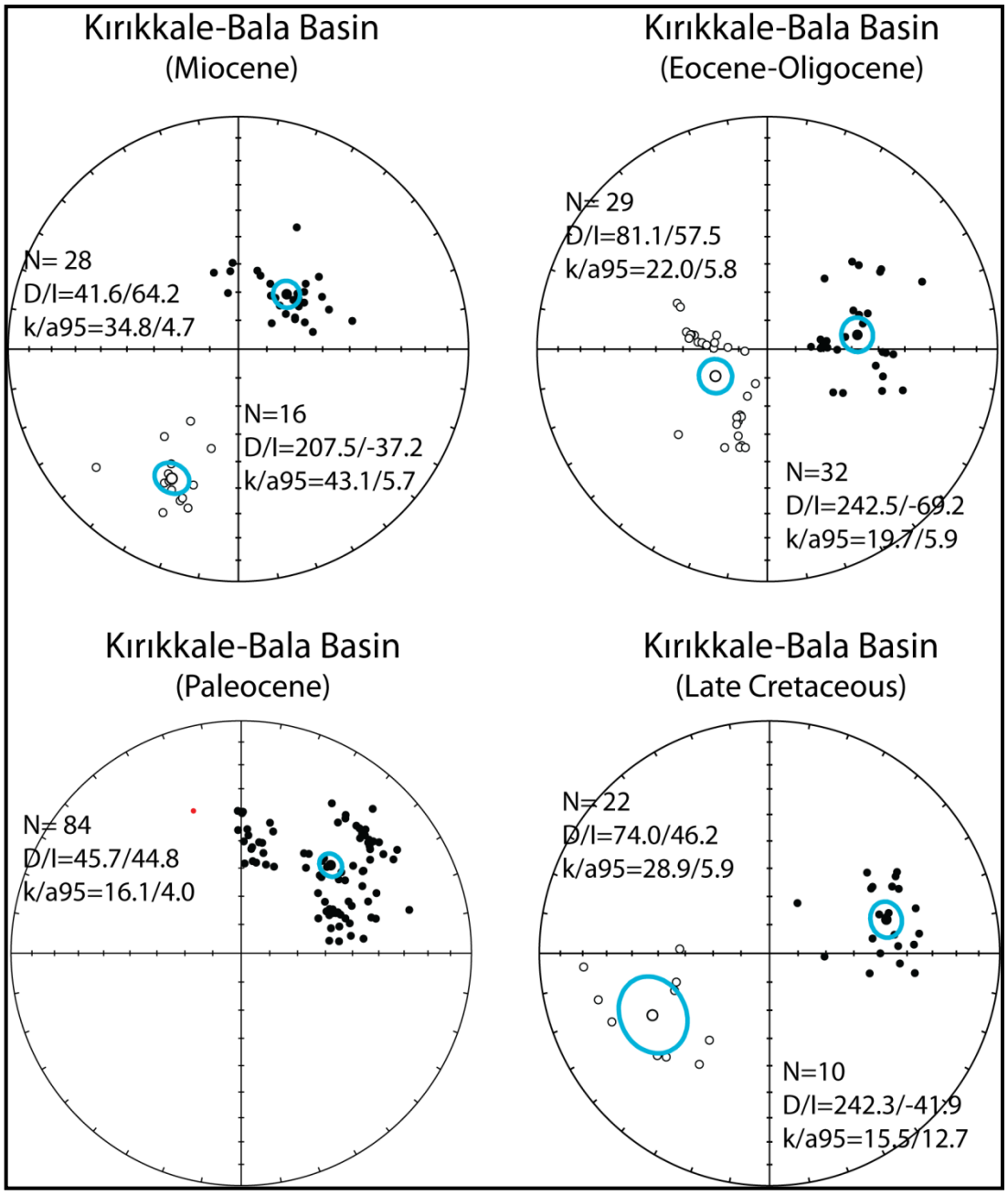

Figure 3.20. Equal area, lower hemisphere projection of all the samples in Kırıkkale-Bala Basin for different times intervals. Large blue circles are mean directions and their error range, black dots are (normal polarity) and small circles (reverse polarity) individual samples and red dots are rejected samples after 45° (Vandamme 1994) filter is applied.

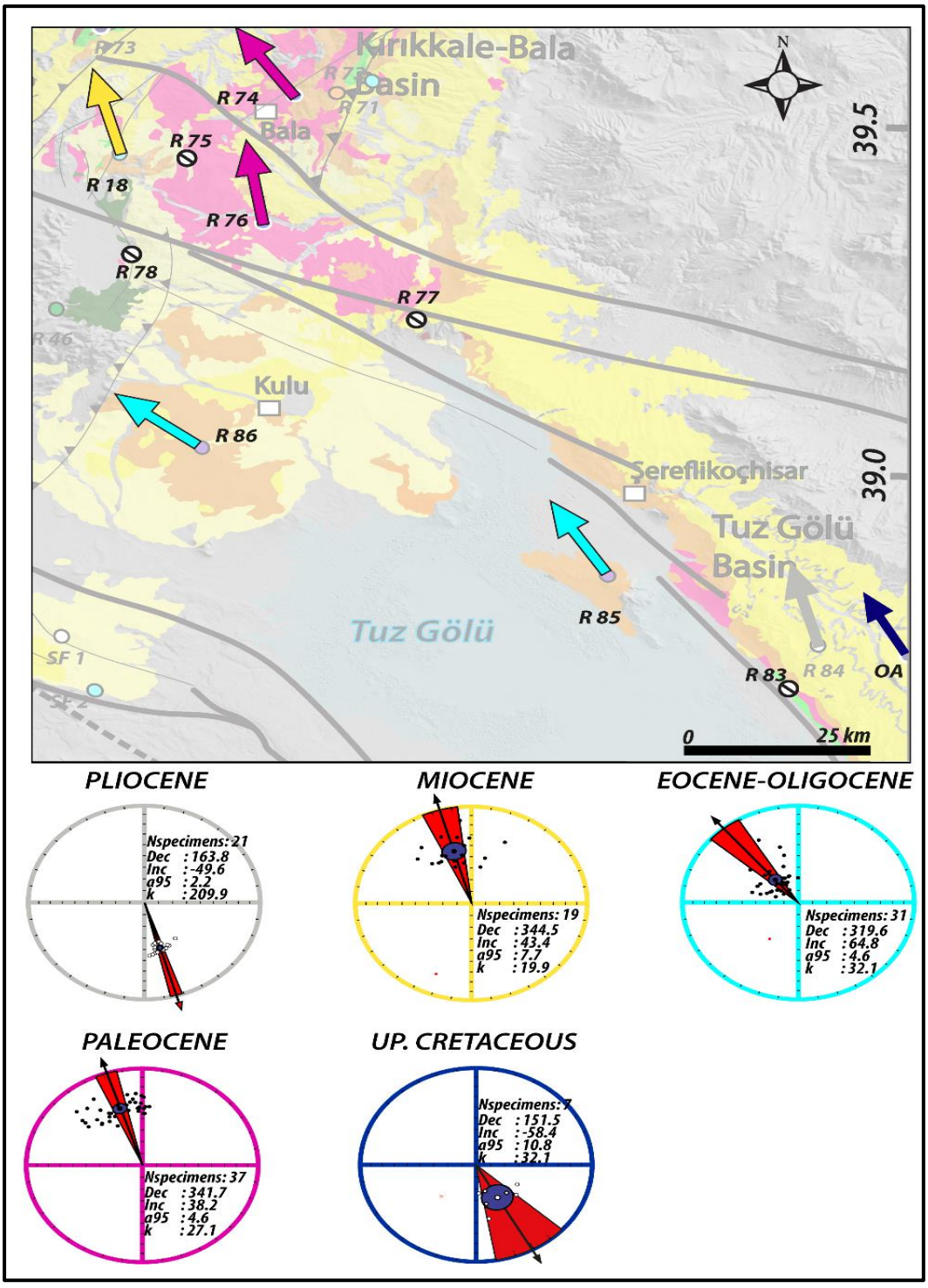

Figure 3.21. Paleomagnetic vector diagrams of Upper Cretaceous to Pliocene rocks in the Tuz Gölü Basin. Equal area projections of the ChRM directions determined from specimens in five time intervals. Open (solid) symbols denote projection on upper (lower) hemisphere. Large symbols indicate respectively the mean directions and their cone of confidence (a95). Red (small) circles indicate the individual directions rejected by the cut-off angle 45° (Vandamme, 1994).

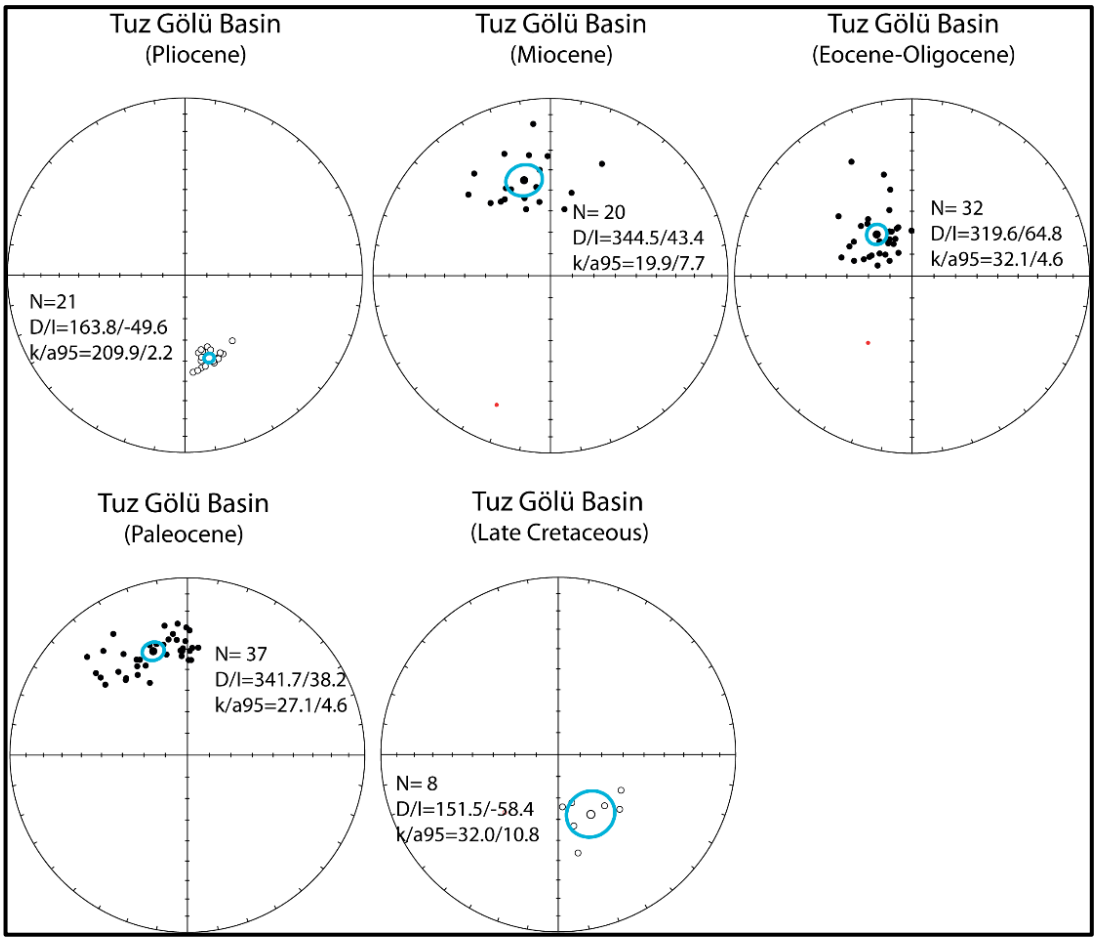

Figure 3.22. Equal area, lower hemisphere projection of all the samples in the Tuz Gölü Basin for different times intervals. Large blue circles are mean directions and their error range, black dots are (normal polarity) and small circles (reverse polarity) individual samples and red dots are rejected samples after 45° (Vandamme 1994) filter is applied.

Similarly, the average Paleocene rotation results are obtained from two sites (R 74 and R 76) in the Tuz Gölü Basin (Figure 3.21, Table 3.2). The combination of these sites, out of 37 samples, indicate 18° counter clockwise rotations (D: 341.7±5.4°, I: 38.2). Low inclination value is most probably due to flattening effect. The late Cretaceous is represented by only one site (OA) in the Tuz Gölü Basin. The other contemporaneous site (R83) did not produce interpretable results and rejected. The site OA belongs to granitoids in the basement of the Tuzgölü Basin. The site mean rotation direction, out of 8 samples, indicate 29° counter-clockwise rotations (D: 151.5±8.9°, I: -58.4°) (Figure 3.22, Table 3.2).

3.5.1.3. The Alcı-Orhaniye Basin

The Alcı-Orhaniye basin is located at the NW part of the study area. It constitutes the integral part of the Haymana Basin and underlain by the Pontide Block. The paleomagnetic results are clustered for five time intervals ranging from the late Cretaceous to Pliocene. The youngest data set represents the Pliocene of the basin and comprises only one site (R28). From 15 samples D: 345.2±9.7°, I: 46.4° results are obtained. Based on this data the basin is said to be rotated 14° counter-clockwise during the Pliocene (Figure 3.23, Table 3.2). All specimens have normal polarity (Figure 3.24). Eight sites (R 13 belongs to volcanic rocks) represent the Miocene of the basin (Figure 3.23). The mean directions calculated from 136 samples indicate 37° counter-clockwise rotation during the Miocene (D: 322.9±8.9°, I: 46.5°). The results from the volcanic site show slightly clockwise rotation of 1.6±7.9°. The data contain both normal and reverse polarities and produced positive reversal test (γ = 14.2° < γc = 8.6°, classification B) (Figure 3.24). For the Eocene-Oligocene rotation results three sites with total 44 samples are available (Figures 3.23 and 24). The resultant mean rotation amount and sense is 34° clockwise (D: 33.9±7.2°, I: 40.1). The sites both normal and revers polarities the applied reversal test is negative (γ = 37.8° < γc = 8.6°, out of classification) (Figure 3.24).

The Alcı-Orhaniye Basin has two Paleocene sites (R1 and R 2) both have normal polarity. Mean direction for the whole basin, based on 56 samples, indicate 70° clockwise rotation (D: 70.1±6.9°, I: 56.3°) (Table 3.2).The site R10 is sampled for the basement of Alcı-Orhaniye Basin and it yielded D: 094.0°, I: 67.7°, from 17 samples. Although, the age of the sampled site is Triassic, however very high inclination values indicate that this site is remagnetized, possible during Eocene-Oligocene interval considering its possible paleolatitudinal position. The late Cretaceous of Alcı-Orhaniye basin is represented by only one site (R6). The results of this site indicate more around 65° clockwise rotation (D: 244.8°, I:-53.5°) based on 20 samples.

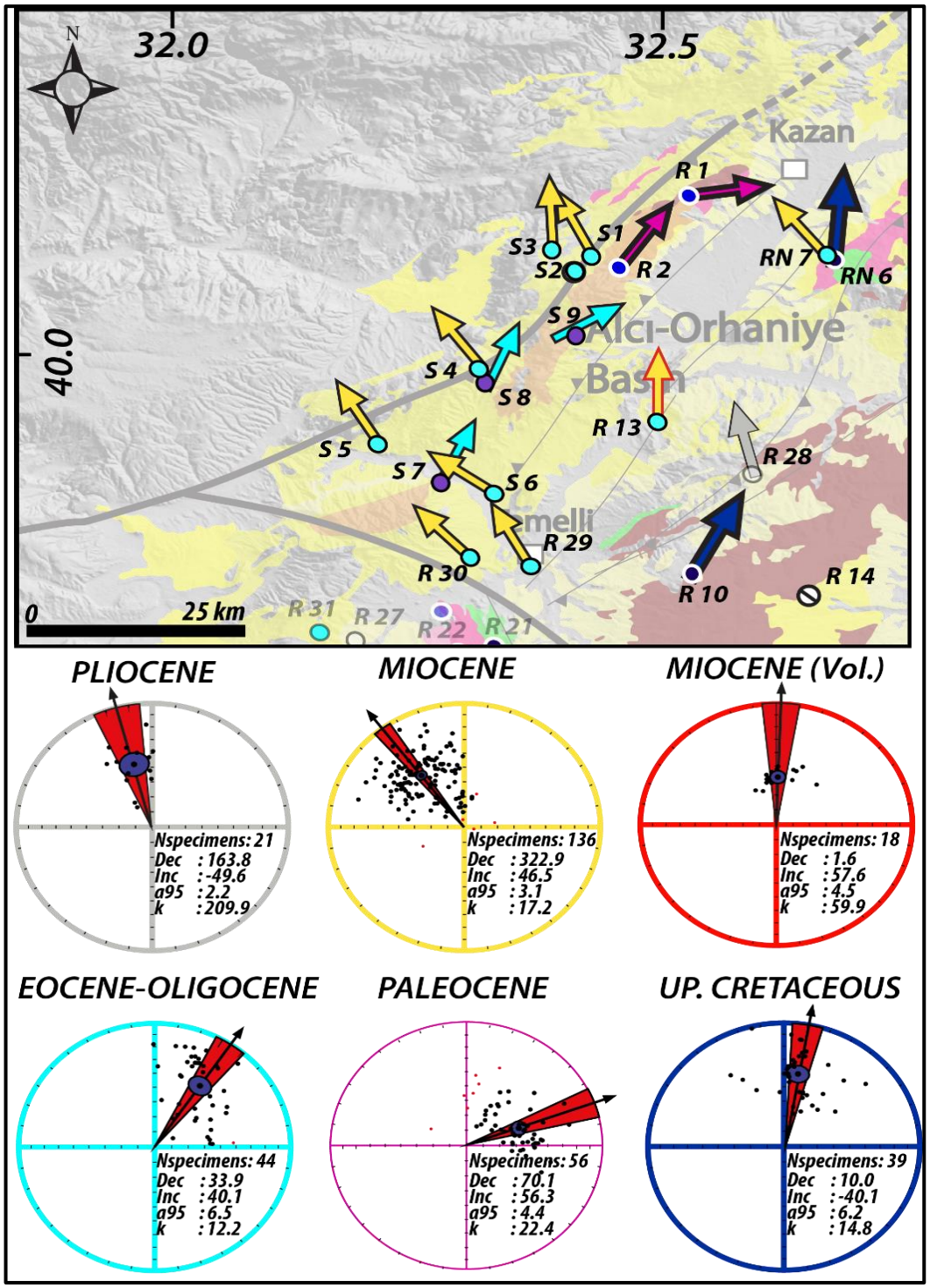

Figure 3.23. Paleomagnetic vector diagrams of Upper Cretaceous to Pliocene age rocks in the Alcı-Orhaniye Basin. Equal area projections of the ChRM directions determined from specimens in five time intervals. Open (solid) symbols denote projection on upper (lower) hemisphere. Large symbols indicate respectively the mean directions and their cone of confidence (a95). Red (small) circles indicate the individual directions rejected by the cut-off angle 45° (Vandamme, 1994).

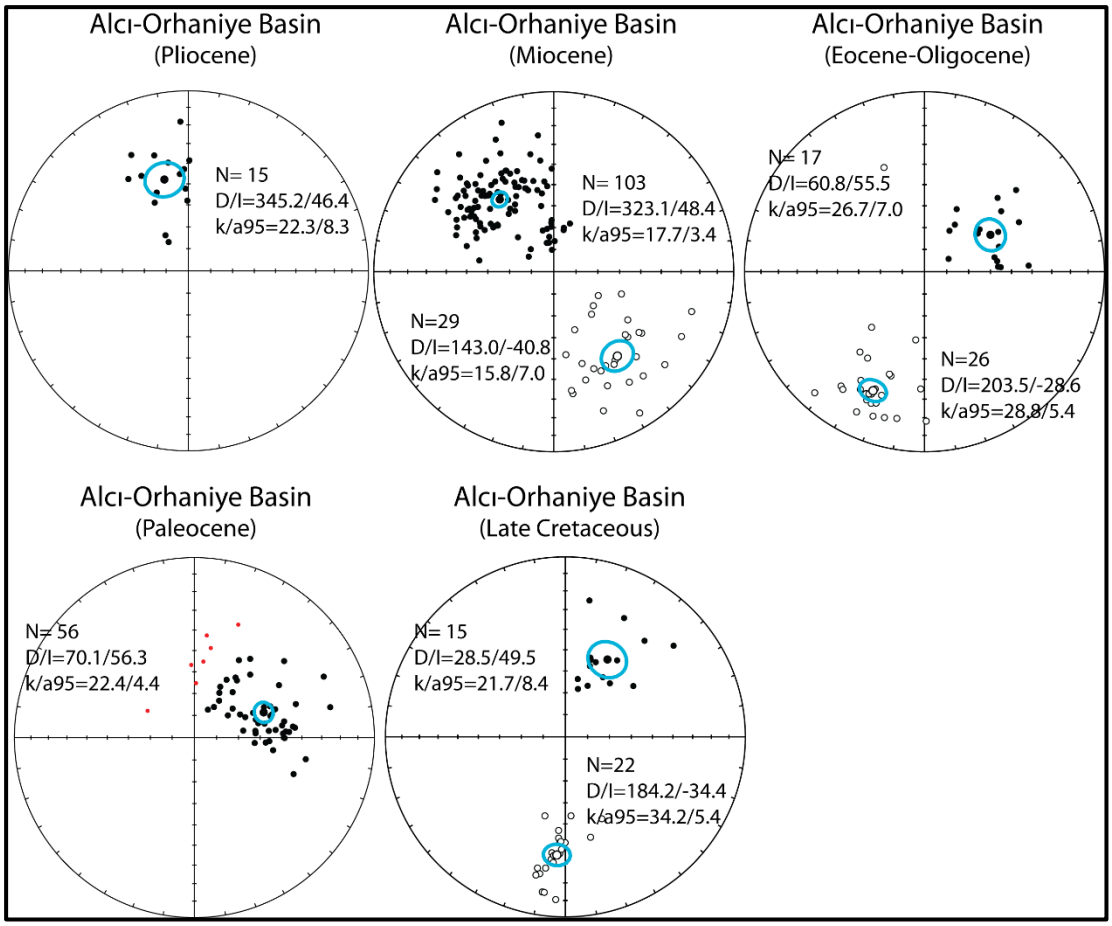

Figure 3.24. Equal area, lower hemisphere projection of all the samples in the Alcı-Orhaniye Basin for different times intervals. Large blue circles are mean directions and their error range, black dots are (normal polarity) and small circles (reverse polarity) individual samples and red dots are rejected samples after 45° (Vandamme 1994) filter is applied.

3.5.1.4. The Haymana Basin

Due to very contrasting paleomagnetic results the Haymana Basin is subdivided into two parts. The northern and southern part of the basin is analyzed separately.

3.5.1.4.1. Northern Part of the Haymana Basin

The northern part of the Haymana Basin characterized by counter clockwise rotation for all time intervals.

The combined result of two Pliocene sites (R 24 and R 27) resulted approximately 30° counterclockwise rotation ((D: 330.5±5.2°, I: 49.0°) out of 37 samples (Table

3.2, Figure 3.25). The sub-basin has both normal and reverse polarity samples. Therefore, we applied reversal test which is positive (γ = 4.4° < γc = 7.2°, classification B) (Figure 3.26).

The Miocene of northern part of Haymana basin is represented by only one site with 20 samples. The results show approximately 10° of counter-clockwise rotation (D: 349.8±4.6°, I: 51.8°) (Figure 3.26, Table 3.2).

Four sites, with 92 samples, represent the Eocene-Oligocene of northern part of the Haymana Basin. Among these one site has reverse polarity samples while the other three sites yielded normal polarity (Table 3.2). The combined results indicate approximately 44° counter-clockwise rotations (D: 315.7±4.5°, I: 40.9) (Table 3.2). Since there are both normal and reverse polarities, the applied reversal test is negative due to shallow and scattered results in the reversal components (I=-34.8, a95=4.9) (γ = 13.6° > γc = 6.5°, out of classification) (Figure 3.26).

Paleocene is represented by 12 sites with 251 samples (Table 3.2, Figure 3.25). Almost half of the samples are reverse polarized. The combined results show large counter-clockwise rotations (D: 312.6±3.0°, I: 47.3°). The ChRM vector distribution show well clustered results (a95=2.6, k=14.2). According to the normal and reverse components, the reversal test shows again shallow inclination (-37.2) in the reversal components so the test is negative (γ = 20.3° > γc = 3.7°, out of classification) (Figure 3.26).

The oldest rotation data in the region belongs Upper Cretaceous sites (Figure 3.25). Only one site show completely reverse polarity and the other two sites have both normal and reverse polarities. The paleomagnetic result out of 449 samples indicate very large counter-clockwise rotations (D: 298.0±2.6°, I: 55.5°) (Table 3.2). The ChRM vectors are well clustered (a95=1.8). The applied reversal test is negative (γ = 23.2° > γc = 3.7°, out of classification) (Figure 3.26). This is most probably due to declination differences (D_{normal}=292.6 and $D_{reverse}$=148.9) and shallower inclination in the reverse polarities (56.3 versus -48.5) (Figure 3.26).

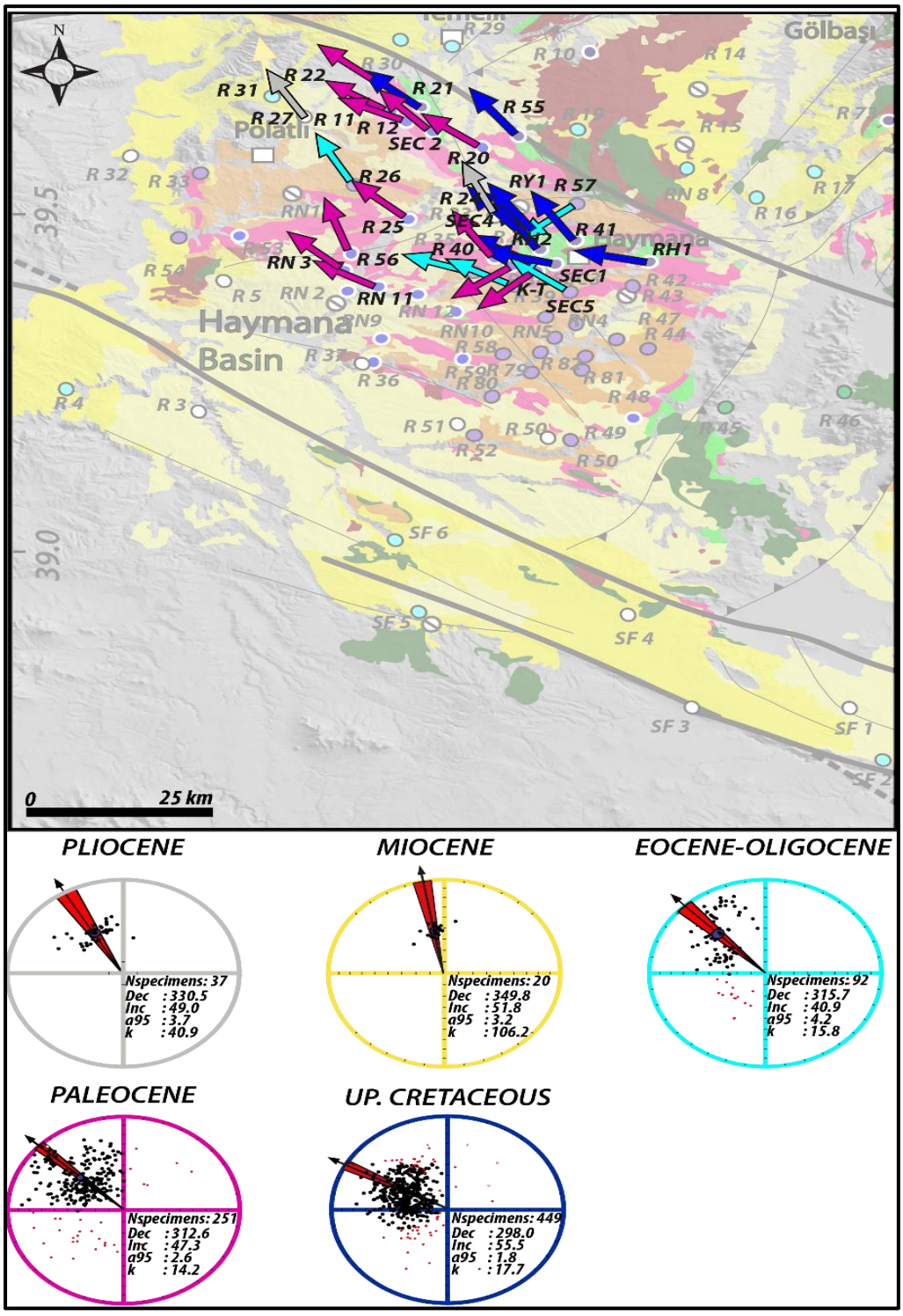

Figure 3.25. Paleomagnetic vector diagrams of Upper Cretaceous to Pliocene rocks in the northern part of Haymana Basin. Equal area projections of the ChRM directions determined from specimens in four intervals. Open (solid) symbols denote projection on upper (lower) hemisphere. Large symbols indicate respectively the mean directions and their cone of confidence (a95). Red (small) circles indicate the individual directions rejected by the cut-off angle 45° (Vandamme, 1994).

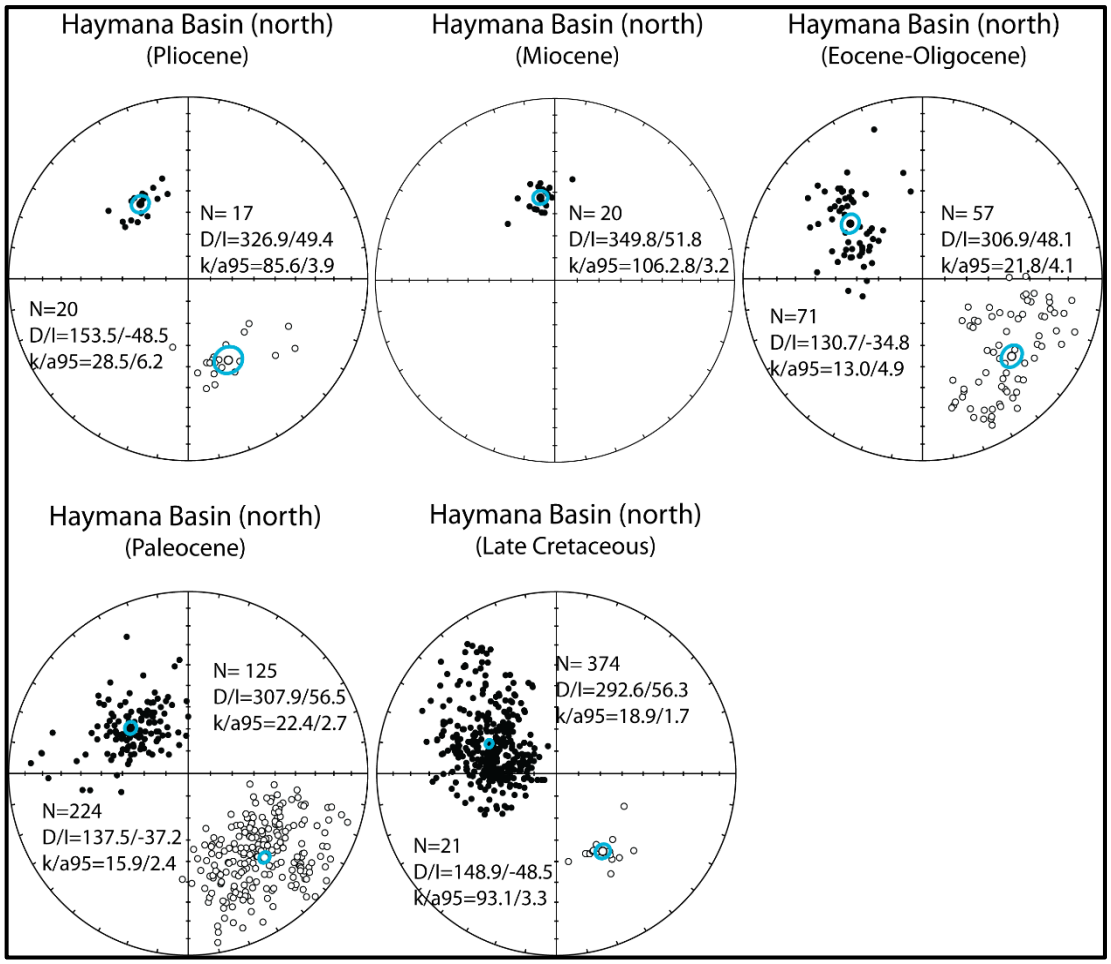

Figure 3.26. Equal area, lower hemisphere projection of all the samples in the northern part of the Haymana Basin for different times intervals. Large blue circles are mean directions and their error range, black dots are (normal polarity) and small circles (reverse polarity) individual samples and red dots are rejected samples after 45° (Vandamme 1994) filter is applied.

3.5.1.4.2. Southern Part of the Haymana Basin

The Pliocene of the southern part of the Haymana Basin is represented by 9 sites (Figure 3.27). The mean of the 9 sites with 449 samples indicate that the sub-basin underwent 17° clockwise rotation (D: 17.2±2.6°, I: 52.3) (Table 3.2). The basin has both normal and reverse polarities and the reversal test is positive ($\gamma = 4.1° < \gamma c = 5.2°$, classification B) (Figure 3.28).

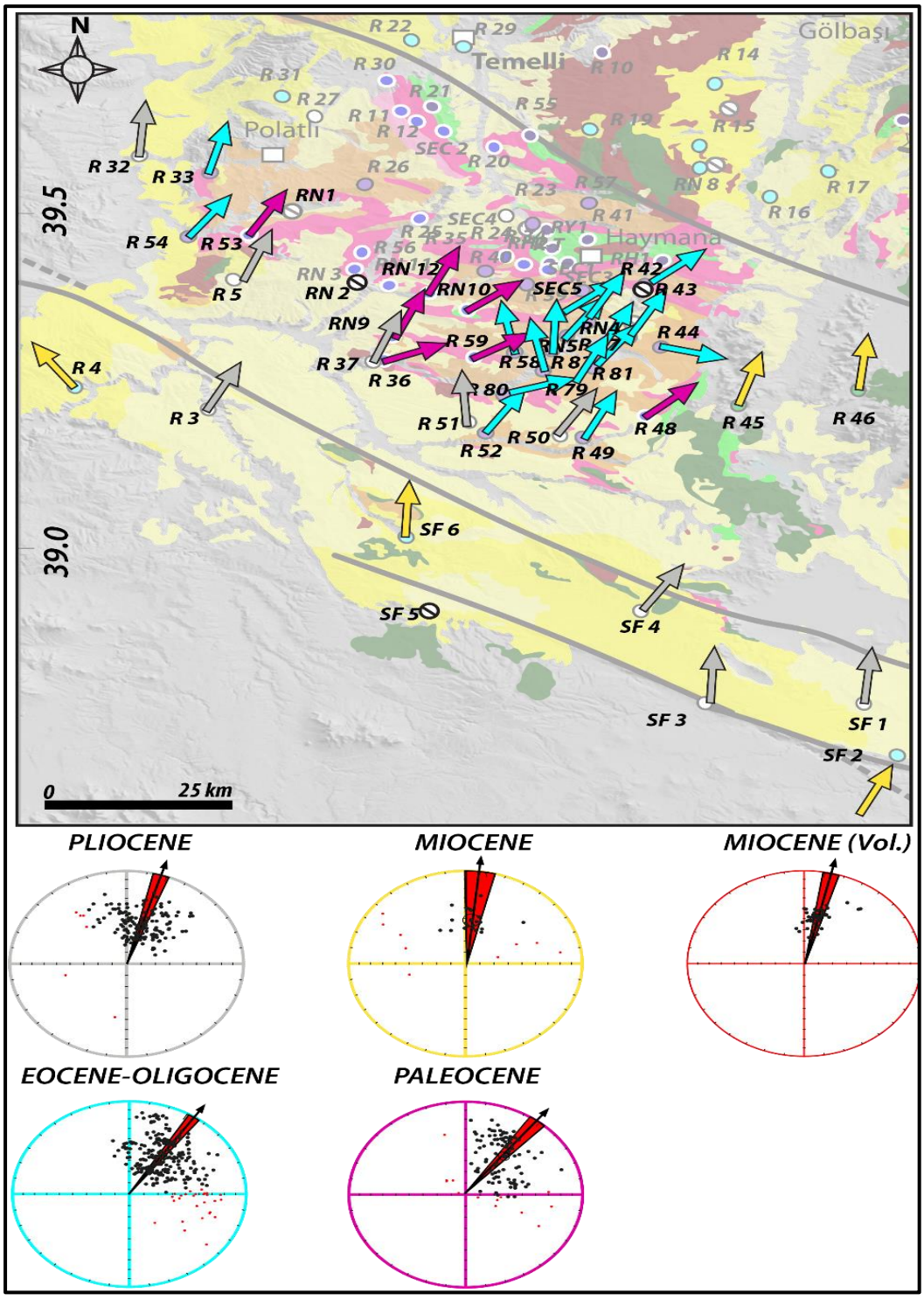

Figure 3.27. Paleomagnetic vector diagrams of Upper Cretaceous to Pliocene age rocks in the Haymana Basin (south). Equal area projections of the ChRM directions determined from specimens in five time intervals. Open (solid) symbols denote projection on upper (lower) hemisphere. Large symbols indicate respectively the mean directions and their cone of confidence (a95). Red (small) circles indicate the individual directions rejected by the cut-off angle 45° (Vandamme, 1994).

Two Miocene sites with total of 30 samples represent the basin. Both of these sites has normal polarity and mean rotation amount is around 6° (D: 6.3±7.5°, I: 51.2°) clockwise. One of these sites is volcanic and reverse polarity the other one is sedimentary and with normal polarity. The mean rotation from volcanic rocks has more clockwise rotation (12.8±3.7°) than the sedimentary ones. The applied reversal test is negative ($\gamma = 11.4° > \gamma c = 5.8°$, out of classification) (Figure 3.28).

The Eocene-Oligocene of the southern part of the Haymana Basin is represented by 15 sites and 254 total samples. Although, some of the results are rejected due to inconsistencies in directions, the general distribution of the ChRM directions are well clustered (a95=2.4). The mean rotation amount is clockwise sense and direction of (D: 34.3±3.0° I: 46.8). According to the reverse and normal polarities, the reversal test is negative ($\gamma = 262° > \gamma c = 7.0°$, out of classification) (Figure 3.29).

The oldest units sampled level in the southern part of the Haymana Basin is Paleocene (Figure 3.27). It is represented by six Paleocene sites (Figure 3.27) with 115 samples. The mean Paleocene rotation is around 38° clockwise (D: 38.3±4.7°, I: 46.2°). The distribution to total number of 115 samples show fair clustering (a95=3.7). The reversal test gives positive result ($\gamma = 4.1° < \gamma c = 7.2°$, classification B) (Figure 3.28).

In addition to two sub areas, the data from Haymana Basin is also evaluated for whole basin. In order to accomplish this all the data from northern southern part of the basin is combined and analyzed. The Pliocene of the basin is represented by 183 samples and they indicate approximately 10° clockwise rotation during the Pliocene with D: 10.5°, I: 52.7° (Figure 3.29).

The Miocene is represented by 41 samples and they yielded D: 356.7°, I: 53.9° which indicates very slight counter-clockwise rotation of the basin. Eocene-Oligocene time interval comprises 303 samples which produced D: 33.9°, I: 46.9°. Very large part of the data is rejected due to 45° cut-off (Vandamme 1994). This value indicates approximately 34° clockwise rotation of the basin during Eocene.

Paleocene time interval in the Haymana Basin is represented by 321 samples and the yielded D: 312.8°, I: 47.5°. It indicates approximately 39° counter-clockwise rotation

during the Paleocene. In the analysis very large part of the data is excluded due to 45° cut-off (Vandamme 1994). Therefore, the obtained ChRM values represent smoothed rotation value of the basin.

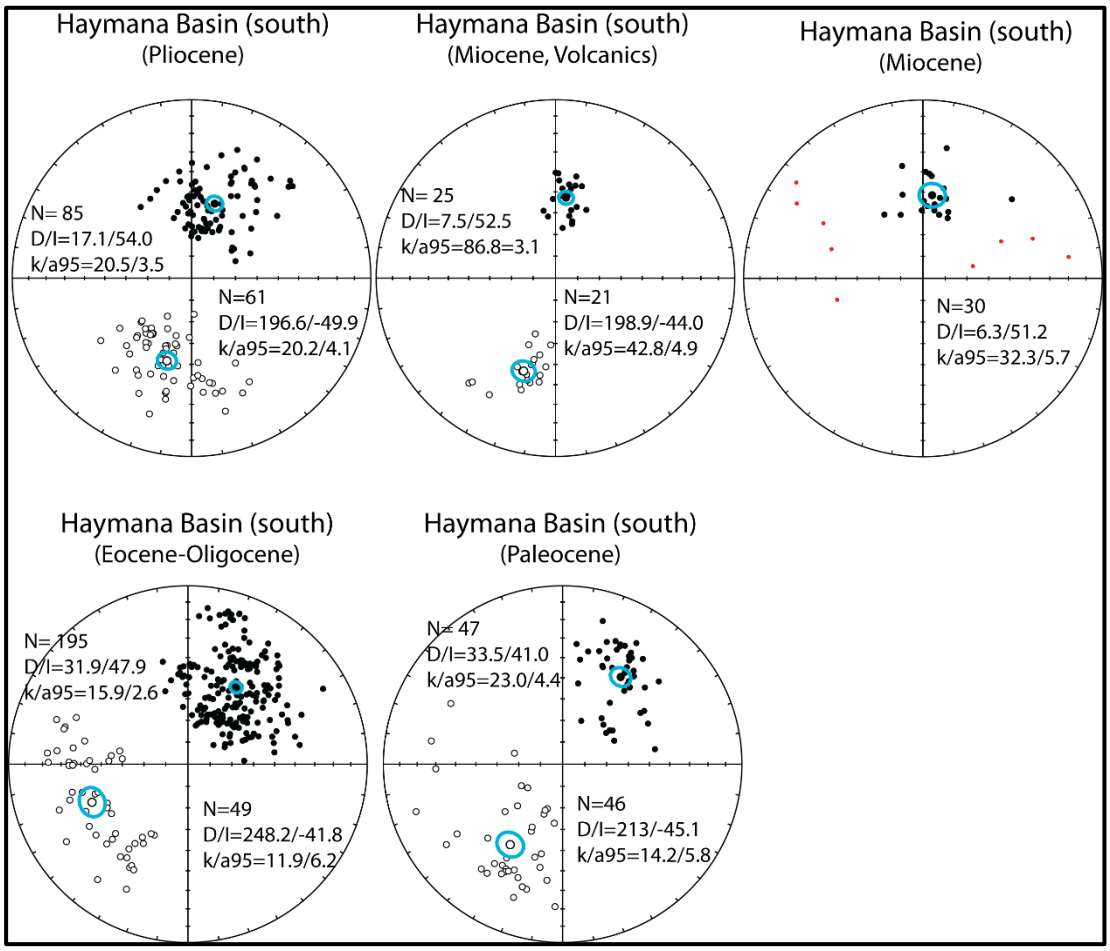

Figure 3.28. Equal area, lower hemisphere projection of all the samples in the southern part of the Haymana Basin for different times intervals. Large blue circles are mean directions and their error range, black dots are (normal polarity) and small circles (reverse polarity) individual samples and red dots are rejected samples after 45° (Vandamme 1994) filter is applied.

The late Cretaceous of the Haymana Basin is represented by 374 samples all of which passed the 45° cut-off indicating that the results are consistent which are; D: 292.6, I: 56.3 (Figure 3.29). These results indicate approximately 67° counterclockwise rotation of the basin at the end of Cretaceous.

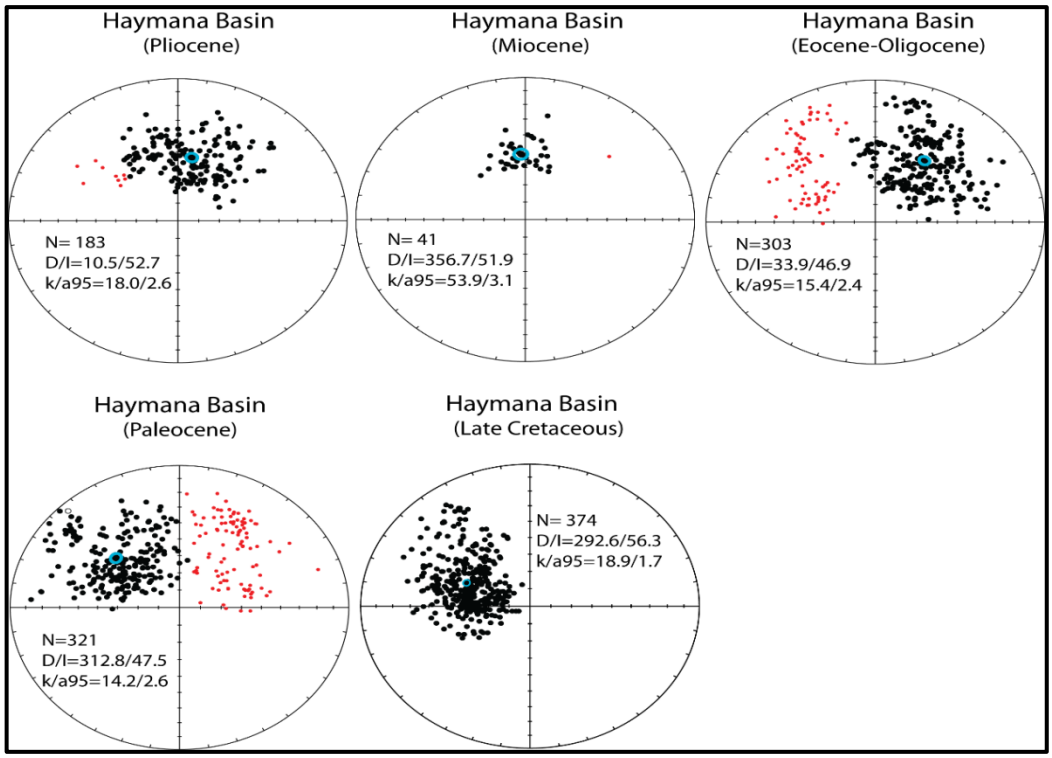

Figure 3.29. Equal area, lower hemisphere projection of all the samples in the Haymana Basin (data includes both northern and southern parts of the basin) for different times intervals. Large blue circles are mean directions and their error range, black dots are (normal polarity) and small circles (reverse polarity) individual samples and red dots are rejected samples after 45° (Vandamme 1994) filter is applied.

3.5.2. Timing of the vertical axis bock rotations

The systematic sampling in the field and detailed paleomagnetic analyses show that there are very significant variations in the vertical axis rotations in the study area since the Late Cretaceous to Pliocene. Based on the spatial consistency of the rotations the study area is subdivided into five sub-areas. Each sub areas are analyzed for their mean rotations (Table 3.2). In order to calculate incremental rotation amounts of each basin for successive time interval, the younger rotation amounts are subtracted from the previous ones (Table 3.3). This would give the paleodeclination values for that particular interval for each basin. As seen in the Table 3.3, the late Cretaceous units in Kırıkkale-Bala Basin had paleodeclination values of 024.6°N. It means that by the end of the Late Cretaceous the basin infill of Kırıkkale-Bala basin must have been rotated clockwise approximately 24°.

Likewise, during the Paleocene in the Kırıkkale-Bala Basin 28° counter-clockwise rotation, in Tuzgölü Basin 6.4° clockwise rotation, in Alcı-Orhaniye Basin 36.2 clockwise rotation, in northern part of Haymana Basin 3.1 counter-clockwise and in the southern part 21.2 clockwise rotations took place.

During the Eocene-Oligocene interval amount of rotation was 39.3° clockwise sense in Kırıkkale-Bala, 6.4° clockwise in Tuzgölü, 36.2° clockwise in Alcı-Orhaniye, -3.1° counter-clockwise in the northern part of Haymana and 21.2 clockwise in the southern part of the Haymana basin.

The rotation amounts during the Miocene is as follows; Kırıkkale-Alcı Basin 34.4°, clockwise, Tuz Gölü Basin 1.5° clockwise, Alcı-Orhaniye Basin 22.3° counter-clockwise, in the northern part of Haymana Basin 19.3° clockwise and in the southern part of Haymana Basin 6.3° clockwise rotations took place.

The largest Pliocene rotation took place in the northern part of Haymana Basin which is -29.5° (counterclockwise). Similarly, Tuzgölü and Alcı-Orhaniye basins were also rotated counterclockwise during the Pliocene time interval (Table 3.3) while overall Hayman Basin and its southern part rotated around 10.5 and 17.2° clockwise respetively. This implies that vertical axis rotations in the region continued until Pliocene and possibly still continuing.

3.6. Conclusions

Obtained results have shown that there has been significant amount of rotations in the region almost each time interval and each basin.

During the late Cretaceous the largest rotations took place in Alcı-Orhaniye Basin and it was as high as -96° (counter-clockwise). The least rotation took place in the Tuz Gölü Basin and it is around 5.5 ° clockwise senses which is an insignificant amount. The other areas rotated both clockwise and counter-clockwise around 15-25°.

Table 3.3. Rotation amounts restored incrementally for each time interval.

Basins	Age	Dec.	Present	End Miocene	End Oligocene	End Paleocene	End Cretaceous
Kırıkkale-Bala	Pliocene	?	**?**				
	Miocene	034.4	34.4	**34.4**			
	Eo-Oligocene	073.7	73.7	73.7	**39.3**		
	Paleocene	045.7	45.7	45.7	11.3	**-28.0**	
	U. Cretaceous	070.3	70.3	70.3	35.9	-3.4	**24.6**
Tuz Gölü	Pliocene	163.8	**-17.0**				
	Miocene	344.5	-15.5	**1.5**			
	Eo-Oligocene	319.6	-40.4	-23.4	**-24.9**		
	Paleocene	341.7	-18.3	-17	-18.5	**6.4**	
	U. Cretaceous	151.5	-28.5	-11.5	-13.0	11.9	**5.5**
Alcı-Orhaniye	Pliocene	345.2	**-14.8**				
	Miocene	322.9	-37.1	**-22.3**			
	Eo-Oligocene	033.9	33.9	48.7	**71.0**		
	Paleocene	070.1	70.1	84.9	107.2	**36.2**	
	U. Cretaceous	010.0	10.0	24.8	47.1	-60.1	**-96.3**
Haymana (north)	Pliocene	330.5	**-29.5**				
	Miocene	349.8	-10.2	**19.3**			
	Eo-Oligocene	315.7	-44.3	-14.8	**-34.1**		
	Paleocene	312.6	-47.4	-17.9	-37.2	**-3.1**	
	U. Cretaceous	298.0	-62.0	-32.5	-51.8	-17.7	**-14.6**
Haymana (south)	Pliocene	017.2	**17.2**				
	Miocene	006.3	6.3	**6.3**			
	Eo-Oligocene	034.3	34.3	17.1	**10.8**		
	Paleocene	038.3	38.3	38.3	32.0	**21.2**	
	U. Cretaceous	?					**?**
Haymana (all)	Pliocene	010.5	**10.5**				
	Miocene	356.7	3.3	**-7.2**			
	Eo-Oligocene	033.9	33.9	23.4	**30.6**		
	Paleocene	312.8	47.2	36.7	43.9	**13.3**	
	U. Cretaceous	292.6	67.1	56.6	63.8	33.2	**19.9**

Red numbers indicate amount of rotation that took place during corresponding time interval. Positive numbers indicate clockwise while negative numbers indicate counter-clockwise rotations. Positive numbers also corresponds to paleodeclination values while negative values need to be added to (subtracted from) 360° to obtain their paleodeclinations.

During the Paleocene, the largest rotations took place in the Alcı-Orhaniye (36.2° clockwise), Kırıkkale-Bala (-28° counterclockwise) and southern part of Haymana

(21.2° clockwise) basins. Rotations in other basins are relatively low to negligible. The least rotation took place in the northern Part of Haymana Basin and it is around -3.1° in counter-clockwise sense. Rotations during the Eocene-Oligocene time interval are very large, in almost all basins, except for the southern part of the Haymana Basin where least rotation values obtained (10.8° clockwise). All other basins experienced clockwise and counterclockwise rotations larger than 25°.

The Miocene rotation values are relatively low except for Kırıkkale-Bala Basin where clockwise rotation reaches up to 34.4°, all other basins experienced rotation less than 23°. Rotations in Tuz Gölü, southern part of Haymana and Hayman Basin combined are negligible. Which implies that only northern part Haymana Basin, Kırıkkale-Bala Basin and Alcı-Orhaniye basin experienced rotation during prior to Pliocene. Kırıkkale-Bala basin does not have any Pliocene rotation data. Northern part of Haymana, Alcı-Orhaniye and Tuz Gölü basins experienced counter-clockwise rotations while only southern part of Haymana Basin experienced clockwise rotation. Clockwise rotation of combined data of overall Haymana Basin is possibly is an artifact of statistical operations. It seems that the data from southern part dominates over the northern part and combined results produced 10.5 ° clockwise rotation.

In conclusion, there has been very large amounts of rotations in all senses and almost in all time intervals and are changed continuously over time. This implies that rotational deformation of the study area has been a continuous process since the Late Cretaceous until recently.

CHAPTER 4

CONCLUSIONS

This study provides a very comprehensive and detailed paleomagnetic and AMS data from the Late Cretaceous to Pliocene time interval mainly from the sedimentary infill of the central Anatolian basins that centered around the Haymana Basin. The other basins include Alcı-Orhaniye, Kırıkkale-Bala and Tuzgölü basins which interrelated and laterally transitional with the Haymana Basin.

These basins straddle the three sutures zones which form a triple junction at the eastern margin of the Haymana Basin, SW and NW margins of Kırıkkale-Bala and Tuzgölü basins, respectively. The Haymana Basin straddles the Izmir-Ankara segment of the İzmir-Ankara-Erzincan Suture Zone while, Kırıkkale-Bala Basin demarcates the Ankara-Erzincan segment of the İzmir-Ankara-Erzincan Suture Zone and Tuzgölü basin is located along the Intra-Tauride Suture Zone.

The study was conducted on by paleomagnetic sampling in 119 sites distributed homogeneously over the study area both temporally and spatially. In these sites more than 4500 samples were collected and measured for both ChRM vector and Anisotropy of Magnetic Susceptibility (AMS) vectors. The majority of the samples are collected from sedimentary rocks ranging in age from late Cretaceous to Pliocene.

Nearly 90% of the measured specimens provided reliable results which are used to investigate the rotational history of the Haymana and adjacent basins including to the Kırıkkale-Bala, Tuz Gölü, and Alcı-Orhaniye basins.

In addition to ChRM results for vertical axes rotations, the AMS results provided deformation history of the study are based on the magnetofabric characteristics of the measured samples.

The major findings of this research are summarized below.

Paleomagnetic studies revealed that;

1. The studied basins and related suture zones are rotated spatially and temporally both clockwise and counter-clockwise (back and forth) since the late Cretaceous continuously.
2. One of the most important outcome of this study is related to the geometry and position of these basins and hence the suture zones. In paleogeograhical maps and palinspastic reconstructions, in the literature, the İzmir-Ankara-Erzincan Suture zone is generally envisaged as E-W belt along which the Neotethys ocean subducted northwards below Pontides. Its complete consumption and obliteration is followed by collision of Taurides into the Pontides from south to north along an E-W oriented suture zone. However, the results of this study have shown that the orientation of the suture İzmir-Ankara and Intra-Tauride zones and possibly also the late Cretaceous configuration of the trench was oriented N-S, contrary to what is known previously. In addition, the longer axes of all the basins were oriented N-S during the late Cretaceous and Tuzgölü and Kırıkkale-Bala basins were collinear while Haymana and Alcı-Orhaniye Basins were collinear.
3. The largest rotation took place at the end of Cretaceous in the Alci-Orhaniye Basin and it was as high as -96°. The other major rotations took place during the Eocene-Oligocene interval and reached up to 71° in Alcı-Orhaniye and 30.6° in Haymana, 39.3° in Kırıkkale-Bala basins. End Paleocene and end Miocene rotations are relatively low except for Alcı-Orhaniye (36.2°) and Kırıkkale-Bala (-28°).
4. The largest Pliocene rotation took place in the northern part of Haymana basin (-29.5°).
5. Rotations along the İzmir-Ankara-Erzincan Suture Zone and the studied basins continued until the recently

The AMS studies revealed that

6. The AMS vectors are related to tectonic deformation and can be used as strain markers. The minimum AMS vector corresponds to maximum principal contraction axis (k_{min}) which is the compaction component of the

sediments, whereas the intermediate axis (k_{int}) corresponds to the major tectonic contraction direction while k_{max} corresponds to principal stretching direction.

7. Based on this assumption late Cretaceous is characterized by multidirectional contraction and extension in different parts of the study area. Whereas, Paleocene is characterized generally by NW-SE directed extension in almost in all areas.
8. Eocene-Oligocene is dominated by NW-SE contraction possible due to indentation of Kırıkkale-Keskin Block into the Kırıkkale-Bala and Alcı-Orhaniye basins, while the Tauride Block squeezed the Tuz Gölü and Haymana basins simultaneously.
9. Miocene is characterized by NW-SE compression in the eastern part of the study area and NE-SW and N-S compression in the western part of the study area.
10. Pliocene is characterized by WNW-ESE compression in the south while it is dominated by NE-SW compression in the Alcı-Orhaniye Basin in the north.
11. There is a very prominent boundary that separates the domains with similar AMS vector orientations. This boundary corresponds to Dereköy-Hirfanlı Fault Zone and was proposed by Lefebvre et al. (2013) and its eastern extension is delineated in this study.

This study successfully applied integration of paleomagnetic and AMS results in unravelling the deformation history as well as spatial and temporal evolution of central Anatolian basins and associated Neotethyan Sutures.

REFERENCES

Advokaat, E.L., van Hinsbergen, D.D.J., Kaymakcı, N., Vissers, R.L.M., and Hendriks, B.W.H., 2014. Late Cretaceous extension and Paleogene rotation related contraction in Central Anatolia recorded in the Ayhan-Büyükkışla basin. International Geology Review, 56, 1813-1836.

Akarsu, İ., 1971. II. Bölge AR/TPO/747 nolu sahanın terk raporu. Pet. İş. Gen. Md., Ankara (Unpublished).

Akıl, B., 2008. Structural Evolution of İnönü-Eskişehir Fault System between Günyüzü (Eskişehir) and Yeniceoba (Konya-Turkey). Ph.D. Thesis, University of Haccettepe, 113 p.

Akyürek, B., Bilginer, E., Akbaş, B., Hepşen, N., Pehlivan, Ş., Sunu, O., Soysal, Y., Dağer, Z., Çatal, E., Sözeri, Z., Yıldırım, H., and Hakyemez, Y., 1984. The geology of the Ankara-Elmadağ-Kalecik region. Jeoloji Mühendisliği Dergisi, 20, 31-46.

Altıner, D., Koçyiğit, A., Farinacci, A., Nicosia, U., and Conti, M.A., 1991. Jurassic-Lower Cretaceous stratigraphy and paleogeographic evolution of the southern part of NW Anatolia, Turkey. Geologica Romana, 27, 13-80.

Andrew, T., and Robertson, A.H.F., 2002. The Beysehir-Hoyran-Hadim nappes: genesis and emplacement of Mesozoic marginal and oceanic units of the northern Neotethys in southern Turkey. Journal of the Geological Society of London, 159, 529-543.

Angelier, J., Lyberis, N., Le Pichon, X., Barrier, E., Huchon, P., 1982. The tectonic development of the Hellenic arc and the Sea of Crete: a synthesis. Tectonophysics 86, 159–196.

Arıkan, Y., 1975. Tuzgölü havzasının jeolojisi ve petrol imkanları. MTA Bülteni, 85, 17-38.

Arni, P., 1965. L'évolution des nummulitinae en tant que facteur de modification des depots littoraux. Coloque International de Micropaléontologie (Daker), Mémoires du BRGM, 32, 7-20.

Arslan, M., Aslan, Z., Sen, C., and Hoskin, P.W.O., 2000. Constraints on Petrology and Petrogenesis of Tertiary Volcanism in the Eastern Pontide Paleo-Arc System, NE Turkey Conference Abstracts, Cambridge Publications, 5(2),157

Arslan, M., Temizel, İ., Abdioğlu, E., Kolaylı, H., Yücel, C., Boztuğ, D., and Şen, C., 2013. 40Ar–39Ar dating, whole-rock and Sr–Nd–Pb isotope geochemistry of post-collisional Eocene volcanic rocks in the southern part of the Eastern Pontides (NE Turkey): implications for magma evolution in extension-induced origin. Contributions to Mineralogy and Petrography, 166,113–142.

Averbuch, O., Frizonde Lamotte, D., and Kissel, C.(1992). Magnetic fabric as a structural indicator of the deformation path within a fold thrust structure: a test case from the Corbieres (NE Pyrenees, France). J. Struct.Geol. 14,461–474.

Aydemir, A., Ates, A., 2006. Structural interpretation of the Tuzgölü and Haymana Basins, Central Anatolia, Turkey, using seismic, gravity and aereomagnetic data. Earth, Planets and Space, 58, 951–961.

Aydın, M., Demir, O., Özçelik, Y., Terzioğlu, N., Satır, M., 1995. A geological revision of İnebolu, Devrekani, Ağlı and Küre areas: new observations in Paleo-Tethys - Neo-Tethys sedimentary successions. In: Erler, A., Ercan, T., Bingöl, E., Örçen, S. (Eds.), Geology of the Black Sea Region. MTA Bülteni, Özel baskı, 33–38.

Aziz, A. 1975. İskilip civarı ile güney ve güneybatısının detay jeolojisi ve petrol olanakları. M.T.A. Ars¸. Rap. No: 6132 (unpublished).

Bailey, E.B., McCallien, W.J., 1950. The Ankara mélange and the Anatolian thrust. MTA Bülteni, 40, 17-21.

Barrier, E., and B. Vrielynck (2008). Paleotectonic Maps of the Middle East: Atlas of 14 Maps, Comm. de la Carte Geol. du Monde, Paris.

Barka, A.A., Hancock, P.L., 1984a. Neotectonic deformation patterns in the convex northwards arc of the North Anatolian Fault. In: Dixon, J.G., Robertson, A.H.F. (Eds.), The Geological Evolution of the Eastern Mediterranean, Geological Society of London Special Publication, vol. 105, pp. 763–773.

Barka, A., 1984b. Geology and tectonic evolution of some Neogene-Quaternary basins in the North Anatolian fault zone. In: Ketin Symposium. In: Geol. Soc. of Turkey, pp.209–227.

Barka, A., 1992. The North Anatolian fault zone. Ann. Tecton.6, 164–195.

Barka, A., Reilinger, R., 1997. Active tectonics of the Eastern Mediterranean region: deduced from GPS, neotectonic and seismicity data. Annali Di Geofisica 40, 587–610.

Barka, A., Reilinger, R., Şaroğlu, F., Şengör, A.M.C., 1999. The Isparta Angle: its importance in the Neotectonics of the Eastern Mediterranean Region. In: Pişkin, Ö., Ergun, M., Savaşcın, M.Y., Tarcan, G. (Eds.), Proceeding of the International Earth Science Colloquium on the Aegean Region, 9–14 October 1995, İzmir, Turkey, pp. 3–17.

Balsley, J. R. and Buddington, A. F., 1960. Magnetic Susceptibility Anisotropy and Fabric of Some Adirondack Granites and Orthogneisses, Amer. J. Sci. 258-A, 6-20.

Batman, B., 1978. Haymana kuzeyinin jeolojik evrimi ve yöredeki melanjin incelenmesi - stratigrafi birimleri. Hacettepe University, Earth Sciences, 4, 95-124

Baydemir, N., 1990. Paleomagnetism of the Eocene volcanic rocks in the eastern Black Sea region (in Turkish). Istanbul University Engineering Department. Journal of Earth Science 7, 167–176.

Bingöl, E., 1974. Discussions on the metamorphic map of Turkey in a scale of 1:2,500,000 and geotectonic evolution of some metamorphic belts. MTA Bülteni, 83, 119–131.

Birgili, S., Yoldaş, R., and Ünalan, G., 1974. Çankırı-Çorum Havzası jeolojisi ve petrol olanakları ön raporu. TPAO Rap. No: 1216 (unpublished).

Biryol, C.B., Beck, S.L., Zandt, G., Özacar, A.A., 2011. Segmented African lithosphere beneath the Anatolian region inferred from teleseismic P-wave tomography. Geophys. J. Int.184, 1037–1057.

Boccaletti, M., Gocev, P., and Manetti, P., 1974. Mesozoic isotopic zones in the Black Sea region. Società Geologica Italiana, Bollettino, 93, 547-565.

Borradaile GJ., Mothersill J., Tarling D., Alford C. (1986). Sources of magnetic susceptibility in a slate. Earth Planet Sci Lett 76:336–340.

Borradaile GJ. (1988). Magnetic susceptibility, petrofabrics and strain. Tectonophysics 156(1–2):1–20.

Borradaile GJ., Henry B. (1997). Tectonic applications of magnetic susceptibility and its anisotropy. Earth Sci Rev 42(1–2):49–93.

Borradaile GJ., Jackson M., (2004). Anisotropy of magnetic susceptibility (AMS): magnetic petrofabrics of deformed rocks. In: Martı´n-Herna´ndez F, Lu¨neburg C, Aubourg C, Jackson M (eds) Magnetic Fabric methods and applications. Geol. Soc. Lond. Spec. Publ. 238:299–360.

Borradaile, G.J., and Jackson, M. (2010). Structural geology, petrofabrics and magnetic fabrics (AMS, AARM, AIRM). J. Struct. Geol. 32, 1519–1551.

Bozkurt, E., Koçyiğit, A., 1996. The Kazova basin: an active negative flower structure on the Almus Fault Zone, a splay fault system of the North Anatolian Fault Zone, Turkey. Tectonophysics 265, 239–254.

Bozkurt, E., 2001. Neotectonics of Turkey—a synthesis. Geodin. Acta14, 3–30.

Boztuğ, D., Harlavan, Y., 2007. K-Ar ages of granitoids unravel the stages of Neo-Tethyan convergence in the eastern Pontides and central Anatolia, Turkey. International Journal of Earth Sciences, 97, 585-599.

Boztuğ, D., G.A. Wagner, A.İ. Erçin, D. Göc ,, Z. Yeğingil, A. İskenderoğlu, M. K. Kuruçelik, İ. Kömür, and Y. Güngör., 2002. Sphene and zircon fission-track geochronology unravelling subduction-and collision related magma surges in the composite Kaçkar Batholith, Eastern Black Sea region, Turkey. 1st International Symposium of the Faculty of Mines (İTÜ) on Earth Sciences and Engineering, 16–18 May 2002, Istanbul, Turkey, Abstracts, p. 121.

Bragin, N.J., Tekin, K., 1996. Age of radiolarian-chert blocks from the Senonian ophiolitic mélange (Ankara, Turkey). Island Arc, 5, 114–122.

Bucha, V., 1975. Geomagnetic field. (In Czech). Academia, Prague.

Butler, R.F., 1992. Paleomagnetism: Magnetic Domains to Geologic Terranes. Black-well Publishing, Boston. 195 pp.

Burbank, D.W., and Anderson, R.S., 2001. Tectonic Geomorphology. Blackwell Science, Massachusetts, 274 p.

Candan, O., Cetinkaplan, M., Oberhänsli, R., Rimmele, G., and Akal, C., 2005. Alpine high Pressure low-Temperature metamorphism of the Afyon Zone and implications for the metamorphic evolution of Western Anatolia, Turkey. Lithos 84(1-2), 102-124.

Carey, E., and Brunier, B., 1974. Analyse théorique et numérique d'un modèle mécanique élémentaire applequé à l'étude d'une population de failles: C. R. hebd. Séanc. Acad. Sci. Paris, D, v. 279, p. 891-894.

Cater, J.M.L., Hanna, S.S., Ries, A.C, and Turner, P., 1991. Tertiary evolution of the Sivas Basin, central Turkey. Tectonophysics, 195, 29-46.

Channell, J.E.T., Tüysüz, O., Bektaş, O., Şengör, A.M.C., 1996. Jurassic–Cretaceous paleomagnetism and palaeogeography of the Pontides (Turkey). Tectonics 15, 201–212.

Chaput, E., 1932. Observations géologiques en Asie Mineure: Le Crétacé supérieur dans l'Anatolie Centrale. C. R. A. S., 194, 1960-1961.

Chaput, E., 1935a. L'Eocene du plateau de Galatie (Anatolie Centrale). C. R. A. S., 200, 767-768.

Chaput, E., 1935b. Les plissements Tertiare de l'Anatolie Centrale. C. R. A. S., 201, 1404-1405.

Chaput, E., 1936. Voyages d'études géologiques et géomorphologiques en Turquie. Mém. Inst. Françaiş D'Archaéo. İstanbul, II, 312 p.

Cifelli, F.; Mattei, M.; Chadima, M.; Hirt, A. & Hansen, A., 2005. The origin of tectonic lineation in extensional basins: Combined neutron texture and magnetic analyses on undeformed clays, *Earth and Planetary Science Letters*, 235, 62 - 78

Clark, M., and Robertson, A., 2002. The role of the Early Tertiary Ulukışla Basin, southern Turkey, in suturing of the Mesozoic Tethys Ocean. Journal of the Geological Society, 159(6), 673-690.

Clark, M. and Robertson, A., 2005. Uppermost Cretaceous–Lower Cenozoic Ulukışla Basin, south-central Turkey: sedimentary evolution of part of a unified basin complex within an evolving Neotethyan suture zone. Sedimentary Geology, 173, 15–51.

Creer, K.M., 1983. Computer analysis of geomagnetic palaeosecular variations. Nature 304, 695–699.

Çelik, Ö.F., Delaloye, M., 2006. Characteristics of ophiolite-related metamorphic rocks in the Beyşehir ophiolitic mélange (Central Taurides, Turkey), deduced from whole rock and mineral chemistry. Journal of Asian Earth Sciences, 26, 461–476.

Çelik, Ö. F., Marzoli, A., Marschik, R., Chiaradia, M., Neubauer, F. and Öz, I., 2011. Early–Middle Jurassic intra-oceanic subduction in the Izmir-Ankara-Erzincan Ocean, Northern Turkey. Tectonophysics, 509, 120–134.

Çemen, İ., Göncüoğlu, M.C., and Dirik, K., 1999. Structural evolution of the Tuzgölü Basin in Central Anatolia, Turkey. Journal of Geology, 107, 693–706.

Çetin, H., Demirel, İ. H., and Gökçen, S.L., 1986. Haymana'nın (SW Ankara) doğusu ve batısındaki Üst Kretase-Alt Tersiyer istifinin sedimantolojik ve sedimanter petrolojik incelemesi. TJK Bülteni , 29/2, 21-33.

Çetinkaplan, M., Candan, O., Oberhänsli, R., Bousquet, R., 2008. Pressure-temperature evolution of lawsonite eclogite in Sivrihisar; Tavşanlı Zone-Turkey. Lithos, 104, 12–32.

Çiner, A., Deynoux, M., Ricou, S., and Koşun, E. 1996a. Cyclicity in the middle Eocene Çayraz Carbonate Formation, Haymana Basin, Central Anatolia. Palaeogeography, Palaeoclimatology, Palaeoecology, 121, 313-329.

Çiner, A., Deynoux, M., and Koşun, E., 1996b. Cyclicity in the Middle Eocene Yamak turbidite complex of the Haymana basin, Central Anatolia, Turkey. Geologische Rundschau, 85, 669-682.

Delaloye, M., and Bingöl, E., 2000. Granitoids from Western and Northwestern Anatolia: Geochemistry and modeling of geodynamic evolution. International Geology Review, 42(3), 241- 268.

Dellaloğlu, A. A., Tüysüz, O., Kaya, O.H., and Harput, B., 1992. Kalecik (Ankara) – Eldivan – Yapraklı (Çankırı) – İskilip (Çorum) ve Devrez Çayı arasindaki alanın jeolojisi ve petrol olanakları. TPAO Rap. No. 3194 (unpublished).

Dellaloğlu, A.A., and Aksu, R., 1984. Polatlı, Haymana, Yenice, Yeniceoba ve Cihanbeyli dolaylarının Ayrıntılı Jeoloji ön raporu. TPAO rapor no.2006 (unpublished)

Dellaloğlu, A.A., and Aksu, R., 1986. Ereğli (Konya)-Ulukışla-Çiftehan-Çamardı(Niğde) dolayının jeolojisi ve petrol olanakları. TPAO rapor no.2205 (unpublished)

Dellaloğlu, A.A., and Aksu, R., 1991. Ankara-Temelli-Haymana-Kulu-Kırıkkale arasındaki alanın jeolojisi ve petrol olanakları. TPAO rapor no.3006 (Unpublished).

Delvaux, D., Moeys, R., Stapel, G., Petit, C., Levi, K., Miroshenko, A., Ruzhıch, V., and Sankov, V., 1997. Paleostress reconstructions and geodynamics of the Baikal region, Central Asia, Part 2. Cenozoic rifting. Tectonophysics, 282, 1–38.

Deenen, M.H.L., Langereis, C.G., van Hinsbergen, D.J.J., Biggin, A.J., 2011. Geomag-netic secular variation and the statistics of palaeomagnetic directions. Geophys. J. Int.186, 509–520.

Deenen, M.H.L., Langereis, C.G., van Hinsbergen, D.J.J., Biggin, A.J., 2014. Erratum to: Geomagnetic secular variation and the statistics of palaeomagnetic directions (Geophys. J. Int. 186 (2011) 509–520]. Geophys. J. Int.197, 643.

Demarest, H.H., 1983. Error analysis for the determination of tectonic rotation from paleomagnetic data. Journal of Geophysical Research 88, 4321–4328.

Demirtaşlı, E., Bilgin, A.Z., Erenler, F., Işılar, S., Sanlı, D., Selim, N. and Turhan, N., 1973. Bolkardağlarının Jeolojisi. Cumhuriyetin 50. yılı Yerbilimleri Kongresi, Tebliğler, MTA Yayını, Ankara, 608 p.

Derman, A.S., 1978. Tuzgölü ve Kuzeyinin Jeolojisi. TPAO rapor no 1512 (unpublished).

Dewey, J.F., Hempton, M.R., Kidd, W.S., Şaroğlu, F., Şengör, A.M.C., 1986. Shortening of continental lithosphere: the neotectonics of eastern Anatolia — a young collision zone. In: Coward, M.P., Reis, A.C. (Eds.), Collision Tectonics: Geological Society of London, Special Publication, vol. 19, pp. 2–36.

Dickinson, W.R., and Seely, D.R., 1979. Structure and stratigraphy of forearc regions. AAPG Bulletin, 63, 2–31.

Dilek, Y. and Thy, P., 2006. Age and petrogenesis of palgiogranite intrusions in the Ankara mélange, central Turkey. Island Arc, 15, 44-57.

Dilek, Y., Thy, P., Hacker, B. & Grundvig, S., 1999. Structure and petrology of Tauride ophiolites and mafic dike intrusions (Turkey): implications for the Neotethyan Ocean.Bull. Geol. Soc. Am. 111, 1192-1216.

Dinçer, A., 1977. Haymana-Kulu yöresinin jeolojisi ve petrol olanakları. TPAO rapor no.1314 (unpublished)

Dirik, K., and Erol, O., 2000. Tuzgölü ve civarının tektonomorfolojik evrimi [Tectonomorphologic evolution of Tuzgölü and surrounding area]. Haymana-Tuzgölü-Ulukışla Basenleri Uygulamalı Çalışması, Aksaray, Abstracts, p. 7–8.

Dirik, K., and Erol, O., 2003. Tuzgölü ve civarının tektonomorfolojik evrimi, Orta Anadolu-Türkiye.TPJD Özel sayı, 27-46.

Dirik, K., and Göncüoğlu, M.C., 1996. Neotectonic characteristics of central Anatolia. International Geology Review, 38, 807–817.

Dodson, M.H., 1973. Closure temperature in cooling geochronological and petrological systems. Contributions to Mineralogy and Petrology, 40, 259-274.

Donelick, R.A., O'Sullivan, P.B., and Ketcham, R.A., 2005. Apatite Fission-Track analysis. Reviews in Minerology and Geochemistry, 58, 49-94.

Duddy, I.R., Green, P.F., and Laslett, G.M., 1988. Thermal annealing of fission tracks in apatite, 3. Variable temperature behavior. Chemical Geology (Isotope Geoscience Section), 73, 25–38.

Duermeijer, C.E., van Vugt, N., Langereis, C.G., Meulenkamp, J.E. and Zachariasse, W.J. (1998). A major late Tortonian rotation phase of the Crotone Basin using AMS as tectonic tilt correction and timing of the opening of the Tyrrhenian Basin, Tectonophysics, 287, 233-249.

Duermeijer, C.E., Nyst, M., Meijer, P.T., Langereis, C.G., Spakman, W., 2000. Neogene evolution of the Aegean arc: Paleomagnetic and geodetic evidence for a rapid and young rotation phase. Earth and Planetary Science Letters 176, 509–525.

Dunlop D, Ozdemir O (1997) Rock magnetism, fundamentals and frontiers. Cambridge Studies in Magnetism, Cambridge University Press, Cambridge, p 272.

Elitok, Ö., Dolmaz, M.N., 2008. Mantle flow-induced crustal thinning in the area between the easternmost part of the Anatolian plate and the Arabian Foreland (E. Turkey) deduced from the geological and geophysical data. Gondwana Research 13 (3), 302–318.

Ellwood, B. B., 1975. Analysis of Emplacement Mode in Basalt from DSDP Holes 319A and 321 Using Anisotropy of Magnetic Susceptibility, J. Geophys. Res. 80, 4805-4808.

Ellwood, B. B., 1978a. Measurement of Anisotropy of Magnetic Susceptibility: A comparison of the Precision of Torque and Spinner Magnetometer Systems for Basaltic Specimens, J. Phys. E.: Sci. Instrum. 11, 71-75.

Ellwood, B. B., 1978b. Flow and Emplacement Direction Determined for Selected Basaltic Bodies Using Magnetic Susceptibility Anisotropy Measurements', Earth Plan. Sci. Letters 41,254-264.

Ellwood, B. B., 1979a. Anisotropy of Magnetic Susceptibility Variations in Icelandic Columnar Basalts', Earth Plan. Sci. Letters 42,209-212.

Ellwood, B. B., 1979b. Magnetic Susceptibility Anisotropy Measurements of Coal from the South Wales Coal Field: A Coalification Process Indicator', Geophys. J. Roy. Astron. Soc. 57, 431-443.

Ellwood, B. B. and Fisk, M. R., 1977. Anisotropy of Magnetic Susceptibility Variations in a Single Icelandic Columnar Basalt', Earth Plan. Sci. Letters 35, 116-122.

Ellwood, B. B. and Noltimier, H. C., 1978. Anisotropy of Magnetic Susceptibility Measurements as a Coal Banding-plane Indicator, Nature 274, 353-354.

Ellwood, B. B. and Ledbetter, M. T., 1979. Paleocurrent Indicators in Deep-sea Sediment', Science 203, 1335-1337.

Erdoğan, B., Akay, E., and Uğur, M.S., 1996. Geology of the Yozgat region and evolution of the collisional Çankiri Basin. International Geology Review, 38, 788-806.

Erler, A., and Göncüoglu, M.C., 1996. Geologic and tectonic setting of the Yozgat batholith, Northern Central Anatolian Crystalline Complex, Turkey. International Geology Review, 38 (8), 714-726.

Erler, A., Akıman, O., Unan, C., Dalkılıç, F., Dalkılıç, B., Geven, A., and Önen, P., 1991. Kaman (Kırşehir) ve Yozgat yörelerinde Kırşehir masifi magmatik kayaçlarının petrolojisi ve jeokimyası: TÜBITAK, Doga-Tr. J. of Eng. and Env. Sc., 15, 76-100.

Espurt, N., Hippolyte, J.-C., Kaymakci, J.C.N., and Sangu, E., 2014. Lithospheric structural control on inversion of the southern margin of the Black Sea Basin, Central Pontides, Turkey. Lithosphere, 6, 26–34.

Faccenna, C., Becker, T.W., Jolivet, L., Keskin, M., 2013. Mantle convection in the middle East: reconciling Afar upwelling, Arabia indentation and Aegean trench rollback. Earth Planet. Sci. Lett.375, 254–269.

Faccenna, C., Bellier, O., Martinod, J., Piromallo, C., Regard, V., 2006. Slab detachment beneath eastern Anatolia: a possible cause for the formation of the North Anatolian Fault. Earth Planet. Sci. Lett.242, 85–97.

Faccenna, C., Jolivet, L., Piromallo, C., Morelli, A., 2003. Subduction and the depth of convection of the Mediterranean mantle. J. Geophys. Res.108 (B2), 2099.

Fayon, A.K., Whitney, D.L., Teyssier, C., Garver, J.I., and Dilek, Y., 2001. Effects of plate convergence obliquity on timing and mechanisms of exhumation of a mid-crustal terrain, the Central Anatolian Crystalline Complex. Earth and Planetary Science Letters, 192, 191–205.

Fernandez-Blanco, D., Bertotti, G., and Çiner, T.A., 2013. Cenozoic tectonics of the Tuzgölü basin (Central Anatolian Plateau, Turkey). Turkish Journal of Earth Science, 22, 715-738.

Gans, C.R., Beck, S.L., Zandt, G., Biryol, C.B., Ozacar, A.A., 2009. Detecting the limit of slab break-off in central Turkey: new high-resolution Pn tomography results. Geophys. J. Int.179, 1566–1577.

Gautier, P., Bozkurt, E., Bosse, V., Hallot, E., Dirik, K., 2008. Coeval extensional shearing and lateral underflow during Late Cretaceous core complex development in the Niğde Massif, Central Anatolia, Turkey. Tectonics, 27, TC1003

Glover, C.P., Robertson, A.H.F., 1998. Neotectonic intersection of the Aegean and Cyprus tectonic arcs: extensional and strike-slip faulting in the Isparta Angle, SW Turkey. Tectonophysics 298, 103–132.

Gökçen, S.L., 1976. Haymana güneyinin sedimentolojik incelemesi. I. Stratigrafik birimler ve tektonik. Yerbilimleri, 2, 161-201.

Gökçen, S.L., Kelling, G., 1983. The Paleogene Yamak sand-rich submarine fan complex, Haymana basin, Turkey. Sedimentary Geology, 34, 219-243.

Göncüoğlu, M.C., and Türeli, K., 1993. Orta Anadolu Ofiyoliti plajiyogranitlerinin petrolojisi ve jeodinamik yorumu (Aksaray-Türkiye). Turkish Journal of Earth Sciences, 2, 195-203.

Guezou, J.C., Temiz, H., Poisson, A., Gürsoy, H., 1996. Tectonics of the Sivas Basin. The Neogene Record of the Anatolian accretion along the Inner Tauric Suture. International Geology Review 38, 901–925.

Gürsoy, H., Piper, J.D.A., Tatar, O., Temiz, H., 1997. A palaeomagnetic study of the Sivas Basin, Central Turkey: crustal deformation during lateral extrusion of the Anatolian Block. Tectonophysics 271, 89–105.

Gürsoy, H., Piper, J.D.A., Tatar, O., Mesci, L., 1998. Palaeomagnetic study of the Karaman and Karapınar volcanic complexes, central Turkey: neotectonic rotation in the south-central sector of the Anatolian Block. Tectonophysics 299, 191–211.

Gürsoy, H., Piper, J.D.A., Tatar, O., 1999. Palaeomagnetic study of the Galatean Volcanic Province, north-central Turkey: Neogene deformation at the northern border of the Anatolian Block. Geological Journal 34, 7–23.

Gürsoy, H., Piper, J.D.A., Tatar, O., 2003a. Neotectonic deformation in the western sector of tectonic escape in Anatolia; palaeomagnetic study of the Afyon region, central Turkey. Tectonophysics 374, 57–79.

Gürsoy, H., Tatar, O., Piper, J.D.A., Heimann, A., Mesci, L., 2003b. Neotectonic deformation in the Gulf of Iskenderun, Southern Turkey, deduced from palaeomagnetic study of the Ceyhan–Osmaniye Volcanics. Tectonics 22, 1067–1079.

Gürsoy, H., Tatar, O., Piper, J.D.A., Heimann, A., Kochulut, F. and Mesci, B.L., 2009. Palaeomagnetic study of Tertiary volcanic domains in Southern Turkey and Neogene anticlockwise rotation of the Arabian Plate, Tectonophysics 465, 114–127.

Govers, R., Wortel, M.J.R., 2005. Lithosphere tearing at STEP faults: response to edges of subduction zones. Earth Planet. Sci. Lett.236, 505–523.

Göncüoğlu, M.C., 1997. İdiş Dağı-Avanos Alanının Jeolojisi (Nevşehir-Orta Anadolu): MTA Bülteni, 119, 73-87.

Göncüoğlu, M.C., Sayıt, K., and Tekin, U.K., 2010. Oceanization of the northern Neotethys: Geochemical evidence from ophiolitic mélange basalts within the Izmir-Ankara suture belt, NW Turkey. Lithos, 116, 175-187.

Göncüoğlu, M.C.,1986. Orta Anadolu Masifinin güney ucundan jeokronolojik yaş bulguları. MTA Bülteni, 105/106, 111-124.

Göncüoğlu, M.C., Toprak, V., Kuşcu, I., Erler, A., and Olgun, E., 1991. Orta Anadolu Masifinin orta bölümünün jeolojisi - bölüm 1: Güney kesim. TPAO Rapor no.2909, 140 p (unpublished).

Göncüoğlu, M.C., 1977. Geologie des westlichen Niğde Massivs. Phd Thesis, Bonn University, 181 pp.

Göncüoğlu, M.C., Erler, A., Toprak, V., Olgun, E., Yaliniz, K.M., Kuşcu, I.,Dirik, K., 1993. Orta Anadolu Masifinin orta bölümünün jeolojisi - bölüm 3: Orta Kızılırmak Tersiyer Baseninin jeolojik evrimi. TPAO Rapor no.3313, 104 pp (unpublished).

Görür, N., Tüysüz, O., Aykol, A., Sakinc, M., Yiğitbaş¸ E. and Akkök, R., 1993. Cretaceous red pelagic carbonates of northern Turkey: their place in the opening history of the Black Sea. Eclogae Geology Helvetica, 86, 819–838.

Görür, N., 1997. Cretaceous Syn- to Post-rift Sedimentation on the Southern Continental Margin of the Western Black Sea Basin. In A. G. Robinson (Ed.), Regional and petroleum geology of the Black Sea and surrounding region. AAPG Memoir, 68, 227-240.

Görür, N., Oktay, F.Y., Seymen, I., and Şengör, A.M.C., 1984. Palaeotectonic evolution of the Tuzgölü basin complex, Central Turkey: sedimentary

record of a Neo-Tethyan closure. Journal of the Geological Society of London Special Publications, 17(1), 467-482.

Görür, N., Tüysüz, O., and Şengör, A.M.C., 1998. Tectonic Evolution of the Central Anatolian Basins. International Geology Review, 40, 831-850.

Graham, J. W. (1954). Magnetic susceptibility anisotropy, an unexploited petro fabric element. Geol. Soc. Am. Bull. 65, 1257–1258.

Graham, J. W. (1966). "Significance of magnetic Anisotropy in Appalachian Sedimentary rocks," in The Earth beneath the Continents. Geophysical Monograph Series 10, eds S. Steinhart and T. J. Smith (Washington, DC: American Geophysical Union), 627–648.

Granar L. 1958. Magnetic measurements on Swedish varved sediments. Arkiv for Geofysik, 3, 1-40.

Gülyüz, E., Kaymakci, N., Meijers, M.J.M., van Hinsbergen, D. J.J., Lefebvre, C.J.C., Vissers, R.L.M., Hendriks, B.W.H., and Peynircioğlu, A.A., 2013. Late Eocene evolution of the Çiçekdağı Basin (central Turkey): Syn-sedimentary compression during microcontinent–continent collision in central Anatolia. Tectonophysics, 602, 286–299.

Gülyüz, E., 2015. Tectono-stratigraphic and thermal evolution of the Haymana Basin, central Anatolia, Turkey, PhD. Thesis, Middle East Technical University, Ankara.

Gürbüz, E., and Evans, C., 1991. A seismic refraction study of the western Tuzgolu Basin, central Turkey. Geophysical Journal International, 106, 239–251.

Gürer, Ö.F., and Aldanmaz, E., 2002. Origin of the Upper Cretaceous–Tertiary sedimentary basins within the Tauride–Anatolide platform in Turkey. Geological Magazine, 139, 191-197.

Gürsoy, H., Piper, J.D.A., Tatar, O., Temiz, H., 1997. A palaeomagnetic study of the Sivas Basin, Central Turkey: crustal deformation during lateral extrusion of the Anatolian Block. Tectonophysics271, 89–105.

Gürsoy, H., Piper, J.D.A., Tatar, O., 1999. Palaeomagnetic study of the Galatean Vol-canic Province, north-central Turkey: neogene deformation at the northern bor-der of the Anatolian Block. Geol. J.34, 7–23.

Gürsoy, H., Piper, J.D.A., Tatar, O., 2003. Neotectonic deformation in the west-ern sector of tectonic escape in Anatolia: palaeomagnetic study of the Afyon region, central Turkey. Tectonophysics374, 57–79. http://dx.doi.org/10.1016/S0040-1951(03)00346-9.

Gürsoy, H., Tatar, O., Piper, J.D.A., Heimann, A., Kochulut, F., Mesci, B.L., 2009. Palaeo-magnetic study of Tertiary volcanic domains in Southern Turkey and Neogene anticlockwise rotation of the Arabian Plate. Tectonophysics465, 114–127

Hippolyte, J.-C., Müller, C., Kaymakci, N., and Sangu, E., 2010. Nannoplankton dating in the Black Sea inverted margin of Central Pontides (Turkey) reveals two episodes of rifting. In M. Sosson, N. Kaymakci, R. A. Stephenson, V. Starostenko & F. Bergerat (Eds.), Sedimentary basin tectonics from the Black Sea and Caucasus to the Arabian Platform.). Geological Society of London, 340, 13-136.

Housen, B.A., van der Pluijm, B.A., 1991, Slaty cleavage development and magnetic anisotropy fabrics. Journal of Geophysical Research, 96, 9937-9946.

Housen, B.A., Tobin, H.J., Labaume, P., Leitch, E.C., Maltman, A.J., and ODP Leg 156 Shipboard ScienceParty, 1996. Strain decoupling across the decollement of the Barbados accretionary prism. Geology 24, 127–130.

Housen, B.A., 1997. Magneticanisotropy of Barbados prism sediments, in Proceedings of the Ocean Drilling Program, Scientific Results, Vol.156, eds T.H. Shipley, Y.Ogawa, P.Blum,and J.M. Bahr (College Station, TX: OceanDrilling Program), 97–105.

Housen, B.A., Richter, C., and van der Pluijm, B.A., 1993. Composite magnetic anisotropy fabrics: experiments, numericalmodels, and implications for the quantification of rock fabrics. Tectonophysics 220,

Housen, B.A., and Sato, T., 1995. Magneticanisotropy fabrics from the Cascadia accretionary prism, in Proceedings of the Ocean Drilling Program, Scientific Results, Vol. 146 (CollegeStation, TX: TexasA & MUniversity), 233–254.

Housen, B. A., and T. Kanamatsu, 2003. Magnetic fabrics from the Costa Rica margin: Sediment deformation during the initial dewatering and underplating process, Earth Planet. Sci. Lett., 206, 215–228.

Hrouda F. and Janak F. (1976). The changes in shape of the magnetic susceptibility ellipsoid during progressive metamorphism and deformation. Tectonophysics 34:135–148.

Hrouda, F., 1982. Magnetic anisotropy of rocks and its application in geology and geophysics. Geophys. Surv.5, 37–82.

Hrouda, F., and Jeliınek, V. (1990). Resolution of ferromagnetic and paramagnetic anisotropies in rocks, using combined low-field and high-field measurements. Geophys. J. Int. 103, 75–84.

Hrouda F, Kahan S (1991) The magnetic fabric relationship between sedimentary and basement nappes in the High Tatra Mts (N Slovakia). J Struct Geol 13:431–442.

Hurford, A.J. 1986. Cooling and uplift patterns in the Lepontine Alps, South Central Switzerland and an age of vertical movement on the Insubric fault line. Contributions to Mineralogy and Petrology, 92, 413-427.

Ising, G. (1942). On the magnetic properties of varved clay. Ark. Mat. Astron. Fys. 29a, 1–37.

İlbeyli, N., and Kibici, Y., 2009. Collision-related granite magma genesis, potential sources and tectono-magmatic evolution: comparison between central, northwestern and western Anatolia (Turkey). International Geology Review, 51, 252-278.

İşseven, T., 1995, Kuzeybatı Anadolu'nun tektoniği ve paleomanyetik sonuçlar. Yüksek Lisans Tezi, İTÜ Fen Bilimleri Enst., 113 sayfa.

İşseven, T., 2001, Batı Anadolu'nun neotektonik rejiminin paleomanyetik çalışmalarla incelenmesi. Doktora Tezi, İTÜ Fen Bilimleri Enstitüsü, 194 sayfa.

Jelinek, V., 1978. Statistical processing of anisotropy of magnetic susceptibility on groups of specimens. Stud. Geophys. Geod.22, 50–62.

Jelinek, V., 1981. Characterization of the magnetic fabrics of rocks. Tectonophysics79 (3–4), T63–T67.

Kadıoğlu, Y.K., Dilek, Y., and Foland, K.A., 2006. Slab break-off and syn-collisional origin of the Late Cretaceous magmatism in the Central Anatolian crystalline complex, Turkey. Geological Society of America Special Paper, 409, 381–415.

Kara, H., and Dönmez, M., 1990. 1/100.000 ölçekli açınsama nitelikli Türkiye jeolojisi haritalar serisi: Kırşehir G-17 paftası. MTA Raporu.

Kaygusuz, A., Aydınçakır, E., 2009. Mineralogy, whole-rock and Sr-Nd isotope geochemistry of mafic microgranular enclaves in Cretaceous Dagbaşı granitoids, eastern Pontides, NE Turkey: evidence of magma mixing, mingling and chemical equilibration. Chemie der Erde, 69, 247-277.

Kaygusuz, A., Siebel, W., Ilbeyli, N., Arslan, M., Satır, M., Şen, C., 2010. Insight into magma genesis at convergent plate margins e a case study from the eastern Pontides (NE Turkey). Journal of Mineralogy and Geochemistry, 187 (3), 265-287.

Kaygusuz, A., Sipahi, F., İlbeyli, N., Arslan, M., Chen, B., Aydınçakır, E., 2013. Petrogenesis of the Late Cretaceous Turnagöl intrusion in the eastern Pontides: implications for magma genesis in the arc setting. Geoscience Frontiers, 4, 423–438.

Kaymakcı, N., 2000. Tectono-stratigraphical evolution of the Cankiri Basin (Central Anatolia, Turkey). Geologica Ultraiectina, 190, 1-247.

Kaymakcı, N., Duermeijer, C.E., Langeris, C., White, S.H., Van Dijk, P.M., 2003. Palaeomagnetic evolution of the Çankırı Basin (Central Anatolia, Turkey): implications for oroclinal bending due to indentation. Geological Magazine 140, 343–355.

Kaymakcı, N., Aldanmaz, E., Langereis, C., Spell, T.L., Gurer, O.F., Zanetti, K.A., 2007. Late Miocene transcurrent tectonics in NW Turkey: evidence from Paleomegntism and 40Ar–39Ar dating of alkaline volcanic rocks. Geol. Mag.144 (2), 379–392.

Kaymakcı, N., Özçelik, Y., White, S.H., and Van Dijk, P.M., 2009. Tectono-stratigraphy of the Çankiri Basin: late Cretaceous to early Miocene evolution of the Neotethyan suture zone in Turkey. Journal of the Geological Society of London Special Publications, 311, 67-106.

Keskin, M., Genç, S.C., and Tüysüz, O., 2008. Petrology and geochemistry of post-collisional Middle Eocene volcanic units in North-Central Turkey: Evidence for magma generation by slab breakoff following the closure of the Northern Neotethys Ocean. Lithos, 104, 267-305.

Ketin, I., 1966. Tectonic units of Anatolia (Asia Minor). MTA Bülteni, 66, 23-34.

Kirschvink, J.L., 1980. The least-squares line and plane and the analysis of palaeomagnetic data. Geophys. J. R. Astron. Soc.62, 699–718.

Kissel, D. 1986, Apport du paleomagnetisme a la comprehension de l'évolutiongeodynamique Tertiaire du domaine Egeen de L'épire a L'anatolie occidentale. Ph.D Thesis, University of Paris-Sud, Centre D'Orsay, 415pp.

Kissel, C., Poisson, A., 1987. Etude paleomagnetique preliminaire des formations cenozoiques des Bey Daglari (Taurides occidentals, Turquie). Comptes Rendus de l'Académie des Sciences. Paris 304 (II (8)), 343–348.

Kissel, C., Kondopoullou, D., Laj, C., Papadopoulos, P., 1986. New palaeomagnetic data from Oligocene formations of northern Aegea. Geophysical Research Letters 13,1039–1041.

Kissel, C., Laj, C., Poisson, A., Savascin, Y., Simeakis, K., Mercier, J.L., 1986. Palaeomagnetic evidence for Neogene rotational deformations in the Aegean domain. Tectonics 5, 783–795.

Kissel, C., Barrier, E., Laj, C., and Lee, T.Q. (1986). Magnetic fabric in 'undeformed' marine clays from compressional zones. Tectonics 5, 769–781.

Kissel, C., Laj, C., Sengor, A.M.C., Poisson, A., 1987. Palaeomagnetic evidence for rotation in opposite senses of adjacent blocks in northeastern Aegea. Geophysical. Research Letters 14, 907–910.

Kissel, C., Laj, C., 1988. The Tertiary geodynamical evolution of the Aegean arc: a palaeomagnetic reconstruction. Tectonophysics 146, 183–201.

Kissel, C., Laj, C., Poisson, A., Simeakis, K., 1989. A pattern of block rotations in Central Aegea. In: Kissel, C., Laj, C. (Eds.), Palaeomagnetic Rotations and Continental Deformation. InKluwer, Dordrecht, pp. 115–130.

Kissel, C., Averbuch, O., Frizon de Lamotte, D., Monod, O., Allerton, S., 1993. First palaeomagnetic evidence for a post-Eocene clockwise rotation of the Western Taurides thrust belt east of the Isparta reentrant (Southwestern Turkey). Earth and Planetary Science Letters 117, 1–14.

Kissel, C., Laj, C., Poisson, A., Görür, N., 2002. Palaeomagnetic reconstruction of the Cenozoic evolution of the Eastern Mediterranean. Tectonophysics 362, 199–217.

Kibici, Y., Ilbeyli, N., Yıldız, A., and Bağcı, M., 2008. Petrology and geochemistry of the Günyüzü pluton, Northwest Anatolia, Turkey. International Geology Review, 50, 931–947.

Kligfield, R., Lowrie, W., and Dalziel, I.W.D. (1977). Magnetic susceptibility anisotropy as a strain indicator in the Sudbury basin, Ontario. Tectonophysics 40, 287–

Kligfield, R., Owens, W.H., and Lowrie, W. (1981). Magnetic susceptibility anisotropy, strain and progressive deformationin Permian sediments from the Maritime Alps (France). Earth Planet. Sci. Lett. 55,181–189.

Kondopoulou, D.P., 1982. Paleomagnetisme et deformations neogenes du Nord de la mer Egee, Ph.D Thesis, University of Strasbourg, France.

Kondopoulou, D., Leci, V., Symeakis, C., 1993. Palaeomagnetic study of the Tertiary volcanics of Chios Island, Greece. Proceedings of the 2nd Congress of the Hellenioc Geophysical Union, FLorina, pp. 676–687.

Koçyiğit, A., 1987. Hasanoğlan (Ankara) yöresinin tektonostratigrafisi: Karakaya orojenik kuşağının evrimi. Yerbilimleri, 14, 269-293.

Koçyiğit, A., Özkan, S., Rojay, B., 1988. Examples of the forearc basin remnants at the active margin of northern Neo-Tethys: development and emplacement ages of the Anatolian Nappe, Turkey. Middle East Technical University Journal of Pure and Applied Sciences, 3, 183-210.

Koçyiğit, A., 1991. Changing stress orientation in progressive intracontinental deformation as indicated by the Neotectonics of the Ankara region, (NW Central Anatolia). Turkish Association of Petroleum Geologists Bulletin 3/I, 48–55.

Koçyiğit, A., 1991. An example of an accretionary forearc basin from Central Anatolia and its implications for the history of subduction of Neo-Tethys in Turkey. Geological Society of America Bulletin, 103, 22-36.

Koçyiğit, A., Beyhan, A., 1998. A new intracontinental transcurrent structure: the Central Anatolian Fault Zone, Turkey. Tectonophysics 284, 317–336.

Koçyiğit, A., Winchester, J.A., Bozkurt, E. and Holland, G., 2003. Saraçköy Volcanic Suite: implications for the subductional phase of arc evolution in the Galatean Arc Complex, Ankara-Turkey. Geological Journal, 37, 1−14.

Kodama, K.P., and Sun, W. W., 1992. Magnetic anisotropy as a correction for compaction-caused paleomagnetic inclination shallowing. Geophys.J.Int. 111,

Kono, M., 1980. Statistics of palaeomagnetic inclination data. Journal of Geophysical Research 85, 3878–3882.

Köksal, S., and Göncüoğlu, M.C., 1997. Geology of the Idiş Dağı - Avanos area (Nevşehir - Central Anatolia). MTA Bülteni, 119, 41-58.

Krijgsman, W., Tauxe, L., 2004. Shallow bias in Mediterranean palaeomagnetic directions caused by inclination error. Earth and Planetary Science Letters 222, 685–695.

Krijgsman, W., Duermeijer, C.E., Langeris, C.G., Bruijn, H., Sarac, G., Andriessen, P.A.M., 1996. Magnetic polarity stratigraphy of late Oligocene to middle Miocene mammalbearing continental deposits in central Anatolia (Turkey). Newsletter of Stratigraphy 34 (1), 13–29.

Laj, C., Jamet, M., Sorel, D., Valente, J.P., 1982. First palaeomagnetic results from the Mio-Pliocene Series of the Hellenic sedimentary arc. Tectonophysics 86, 45–67.

Le Pichon, X., Chamot-Rooke, N., Lallemant, S., Noomen, R., Veis, G., 1995. Geodetic determination of the kinematics of central Greece with respect to Europe: Implications for eastern Mediterranean tectonics. Journal of Geophysical Research 100 (B7), 12675–12690.

Lefebvre, C.J.C., Meijers, M.J.M., Kaymakcı, N., Peynircioğlu, A.A., Langereis, C.G., and Van Hinsbergen, D.J.J., 2013. Reconstructing the geometry of central Anatolia during the late Cretaceous: Large-scale Cenozoic rotations and deformation between the Pontides and Taurides. Earth and Planetary Science Letters, 366, 83-98.

Loucks R.G., Moody R.T.J., Bellis, J.K, Brown, A.A., 1998. Regional depositional setting and pore network systems of the El Garia Formation (Metlaoui

Group, Lower Eocene), offshore Tunisia. Journal of the Geological Society of London Special Publications, 132, 355–374.

Lowrie W., 1989. Magnetic analysis of rock fabric. In: James DE (ed) Encyclopedia of Solid Earth Geophysics. Van Nostrand Reinhold Company, New York, pp 698–706.

Lowrie W., 2007. Fundamentals of Geophysics, 2nd ed. x + 381 pp. Cambridge, New York, Melbourne.

Lytwyn, J.N., and Casey, J.F., 1995. The geochemistry of postkinematic mafic dike swarms and subophiolitic metabasites, Pozanti-Karsanti ophiolite, Turkey. Evidence for ridge subduction. Geological Society of America Bulletin, 107, 830-850.

MacDonald, W.D., 1980. Net tectonic rotation, apparent tectonic rotation and the structural tilt correction in palaeomagnetic studies. Journal of Geophysical Research 85, 3659–3669.

Mattei M, Sagnotti L, Faccenna C, Funiciello R (1997) Magnetic fabric of weakly deformed clay-rich sediments in the Italian peninsula: Relationship with compressional and extensional tectonics. Tectonophysics 271:107–122

Mattei M, Speranza F, Argentieri A, Rossetti F, Sagnotti L, Funiciello R (1999) Extensional tectonics in the Amantea basin (Calabria, Italy): a comparison between structural and magnetic anisotropy data. Tectonophysics 307:33–49

McClusky, S., Balassanian, S., Barka, A., Demir, C., Ergintav, S., Georgiev, I., Gürkan, O., Hamburger, M., Hurst, K., Kahle, H., Kastens, K., Kekelidze, G., King, R., Kotzev, V., Lenk, O., Mahmoud, S., Mishin, A., Nadariya, M., Ouzounis, A., Paradissis, D., Peter, Y., Prilepin, M., Reilinger, R., Sanli, I., Seeger, H., Tealeb, A.,

McFadden, P.L., McElhinny, M.W., 1988. The combined analysis of remagnetization circles and direct observations in paleomagnetism. Earth Planet. Sci. Lett.87, 161–172.

McFadden, P.L., McElhinny, M.W., 1990. Classification of the reversal test in palaeo magnetism. Geophys. J. Int.103, 725–729.

McFadden, P.L., Merrill, R.T., McElhinny, M.W., Lee, S., 1991. Reversals of the Earth's magnetic field and temporal variations in the dynamo families. Journal of Geophysical Research 96, 2023–3933.

McKenzie, D.P., 1978. Active tectonics of the Alpine–Himalayan belt: the Aegean Sea and surrounding regions. Geophysical Journal of the Royal astronomical Society 55, 217–254.

Meijers, M.J.M., Kaymakci, N., Hinsbergen, D.J.J. v., Langereis, C.G., Stephenson, R.A., and Hippolyte, J.-C. (2010a). Late Cretaceous to Paleocene oroclinal bending in the central Pontides (Turkey). Tectonics, 29, TC4016.

Meijers, M.J.M., Langereis, C.G., van Hinsbergen, D.J.J., Kaymakcı, N., Stephenson, R.A. and Altıner, D., 2010b. Jurassic-Cretaceous low paleolatitudes from the circum-Black Sea region (Crimea and Pontides) due to True Polar Wander, Earth and Planetary Science Letters, 296, 210–226.

Meriç, E., Görür, N., 1981. Haymana-Polatlı havzasındaki Çaldağ kireçtaşının kireçtaşının yaş konağı. MTA Bülteni, 93, 137-142.

Moores, E.M., 1981. Ancient suture zones within continents. Science, 213, 41–46.

Morris, A., Robertson, A.H.F., 1993. Miocene remagnetisation of carbonate platform and Antalya Complex units within the Isparta Angle, SW Turkey. Tectonophysics 220,

243–253.

Morris, A., Anderson, M., 1996. First palaeomagnetic results from the Cycladic Massif, Greece, and their implications for Miocene extension directions and tectonic models in the Aegean. Earth and Planetary Science Letters 142, 397–408.

Mullender, T.A.T., van Velzen, A.J., Dekkers, M.J., 1993. Continuous drift correction and separate identification of ferrimagnetic and paramagnetic contribution in thermomagnetic runs. Geophys. J. Int.114, 663–672.

Nagata, T., 1961, Rock Magnetism, Maruzen, Tokyo, p. 350.

Nairn, S., 2011. Testing alternative models of continental collision in Central Turkey by a study of the sedimentology, provenance and tectonic setting of Late Cretaceous-Early Cenozoic syn-tectonic sedimentary basins. University of Edinburgh, PhD. Thesis, 395 p.

Nairn, S.P., Robertson, A.H.F., Ünlügenç, U.C., İnan, N., Taslı, K., 2013. Tectonostratigraphic evolution of the Upper Cretaceous-Cenozoic central Anatolian basins: an integrated model of diachronous ocean basin closure and continental collision. Journal of the Geological Society of London Special Publication, 372, 343–384.

Norman, T., 1973. Ankara Yahşıhan bölgesinde Üst Kretase-Alt Tersiyer sedimantasyonu. TJK Bülteni, 16, 41-66.

Norman, T.N., 1972. Ankara Yahşıhan bölgesinde Üst Kretase-Alt Tersiyer istifinin stratigrafisi. TJK Bülteni, 15, 180-276.

Nye,J.F.(1957). The Physical Properties of Crystals. Oxford: Clarendon Press.

Okay, A.I., 1984. Distribution and characteristics of the northwest Turkish blueschists. Journal of the Geological Society of London Special Publications, 17, 455-466.

Okay, A.I., Şengör, A.M.C., Görür, N., 1994. Kinematic history of the opening of the Black Sea and its effect on the surrounding regions. Geology 22, 267–270.

Okay, A.I., Satır, M., Maluski, H., Siyako, M., Monié, P., Metzger, R., and Akyüz, S., 1996. Paleo- and Neo-Tethyan events in northwestern Turkey: geologic and geochronologic constraints. In A. Yin & T. M. Harrison (Eds.). The tectonic evolution of Asia, Cambridge University Press, 420-441

Okay, A.I., and Şahintürk, Ö., 1997. Geology of the Eastern Pontides. In A. G. Robinson (Ed.), Regional and petroleum geology of the Black Sea and surrounding region. AAPG Memoir, 68, 291-311.

Okay, A.I., Harris, N. B.W., and Kelley, S.P., 1998. Exhumation of blueschists along a Tethyan suture in northwest Turkey. Tectonophysics, 285, 275-299.

Okay, A. I., Tansel, I., and Tüysüz, O., 2001. Obduction, subduction and collision as reflected in the Upper Cretaceous–Lower Eocene sedimentary record of western Turkey. Geological Magazine, 138, 117-142.

Okay, A. I., 2002. Jadeite-chloritoid-glaucophane-lawsonite blueschists in north-west Turkey: unusually high P/T ratios in continental crust. Journal of Metamorphic Geology, 20, 757-768.

Okay, A.I., Monod, O., and Monie, P., 2002. Triassic blueschists and eclogites from northwest Turkey: vestiges of the Paleo-Tethyan subduction. Lithos, 64(3-4), 155-178.

Okay, A.I., and Satır, M., 2006. Geochronology of Eocene plutonism and metamorphism in northwest Turkey: evidence for a possible magmatic arc. Geodinamica Acta, 19, 251-266.

Okay, A.I., Tüysüz, O., Satır, M., Özkan-Altıner, S., Altıner, D., Sherlock, S., and Eren, R.H., 2006. Cretaceous and Triassic subduction-accretion, HP/LT metamorphism and continental growth in the Central Pontides, Turkey. Geological Society of America Bulletin, 118, 1247-1269.

Okay, A.I., Sunal, G., Sherlock, S., Altıner, D., Tüysüz, O., Kylander-Clark, A.R.C., and Aygül, M., 2013. Early Cretaceous sedimentation and orogeny on the southern active margin of Eurasia: Central Pontides, Turkey. Tectonics, 32, 1247–1271.

Orbay, N., 1976, Kuzey Anadolu Fay Zonunun paleomagnetizmasi. Doktora tezi, İÜ, 63 sayfa.

Orbay, N., Bayburdi, A., 1979. Paleomegntism of dykes and tuffs from the Mesudiye region and rotation of Turkey. Geophysical Journal of the Royal Astronomical Society 59, 437–444.

Orbay, N., Düzgit, Z., Gündoğdu, O., Hisarlı, M. and Özçep, F., 1993. Batı Anadolu' nun paleomagnetizması ve tektonik gelişimi. TÜBİTAK raporu (yayınlanmamış).

Orbay, N., Sanver, M., Hisarli, T., Isseven, T., Ozcep, F., 2000. Karaburun Yarımadasının paleomagnetizması ve tektonik evrimi [Paleomagnetism and tectonic evolution of Karaburun Peninsula]. In: Batı Anadolu'nun Depremselliği Sempozyumu Kitabi, pp.59–67 (in Turkish).

Owens, W. H., 1974. Mathematical Model Studies on Factors Affecting the Magnetic Anisotropy of Deformed Rocks, Tectonophysics 24, 115-131.

Owens, W.H., Bamford, D., 1976. Magnetic, seismic, and other anisotropic properties of rock fabrics. Philosophical Transactions of the Royal Society of London 283, 55–68.

Owens, W. H. and Rutter, E. H., 1978. The Development of Magnetic Susceptibility Anisotropy through Crystallographic Preferred Orientation in a Calcite Rock, Phys. Earth Planet. Interiors 16, 215-222

Önen, A.P., 2003. Neotethyan ophiolitic rocks of the Anatolides of NW Turkey and comparison with Tauride ophiolites. Journal of the Geological Society of London, 160, 947-962.

Özcan, E., Sirel, E., Özkan-Altıner, S., Çolakoğlu, S., 2001. Late Paleocene Orthophragminae (foraminifera) from the Haymana-Polatlı Basin, Central Turkey and description of a new taxon, Orbitoclypeus haymanaensis. Micropaleontology, 47/4, 339-357.

Özcan, E., Özkan-Altıner, S., 1997. Late Campanian-Maastrichtian evolution of orbitoid foraminifera in Haymana basin succession (Ankara, Central Turkey). Revue de Paléobiologie, 16/1 , 271-290.

Özcan, E., 2002. Cuisian orthophragminid assemblages (Discocyclina, Orbitoclypeus and Nemkovella) from the Haymana-Polatlı Basin (Central Turkey): biometry and description of two new taxa. Eclogae geol. Helv., 95, 75-97.

Özgül, N., 1984. Stratigraphy and tectonic evolution of the Central Taurides. in Tekeli, O. and Göncüoğlu, M.C. (eds): Geology of the Taurus Belt. MTA Bülteni, Özel Sayı, 78–90.

Özsayın, E. & Dirik, K., 2007. Quaternary activity of Cihanbeyli Fault Zone (southern segment of Eskişehir-Sultanhanı Fault System), Central Anatolia, Türkiye. Turkish Journal of Earth Sciences, 16, 471-492.

Özsayın, E. & Dirik, K., 2011. The role of oroclinal bending in the structural evolution of the Central Anatolian Plateau: Evidence from a regional changeover of shortening to extension. Geologica Carpathica, 62-4, 345-359.

Özsayın, E., Çiner, T.A., Rojay, F.B., Dirik, R.K., Melnick, D., Fernandez-Blanco, D., Bertotti, G., Schildgen, T.F., Garcin, Y., Strecker, M.R., Sudo, M., 2013. Plio-Quaternary Extensional Tectonics of the Central Anatolian Plateau: A case study from the Tuz Gölü Basin, Turkey. Turkish Journal of Earth Sciences, 22, 691-714.

Öztürk, Y.Y., Helvacı, C., and Satır, M., 2012. Geochemical and Isotopic Constraints on Petrogenesis of the Beypazarı Granitoid, NW Ankara, Western Central Anatolia, Turkey. Turkish Journal of Earth Science, 21, 53-77.

Pares JM, Van der Pluijm BA, Dinares-Turell J (1999) Evolution of magnetic fabrics during incipient deformation of mudrocks (Pyrenees, northern Spain). Tectonophysics 307:1–14.

Pares J (2004) How deformed are weakly deformed mudrocks? Insights from magnetic anisotropy. Geol Soc Lond Spec Pub.238:191–203.

Pares, J.M., Hassold, N.J.C., Rea, D.K., van der Pluijm, B.A., 2007. Paleocurrent directions from paleomagnetic reorientation of magnetic fabrics in deep-sea

sediments at the Antarctic Peninsula Pacific margin (ODP Sites 1095, 1101). Mar. Geol. 242, 261–269.

Parlak, O. and Delaloye, M., 1999. Precise 40Ar/39Ar ages from the metamorphic sole of the Mersin Ophiolite (southern Turkey). Tectonophysics, 301, 145–58.

Platzman, E.S., Platt, J.P., Tapırdamaz, C., Sanver, M., Rundle, C.C., 1994. Why are there no clockwise rotations along the North Anatolian Fault Zone? Journal of Geophysical Research 99, 21705–21716.

Platzman, E.S., Tapirdamaz, C., Sanver, M., 1998. Neogene anticlockwise rotation of central Anatolia (Turkey): preliminary palaeomagnetic and geochronological results. Tectonophysics 299 (3), 175–189.

Piper, J.D.A., Moore, J., Tatar, O., Gürsoy, H., Park, R.G., 1996. Palaeomagnetic study of crustal deformation across an intracontinental transform: the North Anatolian Fault Zone in Northern Turkey. In: Morris, A., Tarling, D.H. (Eds.), Paleomagnetism of the Mediterranean Regions, Special Publication of the Geological Society of London, vol. 105, pp. 299–310.

Piper, J.D.A., Tatar, O., Gürsoy, H., 1997. Deformational behaviour of continental lithosphere deduced from block rotations across the North Anatolian Fault Zone in Turkey. Earth and Planetary Science Letters 150, 191–203.

Piper, J.D.A., Gürsoy, H., Tatar, O., 2002. Paleomegntism and Magnetic Properties of the Cappadocian Ignimbrite Succession, Central Turkey and Neogene Tectonics of the Anatolian Collage. Journal of Volcanology and Geothermal Research 117, 237–262.

Piper, J.D.A., Tatar, O., Gürsoy, H., Kocbulut, F., Mesci, B.L., 2006. Palaeomagnetic Analysis of Neotectonic Deformation in the Anatolian accretionary collage, Turkey. In: Dilek, Y., Pavlides, S. (Eds.), Post-Collisional Tectonics and Magmatism in the Eastern Mediterranean Region: Geological Society of America, Special Paper, vol. 409, pp. 417–440.

Poisson, A., Guezou, J., Ozturk, A., Inan, S., Temiz, H., Gürsöy, H., and Özden, S., 1996. Tectonic Setting and Evolution of the Sivas Basin, Central Anatolia, Turkey. International Geology Review, 38(9), 838 – 853.

Pollak, A., 1958. 1957 yılında Akdağmadeni-Yıldızeli sahasında yapılan prospeksiyon hakkında rapor. M.T.A. Rap., no. 2679.

Porath, H., 1968. The Magnetic Anisotropy of the Yampi Sound Hematite Ores', Pure Appl. Geophys. 69, 168-178.

Porath, H.: 1971. Anisotropie der magnetischen Suszeptibilitfit und S~ittigungsmagnetisierung als Hilfmittel der Geffigekunde, Geol. Rundsch. 60, 1088-1102.

Porath, H. and Chamalaun, F. H., 1966. The Magnetic Anisotropy of Hematite Bearing Rocks', Pure Appl. Geophys. 64, 81-88.

Porath, H., and Raleigh, C. B., 1967. An Origin of the Triaxial Basal-plane Anisotropy in Hematite Crystals. J. Appl. Phys. 35, 2401-2402.

Pourteau A, Candan O, Oberhänsli R., (2010). High-pressure metasediments in central Turkey: Constraints on the Neotethyan closure history. Tectonics 29: TC5004.

Pourteau, A., 2011. Closure of the Neotethys Ocean in Anatolia: structural, petrologic & geochronologic insights from low-grade high-pressure metasediments, Afyon Zone. PhD Thesis. Potsdam University, 106 p.

Ramsay, J. G., 1967. Folding and Fracturing of rocks. MacGraw Hill, New York, 1-568

Reckamp, J., U., Özbey, S., 1960. Petroleum geology of Temelli and Kuştepe structures, Polatlı area. Pet. İş. Gen. Md., Ankara.

Rees A.I. (1961). The effect of water currents on the magnetic remanence and anisotropy of susceptibility of some sediments. Geophys. J. Royal Astron Soc. 5:251–635.

Rees, A.I., 1966. 'The Effects of Depositional Slopes on the Anisotropy of Magnetic Susceptibility of Laboratory Deposited sands', J. Geol. 74,856-867.

Rees, A.I., 1968. 'The Production of Preferred Orientation in a Concentrated Dispersion of Elongated and Flattened Grains', J. Geol. 76, 457465. Rees, A. I.: 1971, 'The Magnetic Fabric of a Sedimentary Rock deposited on a Slope', J. Sediment. Petrol. , 307-309.

Rees, A.I., and Woodall, W.A.: 1975: 'The Magnetic Fabric of some Laboratory-deposited Sediments', Earth Planet. Sci. Letters 25, 121-130.

Rees, A.I., Rad, U. von, Shepard, F.P.: 1968, 'Magnetic Fabric of Sediments from the La Jolla Submarine Canyon and Fan, California', Marine Geol. 6, 145-178.

Reilinger, R., McClusky, S., 2001. GPS constraints on block motions and deformation in western Turkey and the Aegean: implications for earthquake hazards. In: Taymaz, T. (Ed.), Symposia on Seismotectonics of the north-western Anatolia–Aegean and recent Turkish earthquakes. Istanbul Technical University, Istanbul, pp. 14–20.

Rice, S.P., Robertson, A.H.F., and Ustaömer, T., 2006. Late Cretaceous-Early Cenozoic tectonic evolution of the Eurasian active margin in the Central and Eastern Pontides, northern Turkey. Journal of the Geological Society of London Special Publications, 260, 413-445.

Rice, S.P., Roberson, A.H.F., Ustaömer, T., İnan, T., Taslı, K., 2009. Late Cretaceous-Early Eocene tectonic development of the Tethyan Suture Zone in the Erzincan area, eastern Pontides, Turkey. Geological Magazine, 146(4), 567-590.

Rigo de Righi, M., and Cortesini, A., 1959. Regional studies in central Anatolian basin. Progress Report 1, Turkish Gulf Oil Co., Pet. İş. Gen. Md., Ankara.

Robertson, A.H.F., and Dixon, J.E., 1984. Aspects of the geological evolution of the Eastern Mediterranean. Journal of the Geological Society of London Special Publications, 17, 1-74.

Robertson, A.H.F., 2002. Overview of the genesis and emplacement of Mesozoic ophiolites in the Eastern Mediterranean Tethyan region. Lithos, 65, 1-67.

Robion, R., Grelaud, S., and Frizon de Lamotte, D. (2007). Prefolding magnetic fabrics in fold-and-thrust belts: why the apparent internal deformation of the sedimentary rocks from the Minervois basin (NE—Pyrenees, France) is so high compared to the Potwarbasin (SW-Himalaya). Sed. Geol. 196, 181–200.

Rochette P (1987) Magnetic susceptibility of the rock matrix related to magnetic fabric studies. J Struct Geol 9:1015–1020

Rochette P, Jackson MJ, Aubourg C (1992) Rock magnetism and the interpretation of anisotropy of magnetic susceptibility. Rev Geophys 30(3):209–226

Rojay, B., 1991. Tectonostratigraphy and neotectonic characteristics of the southern margin of Merzifon-Suluova Basin (Central Pontides, Amasya). PhD. Thesis, Middle East Technical University, Ankara, 105 p.

Rojay, B., 1995. Post-Triassic evolution of Central Pontides: evidence from Amasya region, Northern Anatolia. Geologica Romana 31, 329–350.

Rojay, B., and Altıner, D., 1998. Middle Jurassic–Lower Cretaceous biostratigraphy in the Central Pontides (Turkey): remarks on the paleogeography and tectonic evolution. Rivista Italiana di Paleontologia e Stratigrafia, 104 (2), 167–180.

Rojay, B., Süzen, L., 1997. Tectonostratigraphic evolution of an arc-trench basin on accretionary ophiolitic mélange prism, central Anatolia, Turkey. Association of Turkish Petroleum Geologist Bulletin, 9, 1–12.

Rojay, B., Yalınız, K., Altıner, D., 2001. Age and origin of some pillow basalts from Ankara mélange and their tectonic implications to the evolution of northern branch of Neotethys, Central Anatolia. Turkish Journal of Earth Science 10 (3), 93–102.

Rojay, B., Altıner, D., Özkan Altıner, S., Önen, P., James, S., and Thirwall, M., 2004. Geodynamic significance of the Cretaceous pillow basalts from North Anatolian Ophiolitic Mélange Belt (Central Anatolia, Turkey): geochemical and paleontological constrains. Geodinamica Acta, 17 (5), 349–361.

Rojay, B., 2013. Tectonic evolution of the Cretaceous Ankara ophiolitic mélange during the Late Cretaceous to pre-Miocene interval in Central Anatolia, Turkey. Journal of Geodynamics, 65, 6–81.

Sagnotti, L., Winkler, A., 1999. Rock magnetism and Paleomegntism of greigite-bearing mudstones in the Italian peninsula. Earth Planet Sci Lett 165:67–80

Sagnotti, L., Faccenna, C., Funiciello, R., Mattei, M., 1994. Magnetic fabric and structural setting of Plio-Pleistocene clayey units in an extensional regime: the Tyrrhenian margin of Central Italy. J Struct Geol 16:1243–1257

Sagnotti, L., Speranza F., Winkler A., Mattei, M., Funiciello, R., 1998. Magnetic fabric of clay sediments from the external northern Apennines (Italy). Phys Earth Planet Inter 105:73–93

Sarifakioglu, E., Dilek, Y., and Sevin, M., 2014. Jurassic–Paleogene intra-oceanic magmatic evolution of the Ankara Mélange, north-central Anatolia, Turkey. Solid Earth, 5, 77–108.

Saner, S., 1980. Batı Pontidler'in ve komşu havzaların oluşumlarının levha tektoniği kuramıyla açıklanması, kuzeybatı Türkiye. MTA Dergisi, 93/94 1-19.

Sanver, M., 1968. A palaeomagnetic study of Quaternary volcanic rocks from Turkey. Physics of the Earth and Planetary Interioriors 1, 403–421.

Sanver, M., Ponat, E., 1980. Paleomagnetism of the magmatic rocks in Kırşehir and surrounding area. Bulletin of the Kandilli Observatory. InIstanbul University, pp. 1–11.

Schmidt, G., C., 1960. AR/MEM/365-266-367 sahalarının nihai terk raporu. Pet. İş. Gen. Md., Ankara.

Schmidt, V., Günther, D., Hirt, A.M., 2006. Magnetic anisotropy of calcite at roomtemperature. Tectonophysics 418, 63–73.

Schmidt, V., Hirt, A.M., Rosselli, P., Martin-Hernandez, F., 2007a. Separation of diamagnetic and paramagnetic anisotropy by high-field, low-temperature torque measurements. Geophysical Journal International 168, 40–47.

Schmidt, V., Hirt, A.M., Hametner, K., Günther, D., 2007b. Magnetic anisotropy of carbonate minerals at room temperature and 77 K. American Mineralogist 92, 1673–1684.

Seaton N.C.A., Whitney D.L., Teyssier C., Toraman E., and Heizler M.T., 2009. Recrystallization of high-pressure marble (Sivrihisar, Turkey). Tectonophysics, 479(3-4), 241-253.

Seyitoglu, G., Buyukonal, G., 1995. Geochemistry of the Anakara Volcanics and the implications of their K–Ar dates on the Cenozoic stratigraphy of Central Turkey. Turkish Journal of Earth Sciences 4, 87–92.

Seyitoglu, G., Scott, B.C., 1996. The cause of N–S extensional tectonics in western Turkey: tectonic escape vs back-arc spreading vs orogenic collapse. Journal of Geodynamics 22, 145–153.

Seymen, I., 1981. Stratigraphy and metamorphism of the Kırşehir Massif around Kaman (Kırşehir - Turkey). Bulletin of Geological Society of Turkey, 24, 7-14.

Seymen, I., 1982. Kaman Dolayında Kırşehir masifi'nin Jeolojisi. . ITÙ Maden Fakültesi, Doçentlik Tezi, Istanbul, 164 p.

Sherlock, S., Kelley, S., Inger, S., Harris, N., and Okay, A.I., 1999. 40Ar/39Ar and Rb-Sr geochronology of high-pressure metamorphism and exhumation history of the Tavsanli Zone, NW Turkey. Contributions to Mineralogy and Petrology, 137, 46-58.

Sirel, E., 1975. Polatlı (GB Ankara) güneyinin stratigrafisi. TJK Bülteni, 18/2, 181-192.

Sirel, E., and Gündüz, H., 1976. Description and stratigraphic distribution of some species the genera Nummulites, Assilina and Alveolina from the Ilerdian, Cuisian and Lutetian of Haymana region. TJK Bülteni, 19, 33-44.

Sirel, E., Dağer, Z., and Sözeri, B., 1986. Some biostratigraphic and paleogeographic observations on the Cretaceous-Tertiary boundary in the Haymana-Polatlı region (Central Turkey) in Walliser O. (ed.y) Global Bioevents. Lecture Notes in Earth Sciences, 8, 385-396.

Sirel, E., 1998. Foraminiferal description and biostratigraphy of the PaleoceneLower Eocene shallow-water limestones and discussion on the Cretaceous-Tertiary boundary in Turkey. General Directorate of the Mineral Research and Exploration, Monography Series, 2, 117 p.

Speciale, P.A., Catlos, E.J., Yıldız, G.O., Shina, T.A., and Black, K.N., 2014, Zircon ages from the Beypazarı granitoid pluton (north central Turkey): tectonic implications, Geodinamica Acta, 25:3-4, 162-182.

Stacey, F. D., 1960. Magnetic Anisotropy of Igneous Rocks, J. Geophys. Res. 65, 2429-2442.

Stacey, F. D., Joplin, G., and Lindsay, J., 1960. Magnetic Anisotropy and Fabric of some Foliated Rocks from S.E. Australia, Geofiz. Pura Appl. 47, 30--40.

Sunal, G., and Tüysüz, O., 2002. Palaeostress analysis of Tertiary post-collisional structures in the Western Pontides, northern Turkey. Geological Magazine, 139, 343-359.

Şaroğlu, F., Yılmaz, Y., 1986. Geological evolution and basin modelling in East Anatolia during neotectonic period, MTA Bulletin, pp. 73–94.

Şen, S., Seyitoğlu, G., 2009. Magnetostratigraphy of early–middle Miocene deposits from east–west trending Ala¸sehir and Büyük Menderes grabens in western Turkey, and its tectonic implications. In: van Hinsbergen, D.J.J., *et al.* (Eds.), Col-lision and Collapse at the Africa–Arabia–Eurasia Subduction Zone. In: Geol. Soc. (Lond.) Spec. Publ., vol.311, pp.321–342.

Şengör, A.M.C., 1979. The North Anatolian transform fault: its age, offset and tectonic significance, Journal of the Geological Society of London 136, 269–282.

Şengör, A.M.C., Kidd, W.S.F., 1979. Post-collisional tectonics of the Turkish–Iranian plateau and a comparison with Tibet. Tectonophysics 55, 361–376.

Şengör, A.M.C., and Yilmaz, Y., 1981. Tethyan Evolution of Turkey - a Plate Tectonic Approach. Tectonophysics, 75(3-4), 181-241.

Şengör, A.M.C., Altiner, D., Cin, A., Ustaömer, T., Hsü, K.J., 1988. Origin and assemblage of the Tethyside orogenic collage at the expense of Gondwanaland. In: Audley-Charles, M.G., Hallam, A. (Eds.), Gondwana and the Tethys, Geological Society of London Special Publication, pp. 119–181.

Tapırdamaz, C., Yaltırak, C., 1997. Trakya' da Senozoyik volkaniklerinin paleomanyetik özellikleri ve bölgenin tektonik konumu. MTA Dergisi 119, 27–42.

Tankut, A., Dilek, Y., and Önen, A.P., 1998a. Petrology and geochemistry of the Neo-Tethyan volcanism as revealed in the Ankara mélange, Turkey. Journal of Volcanology and Geothermal Research, 85, 265-284.

Tankut, A., Wilson, M., Yihunie, T., 1998b. Geochemistry and tectonic setting of Tertiary volcanism in the Güvem area. Anatolia, Turkey, Journal of Volcanology and Gethermal Research 85, 285–301.

Tarling DH., Hrouda F., 1993. The magnetic anisotropy of rocks. Chapman and Hall, London 217 pp

Tatar, O., Piper, J.D.A., Park, R.G., Gürsoy, H., 1995. Palaeomagnetic study of block rotations in the Niksar overlap region of the North Anatolian Fault Zone. Central Turkey. Tectonophysics 244, 251–266.

Tatar, O., Piper, J.D.A., Gürsoy, H., Temiz, H., 1996. Regional significance of Neotectonic counterclockwise rotation in Central Turkey. International Geology Review 38, 692–700.

Tatar, O., Piper, J.D.A., Gürsoy, H., 2000. Palaeomagnetic study of the Erciyes sector of the Ecemiş Fault Zone: neotectonic deformation in the southeastern part of the Anatolian Block. In: Bozkurt, E., Winchester, J.A., Piper, J.D.A. (Eds.), Tectonics and

Magmatism in Turkey and the Surrounding Area: Geological Society of London Special Publication, vol. 173, pp. 423–440.

Tatar, O., Gürsoy, H., Piper, J.D.A., 2002. Differential neotectonic rotations in Anatolia and the Tauride Arc: paleomagnetic investigation of the Erenlerdağı Complex and Isparta volcanic district, south-central Turkey. Journal of the Geological Society of London 159, 281–294.

Tatar, O., Piper, J.D.A., Gürsoy, H., Heimann, A., Koçbulut, F., 2004. Neotectonic deformation in the transition zone between the Dead Sea Transform and the East Anatolian Fault Zone, Southern Turkey: a palaeomagnetic study of the Karasu Rift Volcanism. Tectonophysics 385, 17–43.

Tauxe, L., Watson, G.S., 1994.The fold test: an eigen analysis approach, Earth and Planetary Science Letters, 122, 3-4, 331

Tauxe, L., Kent, D.V., 2004. A simplified statistical model for the geomagnetic field and the detection of shallow bias in paleomagnetic inclinations: was the ancient magnetic field dipolar? In: Channell, J.E.T., Kent, D.V., Lowrie, W., Meert, J. (Eds.), Timescales of the Paleomagnetic Field: Geophys. Monogr. Am. Geophys. Union, vol. 145, pp. 101–115.

Tauxe, L., Kodama, K.P., Kent, D.V., 2008. Testing corrections for paleomagnetic inclination error in sedimentary rocks: a comparative approach. Physics of the Earth and Planetary Interiors 169, 152–165.

Tauxe, L., Banerjee, S.K., Butler, R.F. and van der Voo R, 2014. Essentials of Paleomagnetism, 3nd Web Edition, Kluwer Academic, p 299.

Tekeli O., 1981. Subduction complex of pre-Jurassic age, northern Anatolia, Turkey. Geology, 9(2), 68-72.

Temizel, İ., Arslan, M., 2008. Petrology and geochemistry of Tertiary volcanic rocks from the İkizce (Ordu) area, NE Turkey: implications for the evolution of the eastern Pontide paleomagmatic arc. Journal of Asian Earth Sciences, 31, 439–463.

Toksöz, M.N., Veis, G., 2000. Global Positioning System constraints on plate kinematics and dynamics in the eastern Mediterranean and Caucasus. Journal of Geophysical Research 105, 5695–5719.

Toprak, V., Savascı, Y., Güleç, N., and Tankut, A., 1996. Structure of the Galetean Volcanic Province, Turkey. International Geology Review, 38, 747-758.

Topuz, G., Altherr, R., Kalt, A., Satir, M., Werner, O., and Schwarz, W. H., 2004a. Aluminous granulites from the Pulur complex, NE Turkey: a case of partial melting, efficient melt extraction and crystallisation. Lithos, 72, 183-207.

Topuz, G., Altherr, R., Satir, M., and Schwarz, W.H. 2004b. Low-grade metamorphic rocks from the Pulur complex, NE Turkey: implications for the pre-Liassic evolution of the Eastern Pontides. International Journal of Earth Sciences, 93, 72-91.

Tüysüz, O., 1999. Geology of the Cretaceous sedimentary basins of the Western Pontides. Geological Journal, 34, 75-93.

Tüysüz, O. and İşseven, T., 2000, Çankırı havzası doğu kenarının neo-tektonik evrimi. İTÜ Araştırma fonu proje raporu, no. 1151.

Tüysüz, O., and Tekin, U.K., 2007. Timing of imbrication of an active continental margin facing the northern branch of Neotethys, Kargı Massif, northern Turkey. Cretaceous Research, 28, 754-764.

Tüysüz, O., Dellaloğlu, A.A., and Terzioğlu, N., 1995. A magmatic belt within the Neo-Tethyan suture zone and its role in the tectonic evolution of Northern Turkey. Tectonophysics, 243, 173-191.

Ünalan, G., Yüksel, V., Tekeli, T., Gönenç, O., Seyirt, Z., and Hüseyin, S., 1976. Haymana-Polatlı yöresinin (Güneybatı Ankara) Üst Kretase-Alt Tersiyer stratigrafisi ve paleocoğrafik evrimi. TJK Bülteni, 19, 159-176.

Vandamme, D., 1994. A new method to determine palaeosecular variation. Physics of the Earth and Planetary Interiors 85, 131–142.

Van der Voo, R., 1968. Paleomegntism and the Alpine tectonics of Eurasia, Part 4, Jurassic, Cretaceous and Eocene pole positions from NE Turkey. Tectonophysics 6, 251–269.

Van Hinsbergen, D.J.J., Langeris, C.G., Meulenkamp, J.E., 2005. Revision of the timing, magnitude and distribution of Neogene rotations in the western Aegean region. Tectonophysics 396, 1–34.

van Hinsbergen, D.J.J., Krijgsman, W., Langereis, C.G., Cornée, J.J., Duermeijer, C.E., van Vugt, N., 2007. Discrete Plio-Pleistocene phases of tilting and counterclock-wise rotation in the southeastern Aegean arc (Rhodos, Greece): early Pliocene formation of the south Aegean left-lateral strike-slip system. J. Geol. Soc.164, 1133–1144.

van Hinsbergen, D.J.J., Kaymakci, N., Spakman, W., Torsvik, T.H., Amaru, M., 2010. Reconciling geological history with mantle structure in western Turkey. Earth Planet. Sci. Lett.297, 674–686.

van Hinsbergen, D.J.J., Dekkers, M.J., Bozkurt, E., Koopman, M., 2010a. Exhumation with a twist: paleomagnetic constraints on the evolution of the Menderes metamorphic core complex, western Turkey. Tectonics29 (3), TC3009.

van Hinsbergen, D.J.J., Dekkers, M.J., Koç, A., 2010b. Testing Miocene remagnetization of Bey Da˘gları: timing and amount of Neogene rotations in SW Turkey. Turk. J. Earth Sci.19, 123–156.

van Hinsbergen, D.J.J., 2010c. A key extensional metamorphic core complex reviewed and restored: the Menderes Massif of western Turkey. Earth-Sci. Rev.102, 60–76.

van Hinsbergen, D.J.J., Mensink, M., Langereis, C.G., Maffione, M., Spalluto, L., Tro-peano, M., Sabato, L., 2014. Did Adria rotate relative to Africa? Solid Earth Discus.6, 937–983. http://dx.doi.org/10.5194/sed-6-937-2014.

Varol, E., Temel, A., Gourgaud, A., Bellon, H., 2007. Early Miocene adakite-like volcanism in the Balkuyumcu region, central Anatolia, Turkey: Petrology and geochemistry. Journal of Asian Earth Sciences 30, 613–628.

Vasiliev, I., Franke, C., Meeldijk, J.D., Dekkers, M.J., Langereis, C.G., Krijgsman, W., 2008. Putative greigite magnetofossils from the Pliocene epoch. Nat. Geosci.1 (11), 782–786.

Westaway, R., 2003. Kinematics of the Middle East and Eastern Mediterranean updated. Turkish Journal of the Earth Sciences 12, 5–46.

Wilson, R.L., 1971. Dipole offset — the time average palaeomagnetic field over the past 25 million years. Geophysical Journal of the Royal astronomical Society 22, 81–504.

Whitney, D. L., and Davis, P.B., 2006. Why is lawsonite eclogite so rare? Metamorphism and preservation of lawsonite eclogite, Sivrihisar, Turkey. Geology, 34, 473-476.

Whitney, D.L., Teyssier, C., Dilek, Y., and Fayon, A.K., 2001. Metamorphism of the Central Anatolian Crystalline Complex, Turkey: influence of orogen-normal collision vs wrench-dominated tectonics on P-T-t paths. Journal of Metamorphic Geology, 19, 411-432.

Whitney, D.L., Teyssier, C., Fayon, A.K., Hamilton, M.A., and Heizler, M., 2003. Tectonic controls on metamorphism, partial melting, and intrusion: timing and duration of regional metamorphism and magmatism in the Nigde Massif, Turkey. Tectonophysics, 376, 37-60.

Wilson, M., Tankut, A., Gulec, N., 1997. Tertiary volcanism of the Galatean Province. NW Central Anatolia, Turkey, Lithos 42, 105–121.

Voight W, Kinoshita S (1907) Bestimmung absoluter Werte von Magnetiserungszahlen, inbesondere fur Kristalle. Annale der Physic 24:492–514

Wortel, M.J.R., Spakman, W., 2000. Subduction and slab detachment in the Mediterranean–Carpathian region. Science290, 1910–1917.

Yalınız, M.K., 2008. A Geochemical Attempt to Distinguish Forearc and Back Arc Ophiolites from the "Supra-Subduction" Central Anatolian Ophiolites (Turkey) by Comparison with Modern Oceanic Analogues. Ofioliti, 33(2), 119-134.

Yalınız, K.M., and Göncüoğlu, M C., 1998. General geological characteristics and distribution of the Central Anatolian Ophiolites. Yerbilimleri , 20, 19-30.

Yalınız, M.K., Floyd, P.A. and Göncüoğlu, M.C., 1996. Supra-subduction zone ophiolites of Central Anatolia: geochemical evidence from the Sarıkaraman ophiolite, Aksaray. Turkey. Mineralogical Magazine, 60, 697-710.

Yalınız, K.M., Güncüoglu, M. C., and Özkan-Altiner, S., 2000. Formation and emplacement ages of the SSZ-type Neotethyan ophiolites in Central Anatolia, Turkey: palaeotectonic implications. Geological Journal, 35, 53-68.

Yiğitbaş, E., Yılmaz, Y., 1996. Post-Late Cretaceous strike-slip tectonics and its implications for the southeast Anatolian orogen, Turkey. International Geology Review 38, 818–831.

Yılmaz, Y., 1990. Comparison of young volcanic associations of western and eastern Anatolia formed under a compressional regime: a review. Journal of Volcanology and Geothermal Research 44, 69–87.

Yılmaz, Y., 1993. New evidence and model of the evolution of the southeast Anatolian Orogeny. Geological Society of America Bulletin 105, 252–271.

Yılmaz, A., 1994. An example of post-collisional trough: Sivas Basin, Turkey. 10th Petroleum Congress of Turkey, Proceedings, Ankara, pp. 21–23.

Yılmaz, Y., Saroglu, F., Güner, Y., 1987. Initiation of the neomagmatism in East Anatolia. Tectonophysics 134, 177–199.

Yılmaz, Y., Tüysüz, E., Yiğitbaş, S., Genç, C., Şengör, A.M.C., 1997. Geology and tectonic evolution of the Pontides. In: Robinson, A.C. (Ed.), Regional and Petroleum Geology of the Black Sea and Surrounding Region: American Association of Petroleum Geologist, Memoir, vol. 68, pp. 183–226.

Yılmaz, Y., Genç, S.C., Gürer, F., Bozcu, M., Yılmaz, K., Karacık, Z., Altunkaynak, Ş., Elmas, A., 2000. When did the western Anatolian grabens begin to develop? In: Bozkurt, E., Winchester, J.A., Piper, J.D.A. (Eds.), Tectonics and Magmatism in Turkey and the Surrounding Area: Geological Society, London, Special Publications, vol.173, pp. 353–384.

Yoldaş, R., 1982. Tosya (Kastamonu) ile Bayat (Çorum) arasındaki bölgenin jeolojisi. PhD. Thesis. University of İstanbul (unpublished).

Yüksel, S., 1970. Etude geologique de la region d'Haymana (Turquie central): PhD. Thesis. Fac. Sci. Univ. Nancy, France, 179 p.

Zijderveld, J.D.A., 1967. A.C. demagnetization of rocks: analysis of results. In: Collinson, D.W., Creer, K.M., Runcorn, S.K. (Eds.), Methods in Paleomagnetism. Elsevier, Amsterdam, pp.254–286.

APPENDIX A

Up. Cretaceous to Paleocene sites thermomagnetic results

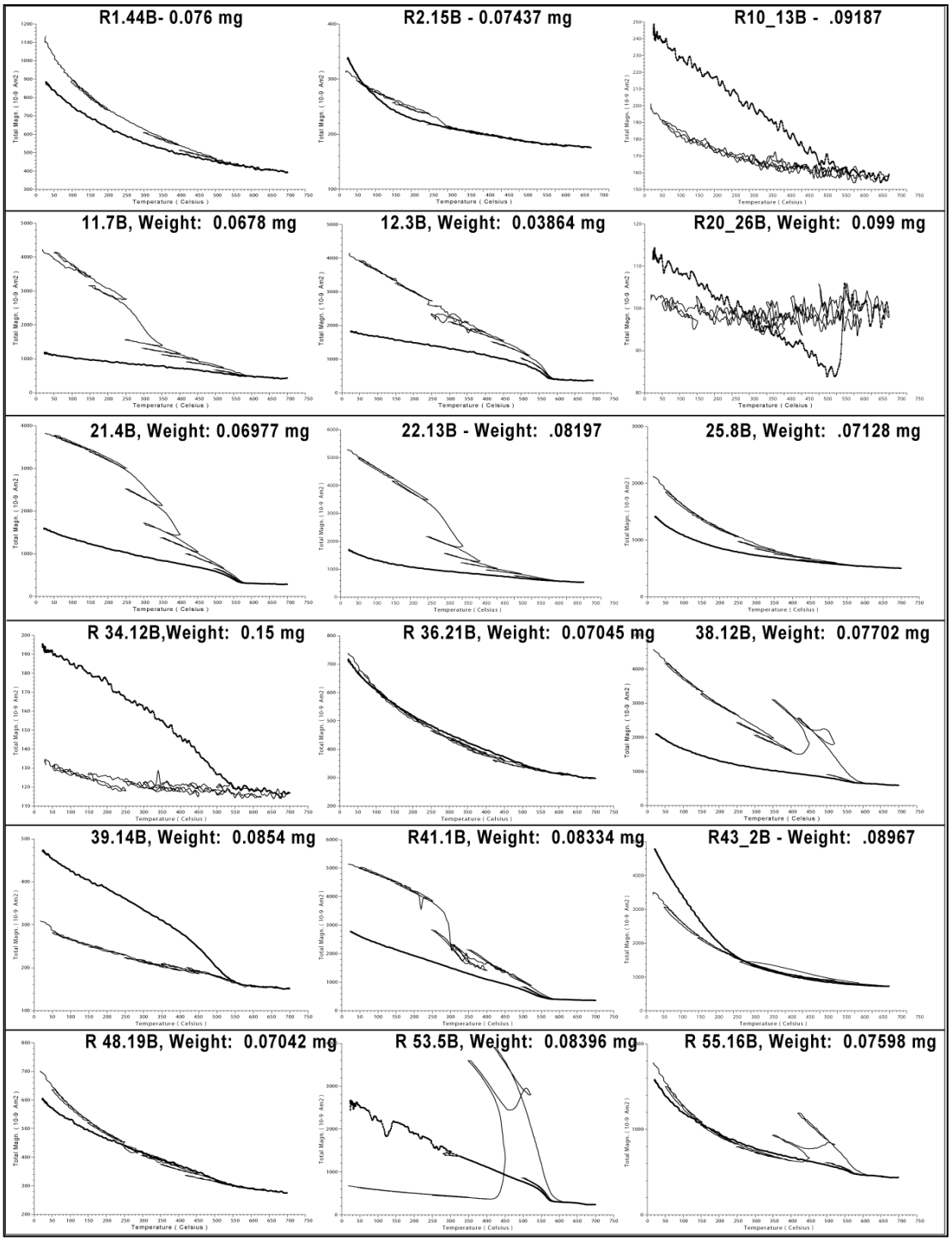

Figure A.1. Curie-balance results of Up. Cretaceous to Paleocene sites.

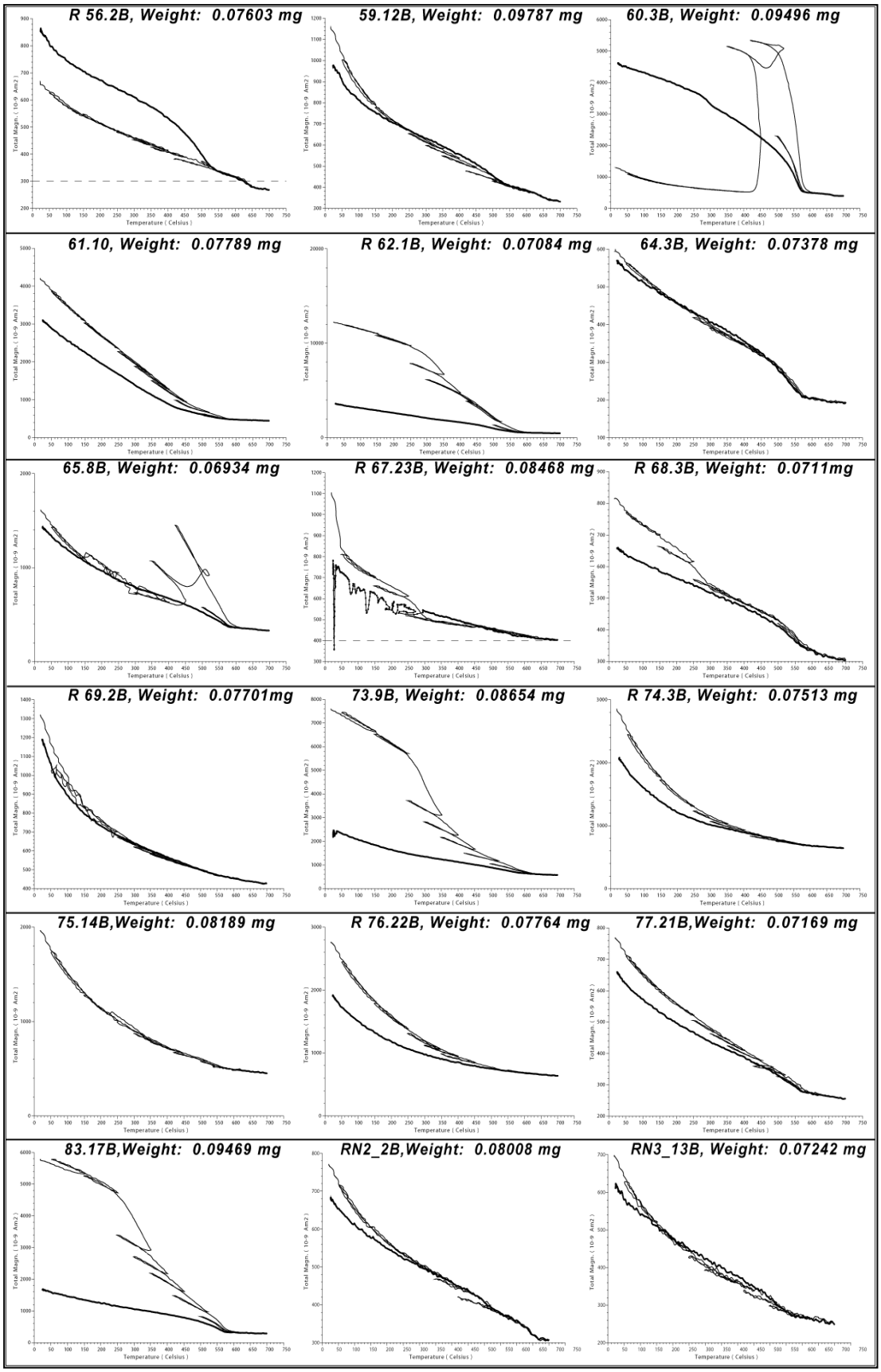

(Figure A.1. continued)

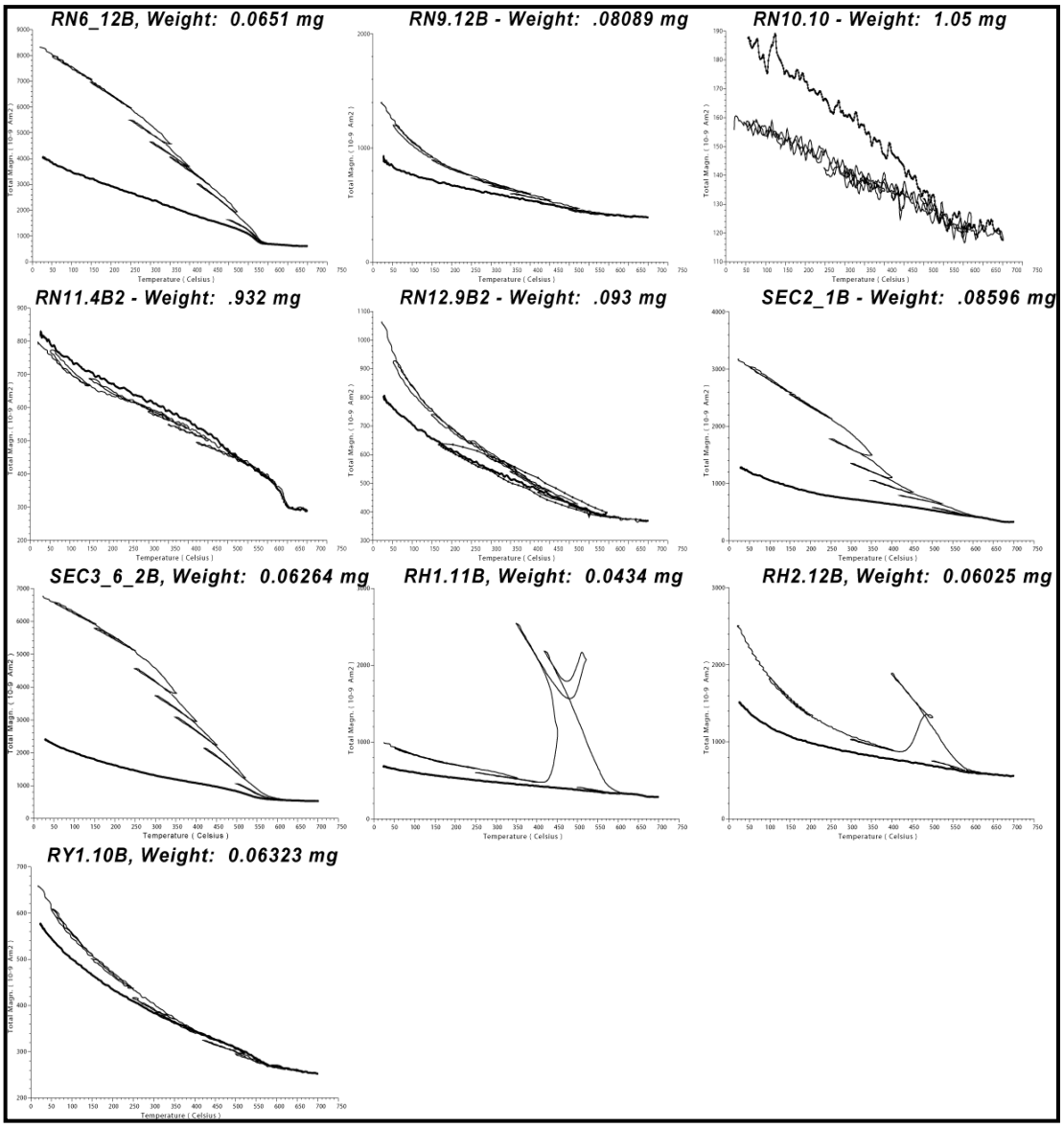

(Figure A.1. continued)

APPENDIX B

Eocene to Pliocene sites thermomagnetic results

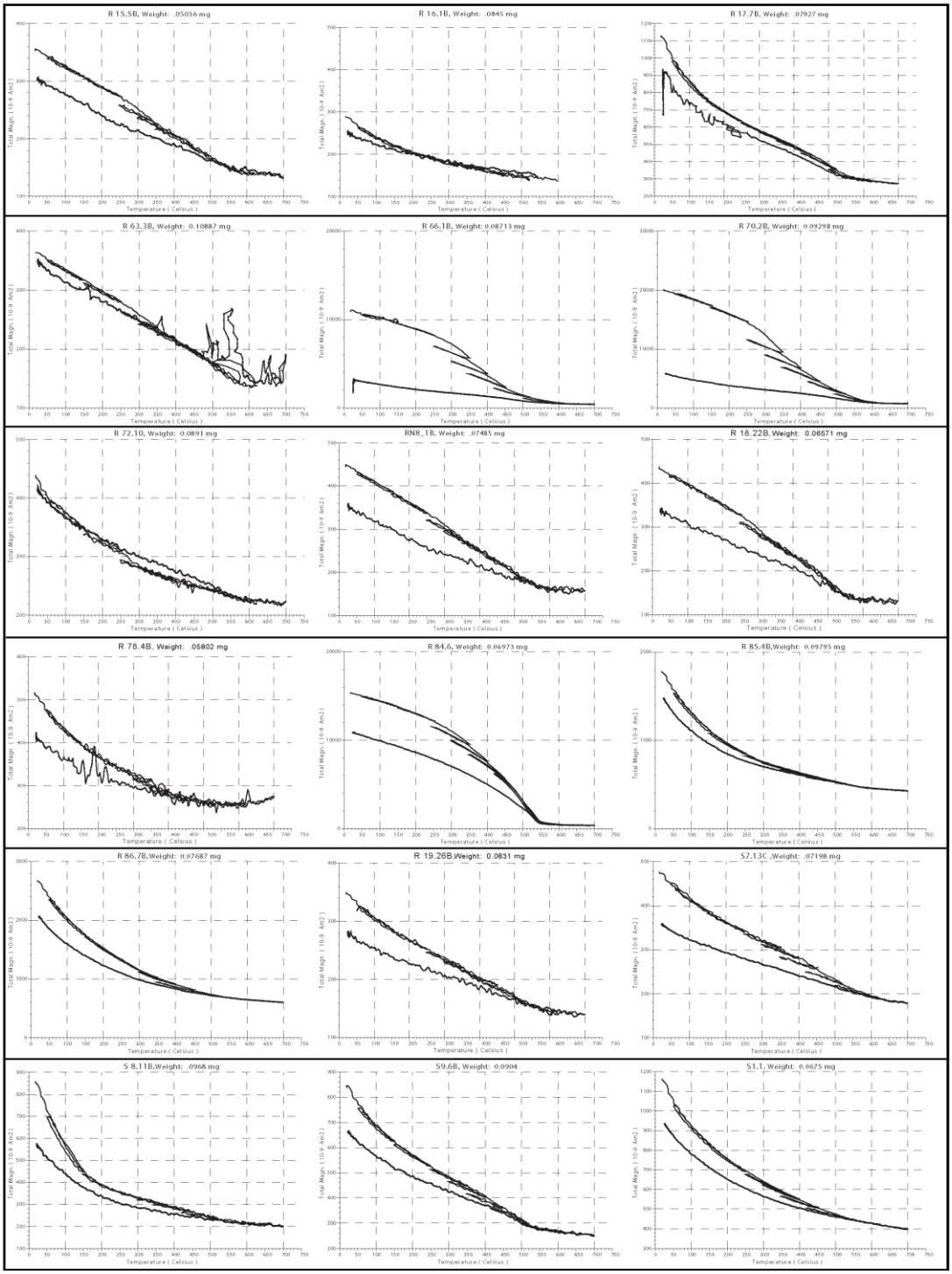

Figure B.1. Curie-balance results of Eocene to Pliocene sites.

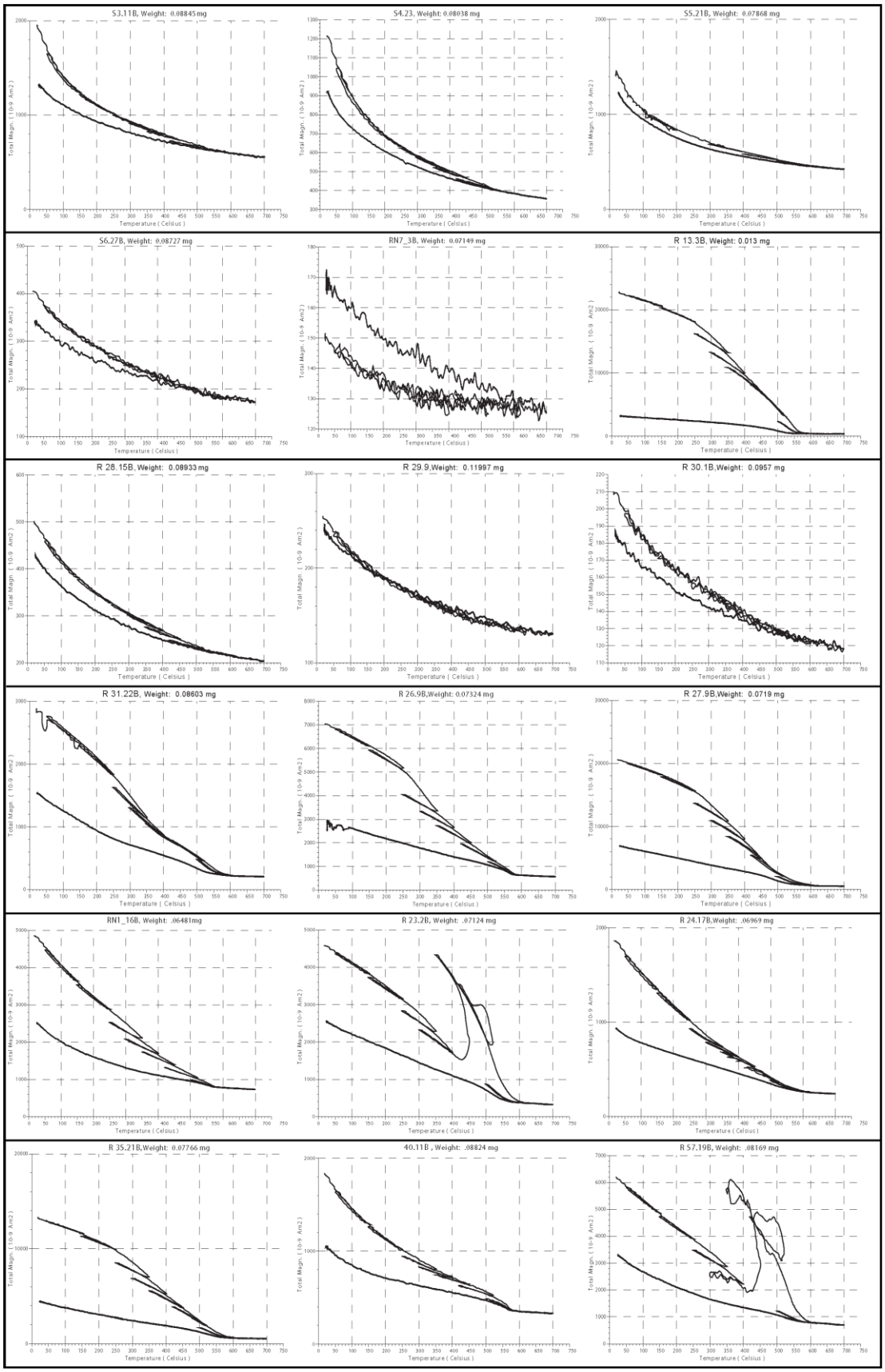

(Figure B.1. continued)

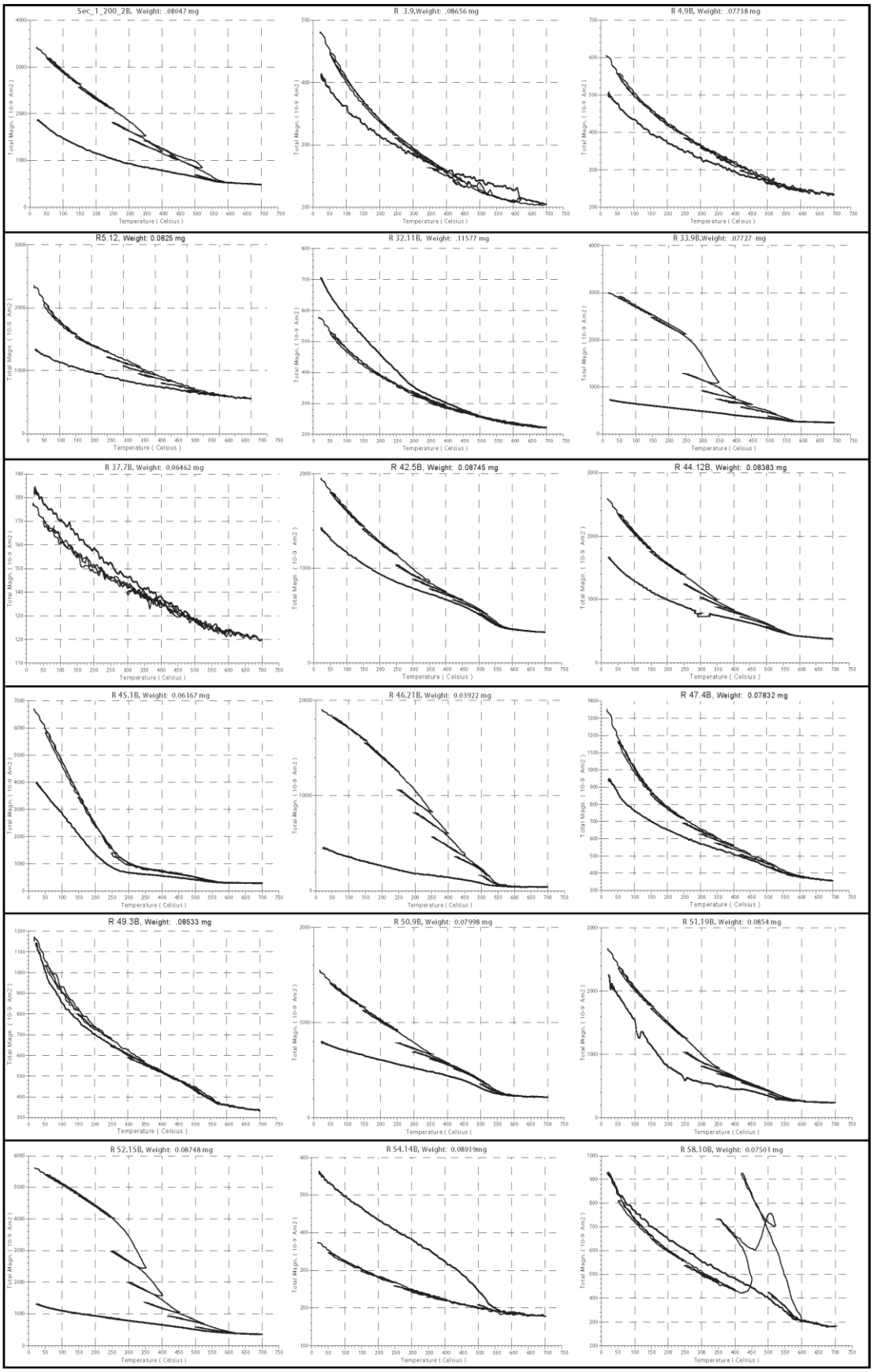

(Figure B.1. continued)

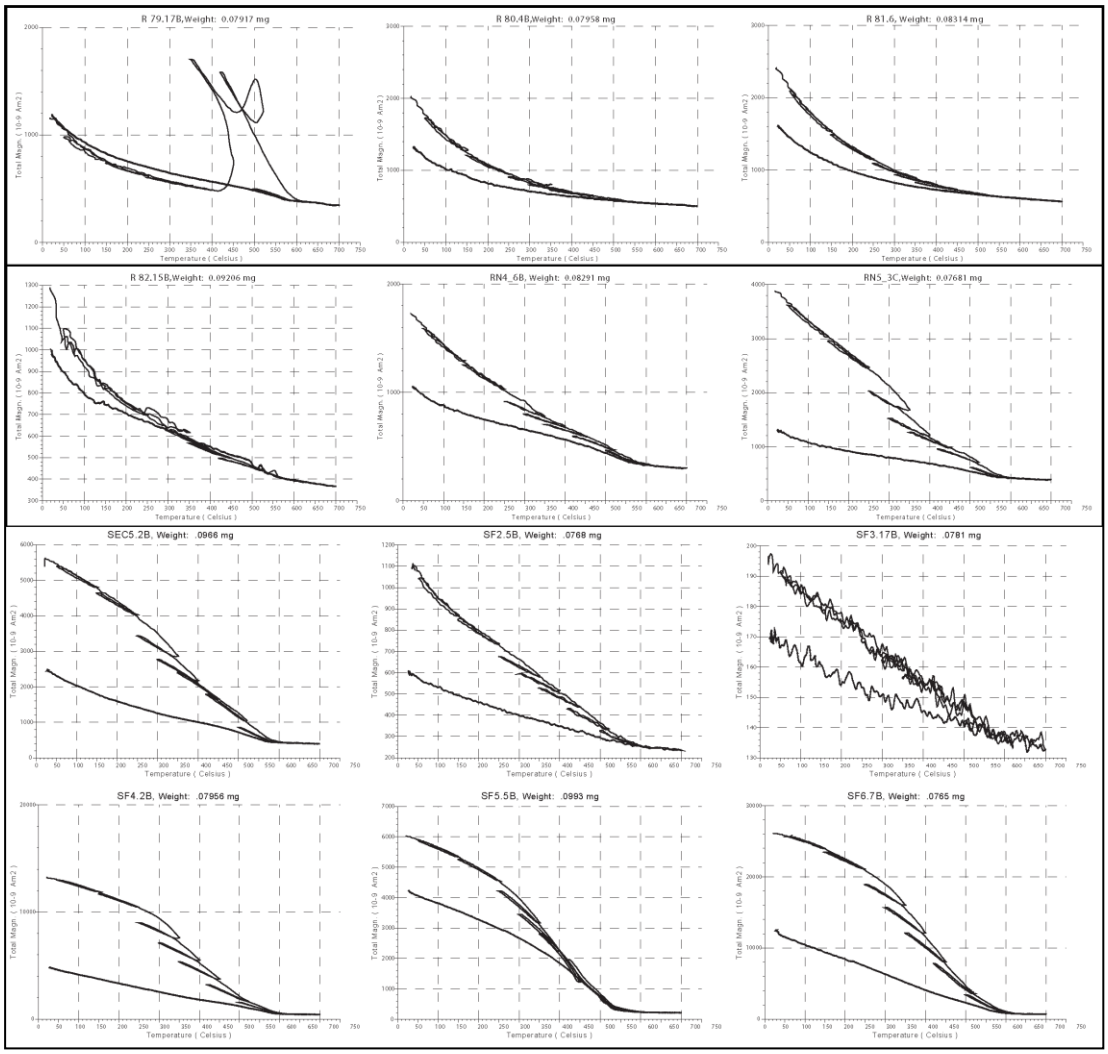

(Figure B.1. continued)

SUPPLEMENTARY A

Up. Cretaceous to Paleocene paleomagnetic site explanations, critical measurement values and mean results.

Site No	*Lithology, Age and Stratigraphy*	*Sample Numbers*	*Demagnetization*	*Initial and Isolated intensities*	*GC and Set Points*	*Results*
R 1	Paleocene in age, bluish to beige, whitish color of fine grain marl. All samples were taken within approximately four meters of stratigraphy.	56 samples were drilled, 34 specimens were demagnetized via AF and TH	5 specimens TH, 23 specimens AF 6 specimens were combined measured	Initial intensities between ~200-500 µA/m. Isolated ranges about 200°C - 450 °C or between 150 °C plus 15 mT and 40 mT	27 specimens GC and 3 specimens Set Point	ChRM (N=30) result is D= 82 °, I= 52°. 12 specimens of them get magnetized as a reverse polarity.
R 2	Paleogene in age and reddish to brown color, fine grain mudstone, mixed clay and sandstone material within approximately 5 meters sedimentary thickness.	Total 30 number of samples were taken and those 26 samples were demagnetized	4 specimens TH, 17 specimens AF, 5 specimens were combine measured.	Lower level, initial intensities between 25µA/m-80 µA/m, upper level show the intensities between 175-600 µA/m	12 specimens GC and 14 specimens selected as a Set Point	ChRM (N=25) result is D=35.4°, I= 58.9°. Inclination value is similar with the present day-field inclination.
R 10	Permian in age and dark to blue color, limestone material approximately in 5 meters thickness.	17 samples were drilled, 17 specimens were demagnetized via AF	17 specimens were measured AF	Initial intensities between ~250-800 µA/m. Isolated ranges about between 8 mT and 50 mT	7 specimens GC and 10 specimens selected as a Set Point	ChRM (N=16) result is D=28.5°, I= 49.5°. All specimens normally magnetized.

R 11	Up. Paleocene-Eocene in age and yellow to green, fine-medium grain sandstone material approximately in 12 meters thickness. (Kirkkavak Formation)	24 samples were drilled, 18 specimens were demagnetized via AF and TH	4 specimens TH,9 specimens AF, 5 specimens were measured combine	Initial intensities between ~7500-15000 µA/m. Isolated ranges about 220°C - 430°C or between 150°C plus 30 mT and 80 mT	All specimens interpreted without GC	ChRM (N=16) result is D=301.2°, I= 61.6°. All specimens normally magnetized.
R 12	Up. Paleocene-Eocene in age and yellow to green, fine-medium grain sandstone material approximately in 12 meters thickness. (Kirkkavak Formation)	27 samples were drilled, 18 specimens were demagnetized via AF and TH	4 specimens TH,8 specimens AF, 6 specimens were measured combine	Initial intensities between ~10000-30000 µA/m. Isolated ranges about 320°C - 580°C or between 150°C plus 30 mT and 80 mT	All specimens interpreted without GC	ChRM (N=18) result is D=292.7°, I= 50°. There are four reversely magnetized specimens.
R 20	Paleocene in age white color, limestone material approximately in 3 meters thickness. Caldag formation.	30 samples were drilled, 20 specimens were demagnetized via AF and TH	4 specimens TH,10 specimens AF, 6 specimens were measured combine	Initial intensities between 50-700 µA/m. Isolated ranges about 230°C -380°C or between 150°C plus 20 mT and 60 mT	All specimens interpreted without GC	ChRM (N=11) result is D=125.8°, I= -46.4°. There are 11 reversely magnetized specs.
R 21	Up. Cretaceous in age dark green to blue color, clay, sandy-mudstone material approximately in 4 meters thickness. Haymana formation.	28 samples were drilled, 20 specimens were demagnetized via AF and TH	4 specimens TH,9 specimens AF, 7 specimens were measured combine	Initial intensities between 5000- 22000 µA/m. Isolated ranges about 230°C -650°C or between 150°C plus 20 mT and 70 mT	All specimens interpreted without GC	ChRM (N=18) result is D=309.4°, I= 55.9°. All specimens normally magnetized.

R 22	Mid. Paleocene-Eocene in age yellow to green color, sandstone material approximately in 3 meters thickness. Kirkkavak formation.	24 samples were drilled, 20 specimens were demagnetized via AF and TH	4 specimens TH,10 specimens AF, 6 specimens were measured combine	Initial intensities between 10000- 40000 µA/m. Isolated ranges about 230°C -650°C or between 150°C plus 25 mT and 70 mT	5 specimens GC and 11 specimens selected as a Set Point	ChRM (N=16) result is D=127.9°, I= -16.2°. All specimens reversely magnetized.
R 25	Mid. Paleocene-Eocene in age yellow to green color, sandstone material approximately in 4 meters thickness. Kirkkavak formation.	18 samples were drilled, 18 specimens were demagnetized via AF and TH	4 specimens TH, 8 specimens AF, 6 specimens were measured combine	Initial intensities between 1400- 6000 µA/m. Isolated ranges about 230°C -560°C or between 150°C plus 25 mT and 70 mT	15 specimens GC and 3 specimens selected as a Set Point	ChRM (N=18) result is D=129.4°, I= -20.9°. All specimens reversely magnetized.
R 34	Paleocene in age white color, limestone material approximately in 3 meters thickness. Caldag formation.	20 samples were drilled, 19 specimens were demagnetized via AF and TH	4 specimens TH, 9 specimens AF, 6 specimens were measured combine	Initial intensities between 50-500 µA/m. Isolated ranges about 80°C-300°C or between 150°C plus 10 mT and 30 mT	15 specimens GC and 1 specimens selected as a Set Point	ChRM (N=16) result is D=324.4°, I= 60.2°. There are 3 reversely magnetized specimens.
R 36	Mid. Paleocene-Eocene in age yellow to green color, sandstone material approximately in 5 meters thickness. Kirkkavak formation.	26 samples were drilled, 20 specimens were demagnetized via AF and TH	4 specimens TH, 10 specimens AF, 6 specimens were measured combine	Initial intensities between 50-500 µA/m. Isolated ranges about 80°C-225°C or between 150°C plus 8 mT and 30 mT	14 specimens GC and 6 specimens selected as a Set Point	ChRM (N=20) result is D=252.1°, I= -56.6°. All specimens reversely magnetized.
R 38	Up. Cretaceous in age dark green to blue color, clay, sandy-mudstone material approximately	24 samples were drilled, 20 specimens were	4 specimens TH, 10 specimens AF, 6 specimens were	Initial intensities between 1100- 2200 µA/m. Isolated ranges about 80°C-450°C or	All specimens interpreted without GC	ChRM (N=20) result is D=299.8°, I= 55.1°. All specimens

	in 6 meters thickness. Haymana formation.	demagnetized via AF and TH	measured combine	between 150°C plus 24 mT and 50 mT		normally magnetized.
R 39	Paleocene in age yellow to green color sandstone, material approximately in 5 meters thickness. Yesilyurt formation.	21 samples were drilled, 20 specimens were demagnetized via AF and TH	4 specimens TH, 10 specimens AF, 6 specimens were measured combine	Initial intensities between 200- 600 µA/m. Isolated ranges about 180°C-500°C or between 150°C plus 6 mT and 35 mT	All specimens interpreted without GC	ChRM (N=11) result is D=224.1°, I= 48.3°. All specimens normally magnetized.
R 41	Up. Cretaceous in age dark green to blue color, clay, sandy-mudstone material approximately in 8 meters thickness. Haymana formation.	22 samples were drilled, 22 specimens were demagnetized via AF and TH	4 specimens TH, 12 specimens AF, 6 specimens were measured combine	Initial intensities between 6500- 20000 µA/m. Isolated ranges about 420°C-650°C or between 150°C plus 40 mT and 80 mT	17 specimens GC and 4 specimens selected as a Set Point	ChRM (N=21) result is D=148.9°, I= -48.5°. All specimens reversely magnetized.
R 43	Mid. Paleocene-Eocene in age yellow to green color, sandstone material approximately in 3 meters thickness. Kirkkavak formation.	16 samples were drilled, 15 specimens were demagnetized via AF and TH	4 specimens TH, 5 specimens AF, 6 specimens were measured combine	Initial intensities between 500- 2000 µA/m. Isolated ranges about?	no set points and no GC	No result, because of remagnetization or big overprint over
R 48	Paleocene in age green to brown color, sandstone material approximately in 3 meters thickness.	24 samples were drilled, 21 specimens were demagnetized via AF and TH	4 specimens TH, 11 specimens AF, 6 specimens were measured combine	Initial intensities between 150- 400 µA/m. Isolated ranges about 150°C-420°C or between 150°C plus 20 mT and 60 mT	All specimens interpreted without GC	ChRM (N=15) result is D=229.4°, I= -52.6°. All specimens reversely magnetized.

R 53	Mid. Paleocene-Eocene in age yellow to green color, sandstone material approximately in 3 meters thickness. Kartal-Kirkkavak boundary.	25 samples were drilled, 21 specimens were demagnetized via AF and TH	4 specimens TH, 11 specimens AF, 6 specimens were measured combine	Initial intensities between 3000- 18000 µA/m. Isolated ranges about 80°C-300°C or between 150°C plus 10 mT and 40 mT	19 specimens GC and 2 specimens selected as a Set Point	ChRM (N=21) result is D=33.4°, I= 35.2°. All specimens normally magnetized.
R 55	Up. Cretaceous in age dark green to blue color, clay, sandy-mudstone material approximately in 12 meters thickness. Haymana formation.	26 samples were drilled, 21 specimens were demagnetized via AF and TH	4 specimens TH, 11 specimens AF, 6 specimens were measured combine	Initial intensities between 1000- 2000 µA/m. Isolated ranges about 100°C-400°C or between 150°C plus 20 mT and 80 mT	All specimens interpreted without GC	ChRM (N=21) result is D=321.3°, I= 50°. All specimens normally magnetized.
R 56	Paleocene in age red to pink color sandstone-clay material approximately in 7 meters thickness. Kartal formation.	20 samples were drilled, 23 specimens were demagnetized via AF and TH	4 specimens TH, 13 specimens AF, 6 specimens were measured combine	Initial intensities between 1200- 3000 µA/m. Isolated ranges about 100°C-450°C or between 150°C plus 20 mT and 80 mT	14 specimens GC and 9 specimens selected as a Set Point	ChRM (N=23) result is D=135.3°, I= 61.2°. All specimens normally magnetized.
R 59	Paleocene in age red to pink color sandstone-clay material approximately in 5 meters thickness. Kartal formation.	23 samples were drilled, 21 specimens were demagnetized via AF and TH	4 specimens TH, 11 specimens AF, 6 specimens were measured combine	Initial intensities between 800- 1100 µA/m. Isolated ranges about 80°C-350°C or between 150°C plus 45 mT and 90 mT	All specimens interpreted without GC	ChRM (N=17) result is D=61.2°, I= 68.2°. All specimens normally magnetized.
R 60	Paleocene in age yellow to green color sandstone-mudstone material approximately in 6 meters	15 samples were drilled, 15 specimens were	4 specimens TH, 5 specimens AF, 6 specimens were	Initial intensities between 800- 1000 µA/m. Isolated ranges about 250°C-420°C or	All specimens interpreted without GC	ChRM (N=14) result is D=122.3°, I= -46.3°. All specimens

	thickness.	demagnetized via AF and TH	measured combine	between 150°C plus 45 mT and 80 mT		reversely magnetized.
R 61	Paleocene in age yellow to green color sandstone-mudstone material approximately in 13 meters thickness.	17 samples were drilled, 16 specimens were demagnetized via AF and TH	4 specimens TH, 6 specimens AF, 6 specimens were measured combine	Initial intensities between 4500- 7000 μA/m. Isolated ranges about 250°C-420°C or between 150°C plus 30 mT and 60 mT	14 specimens GC and 2 specimens selected as a Set Point	ChRM (N=16) result is D=46.2°, I= 26.9°. There are 4 specimens reversely magnetized.
R 62	Paleocene in age yellow to green color sandstone-mudstone material approximately in 3 meters thickness.	17 samples were drilled, 16 specimens were demagnetized via AF and TH	4 specimens TH, 6 specimens AF, 6 specimens were measured combine	Initial intensities between 10200- 67000 μA/m. Isolated ranges about 150°C-530°C or between 150°C plus 5 mT and 45 mT	9 specimens GC and 3 specimens selected as a Set Point	ChRM (N=12) result is D=56.0°, I= 36.5°. There are 4 specimens reversely magnetized.
R 64	Paleocene in age yellow to green color sandstone-mudstone material approximately in 2 meters thickness.	18 samples were drilled, 18 specimens were demagnetized via AF and TH	4 specimens TH, 8 specimens AF, 6 specimens were measured combine	Initial intensities between 400- 3300 μA/m. Isolated ranges about 180°C-420°C or between 150°C plus 10 mT and 30 mT	15 specimens GC and 2 specimens selected as a Set Point	ChRM (N=17) result is D=4.3°, I= 49.5°. There are 12 specimens reversely magnetized.
R 65	Up. Cretaceous in age yellow to green color sandstone-mudstone material approximately in 11 meters thickness.	27 samples were drilled, 21 specimens were demagnetized via AF and TH	4 specimens TH, 11 specimens AF, 6 specimens were measured combine	Initial intensities between 5000- 127000 μA/m. Isolated ranges about 180°C-450°C or between 150°C plus 12 mT and 50 mT	21 specimens GC and 1 specimens selected as a Set Point	ChRM (N=20) result is D=74°, I= 46.2°. There are 10 specimens reversely magnetized.

R 67	Up. Cretaceous-Paleogene age yellow to red color sand-mudstone material approximately in 8 meters m.	25 samples were drilled, 21 were demagnetized via AF and TH	4 spec. TH, 11 spec. AF, 6 spec. were measured combine	Initial inten. between 3000-8500 μA/m. Isolated ranges about 80°C-300°C or 20 mT and 90 mT	All specimens interpreted without GC	ChRM (N=21) result D=352°, I= 68.9°. All specimens normally magnetized.
R 68	Paleocene in age yellow to green color sandstone-mudstone material approximately in 4 meters thickness.	20 samples were drilled, 20 specimens were demagnetized via AF and TH	4 specimens TH, 10 specimens AF, 6 specimens were measured combine	Initial intensities between 1500- 17000 μA/m. Isolated ranges about 80°C-650°C or between 150°C plus 40 mT and 90 mT	6 specimens GC and 14 specimens selected as a Set Point	ChRM (N=20) result is D=44.5°, I= 44.9°. All specimens normally magnetized.
R 69	Paleocene in age yellow to green color sandstone-mudstone material approximately in 5 meters thickness.	21 samples were drilled, 19 specimens were demagnetized via AF and TH	4 specimens TH, 9 specimens AF, 6 specimens were measured combine	Initial intensities between 500- 1700 μA/m. Isolated ranges about 80°C-300°C or between 150°C plus 30 mT and 80 mT	All specimens interpreted without GC	ChRM (N=19) result is D=71.5°, I= 52.4°. All specimens normally magnetized.
R 73	Up. Cretaceous in age yellow to green color sandstone-mudstone material approximately in 3 meters thickness.	17 samples were drilled, 17 specimens were demagnetized via AF and TH	4 specimens TH, 7 specimens AF, 6 specimens were measured combine	Initial intensities between 7000- 21000 μA/m. Isolated ranges about 180°C-500°C or between 150°C plus 20 mT and 50 mT	All specimens interpreted without GC	ChRM (N=10) result is D=242.3°, I= -41.9°. All specimens reversely magnetized.
R 74	Paleocene in age yellow to green color sandstone-mudstone material approximately in 8 meters thickness.	16 samples were drilled, 15 specimens were demagnetized via	4 specimens TH, 5 specimens AF, 6 specimens were measured combine	Initial intensities between 2500- 5200 μA/m. Isolated ranges about 80°C-450°C or between 150°C plus 20 mT	All specimens interpreted without GC	ChRM (N=15) result is D=324.3°, I= 37.3°. All specimens normally magnetized.

		AF and TH		and 80 mT		
R 75	Paleocene in age yellow to green color sandstone-mudstone material approximately in 10 meters thickness.	17 samples were drilled, 16 specimens were demagnetized via AF and TH	4 specimens TH, 6 specimens AF, 6 specimens were measured combine	Initial intensities between 3000- 13000 μA/m. Isolated ranges about 225°C-610°C or between 150°C plus 35 mT and 90 mT	All specimens interpreted without GC	ChRM (N=16) result is D=232.6°, I= 53.1°. All specimens normally magnetized.
R 76	Paleocene in age yellow to green color sandstone-mudstone material approximately in 6 meters thickness.	22 samples were drilled, 22 specimens were demagnetized via AF and TH	4 specimens TH, 12 specimens AF, 6 specimens were measured combine	Initial intensities between 1000- 2700 μA/m. Isolated ranges about 120°C-320°C or between 150°C plus 6 mT and 45 mT	All specimens interpreted without GC	ChRM (N=22) result is D=353.5°, I= 37.3°. All specimens normally magnetized.
R 77	Paleocene in age yellow to green color sandstone-mudstone material approximately in 5 meters thickness.	25 samples were drilled, 18 specimens were demagnetized via AF and TH	4 specimens TH, 8 specimens AF, 6 specimens were measured combine	Initial intensities between 500- 3600 μA/m. Isolated ranges about 120°C-380°C or between 150°C plus 3 mT and 33 mT	13 specimens GC and 5 specimens selected as a Set Point	ChRM (N=18) result is D=77.2°, I= 46.3°. There are 7 specimens reversely magnetized.
R 83	Up. Cretaceous in age yellowish color sandstone material approximately in 12 meters thickness.	33 samples were drilled, 21 specimens were demagnetized via AF and TH	4 specimens TH, 11 specimens AF, 6 specimens were measured combine	Initial intensities between 12000- 63000 μA/m. Isolated ranges about 120°C-560°C or between 150°C plus 4 mT and 70 mT	All specimens interpreted without GC	ChRM (N=21) result is D=14.3°, I= 42.4°. All specimens normally magnetized.
RN2	Paleocene in age red to pink color sandstone-clay material	14 samples were drilled, 14	4 specimens TH, 4 specimens AF, 6	Initial intensities between 1300- 2500 μA/m. Isolated	8 specimens GC and 2 specimens	ChRM (N=10) result is D=124.2°, I= 62.6°.

	approximately in 7 meters thickness. Kartal formation.	specimens were demagnetized via AF and TH	specimens were measured combine	ranges about 400°C-650°C or between 150°C plus 40 mT and 80 mT	selected as a Set Point	All specimens normally magnetized.
RN3	Mid. Paleocene-Eocene in age yellow to green color, sandstone material approximately in 3 meters thickness. Kirkkavak formation.	13 samples were drilled, 20 specimens were demagnetized via AF and TH	4 specimens TH, 10 specimens AF, 6 specimens were measured combine	Initial intensities between 1000- 2100 μA/m. Isolated ranges about 320°C-520°C or between 150°C plus 8 mT and 40 mT	18 specimens GC and 1 specimens selected as a Set Point	ChRM (N=18) result is D=129.8°, I= 65.3°. All specimens normally magnetized.
RN6	Paleocene in age yellow to green color sandstone-claystone material approximately in 20 meters thickness.	20 samples were drilled, 21 specimens were demagnetized via AF and TH	4 specimens TH, 11 specimens AF, 6 specimens were measured combine	Initial intensities between 3000- 15000 μA/m. Isolated ranges about 350°C-500°C or between 150°C plus 20 mT and 50 mT	21 specimens GC and 1 specimens selected as a Set Point	ChRM (N=22) result is D=184.2°, I=-34.4°. All specimens reversely magnetized.
RN9	Paleocene in age yellow to green color sandstone-claystone material approximately in 12 meters thickness.	22 samples were drilled, 20 specimens were demagnetized via AF and TH	4 specimens TH, 10 specimens AF, 6 specimens were measured combine	Initial intensities between 500- 3500 μA/m. Isolated ranges about 150°C-550°C or between 150°C plus 12 mT and 70 mT	All specimens interpreted without GC	ChRM (N=20) result is D=203.6°, I=-35.9°. All specimens reversely magnetized.
RN10	Paleocene in age yellow to green color sandstone-mudstone material approximately in 5 meters thickness.	20 samples were drilled, 19 specimens were demagnetized via AF and TH	5 specimens TH, 14 specimens were measured AF	Initial intensities between 100- 600 μA/m. Isolated ranges about 330°C-500°C or between 150°C plus 9 mT and 50 mT	6 specimens GC and 4 specimens selected as a Set Point	ChRM (N=22) result is D=55.5°, I= 61.6°. All specimens normally magnetized.

RN11	Paleocene in age yellow to green color sandstone-mudstone material approximately in 7 meters thickness.	20 samples were drilled, 20 specimens were demagnetized via AF and TH	5 specimens TH, 15 specimens were measured AF	Initial intensities between 500- 3600 µA/m. Isolated ranges about 120°C-380°C or between 150°C plus 3 mT and 33 mT	14 specimens GC and 5 specimens selected as a Set Point	ChRM (N=18) result is D=117°, I=-43.8°. All specimens reversely magnetized.
RN12	Paleocene in age yellowish color sandstone material approximately in 12 meters thickness.	25 samples were drilled, 17 specimens were demagnetized via AF and TH	5 specimens TH, 12 specimens were measured AF	Initial intensities between 200- 3000 µA/m. Isolated ranges about 120°C-370°C or between 150°C plus 4 mT and 60 mT	All specimens interpreted without GC	ChRM (N=21) result is D=26.3°, I= 35.6°. All specimens normally magnetized.
OA	Up. Cretaceous in age granitoid in 12 meters thickness.	20 samples were drilled, 20 specimens were demagnetized via AF and TH	All specimens were measured AF	Initial intensities between 500- 55000 µA/m. Isolated ranges between 4 mT and 100 mT	All specimens interpreted without GC	ChRM (N=21) result is D=14.3°, I= 42.4°. All specimens normally magnetized.
SEC2	Mid. Paleocene-Eocene in age red, yellow to green color, sandstone-clay, and mudstone material approximately in 700 meters thickness. Kartal-Kirkkavak boundary.	624 samples were drilled, 416 specimens were demagnetized via AF and TH	208 specimens TH, 208 specimens AF were measured	Initial intensities between ~10000-15000 µA/m. Isolated ranges about 200°C -650°C or between 15 mT and 60 mT	All specimens interpreted without GC	ChRM (N=196) result is D=314.1°, I= 56°. There are normal and reverse magnetization
SEC3	Up. Cretaceous in age dark green to blue color, clay, sandy-	202 samples were drilled, 202	101 specimens TH, 101 specimens AF	Initial intensities between ~2000-50000 µA/m.	All specimens interpreted without	ChRM (N=103) result is D=279.7°, I= 61.9°.

	mudstone material approximately in 288 meters thickness. Haymana formation.	specimens were demagnetized via AF and TH	were measured	Isolated ranges about 200℃ - 580℃ or between 15 mT and 80 mT	GC	There are normal and reverse magnetization
SEC4	Paleocene in age yellow to green color sandstone-marl, material approximately in 64 meters thickness. Yeşilyurt formation.	64 samples were drilled, 64 specimens were demagnetized via AF and TH	32 specimens TH, 32 specimens AF were measured	Initial intensities between ~150-1400 µA/m. Isolated ranges about 200℃ - 450℃ or between 8 mT and 50 mT	All specimens interpreted without GC	ChRM (N=14) result is D=337.1°, I= 17.6°. All specimens normally magnetized.
K-T	Cretaceous-Paleogene boundary limestone-marl-sandstone-mudstone material approximately in 35 meters thickness.	20 samples were drilled, 20 specimens were demagnetized via AF	20 specimens were measured AF	Initial intensities between 450- 12500 µA/m. Isolated ranges between 10 mT and 80 mT	All specimens interpreted without GC	ChRM (N=20) result is D=236.6°, I= 51.6°. There are 7 specimens reversely magnetized.
RH 1	Up. Cretaceous in age dark green to blue color, clay-mudstone material approximately in 9 meters thickness. Haymana formation.	Total 45 number of samples were taken and those 24 samples were demagnetized	4 specimens TH, 15 specimens AF, 5 specimens were combine measured.	Initial intensities between 2700-9000 µA/m. Isolated ranges about 180°C -500°C or between 150°C plus 20 mT and 80 mT	All specimens interpreted without GC	ChRM (N=24) result is D=281.7°, I= 49.9°. All specimens normally magnetized.
RH 2	Up. Cretaceous in age dark green to blue color, clay-mudstone material approximately in 11 meters thickness. Haymana formation.	Total 57 number of samples were taken and those 26 samples were demagnetized	4 specimens TH, 17 specimens AF, 5 specimens were combine measured.	Initial intensities between 1200-3200 µA/m. Isolated ranges about 180°C -500°C or between 150°C plus 40 mT and 80 mT	All specimens interpreted without GC	ChRM (N=25) result is D=329.4°, I= 28.5°. All specimens normally magnetized.

RY 1	Paleogene in age and reddish to green color, fine grain mudstone-sandstone material within approximately 6 meters sedimentary thickness.	Total 60 number of samples were taken and those 22 samples were demagnetized	4 specimens TH, 13 specimens AF, 5 specimens were combine measured.	Initial intensities between 1200-3200 μA/m. Isolated ranges about 180°C -480°C or between 150°C plus 40 mT and 80 mT	All specimens interpreted without GC	ChRM (N=22) result is D=323.7°, I= 27.4°. All specimens normally magnetized.

SUPPLEMENTARY B

Eocene Pliocene paleomagnetic site explanations, critical measurement values and mean results.

Site No	***Lithology, Age and Stratigraphy***	***Sample Numbers***	***Demagnetization***	***Initial and Isolated intensities***	***GC and Set Points***	***Results***
R 3	Up. Miocene-Pliocene in age brown to yellow color, mudstone material approximately in 3 meters thickness.	Total 35 number of samples were taken and those 26 samples were demagnetized	4 specimens TH, 17 specimens AF, 5 specimens were combine measured.	Initial intensities between 40-162 μA/m. Isolated ranges about 120°C -300°C or between 150°C plus 5 mT and 40 mT	6 specimens GC and 17 specimens selected as a Set Point	ChRM (N=23) result is D=29.5°, I= 65°. All specimens normally magnetized.
R 4	Lower-Middle Miocene in age, brown color of fine grain mudstone. All samples were taken within approximately 2 meters of stratigraphy.	Total 46 number of samples were taken and those 34 samples were demagnetized	4 specimens TH, 25 specimens AF, 5 specimens were combine measured.	Initial intensities between 240-550 μA/m. Isolated ranges about 150°C -390°C or between 150°C plus 15 mT and 80 mT	All specimens interpreted without GC	ChRM (N=29) result is D=319.7°, I= 52.9°. All specimens normally magnetized.
R 5	Up. Miocene-Pliocene in age reddish to yellow color, mudstone-marl material approximately in 3 meters thickness.	Total 23 number of samples were taken and those 18 samples were demagnetized.	4 specimens TH, 9 specimens AF, 5 specimens were combine measured.	Initial intensities between 200-2000 μA/m. Isolated ranges about 150°C -390°C or between 150°C plus 5 mT and 50 mT.	5 specimens GC and 7 specimens selected as a Set Point.	ChRM (N=11) result is D=203.4°, I= -43.1°. All specimens reversely magnetized.

R 13	Middle Miocene in age and dark brown color, fine grain andesite, approximately in 11 meters thickness.	22 samples were drilled, 18 specimens were demagnetized via AF and TH	4 specimens TH,8 specimens AF, 6 specimens were measured combine	Initial intensities between 550000- 120000 μA/m. Isolated ranges about 80°C - 580°C or between 150°C plus 10 mT and 100 mT	All specimens interpreted without GC	ChRM (N=18) result is D=1.6°, I= 57.6°. All specimens normally magnetized.
R 14	Lower-Mid. Miocene in age and purple to white color, marl material approximately in 3 meters thickness.	14 samples were drilled, 8 specimens were demagnetized via AF	8 specimens AF	Initial intensities between 20-80 μA/m. Isolated ranges?	all scattered data	Low Intensities.
R 15	Lower-Mid. Miocene in age and purple to white color, marl material approximately in 3 meters thickness.	28 samples were drilled, 10 specimens were demagnetized via AF and TH	3 specimens TH, 7 specimens combined	Initial intensities between 100000- 200000 μA/m. Isolated ranges?	all scattered data	Lightning.
R 16	Lower-Mid. Miocene in age grey to white color, Limestone, marl material approximately in 3 meters thickness.	29 samples were drilled, 18 specimens were demagnetized via AF and TH	4 specimens TH,8 specimens AF, 6 specimens were measured combine	Initial intensities between 100- 500 μA/m. Isolated ranges about 80°C -280°C or between 150°C plus 10 mT and 30 mT	14 specimens GC and 2 specimens selected as a Set Point	ChRM (N=16) result is D=207.5°, I= -37.2°. There are twelve reversely magnetized specimens.

R 17	Lower-Mid. Miocene in age yellowish to purple color, sandstone, mudstone material approximately in 4 meters thickness.	21 samples were drilled, 18 specimens were demagnetized via AF and TH	4 specimens TH,8 specimens AF, 6 specimens were measured combine	Initial intensities between 1500-18000 μA/m. Isolated ranges about 80°C -330°C or between 150°C plus 20 mT and 50 mT	15 specimens GC and 2 specimens selected as a Set Point	ChRM (N=17) result is D=55.5°, I= 63.2°. There are 14 reversely magnetized specimens.
18	Up. Miocene-Pliocene in age purple to white color, limestone material approximately in 2 meters thickness.	33 samples were drilled, 20 specimens were demagnetized via AF and TH	4 specimens TH,10 specimens AF, 6 specimens were measured combine	Initial intensities between 3000- 5000 μA/m. Isolated ranges about 150°C -500°C or between 150°C plus 20 mT and 65 mT	8 specimens GC and 12 specimens selected as a Set Point	ChRM (N=19) result is D=344.5°, I= 43.4°. There are 8 reversely magnetized specimens.
R 19	Up. Miocene-Pliocene in age reddish to yellow color, limestone material approximately in 3 meters thickness.	27 samples were drilled, 20 specimens were demagnetized via AF and TH	4 specimens TH,10 specimens AF, 6 specimens were measured combine	Initial intensities between 400- 2200 μA/m. Isolated ranges about 80°C -280°C or between 150°C plus 10 mT and 40 mT	15 specimens GC and 3 specimens selected as a Set Point	ChRM (N=18) result is D=199.9°, I= -49.4°. There are 14 reversely magnetized specimens.
R 23	Mid. Paleocene-Eocene in age yellow to green color, sandstone material approximately in 2 meters thickness. Kirkkavak formation.	16 samples were drilled, 16 specimens were demagnetized via AF and TH	4 specimens TH,6 specimens AF, 6 specimens were measured combine	Initial intensities between 10000- 20000 μA/m. Isolated ranges about?	no set points and no GC	No result, because of demagnetization or big overprint

R 24	Pliocene in age reddish to purple color, marl, mudstone material approximately in 3 meters thickness.	25 samples were drilled, 24 specimens were demagnetized via AF and TH	4 specimens TH, 14 specimens AF, 6 specimens were measured combine	Initial intensities between 5000- 170000 μA/m. Isolated ranges about 230°C -560°C or between 150°C plus 25 mT and 70 mT	All specimens interpreted without GC	ChRM (N=20) result is D=153.5°, I= -48.5°. All specimens reversely magnetized.
R 26	Low-Middle Eocene in age yellow to green color, sandstone material approximately in 3 meters thickness. Eskipolatli formation.	29 samples were drilled, 21 specimens were demagnetized via AF and TH	4 specimens TH, 11 specimens AF, 6 specimens were measured combine	Initial intensities between 7000- 45000 μA/m. Isolated ranges about 200°C -500°C or between 150°C plus 10 mT and 35 mT	17 specimens GC and 4 specimens selected as a Set Point	ChRM (N=21) result is D=118.2°, I= 67.5°. All specimens normally magnetized.
R 27	Lower-Mid. Miocene in age and yellow to brown color, fine grain marl, sandstone material approximately in 2 meters thickness.	17 samples were drilled, 18 specimens were demagnetized via AF and TH	4 specimens TH, 8 specimens AF, 6 specimens were measured combine	Initial intensities between 30000- 225000 μA/m. Isolated ranges about 180°C - 610°C or between 150°C plus 35 mT and 70 mT	All specimens interpreted without GC	ChRM (N=17) result is D=326.9°, I= 49.4°. All specimens normally magnetized.
R 28	Pliocene in age reddish to yellow color, marl, mudstone material approximately in 3 meters thickness.	26 samples were drilled, 20 specimens were demagnetized via AF and TH	4 specimens TH, 10 specimens AF, 6 specimens were measured combine	Initial intensities between 100- 400 μA/m. Isolated ranges about 80°C-275°C or between 150°C plus 20 mT and 50 mT	All specimens interpreted without GC	ChRM (N=15) result is D=345.2°, I= 46.4°. There are 1 reversely magnetized specimens.

R 29	Lower-Mid. Miocene in age and yellow to white color, fine grain marl, material approximately in 2 meters thickness.	18 samples were drilled, 17 specimens were demagnetized via AF and TH	4 specimens TH, 7 specimens AF, 6 specimens were measured combine	Initial intensities between 50-200 μA/m. Isolated ranges about 80°C-350°C or between 150°C plus 18 mT and 40 mT	All specimens interpreted without GC	ChRM (N=14) result is D=330.3°, I= 49.1°. All specimens normally magnetized.
R 30	Lower-Mid. Miocene in age and yellow to white color, fine grain marl, limestone material approximately in 5 meters thickness.	19 samples were drilled, 19 specimens were demagnetized via AF and TH	4 specimens TH, 9 specimens AF, 6 specimens were measured combine	Initial intensities between 175- 900 μA/m. Isolated ranges about 80°C-280°C or between 150°C plus 20 mT and 60 mT	All specimens interpreted without GC	ChRM (N=15) result is D=134.9°, I= -40.9°. There are 13 reversely magnetized specimens.
R 31	Lower-Mid. Miocene in age and reddish to yellow color, fine grain marl, material approximately in 3 meters thickness.	20 samples were drilled, 20 specimens were demagnetized via AF and TH	4 specimens TH, 10 specimens AF, 6 specimens were measured combine	Initial intensities between 17000- 32000 μA/m. Isolated ranges about 180°C-580°C or between 150°C plus 20 mT and 60 mT	All specimens interpreted without GC	ChRM (N=15) result is D=349.8°, I= 51.8°. All specimens normally magnetized.
R 32	Up. Miocene-Pliocene in age and white to yellowish color, fine grain marl, material approximately in 3 meters thickness.	32 samples were drilled, 24 specimens were demagnetized via AF and TH	4 specimens TH, 14 specimens AF, 6 specimens were measured combine	Initial intensities between 150- 300 μA/m. Isolated ranges about 80°C-300°C or between 150°C plus 20 mT and 50 mT	All specimens interpreted without GC	ChRM (N=24) result is D=4.9°, I= 56.5°. All specimens normally magnetized.

R 33	Low-Middle Eocene in age yellow to red color, sandstone material approximately in 7 meters thickness. Ilginlikdere formation.	17 samples were drilled, 17 specimens were demagnetized via AF and TH	4 specimens TH, 7 specimens AF, 6 specimens were measured combine	Initial intensities between 2000- 15000 µA/m. Isolated ranges about 80°C-280°C or between 150°C plus 12 mT and 35 mT	13 specimens GC and 4 specimens selected as a Set Point	ChRM (N=17) result is D=16.3°, I= 18.2°. There are 12 reversely magnetized specimens.
R 35	Low-Middle Eocene in age red color sandstone material approximately in 6 meters thickness. Ilginlikdere formation.	25 samples were drilled, 22 specimens were demagnetized via AF and TH	4 specimens TH, 12 specimens AF, 6 specimens were measured combine	Initial intensities between 20000- 36000 µA/m. Isolated ranges about 300°C-630°C or between 150°C plus 30 mT and 80 mT	15 specimens GC and 7 specimens selected as a Set Point	ChRM (N=22) result is D=287.5°, I= 61.5°. All specimens normally magnetized.
R 37	Pliocene in age yellow to white color, marl, limestone material approximately in 3 meters thickness.	26 samples were drilled, 20 specimens were demagnetized via AF and TH	4 specimens TH, 10 specimens AF, 6 specimens were measured combine	Initial intensities between 50-200 µA/m. Isolated ranges about between 150°C plus 8 mT and 30 mT	8 specimens GC and 7 specimens selected as a Set Point	ChRM (N=15) result is D=202.8°, I= -52.2°. There are 12 specimens reversely magnetized.
R 40	Mid. Paleocene-Eocene in age dark green to reddish color, sandstone, claystone material approximately in 6 meters thickness. Kirkkavak formation.	27 samples were drilled, 24 specimens were demagnetized via AF and TH	4 specimens TH, 14 specimens AF, 6 specimens were measured combine	Initial intensities between 2000- 8000 µA/m. Isolated ranges about 100°C-250°C or between 150°C plus 16 mT and 40 mT	11 specimens GC and 13 specimens selected as a Set Point	ChRM (N=24) result is D=296.3°, I= 57.7°. All specimens normally magnetized.

R 42	Low-Middle Eocene in age yellow- to green color sandstone-clay material approximately in 3 meters thickness. Ilginlikdere formation.	23 samples were drilled, 21 specimens were demagnetized via AF and TH	4 specimens TH, 11 specimens AF, 6 specimens were measured combine	Initial intensities between 2500- 10000 µA/m. Isolated ranges about 420°C-650°C or between 150°C plus 40 mT and 90 mT	All specimens interpreted without GC	ChRM (N=13) result is D=52.1°, I= 38.8°. All specimens normally magnetized.
R 44	Low-Middle Eocene in age yellowish to green color sandstone material approximately in 5 meters thickness. Eskipolatli formation.	26 samples were drilled, 21 specimens were demagnetized via AF and TH	4 specimens TH, 11 specimens AF, 6 specimens were measured combine	Initial intensities between 6500- 10000 µA/m. Isolated ranges about 350°C-580°C or between 150°C plus 40 mT and 80 mT	All specimens interpreted without GC	ChRM (N=21) result is D=283°, I= -38.9°. All specimens reversely magnetized.
R 45	Mid. Miocene in dark color, pyroclastic material approximately 3 samples in three meters and 7 different levels.	34 samples were drilled, 23 specimens were demagnetized via AF and TH	4 specimen's TH, 13 specimen's AF, 6 specimens were measured combine	Initial intensities between 100000- 350000 µA/m. Isolated ranges about 80°C-500°C or between 150°C plus 20 mT and 70 mT	16 specimens GC and 5 specimens selected as a Set Point	ChRM (N=21) result is D=198.9°, I= -44°. All specimens reversely magnetized.
R 46	Mid. Miocene in dark color, pyroclastic material approximately 3 samples in three meters and 7 different levels.	24 samples were drilled, 21 specimens were demagnetized via AF and TH	4 specimens TH, 11 specimens AF, 6 specimens were measured combine	Initial intensities between 150000- 200000 µA/m. Isolated ranges about 80°C-300°C or between 150°C plus 20 mT and 40 mT	12 specimens GC and 9 specimens selected as a Set Point	ChRM (N=21) result is D=6°, I= 51°. There are 5 reversely magnetized specimens.

R 47	Low-Middle Eocene in age yellowish to green color sandstone material approximately in 5 meters thickness. Yamak formation.	27 samples were drilled, 21 specimens were demagnetized via AF and TH	4 specimens TH, 11 specimens AF, 6 specimens were measured combine	Initial intensities between 2500- 7000 µA/m. Isolated ranges about 150°C-300°C or between 150°C plus 20 mT and 80 mT	All specimens interpreted without GC	ChRM (N=21) result is D=28.3°, I= 65°. All specimens normally magnetized.
R 49	Low-Middle Eocene in age yellowish to green color sandstone-clay material approximately in 5 meters thickness. Eskipolatli formation.	23 samples were drilled, 20 specimens were demagnetized via AF and TH	4 specimens TH, 10 specimens AF, 6 specimens were measured combine	Initial intensities between 2000- 5000 µA/m. Isolated ranges about?	no set points and no GC	No result, because of remagnetization or big overprint over
R 50	Pliocene in age yellowish to brown color sandstone-clay material approximately in 3 meters thickness.	20 samples were drilled, 21 specimens were demagnetized via AF and TH	4 specimens TH, 11 specimens AF, 6 specimens were measured combine	Initial intensities between 1300- 9500 µA/m. Isolated ranges about 80°C-300°C or between 150°C plus 10 mT and 40 mT	17 specimens GC and 3 specimens selected as a Set Point	ChRM (N=20) result is D=214.1°, I= -56.2°. There are 16 specimens reversely magnetized.
R 51	Pliocene in age yellowish to brown color sandstone-clay material approximately in 4 meters thickness.	20 samples were drilled, 19 specimens were demagnetized via AF and TH	4 specimens TH, 9 specimens AF, 6 specimens were measured combine	Initial intensities between 5000- 30000 µA/m. Isolated ranges about 80°C-380°C or between 150°C plus 20 mT and 60 mT	10 specimens GC and 8 specimens selected as a Set Point	ChRM (N=20) result is D=165.1°, I= -38.7°. All specimens reversely magnetized.

R 52	Low-Middle Eocene in age yellowish to green color sandstone material approximately in 4 meters thickness. Eskipolatli formation.	28 samples were drilled, 21 specimens were demagnetized via AF and TH	4 specimens TH, 11 specimens AF, 6 specimens were measured combine	Initial intensities between 6000- 10000 µA/m. Isolated ranges about 80°C-350°C or between 150°C plus 20 mT and 60 mT	11 specimens GC and 10 specimens selected as a Set Point	ChRM (N=20) result is D=232.3°, I= 54.9°. There are 14 specimens reversely magnetized.
R 54	Low-Middle Miocene in age yellowish to white color marl-sandstone material approximately in 5 meters thickness.	17 samples were drilled, 17 specimens were demagnetized via AF and TH	4 specimens TH, 7 specimens AF, 6 specimens were measured combine	Initial intensities between 2000- 62000 µA/m. Isolated ranges about 80°C-530°C or between 150°C plus 30 mT and 70 mT	All specimens interpreted without GC	ChRM (N=11) result is D=38.2°, I= 53.4°. There are 3 specimens reversely magnetized.
R 57	Low-Middle Eocene in age yellowish to green color sandstone-clay material approximately in 6 meters thickness. Ilginlikdere formation.	19 samples were drilled, 17 specimens were demagnetized via AF and TH	4 specimens TH, 7 specimens AF, 6 specimens were measured combine	Initial intensities between 2000- 7000 µA/m. Isolated ranges about 100°C-450°C or between 150°C plus 20 mT and 80 mT	All specimens interpreted without GC	ChRM (N=17) result is D=232.6°, I= 59°. All specimens normally magnetized.
R 58	Low-Middle Eocene in age dark blue color claystone material approximately in 7 meters thickness. Yamak formation.	18 samples were drilled, 18 specimens were demagnetized via AF and TH	4 specimens TH, 8 specimens AF, 6 specimens were measured combine	Initial intensities between 800- 3100 µA/m. Isolated ranges about 100°C-530°C or between 150°C plus 30 mT and 90 mT	All specimens interpreted without GC	ChRM (N=17) result is D=337.2°, I= 49.3°. All specimens normally magnetized.

R 63	Eocene in age purple to whitish color limestone material approximately in 4 meters thickness.	16 samples were drilled, 16 specimens were demagnetized via AF and TH	4 specimens TH, 6 specimens AF, 6 specimens were measured combine	Initial intensities between 200- 4300 μA/m. Isolated ranges about 80°C-580°C or between 150°C plus 20 mT and 80 mT	All specimens interpreted without GC	ChRM (N=14) result is D=95.4°, I= 65.1°. All specimens normally magnetized.
R 66	Oligocene in age red to yellow color sandstone-conglomerate and mudstone material approximately in 15 meters thickness.	15 samples were drilled, 15 specimens were demagnetized via AF and TH	4 specimens TH, 5 specimens AF, 6 specimens were measured combine	Initial intensities between 4000- 82000 μA/m. Isolated ranges about 180°C-450°C or between 150°C plus 12 mT and 50 mT	12 specimens GC and 1 specimens selected as a Set Point	ChRM (N=13) result is D=202.5°, I= -61.5°. There are 9 specimens reversely magnetized.
R 70	Paleocene in age green to yellow color sandstone-claystone and mudstone material approximately in 6 meters thickness.	21 samples were drilled, 15 specimens were demagnetized via AF and TH	4 specimens TH, 5 specimens AF, 6 specimens were measured combine	Initial intensities between 30000- 60000 μA/m. Isolated ranges about 450°C-650°C or between 150°C plus 40 mT and 90 mT	All specimens interpreted without GC	ChRM (N=15) result is D=72.4°, I= 49.3°. All specimens normally magnetized.
R 71	Up Miocene-Pliocene in age red to yellow color mudstone material approximately in 5 meters thickness.	18 samples were drilled, 17 specimens were demagnetized via AF and TH	4 specimens TH, 7 specimens AF, 6 specimens were measured combine	Initial intensities between 6000- 18000 μA/m. Isolated ranges about 200°C-650°C or between 150°C plus 40 mT and 90 mT	All specimens interpreted without GC	ChRM (N=15) result is D=8°, I= 63.7°. There are 1 specimen reversely magnetized.

R 72	Oligocene in age red to yellow color sandstone-mudstone material approximately in 4 meters thickness.	21 samples were drilled, 20 specimens were demagnetized via AF and TH	4 specimens TH, 8 specimens AF, 6 specimens were measured combine	Initial intensities between 160- 650 μA/m. Isolated ranges about 80°C-380°C or between 150°C plus 6 mT and 45 mT	18 specimens GC and 1 specimens selected as a Set Point	ChRM (N=18) result is D=280°, I= -66.5°. All specimens reversely magnetized.
R 79	Low-Middle Eocene in age yellowish to green color sandstone-claystone material approximately in 7 meters thickness. Yamak formation?	17 samples were drilled, 17 specimens were demagnetized via AF and TH	4 specimens TH, 7 specimens AF, 6 specimens were measured combine	Initial intensities between 400- 1300 μA/m. Isolated ranges about 180°C-380°C or between 150°C plus 6 mT and 40 mT	13 specimens GC and 4 specimens selected as a Set Point	ChRM (N=17) result is D=36.6°, I= 63.3°. All specimens normally magnetized.
R 80	Low-Middle Eocene in age yellowish to green color sandstone-claystone material approximately in 4 meters thickness. Eskipolatli formation?	11 samples were drilled, 13 specimens were demagnetized via AF and TH	4 specimens TH, 3 specimens AF, 6 specimens were measured combine	Initial intensities between 200- 14500 μA/m. Isolated ranges about 80°C-500°C or between 150°C plus 6 mT and 60 mT	All specimens interpreted without GC	ChRM (N=13) result is D=264°, I= 44.4°. All specimens normally magnetized.
R 81	Low-Middle Eocene in age yellowish to green color sandstone-claystone material approximately in 4 meters thickness. Yamak formation?	14 samples were drilled, 13 specimens were demagnetized via AF and TH	4 specimens TH, 3 specimens AF, 6 specimens were measured combine	Initial intensities between 500- 1250 μA/m. Isolated ranges about 80°C-340°C or between 150°C plus 6 mT and 80 mT	All specimens interpreted without GC	ChRM (N=13) result is D=38°, I= 46.2°. All specimens normally magnetized.

R 82	Low-Middle Eocene in age yellowish to green color sandstone-claystone material approximately in 8 meters thickness. Yamak formation?	20 samples were drilled, 20 specimens were demagnetized via AF and TH	4 specimens TH, 10 specimens AF, 6 specimens were measured combine	Initial intensities between 1000- 30000 μA/m. Isolated ranges about 80°C-560°C or between 150°C plus 6 mT and 80 mT	All specimens interpreted without GC	ChRM (N=20) result is D=333.6°, I= 39.5°. All specimens normally magnetized.
R 84	Up Miocene-Pliocene in age white color tuff approximately in 11 meters thickness.	28 samples were drilled, 21 specimens were demagnetized via AF and TH	21 specimens were measured AF	Initial intensities between 80000- 350000 μA/m. Isolated ranges between 8 mT and 60 mT	All specimens interpreted without GC	ChRM (N=21) result is D=163.8°, I= -49.6°. All specimens reversely magnetized.
R 85	Low-Middle Eocene in age yellowish to green color sandstone material approximately in 16 meters thickness.	27 samples were drilled, 21 specimens were demagnetized via AF and TH	4 specimens TH, 11 specimens AF, 6 specimens were measured combine	Initial intensities between 500- 13500 μA/m. Isolated ranges about 150°C-420°C or between 150°C plus 8 mT and 80 mT	All specimens interpreted without GC	ChRM (N=20) result is D=326.7°, I= 62.6°. All specimens normally magnetized.
R 86	Low-Middle Eocene in age yellowish to green color sandstone material approximately in 5 meters thickness.	13 samples were drilled, 13 specimens were demagnetized via AF and TH	4 specimens TH, 3 specimens AF, 6 specimens were measured combine	Initial intensities between 500- 3500 μA/m. Isolated ranges about 150°C-420°C or between 150°C plus 6 mT and 27 mT	9 specimens GC and 3 specimens selected as a Set Point	ChRM (N=11) result is D=304.2°, I= 67.6°. All specimens normally magnetized.

RN1	Low-Middle Eocene in age yellowish to green color sandstone material approximately in 5 meters thickness. Eskipolatli formation.	19 samples were drilled, 21 specimens were demagnetized via AF and TH	4 specimens TH, 11 specimens AF, 6 specimens were measured combine	Initial intensities between 100- 3500 μA/m. Isolated ranges about?	no set points and no GC	No result, because of remagnetization or big overprint over
RN4	Low-Middle Eocene in age yellowish to green color sandstone material approximately in 15 meters thickness. Yamak formation.	18 samples were drilled, 21 specimens were demagnetized via AF and TH	4 specimens TH, 11 specimens AF, 6 specimens were measured combine	Initial intensities between 6000- 25000 μA/m. Isolated ranges about 450°C-580°C or between 150°C plus 10 mT and 35 mT	19 specimens GC and 2 specimens selected as a Set Point	ChRM (N=21) result is D=31.4°, I= 34.7°. There are 7 specimens reversely magnetized.
RN5	Low-Middle Eocene in age reddish to green color sandstone material approximately in 5 meters thickness. Yamak formation.	16 samples were drilled, 21 specimens were demagnetized via AF and TH	4 specimens TH, 11 specimens AF, 6 specimens were measured combine	Initial intensities between 15000- 33000 μA/m. Isolated ranges about 180°C-580°C or between 150°C plus 10 mT and 80 mT	All specimens interpreted without GC	ChRM (N=20) result is D=1.1°, I= 48.5°. All specimens normally magnetized.
RN7	Low-Middle Eocene in age yellowish to white color fossilliferrious limestone-marl material approximately in 8 meters thickness.	19 samples were drilled, 21 specimens were demagnetized via AF and TH	4 specimens TH, 11 specimens AF, 6 specimens were measured combine	Initial intensities between 20-40 μA/m. Isolated ranges about 100°C-350°C or between 150°C plus 16 mT and 50 mT	13 specimens GC and 8 specimens selected as a Set Point	ChRM (N=21) result is D=319.9°, I=44.0°. All specimens normally magnetized.
RN8	Lower-Mid. Miocene in age and purple to white color marl	13 samples were drilled, 11	4 specimens TH, 7	Initial intensities between 10000- 40000 μA/m. Isolated	no remnant	Lightning.

	approximately in 12 meters thickness.	specimens were demagnetized via AF and TH	specimens AF	ranges?		
SEC1	Low-Middle Eocene in age yellowish to green color sandstone-clay material approximately in 564 meters thickness. Eskipolatli formation.	610 samples were drilled, 400 specimens were demagnetized via AF and TH	200 specimens TH, 200 specimens AF were measured	Initial intensities between ~350-34000 µA/m. Isolated ranges about 350°C - 580°C	All specimens interpreted without GC	ChRM (N=79) result is D=120.4°, I= -39.2°. There are normal and reverse magnetization
SEC5	Low-Middle Eocene in age yellowish to green color sandstone-clay material approximately in 564 meters thickness. Eskipolatli formation.	394 samples were drilled, 197 specimen with AF and 146 were demagnetized wit TH	46 specimens with TH were interpreted	Initial intensities between ~350-32000 µA/m. Isolated ranges about 350°C - 550°C	All specimens interpreted without GC	ChRM (N=46) result is D=52.9°, I= 53.1°. There are normal and reverse magnetization
S 1	Lower-Mid. Miocene in age and bluish to white color, fine grain marl, mixed clay and sandstone material approximately in 7 meters thickness.	24 samples were drilled, 20 specimens were demagnetized via AF and TH	4 specimens TH,10 specimens AF,6 specimens were combine measured	Initial intensities between ~120-1600 µA/m. Isolated ranges about 100°C - 310°C or between 150°C plus 4 mT and 70mT	All specimens interpreted without GC	ChRM (N=46) result is D=332.6°, I= 45°. All specimens normally magnetized.
S 2	Lower-Mid. Miocene in age and bluish to white color, fine grain muddy loose material	3 samples were drilled, 0 specimens were	-	-	-	-

	approximately in 3 meters thickness.	demagnetized				
S 3	Lower-Mid. Miocene in age and bluish to white color, fine grain marl, mixed clay and sandstone material approximately in 3 meters thickness.	27 samples were drilled, 20 specimens were demagnetized via AF and TH	4 specimens TH,11 specimens AF, 5 specimens were measured combine	Initial intensity ranges between ~2000-4200 µA/m. Isolated intensities about 180°C -540°C or between 150°C plus 15 mT and 80 mT	All specimens interpreted without GC	ChRM (N=19) result is D=358.3°, I= 75°. All specimens normally magnetized.
S 4	Up. Miocene-Pliocene in age and reddish to blue color, fine grain marl, mixed clay and sandstone material approximately in 3 meters thickness.	24 samples were drilled, 14 specimens were demagnetized via AF and TH	4 specimens TH,4 specimens AF, 6 specimens were measured combine	Initial intensity ranges between ~100-300 µA/m. Isolated intensities about 80°C -290°C or between 150°C plus 4 mT and 50 mT	All specimens interpreted without GC	ChRM (N=12) result is D=322.9°, I= 33°. There are two reversely magnetized specimens.
S 5	Lower-Mid. Miocene in age and bluish to white color, fine grain marl, claystone material approximately in 6 meters thickness.	28 samples were drilled, 20 specimens were demagnetized via AF and TH	4 specimens TH,9 specimens AF, 7 specimens were measured combine	Initial intensity ranges between ~240-810 µA/m. Isolated intensities about 180°C -250°C or between 150°C plus 30 mT and 80 mT	All specimens interpreted without GC	ChRM (N=14) result is D=151.6°, I=-40.1°. All specimens reversely magnetized.
S 6	Lower-Mid. Miocene in age and bluish to green color, fine grain marl, shale material approximately in 3 meters	39 samples were drilled, 20 specimens were demagnetized via	4 specimens TH,10 specimens AF, 6 specimens were	Initial intensity ranges between ~200-1400 µA/m. Isolated intensities about 80°C -230°C or between	All specimens interpreted without GC	ChRM (N=20) result is D=303.3°, I=41.5°. All specimens normally

	thickness.	AF and TH	measured combine	150°C plus 30 mT and 70 mT		magnetized.
S 7	Eocene in age and dark brown color, fine grain andesite, approximately in 11 meters thickness.	23 samples were drilled, 20 specimens were demagnetized via AF and TH	4 specimens TH,10 specimens AF, 6 specimens were measured combine	Initial intensity ranges between ~2000-12000 µA/m. Isolated intensities about 350°C -280°C or between 150°C plus 40 mT and 90 mT	All specimens interpreted without GC	ChRM (N=16) result is D=206.3°, I=-23.2°. All specimens normally magnetized.
S 8	Up. Eocene-Low. Miocene in age and reddish to blue color, fine grain marl, mixed clay and sandstone material approximately in 4 meters thickness.	27 samples were drilled, 20 specimens were demagnetized via AF and TH	4 specimens TH,10 specimens AF, 6 specimens were measured combine	Initial intensity ranges between ~1000-2200 µA/m. Isolated intensities about 80°C -200°C or between 150°C plus 15 mT and 50 mT	All specimens interpreted without GC	ChRM (N=10) result is D=198.4°, I= -37.2°. There are six reversely magnetized specimens.
S 9	Up. Eocene-Low. Miocene in age and reddish to blue color, fine grain marl, mixed clay and sandstone material approximately in 4 meters thickness.	24 samples were drilled, 20 specimens were demagnetized via AF and TH	4 specimens TH,10 specimens AF, 6 specimens were measured combine	Initial intensities between ~50-120 µA/m. Isolated ranges about 80°C -200°C or between 150°C plus 15 mT and 50 mT	All specimens interpreted without GC	ChRM (N=17) result is D=60.8°, I= 55.5°. All specimens normally magnetized.
SF 1	Pliocene in age and white color, fine grain marl, mixed clay material approximately in 8	20 samples were drilled, 20 specimens were demagnetized via	5 specimens TH,15 specimens were measured AF	Initial intensities between ~50-1200 µA/m. Isolated ranges about 20 -	5 specimens GC and 9 specimens selected as a Set	ChRM (N=14) result is D=5.9°, I= 42.1°. All specimens normally

	meters in thickness.	AF and TH		310°C or 4 mT and 45mT	Point	magnetized.
SF 2	Miocene in age and white color, fine grain marls/mudstones approximately in 5 meters in thickness.	20 samples were drilled, 20 specimens were demagnetized via AF and TH	5 specimens TH,15 specimens were measured AF	Initial intensities between ~50-1200 µA/m. Isolated ranges about 20 - 310°C or 4 mT and 45mT	6 specimens GC and 10 specimens selected as a Set Point	ChRM (N=16) result is D=27.4°, I= 48.9°. All specimens normally magnetized.
SF 3	Pliocene in age and white color, fine grain marl, mixed clay material approximately in 6 meters in thickness.	20 samples were drilled, 20 specimens were demagnetized via AF and TH	5 specimens TH,15 specimens were measured AF	Initial intensity ranges between ~50-4200 µA/m. Isolated ranges about 150 - 550°C or 12 mT and 50 mT	All specimens interpreted without GC	ChRM (N=10) result is D=2.7°, I= 59.1°. All specimens normally magnetized.
SF 4	Pliocene in age and white color, fine grain marl, mixed clay material approximately in 9 meters in thickness.	16 samples were drilled, 16 specimens were demagnetized via AF and TH	5 specimens TH,11 specimens were measured AF	Initial intensity ranges between ~7500-103000 µA/m. Isolated intensities about 80°C -290°C or between 150°C plus 4 mT and 50 mT	6 specimens GC and 10 specimens selected as a Set Point	ChRM (N=12) result is D=35.5°, I= 35.3°. There are two reversely magnetized specimens.
SF 5	Miocene in age and white color, fine grain marls/mudstones approximately in 6 meters in	15 samples were drilled, 15 specimens were demagnetized via	5 specimens TH,10 specimens were measured AF	Initial intensity ranges between 17000-1200000 µA/m. Isolated ranges about 410 -600°C or 25 mT and 60	2 specimens GC and 10 specimens selected as a Set	ChRM (N=12) result is scattered

	thickness.	AF and TH		mT	Point	
SF 6	Miocene in age and white color, fine grain marls/mudstones approximately in 8 meters in thickness.	16 samples were drilled, 16 specimens were demagnetized via AF and TH	5 specimens TH,11 specimens were measured AF	Initial intensity ranges between ~5000-10400 µA/m. Isolated ranges about 100 - 500°C or 12 mT and 45 mT	All specimens interpreted without GC	ChRM (N=20) result is D=2.5°, I=54.6°. All specimens normally magnetized.

CURRICULUM VITAE

PERSONAL INFORMATION

Surname, Name: Murat, Özkaptan
Nationality: Turkish (TC)
Date and Place of Birth: 09 March 1981, Sinop
Marital Status: Single
Phone: +90 505 585 18 88
Fax: +90 312 210 57 50
E-mail: muratozkaptan@gmail.com

EDUCATION

Degree	Institution	Graduation Year
MS	KTÜ Geophysical Engineering	2006
BS	KTÜ Geophysical Engineering	2002
High School	Gerze High School, Gerze-SİNOP	1998

WORK EXPERIENCE

Year	Place	Enrollment
2008-Present	METU Department of Geological Engineering	Research Assistant
2005-2007	KTÜ Department of Geophysical Engineering	Research Assistant
2005-2005	Çelebi Ground Handling	Ground Operator

FOREIGN LANGUAGES

Fluent English

PUBLICATIONS

1. Malandri C., Hinsbergen, D.J.J.V., Soukis, K., Özkaptan, M., Maffione,. M., Kriegsman, L., Langereis, C., 2016. A major post-middle Miocene vertical axis rotation difference across the 'Mid-Cycladic Lineament' on Paros Island, Cyclades, Greece, Tectonics (under preparation).

2. Uzel, B., Ökmen, S., Özkaptan, M., Özkaymak, Ç., Kuiper, K., Sözbilir, H., İnci, U., Kaymakcı, N., Langereis, C., 2016. Paleomagnetic and geochronologic

evidence for a major middle Miocene unconformity in western Anatolia, Journal of the Geological Society (submitted, under review).

3. Meijers, M.J.M., Strauss, B., Özkaptan, M., Feinberg, J.M., Mulch, A., Whitney, D.L., Kaymakci, N., 2016. Age and paleoenvironmental reconstruction of partially remagnetized lacustrine sedimentary rocks (Oligocene Aktoprak basin, central Anatolia, Turkey). Geochem. Geophys. Geosyst (accepted).

4. Uzel, B., Langereis, C.G., Kaymakci, N., Sözbilir, H., Özkaymak, Ç., Özkaptan, M., 2015. Reply to Karaoğlu and Erkül's comment on: "Paleomagnetic evidence for an inverse rotation history of Western Anatolia during the exhumation of Menderes core complex", Earth Planetary Science Letters, 427, 312.

5. Uzel, B., Langereis, C.G., Kaymakci, N., Sözbilir, H., Özkaymak, Ç., Özkaptan, M., 2015. Paleomagnetic evidence for an inverse rotation history of Western Anatolia during the exhumation of Menderes metamorphic core complex, Earth Planetary Science Letters, 414, 108-125.

HOBBIES

Basketball, Fishing, Football, Table Tennis, Cinema